

EXPERIMENTAL OBSERVATIONS OF THE EFFECT OF
FOUNDATION EMBEDMENT ON STRUCTURAL RESPONSE

Thesis by

Albert Niu Lin

In Partial Fulfillment of the Requirements
for the Degree of Doctor of Philosophy

California Institute of Technology
Pasadena, California

1982

(Submitted May 17, 1982)

ABSTRACT

Ambient, ring-down, and forced vibration tests were used to determine the effect of foundation embedment on the response of a one-story model structure 10 ft square in plan and 11.4 ft high. The tests, conducted at the full-, half- and unembedded foundation conditions, led to the identification of the fundamental translatory mode in the primary (east-west) and secondary (north-south) directions, and two torsional modes. The forced vibration consisted of horizontally incident SH-waves generated at an excitation structure located 47.5 ft (center-to-center) away. During these tests, detailed measurements of the near-field ground motion and modal displacement ratios were obtained at the fundamental mode in the primary direction. The displacement ratios were used to calculate the structural and foundation-soil stiffnesses and damping coefficients for comparison to theoretical results. Foundation embedment increased the model frequencies and decreased the contribution of the foundation motion to the overall displacement of the superstructure. For the fundamental mode response, which consisted of translatory and rocking motions, the resonant frequency predicted by lumped parameter analysis was higher than that measured experimentally by 25% for the unembedded case. While the experimental and theoretical fundamental mode shapes were in close agreement, the calculated effect of embedment on the response was less than that measured. These results were consistent with the comparison of the impedances and embedment factors. Serious discrepancies between analytical and experimental results were

found for the case of torsion; a simple two-degree-of-freedom model was consistent only with the first of the two measured resonant frequencies.

ACKNOWLEDGMENTS

This study would not have been possible without the generous help and cooperation that I have received from my friends and colleagues at Caltech. Space prevents me from listing every contributor, but certain individuals deserve special recognition.

My advisor, Professor Paul Jennings deserves much credit for his help, advice and encouragement during the progress of my graduate study and research. His insight and ability to simplify problems to their essential points were especially valuable contributions.

Professors Charles D. Babcock, Jr, George W. Housner, Ronald F. Scott and James L. Beck provided me with fresh and different perspectives in our many discussions. Their experience and individual abilities helped me understand other aspects of my research area.

Raul Relles deserves a hearty note of gratitude for his competent maintenance (and repair) of the equipment used in the field and in the lab. The expedient word processing assistance of Sharon Beckenbach, and library help of Donna Covarrubias are happily acknowledged.

Many fellow students offered their help and assistance. Special recognition is due Catherine Petroff for her eager and competent assistance in the field and lab. Garrett Jeong played a key role in the operation and upkeep of the laboratory's computer. His assistance in programming and debugging was invaluable. The help of Michael Karyeaclis and Nicholas Jones is also appreciated.

The generous loan of the vibration generating equipment by Professor Gary Hart and Mr. Ed Reuben of the University of California, Los Angeles made the forced vibration tests possible. The Caltech Azusa Hydraulics Laboratory, made available by Professor Frederic Raichlen and Mr. Elton Daly, successfully ended what could have been a long search for an undeveloped level site in the Los Angeles area.

Tse-Wen Lin, my father, checked all of my project design calculations and drawings, and offered many valuable suggestions to improve their clarity and accuracy. Both he and my mother, Tzi-Ing Lin, have steadfastly guided, nurtured, loved, and supported me. By their example, I have learned the meaning of humanity. This thesis is dedicated to them with my love and devotion.

The financial support of this study was provided by the Earthquake Research Affiliates of the California Institute of Technology and the National Science Foundation under Grant No. PFR77-23687. Finally, I acknowledge the educational support through the Earle C. Anthony Fellowship, as well as tuition scholarships, of the California Institute of Technology. I am proud to join the ranks of its alumni.

TABLE OF CONTENTS

ABSTRACT	ii
ACKNOWLEDGMENTS	iv
CHAPTER ONE - INTRODUCTION	1
1.1. GENERAL	1
1.2. CURRENT STATUS	3
1.3. SYNOPSIS OF PERTINENT WORK	6
1.3.1. Response of Embedded Foundations	6
1.3.2. Response of Structures Subjected to Incident Waves	10
1.3.3. Multiple Structure Interaction	12
1.3.4. Summary	13
1.4. OBJECTIVES OF THIS STUDY	15
1.5. SUMMARY OF THIS STUDY	16
1.6. ORGANIZATION OF THIS REPORT	19
CHAPTER REFERENCES	21
CHAPTER TWO - THE DESIGN OF THE EXPERIMENTAL STRUCTURES	26
2.1. SCHEMATIC PLANS	26
2.2. DESCRIPTION OF THE EXPERIMENTAL SITE	30
2.3. DERIVATION AND DEFINITION OF PARAMETERS	31
2.4. PRELIMINARY WAVE VELOCITY DETERMINATION	35
2.5. REQUIREMENTS AND CHARACTERISTICS OF VIBRATION GENERATORS	37

TABLE OF CONTENTS (CONTINUED)

2.6. DESIGN OF THE SPECIMEN STRUCTURE	39
2.6.1. Foundation Dimensions	39
2.6.2. Foundation and Superstructure Weight	40
2.6.3. Superstructure Stiffness	40
2.6.4. Miscellaneous Details	41
2.6.5. Comparison of Specimen Structure to Prototype Structures	44
2.6.6. Characteristics of the Specimen Structure "As-Built"	49
2.7. DESIGN OF THE EXCITATION STRUCTURE	50
CHAPTER REFERENCES	53
CHAPTER THREE - EQUIPMENT AND PROCEDURES	54
3.1. DESCRIPTION OF EQUIPMENT	54
3.1.1. Force Generation	54
3.1.2. Data Acquisition	57
3.1.2.1. Motion transducers	58
3.1.2.2. Signal conditioners	60
3.1.2.3. Data recorders	61
3.1.3. Data Reduction	63
3.2. PROCEDURE	65
3.2.1. Data Acquisition	66
3.2.1.1. Preliminary phase: free-field motion	66
3.2.1.2. Major phase: response of the spectrum structure	75
3.2.1.2.a. Ambient vibration	76
3.2.1.2.b. Ring-down test	77
3.2.1.2.c. Forced vibration tests	77

TABLE OF CONTENTS (CONTINUED)

3.2.2. Data Reduction	79
3.2.2.1. Ambient vibration	80
3.2.2.2. Forced vibration	81
3.2.2.2.a. Determination of frequency	82
3.2.2.2.b. Determination of amplitude	83
3.2.2.2.c. Determination of phase	85
3.2.3. Data Analysis	86
3.2.3.1. Free-field motion data	87
3.2.3.2. Structural response data	88
3.2.4. Errors analysis for forced vibration tests	89
CHAPTER REFERENCES	95
CHAPTER FOUR - THE EXPERIMENTAL RESULTS	96
4.1. FREE-FIELD MOTION DETERMINATION	96
4.1.1. Ground Motion at Specimen Structure	109
4.1.2. Shear Wave Velocity	109
4.2. SPECIMEN STRUCTURE RESPONSE	115
4.2.1. Ambient Vibration Test Results	115
4.2.2. Ring-Down Results	127
4.2.3. Forced Vibration Test Results	130
4.2.3.1. Determination of response modes	130
4.2.3.2. Mode shape at resonance	180
4.2.3.3. Resonance induced ground motions	188
4.3. ANALYSIS OF EXPERIMENTAL RESULTS	193
4.3.1. Determination of Equivalent Oscillators	194
4.3.2. Calculation of Translatory and Rocking Impedances	200

TABLE OF CONTENTS (CONTINUED)

4.3.2.1.	Determination of system stiffnesses	201
4.3.2.2.	Determination of system damping coefficients	205
4.3.3.	Determination of Torsional Properties	207
4.4.	COMPARISON OF RESULTS	214
4.5.	CHAPTER SUMMARY	216
	CHAPTER REFERENCES	219
CHAPTER FIVE - RESULTS OF ANALYSIS		220
5.1.	METHODS OF ANALYSIS	221
5.2.	DYNAMIC PROPERTIES	228
5.2.1.	Superstructure Stiffness and Damping in Translation	228
5.2.2.	Superstructure Stiffness and Damping in Torsion	232
5.2.3.	Equivalent Radii	239
5.2.4.	Soil Properties	241
5.3.	FUNDAMENTAL MODE RESPONSE	241
5.3.1.	Foundation-Soil Impedances	241
5.3.1.1.	Horizontal translation	246
5.3.1.2.	Rocking	252
5.3.2.	Analysis with Unembedded Foundation	257
5.3.3.	Modification of Foundation-Soil System for Embedment	262
5.3.4.	Response of Structure with Embedded Foundation	270
5.3.5.	Summary of Fundamental Mode Analysis	274

TABLE OF CONTENTS (CONCLUDED)

5.4. TORSIONAL RESPONSE	275
5.4.1. Foundation-Soil Impedance	276
5.4.2. Analysis of Torsional Behavior with Unembedded Foundation	278
5.4.2.1. Analysis with analytically obtained properties	279
5.4.2.2. Analysis with measured superstructure stiffness	281
5.4.2.3. Analysis using hybrid input values	284
5.4.3. Modification of Foundation-Soil System for Embedment	288
5.4.4. Torsional Response of Structure with Embedded Foundation	289
5.4.5. Summary of Torsion Analysis	291
5.5. CHAPTER SUMMARY	294
CHAPTER REFERENCES	297
CHAPTER SIX - SUMMATION	300
6.1. SUMMARY	300
6.2. CONCLUSIONS	308
APPENDIX A - COMPUTER PROGRAM LISTINGS	314
APPENDIX B - CONTRACT DRAWINGS	320

CHAPTER ONE

INTRODUCTION

This introductory chapter is divided into six sections. The first section is a broad overview of the significance of soil-structure interaction. Section 1.2 presents a summary of the current methods used for soil-structure interaction analysis. Pertinent works in the field are listed in the third section. The objectives and summary of this study are described in Sections 1.4 and 1.5 respectively. The organization of this report is given in the last section.

1.1. GENERAL.

The reduction of seismic risk to construction and human life is the principal objective of research and practice in the field of earthquake engineering. The reduction of this risk, through design of economical earthquake resistant structures, requires the accurate prediction of the structural response. Such response is dependent chiefly upon the characteristics of the structure and of the ground acceleration. Experience with structures subjected to earthquakes and the analysis of measured responses, however, have shown that the character of the soil-foundation interface is also an important factor in structural behavior. Identical structures subjected to the same free-field motion, but founded on different types of soil, will respond differently because of their different resonant frequencies and effective dampings.

It is this area of the soil-foundation interface, or more generally, the soil-structure interaction, that has been selected for study.

The nature of the soil-foundation interface governs the transmission of strong ground motion to the structural foundation. A typical structure founded on stiff soil or rock, for example, will have a foundation motion very similar to that which would have existed at the site in the absence of the structure. In soft soils, the coupling of the soil and structure during the earthquake causes the foundation motion to differ substantially from the free-field motion. In a limited number of cases where data are available, comparison of the records obtained in the foundation and at the free-field near the structure show considerable variation in the amplitude and frequency content. The majority of present analytical techniques for earthquake resistant design, however, are based on the assumption that the foundation of the structure moves identically with the soil around it.

Soil-structure interaction also affects the response of the structure. Compared to a structure with a "fixed base", the effect of soil-structure interaction is to lower the resonant frequencies and increase the modal damping through the phenomenon of radiation damping. Furthermore, there can be significant translational and rocking contributions to the structure's motion from the compliance of the supporting soil. For example, in forced vibration tests of the nine-story reinforced concrete Robert Millikan Memorial Library at the California Institute of Technology, Foutch (1976) found that 4% of the

roof translation was due to translation of the base, and 20% of the roof motion was due to rocking of the foundation. The soil strains involved were very small, and the soil was still behaving nearly elastically. In an earthquake, however, where soil yielding may occur, the contribution of the soil deformation to the structural response may be even greater.

1.2. CURRENT STATUS.

The soil-structure interaction problem has been the subject of many analytical and experimental studies both here in the United States and abroad, mainly in Japan. Many of these studies were concerned with the response, to forced vibration, of foundations bonded to the surface of an elastic half-space or to a stratum overlying a rigid half-space. Some idealizations were required to permit closed form solution of the resulting equations. Furthermore, while perhaps applicable to foundations supporting vibrating machinery, these solutions are not entirely relevant to structures responding to earthquake motions.

Recent studies have tried to overcome the shortcomings of these analyses when applied to earthquake engineering. There have been several analytical and experimental studies that have sought to ascertain the effect of embedment and backfill on the response of foundations to forced vibrations. The response of foundations to waves of arbitrary horizontal and vertical angles of incidence has also been examined. Increasing relevance to structural applications has been achieved by the examination of the response of single or multistory structures, both analytically and by experimentation on model or prototype structures. A

more detailed summary of research relevant to this study will be presented in Section 1.3, "Synopsis of Pertinent Work".

At present, the design of nuclear power facilities is the principal application of soil-structure interaction analysis. Two general methods of analysis have been used, the direct and substructure techniques. The direct method of analysis consists of modelling the entire soil-structure system with discrete finite element or finite difference networks. The free-field motion is then applied as a displacement boundary condition and the responses of both soil and structure are determined simultaneously. The resulting dynamic response of the structure is then used as the input in a second analysis to calculate the detailed structural behavior. In these analyses, the structure's response will induce waves into the soil that will radiate to the boundaries. Special boundary conditions are required to prevent the reintroduction of these waves into the system (Cohen, 1980). The use of the direct method, in theory, should permit the solution of three-dimensional, nonlinear problems.

The substructure method (e.g., Chopra and Guttierrez, 1977) considers the soil-structure interaction as the linear superposition of three simpler problems, (i) the determination of the foundation input motion, as it differs from the free-field motion, (ii) calculation of the impedance of the foundation-soil system, and finally, (iii) the determination of the structural response by solution of the appropriate equations of motion. Normally, because of the frequency dependence of

some of the system's parameters, the problem is solved in the frequency domain.

The foundation input motion depends on the angle of incidence of the wave with respect to the foundation. For surface foundations, the foundation input motion is identical to the free-field motion only for vertical incidence. The motion of the foundation is different from the free-field motion in the non-vertical incidence case because of the difference in rigidity between the soil and the foundation, and because the motion of different parts of the foundation is constrained. In the limiting case where the foundation is much stiffer than the soil, the foundation can be assumed to be rigid, and possesses only the six rigid body degrees-of-freedom. The calculated foundation input motion does not correspond to any measured earthquake motion in the prototype structure, and represents only an intermediate computational result.

Impedance functions relate the forces and displacements of the soil-foundation system. The coupling of the structure and the soil is represented by frequency dependent stiffness and damping terms. For the rigid foundation, the impedance functions can be expressed in a 6×6 matrix which corresponds to the six-degrees-of-freedom of a rigid body. The foundation input motion and the foundation-soil impedances are required to analyze the entire soil-structure system. The structure is modelled by mass, spring, and dashpot elements to represent the modal inertias, stiffnesses, and dampings. Equations of motion that represent the coupled behavior of the soil and foundation are then solved, subject to the forces corresponding to the foundation input motion.

The substructure approach, however, will only yield exact solutions to linear problems. Since superposition is required to obtain the complete solution, nonlinear problems can be solved only approximately.

1.3. SYNOPSIS OF PERTINENT WORK.

Initial investigations of the soil-structure interaction problem, such as those conducted by Reisner (1936), Reisner and Sagoci (1944), Arnold, Bycroft, and Warburton (1955), and Bycroft (1956), were concerned with the response of a rigid, massless, circular plate bonded to an elastic half-space or stratum, to harmonic transverse, vertical, torsional, and rocking forces. These contributions (particularly those of Bycroft) set the stage for almost all subsequent work in this area of study.

Extensive bibliographies in this subject are given by Luco and Westmann (1971), Jennings and Bielak (1973) and more recently by Johnson (1981).

1.3.1. Response of Embedded Foundations.

The response of embedded foundations has only been examined recently. One of the first major studies was conducted by Tajimi (1969) who examined the dynamic properties of a cylindrical, rigid foundation vertically supported on a rigid half-space and partially embedded in an overlying elastic stratum. The input motion consisted of a known acceleration of the supporting half space.

Analytical and experimental studies by Beredugo (1971), Beredugo and Novak (1971), Beredugo and Novak (1972a, 1972b), and Novak (1974) examined the response of two foundations 5.0 ft^2 (0.45 m^2) in area, one square in plan, the other rectangular, to horizontal, vertical, and rocking harmonic forces. The embedment of the foundations was changed by excavating the soil around the side of the foundation. The effect of the density of the surrounding soil was examined by varying the compaction of the backfill. The experimental results were compared to the analytical results obtained by Baranov (1967), who used a model similar to that of Tajimi, except that the foundation was supported by an elastic half-space.

Novak and Sachs (1973) determined the analytical solution for the torsional vibration of a partially embedded footing. The coupling of horizontal translation, rocking, and torsion was also studied. One of the results was the determination of coefficients that could be used to modify the stiffness and dampings obtained for a surface foundation to account for the effect of embedment.

Stokoe and Richart (1974) conducted forced vibration tests on two prototype machine foundations to determine the effect of embedment on the response. These two foundations measured $7.25 \times 4.60 \text{ ft}$ ($2.21 \times 1.40 \text{ m}$) and $15.8 \times 5.0 \text{ ft}$ ($4.80 \times 1.52 \text{ m}$). The effect of in situ soil properties was also examined. In the same year, Kinoshita and Kushida completed shaking table tests of a 6 in (0.15 m) square model. The finite element method was used by Seed and Idriss (1974) to show the effects of soil characteristics, embedment depth, and bedrock on the

response of massive embedded structures, such as nuclear reactor containment buildings.

Parmalee, Perelman, and Lee (1969) removed the frequency dependence of the impedance coefficients by averaging over the non-dimensional frequency range. The effect of embedment on the compliance of wall footings was presented by Parmalee and Kudder (1974). The study also showed that intermodal coupling between translation and rocking was not very significant in the response of embedded foundations.

The response of rigid circular and strip foundations embedded in an elastic stratum was evaluated by the finite element technique by Johnson, Epstein, and Christiano (1976). Bielak (1975) showed that a foundation embedded in a soil with hysteretic damping could be modelled as a single degree-of-freedom system with a linear, viscously damped oscillator subjected to a modified foundation excitation.

Experimental tests of small, rigid model structures, 4 to 6 in (0.10 to 0.15 m) in height, of various shapes and densities, on a shaking table were undertaken by Hadjian, Howard, and Smith (1975) to determine the effect of geometry, soil, and embedment on response. The overturning of these blocks was also examined. Field tests of a cylindrical rigid structure 6.0 ft (1.8 m) high and 3.54 ft (1.1 m) in diameter were conducted at two different field locations to obtain additional information on the effect of soil on response.

The earthquake response of a rigid cylinder, partially embedded in a layered soil medium overlying a rigid half-space, was analyzed ana-

lytically and experimentally by Abe and Ang (1974). The model structure had a radius of 6.48 ft (2.0 m) and a height of 35.2 ft (10.7 m).

Harada and Kubo (1978) extended the work of Tajimi and Novak, et al., to obtain an approximate theory for the calculation of the dynamic stiffness for coupled translation and rocking of an embedded foundation. Masao, et al., (1977, 1979, 1980) attached a vibration generator to the top of a 16.4 ft (5.0 m) square, 12.3 ft (3.75 m) thick concrete block founded 12.3 ft below grade. The response of the structure and the surrounding soil were measured with motion transducers and earth pressure cells. Variable parameters of the study were embedment and excitation frequency. After completion of the forced vibration tests, an additional 4.10 ft (1.25 m) of concrete were added to the top, and the structure was monitored for earthquake response. The experimental results were then compared to the results obtained by analysis of lumped parameter, finite element, and cylindrical rigid body models.

Another experimental study was conducted by Tanaka, Ohta, and Uchiyama (1979) who constructed a model structure consisting of a 20.0 ft (6.1 m) square concrete shear wall foundation and two-story, 10.0 ft (3.0 m) square superstructure, consisting of shear walls and steel frame. A vibration generator was then mounted on the roof of the structure. The effect of embedment was determined by increasing the backfill of the foundation during the experiment.

The inelastic deformation of a deeply embedded reactor building was the subject of an analysis by Celebi, Chatterjee, and Mark (1979).

1.3.2. Response of Structures Subjected to Incident Waves.

Since the earthquake excitation of a structure takes the form of incident waves, several analytical studies have been undertaken to determine the response of a structure subjected to waves of arbitrary vertical or horizontal incidence. Luco (1969) studied the response of a two-dimensional elastic shear wall on a rigid foundation of semicircular cross-section to horizontally polarized shear (SH) waves of vertical incidence. The work was subsequently expanded by Trifunac (1972), and Wong and Trifunac (1974), to include other angles of incidence for foundations of semicircular and semielliptical cross-section. The latter two studies also determined the ground surface displacements induced by the response of the shear wall systems. It was found that the response of the semicircular foundation system was independent of the angle of incidence, while the response of the semielliptical foundation system, as well as the induced ground surface displacements of both cases, were strongly dependent upon the incidence angle.

The general solution of the response of a rigid embedded foundation subjected to external forces, or to seismic excitation, was obtained by Luco, Wong, and Trifunac (1975). A specific solution for the two-dimensional, rigid, semielliptical foundation was determined. Significant rocking and torsional motions were found to be coupled with the translational response under SH-wave excitation.

A two-dimensional strip foundation with rectangular cross-section subjected to an SH-wave of arbitrary profile was examined by Thau and Umek (1973). Response to an incident compression (P) wave was studied

subsequently by Thau and Umek one year later. The response was found by transform techniques as an exact solution for the time period during which wave traverses the footing base for the first time, and as an approximate solution afterward. Thau, Umek, and Rostamian (1974) determined the response of an embedded rectangular foundation with an elastically mounted superstructure subjected to an SH-wave of arbitrary profile.

Shibuya and Shiga (1978) analyzed the response of a rectangular cross-sectioned foundation excited by vertically incident SH-waves as a boundary value problem, and obtained coupled integral equations.

Wolf and Obernhuber (1979), who noted that the majority of incident wave studies considered only vertically incident shear (S) and P-waves, completed a parametric analysis of various foundation models subjected to SH, P, SV (vertically polarized shear), and Rayleigh waves. For foundation models with mass, it was found that the transverse motion caused by non-vertically incident SH-waves was larger than that caused by any other type of wave. The response of foundations to incident S-waves with wavelengths comparable to the length of the foundation was considered by Lam and Scavuzzo (1979). The study found that the lateral motion of a foundation subjected to incident traveling waves was less than that of a foundation subjected to single point uniform motion (such as when the soil under the foundation is assumed to move uniformly). The lateral motion caused by the torsion of the foundation was of the same order of magnitude as that caused by pure translation. For design purposes, spring and dashpot analyses were found to be sufficiently

accurate; the additional complexity of closed form analyses or finite element modeling was not necessary.

The torsional response of a structure subjected to incident SH-waves was examined by Luco (1976). For the case of horizontal incidence, the tangential motions at the edges of the foundation and superstructure were several times larger than the free-field motion.

The diffraction of incident waves, by an embedded rigid foundation, was examined by Dravinski and Thau (1976a, 1976b) by transform techniques, and by Ray and Reed (1979) as a filtering problem.

1.3.3. Multiple Structure Interaction.

The coupling of two structures through the soil is an important manifestation of soil-structure interaction. A small building next to a massive nuclear reactor containment vessel, for instance, may be subjected to an increased ground surface displacement caused by the response of the reactor building.

Experimental studies include one by MacCalden (1969), who measured the coupled response of two 4.0 ft (1.21 m) diameter unembedded concrete foundations. One foundation, designated the active foundation, was subjected to vertical and horizontal translation and rocking forces, while the response of the other (passive) foundation, was measured.

The coupling through the soil between two 6.6 ft (2.0 m) square surface foundations was the subject of an experimental and analytical study by Kobori, Minai, and Kusakabe (1977). The test procedure was similar to that used by MacCalden. The interaction response of two

cylindrical rigid foundations was determined by Kobori and Kusakabe (1978). In 1980, Mizuno and Sugiyama, et al., reported on the results of forced vibration tests on two adjacent nuclear reactor buildings. Vibration generators were installed in one reactor, and the response of the second reactor was measured by motion transducers and earth pressure cells.

1.3.4. Summary.

The above synopsis was presented to illustrate the interest in the soil-structure interaction problem. Many investigators have tried different approaches to increase understanding of the phenomenon in order to develop some simple but accurate methods for analysis and design. This summary is by no means complete, but should allow the reader to gain some appreciation of the past effort in the area, and provides a starting point for further discussion.

Existing analytical models vary in complexity and relevance. The most fundamental solutions require severe assumptions about the shape and contact conditions of the foundation, uniformity and linearity of the soil, and the nature of the excitation. Inclusion of less ideal conditions, such as soil layering, noncircular plan foundations, foundation embedment, and so on, introduce additional complexities that preclude closed form solutions. These more realistic problems require numerical solutions, usually by finite element or lumped parameter analyses.

Experimental studies have also increased in scale and complexity. The earliest forced vibration tests were used to determine impedances of the foundation-soil system. The most recent tests, particularly in Japan, have examined the effect of foundation embedment on the response, to forced vibration, of multistory model structures. In addition, multiple structure systems, shear and moment resisting superstructures, and embedded foundations have been subjected to harmonically forced, ambient, and earthquake excitation.

The results of forced vibration tests provide accurate descriptions of the dynamic properties of the structure. Modal frequencies, dampings, and deformations can be used to determine the impedance of the soil-structure system. Use of this approach to predict the earthquake response of a prototype structure is, however, limited. Earthquake excitation consists of incident waves that transmit motion to the structure via the foundation. For higher excitation frequencies and large structures, the foundation does not move as a rigid body. Analysis has shown that if foundation flexibility is included the response of the structure is more complex, and possibly of smaller amplitude, than if the foundation is assumed to be rigid. Hence, even though the total displacement of the structure is lessened, the multimodal response may pose hazards of a different nature than previously anticipated.

The excitation of structures by incident waves is the central problem of earthquake engineering. The literature does not include any experimental studies of the response of structures to steady-state, incident wave excitation. Furthermore, existing analytical results have

generally examined only the cases of vertical incidence and non-embedded foundations. These two idealizations severely restrict the applicability of such results to structural analysis. Thus, for multistory structures with embedded foundations subjected to non-vertically incident waves, experimental results would not only verify analytical results, but also provide the first pieces of information in an important but as yet unexamined area.

1.4. OBJECTIVES OF THIS STUDY.

As stated previously, the analysis of soil-structure interaction depends upon the foundation input motion, the impedance of the soil-foundation and the structure itself. In order to validate the simplifications and idealizations used in theoretical analysis, it is necessary to experimentally verify the methods used to compute the foundation input motion from specified free-field motion, and the foundation impedance functions.

If existing theories can be experimentally verified for a small number of cases, then some conclusions can be drawn with regard to the overall accuracy of the analytical techniques involved. Since many more prototypical conditions can be included in an analytic study simply by changing parametric values than can be simulated by changes in the experimental conditions, the validation of a wider range of analytical cases by limited experimentation must be accepted.

This study will provide experimental data on the response of a single-story system with variable foundation embedment to horizontally

incident waves. The observed response will be compared to the response calculated by a lumped parameter analysis of the specimen structure. The comparison of these two results should give an indication of the validity of current methods of analysis, and of the approximations required for their use.

1.5. SUMMARY OF THIS STUDY.

In this study, the effect of foundation embedment on the response of a one-story structure will be determined. The study will consist of the measurement of the response to ambient and forced vibration of the structure shown, in the unembedded case, in Figure 1.1. The structure measures 10.0×10.0 ft (3.05×3.05 m) feet in plan, and has an overall height of 11.4 ft (3.5 m). The total weight of the structure is 50,000 lb (224 kN). The forced vibration will consist of horizontally incident, anti-plane SH-waves. The excitation frequencies will be in the range of 7 to 70 Hertz. These dimensions and frequencies will allow the structure to represent, dynamically, a wide range of prototype structures.

A bird's-eye view of the excitation and specimen structures is shown in Figure 1.2.

The experimental program was divided into two phases. The preliminary phase consisted of the measurement of the free-field ground motion caused by the vibration of the excitation structure. Therefore, this phase had to be completed prior to the construction of the specimen structure. In the second, or major, phase of the experiment, the

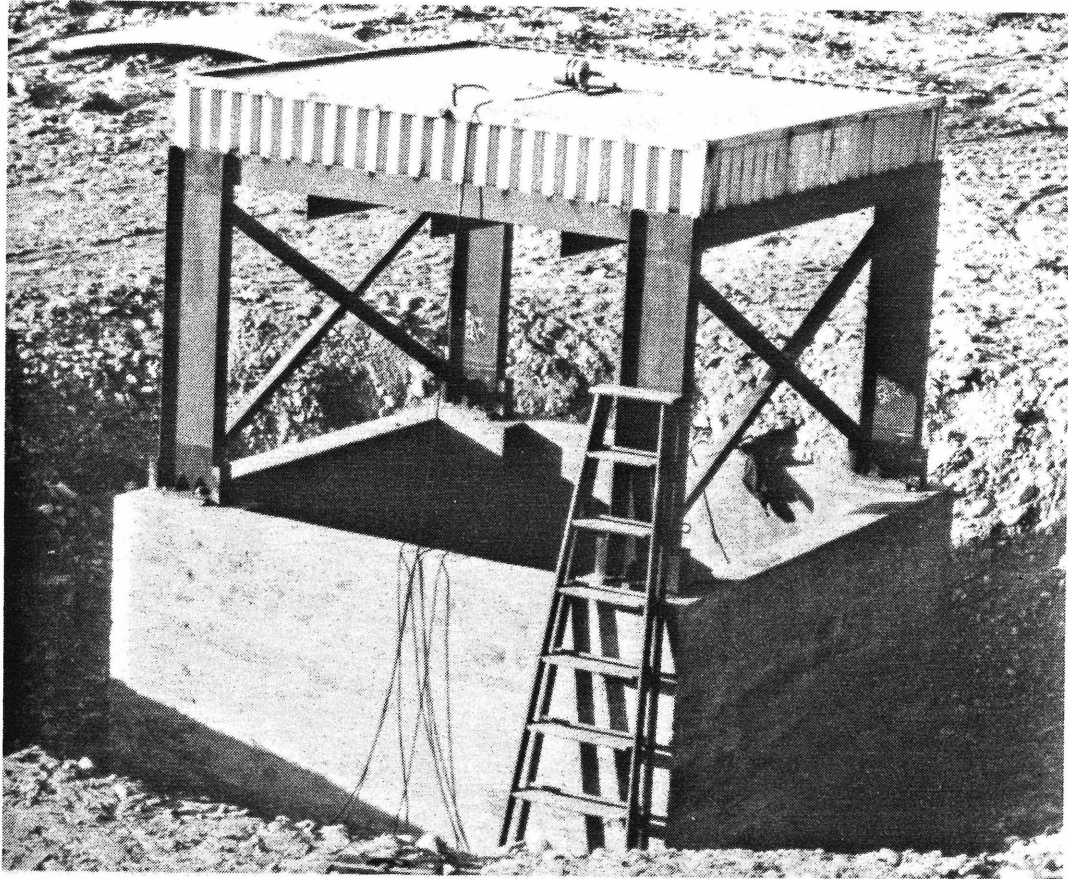


Figure 1.1. Specimen structure with unembedded foundation.

response of the specimen structure to ambient and forced vibration was determined. Sweeps of the frequency range were required to determine the resonant frequencies and modal dampings of the structure. Thorough measurements of the mode shape and ground motion at the fundamental translatory frequencies were completed for each embedment case.

The specimen structure was initially constructed with full-embedment of the foundation. After completion of the response measurements, the foundation was partially excavated to a condition of half-

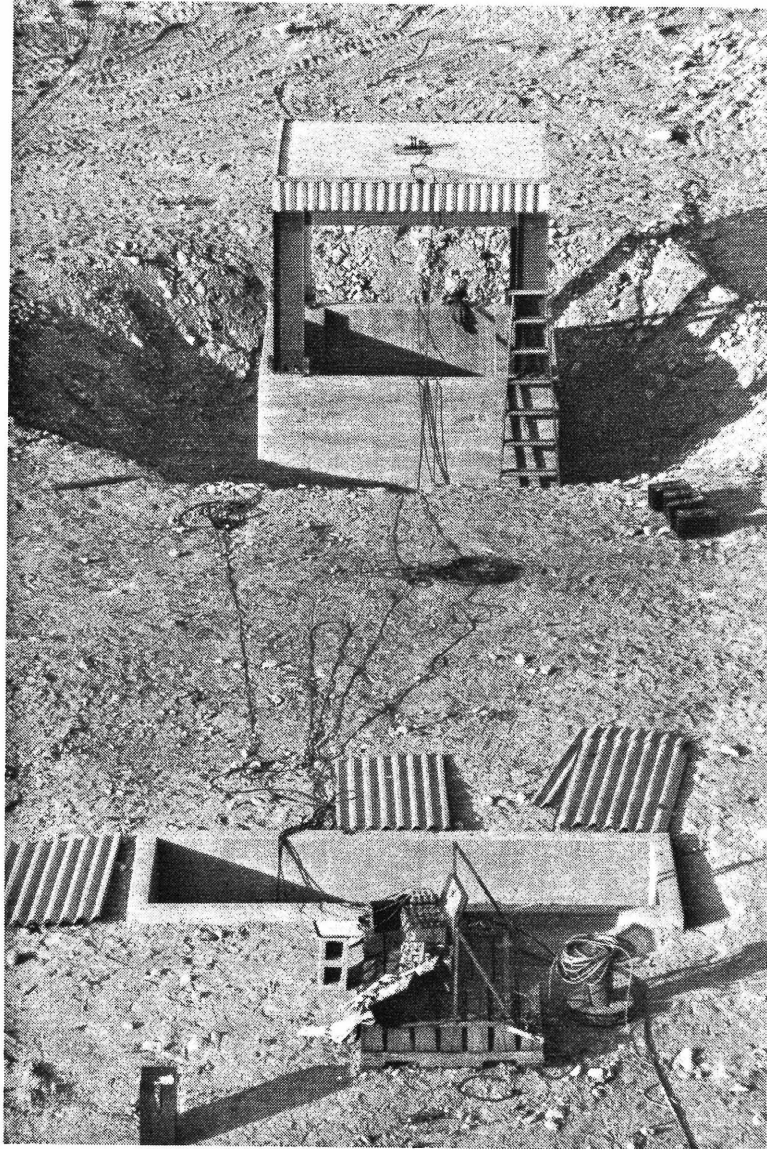


Figure 1.2. Overall view of experimental site.

embedment. The response measurements were repeated for this, and the final unembedded case.

After the experimental measurements were completed, lumped parameter analysis of the specimen structure was used to calculate the dynamic response. The comparison of the calculated and measured responses provided an indication of the validity of current methods of analysis, and the assumptions used therein.

1.6. ORGANIZATION OF THIS REPORT.

The remainder of this report is divided into five additional chapters. Chapter 2 describes the preliminary analysis that led to the design of the excitation and specimen structures. The chapter will include a discussion of the dimensionless parameters that were used in the study. The equipment and procedures for data acquisition, reduction, and analysis are discussed in Chapter 3. It should be noted that all of the field measurements were made with manufactured motion transducers, signal conditioners, and data recorders. Most of this equipment has been used in past experiments.

The results of the experiment, as well as the analysis of these results, are contained in Chapter 4. These results include the Fourier amplitude spectra that result from the ambient vibration tests, and response curves obtained from the forced vibration. The analysis of these results includes the calculation of system impedances and the empirical determination of factors that are applied to these impedances to account for embedment.

Chapter 5 presents the lumped parameter analysis of the specimen structure. Existing methods of calculating foundation-soil impedances

and embedment factors are presented and compared. These methods are used to obtain analytical response curves that can be compared with the experimental results. The summary and conclusions are discussed in Chapter 6.

CHAPTER REFERENCES.

- Abe, T., and Ang, A. H.-S., "Seismic response of structures buried partially in a multi-layered soil medium," Proceedings of the Fifth World Conference on Earthquake Engineering (WCEE), Rome, 1974, pp. 2098-2107.
- Arnold, R.N., Bycroft, G.N., and Warburton, G.B., "Forced vibration of a body on an infinite elastic solid," ASME Journal of Applied Mechanics, Sept. 1955, pp. 391-400.
- Baranov, V.A., "On the calculation of excited vibrations of an embedded foundation," (in Russian) Voprosy Dynamiki i Prochnosti, Polytechnical Institute of Riga, No. 14, 1967, pp. 195-206.
- Beredugo, Y.O., Vibration of Embedded Symmetric Footings, Ph.D. Thesis, Faculty of Engineering Science, The University of Western Ontario, London, Canada, 1971.
- Beredugo, Y.O., and Novak, M., "The effect of embedment on footing vibrations," Proceedings of the First Canadian Conference on Earthquake Engineering Research, Vancouver, 1971, pp. 111-125.
- Beredugo, Y.O., and Novak, M., "Coupled horizontal and rocking vibration of embedded footings," Canadian Geotechnical Journal, Vol. 9, Nov. 1972, pp. 477-497.
- Beredugo, Y.O., and Novak, M., "Vertical vibration of embedded footings," Journal of Soil Mechanics and Foundations Division, ASCE, Vol. 92, No. SM12, Dec. 1972, pp. 1291-1310.
- Bielak, J., "Dynamic behavior of structures with embedded foundations," International Journal of Earthquake Engineering and Structural Dynamics, Vol. 3, No. 3, Jan.-March 1975, pp. 259-274.
- Bycroft, G.N., "Forced vibrations of a rigid circular plate on a semi-infinite elastic space and on an elastic stratum," Philosophical Transactions of the Royal Society, Vol. A248, No. 948, 1956, pp. 327-368.
- Celebi, M., Chatterjee, M., and Mark, K., "Inelastic seismic analysis of a deeply embedded reinforced concrete reactor building," Transactions of the Fifth International Conference on Structural Mechanics in Reactor Technology (SMiRT), 1979, Paper K7/7.

- Chopra, A.K., and Guttierrez, J.A., "Earthquake analysis of structures including structure-soil interaction by a substructure method," Transactions of the Fourth International Conference on SMiRT, 1977, Paper K2/8.
- Cohen, M.F., Silent Boundary Method for Transient Wave Analysis, Earthquake Engineering Research Laboratory (EERL) 80-09, California Institute of Technology (Caltech), Pasadena, California, 1980.
- Dravinski, M., and Thau, S.A., "Multiple diffractions of elastic waves by a rigid rectangular foundation: plane-strain model," ASME Journal of Applied Mechanics, Vol. 43, Series E, No. 2, June 1976, pp. 291-294.
- Dravinski, M., and Thau, S.A., "Multiple diffractions of elastic shear waves by a rigid rectangular foundation embedded in an elastic half space," ASME Journal of Applied Mechanics, Vol. 43, Series E, No. 2, June 1976, pp. 295-299.
- Foutch, D.A., A Study of the Vibrational Characteristics of Two Multi-Story Buildings, EERL 76-03, Caltech, Pasadena, California, Sept. 1976.
- Hadjian, A.H., Howard, G.E., and Smith, C.B., "A comparison of experimental and theoretical investigations of embedment effects on seismic response," Proceedings of the Third International Conference on SMiRT, Sept. 1975, Paper K2/5.
- Harada, T., and Kubo, K., "Dynamic (complex) stiffness and vibration of embedded cylindrical rigid foundation," Proceedings of the Fifth Japan Earthquake Engineering Symposium, Tokyo, Nov. 1978, pp. 401-408.
- Jennings, P.C., and Bielak, J., "Dynamics of building-soil interaction," Bulletin of the Seismological Society of America, Vol. 63, No. 1, Feb. 1973, pp. 9-48.
- Johnson, J.J., Soil-Structure Interaction: The Status of Current Analysis Methods and Research, Lawrence Livermore Laboratory, Livermore, California, Jan. 1981.
- Johnson, G.R., Epstein, G.R., and Christiano, P., "Some comparisons of dynamic soil-structure analyses," Proceedings of the International Symposium on Earthquake Structural Design, Vol I, St. Louis, 1976, pp. 199-214.
- Kinoshita, K., and Kushida, H., "Experimental study on vibrational characteristics of the structures with embedded foundation," Proceedings of the Fifth WCEE, Rome, 1974, pp. 2638-2647.

- Kobori, T., and Kusakabe, K., "Dynamic cross-interaction between two embedded structures," Proceedings of the Fifth Japan Conference on Earthquake Engineering, Tokyo, Nov. 1978, pp. 521-528.
- Kobori, T., Minai, R., and Kusakabe, K., "Dynamical cross-interaction between two foundations," Proceedings of Sixth WCEE, New Delhi, 1977, pp. 1484-1489.
- Lam, P.C., and Scavuzzo, R.J., "Torsional structure response from free-field ground motion," Transactions of the Fifth International Conference on SMiRT, 1979, Paper K5/5.
- Luco, J.E., "Dynamic interaction of a shear wall with the soil," Journal of the Engineering Mechanics Division, ASCE, Vol. 95, No. EM2, Apr. 1969, pp. 333-346.
- Luco, J.E., "Torsional response of structures to obliquely incident seismic SH-waves," Earthquake Engineering and Structural Dynamics, Vol 4. No. 4, Jan-March, 1976, pp. 207-219.
- Luco, J.E., and Westmann, R.A., "Dynamic response of circular footings," Journal of the Engineering Mechanics Division, ASCE, Vol. 97, No. EM5, Proc. Paper 8410, Oct. 1971, pp. 1381-1395.
- Luco, J.E., Wong H.L. and Trifunac, M.D., "A note on the dynamic response of rigid embedded foundations," International Journal of Earthquake Engineering and Structural Dynamics, Vol. 4, No. 2, Oct.-Dec. 1975, pp. 119-125.
- MacCalden, P.B., Transmission of Steady-State Vibrations Between Rigid Circular Foundations, Ph.D. Thesis, University of California-Los Angeles, 1969.
- Masao, T., Hirasawa, M., Yamamoto, S., and Koori, Y., "Earthquake response of nuclear reactor building deeply embedded in soil," Transactions of the Fourth International Conference on SMiRT, 1977, Paper K2/7.
- Masao, T., Hirasawa, M., Yamamoto, S., and Koori, Y., "Earthquake response of nuclear reactor building deeply embedded in soil," Transactions of the Fifth International Conference on SMiRT, 1979, Paper K7/1.
- Masao, T., Takasaki, Y., Hirasawa, M., Okajima, M., Yamamoto, S., Kawata, E., Koori, E., Ochiai, S., and Shimuzu, N., "Earthquake response of nuclear reactor buildings deeply embedded in soil," Nuclear Engineering and Design, North-Holland Publishing Company, Vol. 58, 1980, pp. 393-403.

- Mizuno, N., Sugiyama, N., et al., "Forced vibration test of BWR type nuclear reactor buildings considering through soil coupling between adjacent buildings," Takenaka Technical Research 23, April 1980, pp. 27-36.
- Novak, M., "The effect of embedment on vibration of footings and structures," Proceedings of the Fifth WCEE, Rome, 1974, pp. 2658-2661.
- Novak, M., and Sachs, K., "Torsional and coupled vibrations of embedded footings," International Journal of Earthquake Engineering and Structural Dynamics, Vol. 2, No. 1, July-Sept. 1973, pp 11-34.
- Parmalee, R. A., and Kudder, R. J., "Seismic soil-structure interaction of embedded buildings," Proceedings of the Fifth WCEE, Rome, 1974, pp. 1941-1950.
- Parmalee, R.A., Perelman, D.S., and Lee, S-L, "Seismic response of multiple-story structures on flexible foundations," Bulletin of the Seismological Society of America, Vol. 59, No. 3, June 1969, pp. 1061-1070.
- Ray, Debrarata, and Reed, R.C., "Dynamic response of surface and embedded rectangular foundations for body and surface wave excitation," Proceedings of the Third Canadian Conference on Earthquake Engineering, Montreal, 1979, pp. 241-261.
- Reisner, E., "Stationäre, axialsymmetrische, durch eine schüttelnde Masse erregte Schwingungen eines homogenen elastischen Halbraumes," Ingenieur-Archiv, Vol. 7, 1936, pp. 381-396.
- Reisner, E. and Sagoci, H.F., "Forced torsional oscillations of an elastic half-space," Journal of Applied Physics, Vol. 15, 1944, pp. 652-662.
- Seed, H.B., and Idriss, I.M., "Soil-structure interaction of massive embedded structures during earthquakes," Proceedings of the Fifth WCEE, Rome, 1974, pp. 1881-1890.
- Shibuya, J., and Shiga, T., "Dynamic response of embedded foundations subjected to incident seismic waves," Proceedings of the Fifth Japan Earthquake Engineering Symposium, Tokyo, Nov. 1978, pp. 417-424.
- Stokoe, K. H., and Richart, F.E., Jr., "Dynamic response of embedded machine foundations," Journal of the Geotechnical Engineering Division, ASCE, Vol. 100, No. GT4, April 1974, pp. 427-447.

- Tajimi, H., "Dynamic analysis of a structure embedded in an elastic stratum," Proceedings of the Fourth WCEE, Santiago, Chile, 1969, pp. 53-69.
- Tanaka, N., Ohta, T., and Uchiyama, S., "Experimental and analytical studies of a deeply embedded reactor building model considering soil-building interaction, part I," Transactions of the Fifth International Conference on SMiRT, 1979, Paper K7/8.
- Thau, S.A., and Umek, A. "Transient response of a buried foundation to antiplane shear waves," ASME Journal of Applied Mechanics, Vol. 40, Series E, No. 4, Dec. 1973, pp. 1061-1066.
- Thau, S.A., and Umek, A. "Coupled rocking and translating vibrations of a buried foundation," ASME Journal of Applied Mechanics, Vol. 41, Series E, No. 3, Sept. 1974, pp. 697-702.
- Thau, S.A., Umek, A., and Rostamian, R., "Seismic motion of buildings with buried foundations," Journal of the Engineering Mechanics Division, ASCE, Vol. 100, No. EM5, Proc. Paper 10870, Oct. 1974, pp. 919-933.
- Trifunac, M.D., "Interaction of a shear wall with the soil for incident plane SH waves," Bulletin of the Seismological Society of America, Vol. 62, No. 1, Feb. 1972, pp. 63-83.
- Wolf, J.P., and Obernhuber, P., "Traveling wave effects on soil-structure interaction," Transactions of the Fifth International Conference on SMiRT, 1979, Paper K5/1.
- Wong, H.L., and Trifunac, M.D., "Interaction of a shear wall with the soil for incident plane SH waves: elliptical rigid foundation," Bulletin of the Seismological Society of America, Vol. 64, No. 6, Dec. 1974, pp. 1825-1842.

CHAPTER TWO

THE DESIGN OF THE EXPERIMENTAL STRUCTURES.

This chapter explains the rationale behind the design of the specimen and excitation structures. The design of the specimen structure was based on the site conditions, desired values of the dimensionless parameters, vibration generator capacity, and construction and cost constraints.

This chapter is divided into six sections. The schematic plan of the site and the specimen and excitation structures are presented in the first section. Section 2.2 describes the experimental site in Azusa, California. The key dimensionless parameters are defined and assigned values in the third section. Section 2.4 describes the preliminary determination of the in-situ shear wave velocity. The vibration generator is discussed in Section 2.5. The final design of the specimen and excitation structures are discussed in Sections 2.6 and 2.7, respectively.

2.1. SCHEMATIC PLANS.

Schematic plans of the site and the specimen and excitation structures are shown in Figures 2.1, 2.2, and 2.3. A full set of construction drawings is contained in the Appendix.

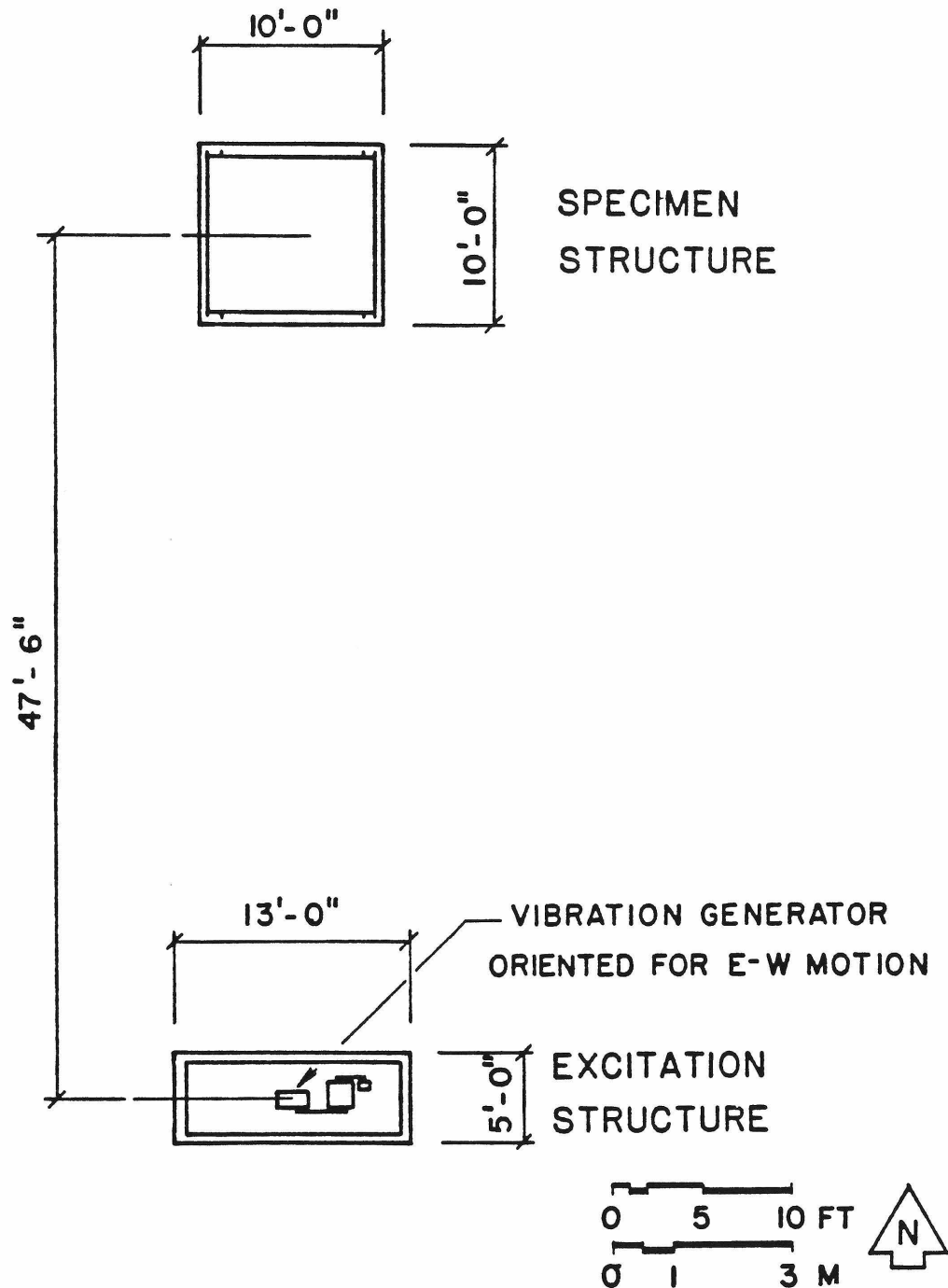


Figure 2.1. Schematic plan of experimental site.

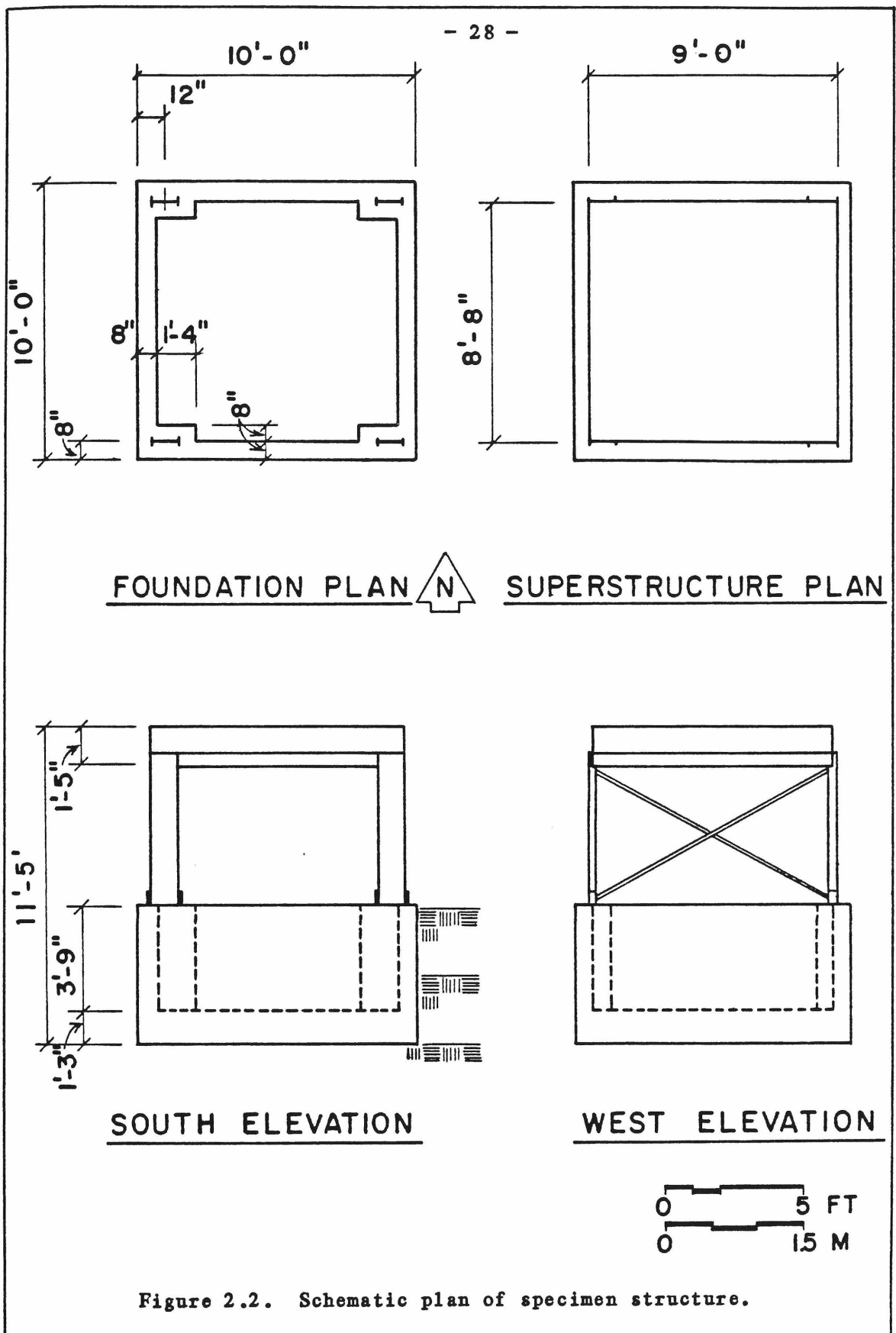


Figure 2.2. Schematic plan of specimen structure.

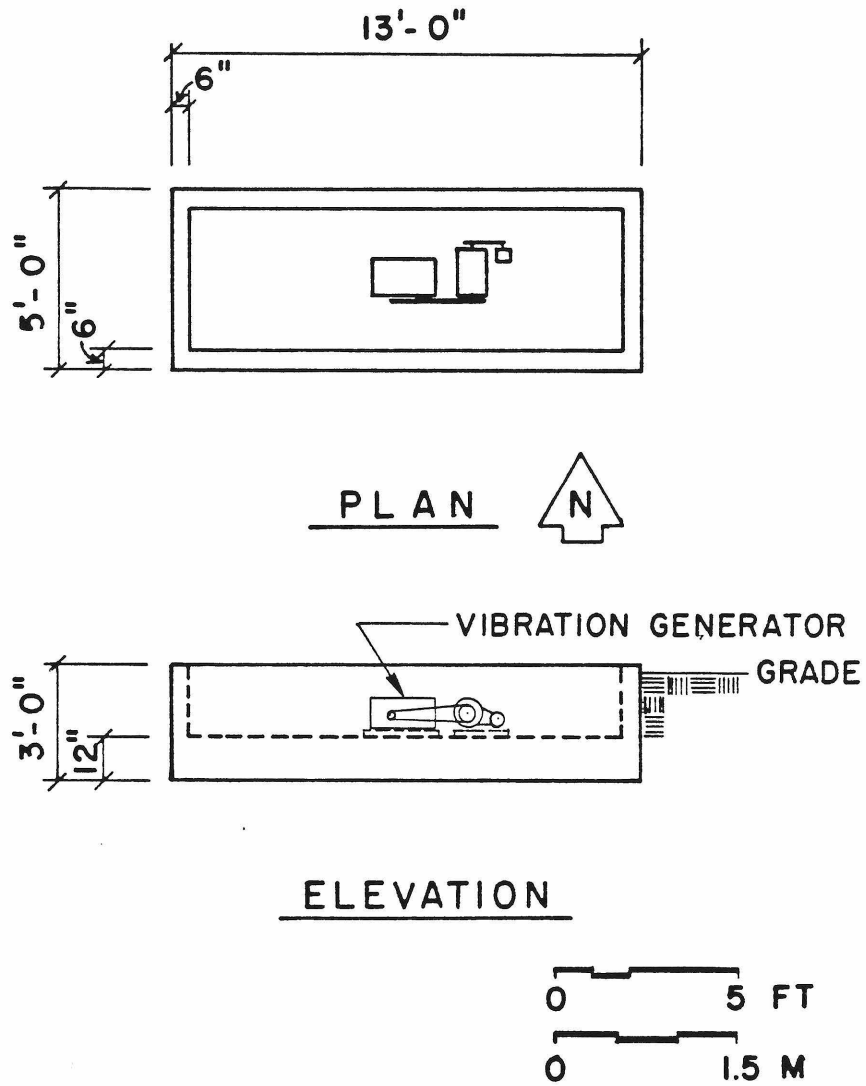


Figure 2.3. Schematic plan of excitation structure.

2.2. DESCRIPTION OF THE EXPERIMENTAL SITE.

The field tests were conducted at the California Institute of Technology's Azusa Hydraulics Laboratory, located 12 miles east of the Pasadena campus in Azusa, California. The site is located on geologically recent alluvium of the flood plain of the San Gabriel River. The structures were constructed on a level and undisturbed surface.

The soil consists of unconsolidated granular materials that include sandy silt, sand, gravel, cobbles, and boulders up to 18 in (0.5m) diameter. The depth of the deposits is approximately 1000 ft (300 m). While no soil tests were conducted at the site, a sand and gravel quarry, located 0.25 mi (0.40 km) to the west, exposed approximately 200 to 250 ft (60 to 75 m) of deposits to view. The exposed material appeared to be almost uniform. There was no evidence of layering, lenses, or significant changes in composition. The water table was approximately 200 ft (60 m) below the ground surface.

Soil tests were conducted by the geotechnical consulting firm of Converse, Ward, Davis, and Dixon, Inc., at two locations within 1 mi (1.6 km) of the site. These tests indicated that the natural ground consists of fine to coarse gray and light brown sands, with up to 60 to 70% gravel, rocks, and boulders up to 18 in (0.5 m) diameter. The dry density ranged from 89 to 103 lb/ft³ (14 - 16.2 kN/m³). The shear resistance ranged from 220 lb/ft² (10.5 kP) for samples consisting chiefly of fine sands, to 610 lb/ft² (30 kP) for sand and gravel mixtures. The boring depths ranged from 6 to 15 ft (2 to 4.5 m).

The winter of 1980-81 was drier than normal. The total precipitation from October 1, 1980 to April 30, 1981 (the usual rainy season) was 12 in (0.30 m). This compares to an average precipitation of 22 in (0.56 m). In contrast, 42 in (1.1 m) of rain fell during the 1977-78 season. There was no significant rainfall during the test program, which lasted from July to early December of 1981. The surface soil remained dry during the period of testing.

2.3. DERIVATION AND DEFINITION OF PARAMETERS.

Conclusions that are drawn from the observation of models can be applied to prototypes only if the similarity between model and prototype can be guaranteed. In a linear system, use of direct scaling is sufficient to guarantee similitude. Soil, however, is not a truly linear material even at small strains, much of its behavior depends on the stress and strain level. Therefore, simple dimensional scaling is not always sufficient.

Under these conditions, dimensionless parameters can be used to advantage. Depending on what aspect of prototype behavior is being studied, the model can be designed to have the same characteristics. The selection of these parametric values is one of compromise; it is not possible for the model and prototype to have the same values for all possible dimensionless parameters. Judgement must be used to determine which parameters should be the same, and which parameters can be allowed to differ.

Dimensional analysis requires, as a first step, the identification of significant variables and the determination of their units. There should be only one dependent variable; if several dependent variables are found, then a separate analysis must be completed for each one. In this experiment, the following variables were judged to be most significant:

1. Shear wave velocity, C_s ;
2. Excitation frequency, f ;
3. Equivalent radius of the foundation, r_o ;
4. Depth of embedment of the foundation, d ;
5. Fixed base natural frequency of the superstructure, f_n ;
6. Mass of the superstructure, M_s ;
7. Mass of the foundation, M_f ;
8. Mass of the excavated soil, M_e , and;
9. Displacement amplification factor (the dependent variable).

The Buckingham Pi Theorem states that the number of dimensionless groups is equal to the number of variables less the number of dimensions. In this case, there are nine variables, and three physical dimensions (force, time, and length); hence, there should be six dimensionless groups. One possible set of groups is:

1. $\pi_1 =$ Displacement amplification factor;
2. $\pi_2 =$ Dimensionless frequency, $a_o = \frac{2\pi f r_o}{C_s}$;

3. π_3 = Frequency ratio, f/f_n ;
4. π_4 = Embedment ratio, $\delta = d/r_o$;
5. π_5 = Mass ratio (1), $\mu_1 = M_s/M_f$; and
6. π_6 = Mass ratio (2), $\mu_2 = (M_s + M_f)/M_e$;

The dependent group π_1 is a function of the five independent groups, π_2 through π_6 . The functional dependence of π_1 on the independent groups may change for each mode. The identification of five independent groups would normally indicate that the list of variables is too long. In this experiment, however, only one model structure will be constructed. Therefore, the value of some of the independent groups will not change.

The next step in the analysis is the determination of the value, or range in values, that will be assigned to each group. For this test, the assigned values were chosen such that:

1. The parametric values are representative of the general class of problems, i.e., they are as close as possible to the assumed idealized conditions of existing analyses, and
2. The model structure is representative of actual structures for which experimental data of a similar nature have already been obtained. This permits direct comparison of the experimental results to past observations.

Based on this discussion, certain features of the specimen structure become apparent:

1. The foundation should be square in plan. Most of the analytical results, for mathematical simplicity, have been obtained for circular foundations. Not many prototype structures, however, are circular in plan. A square foundation is acceptable since there have been some analyses that have compared the behavior of round and square or rectangular foundations. Furthermore, a square foundation will have the same vibrational characteristics in two directions. This facilitates the separation of superstructure effects from foundation effects.
2. The range in dimensionless frequency of the experiment will be between zero and approximately two. This range has been considered extensively in analytical studies, and is most applicable to structures. Higher values of a_0 are applicable to machine and other non-building foundations.
3. The superstructure will have a height of one story. Analytical results have modelled structures as foundations supporting single degree-of-freedom (SDF) oscillator superstructures. Prototype structures, though, while usually multistoried, can be reduced to a SDF system by calculation of an equivalent simple oscillator (Housner, 1970).
4. The embedment ratio will vary from a value of zero to unity. Three embedment cases, hereinafter referred to as zero-

embedment, half-embedment, and full-embedment, will be examined. While few prototype structures are embedded to a depth equal to the foundation radius (the full-embedment case), the large range will emphasize the effect of embedment on the structural response, in the event that the effect is small in the range of embedment normally encountered. Most analyses have examined embedment ratios in this range, as well.

5. The total mass of the structure will be the same as the mass of the soil displaced by the foundation. In this way, there is no change in the load applied to the supporting soil.

The following values for the dimensionless parameters satisfy the conditions set forth above:

1. Dimensionless frequency $0 \leq a_0 \leq 2$;
2. Embedment ratio $0 \leq \delta \leq 1.0$;
3. Frequency ratio $1/3 \leq f/f_n \leq 3$;
4. Mass ratio (1) $\mu_1 = 0.5$;
5. Mass ratio (2) $\mu_2 = 1.0$;

2.4. PRELIMINARY WAVE VELOCITY DETERMINATION.

Wave velocity of the soil is important in soil-structure interaction analysis. The wave velocity determines the wavelength in the soil, and can be used to calculate other soil properties. Several attempts were made to obtain an approximate value of the shear wave velocity C_s for use in the design of the experimental structures.

One attempt consisted of a linear deployment of geophones at 20 ft (6.0 m) intervals. A large wooden timber, partially buried in the soil, was struck laterally to generate a shear disturbance that could be picked up by each geophone and recorded. A Nimbus multi-channel recorder, with inboard additive memory, was used to successively record these signals. By adding the records of successive impacts, random noise would be averaged out, and the desired signal would be enhanced. Unfortunately, the geophones were not sensitive enough to pick up the low amplitude motions. Furthermore, the recorder output was on photosensitive paper, which quickly became overexposed in the daylight.

The same apparatus was used with vertical force input to the ground. This attempt was also unsuccessful.

Finally, eight seismometers were deployed in a linear array at 20 ft (6.0 m) centers and connected to a thermal-tip recorder. A 60 lb (270 N) rock was dropped from a height of approximately 30 ft (9.1 m) to generate a vertical input force that was received by each seismometer and recorded in real time. The first arrival time and seismometer separation distances could be used to find the compression wave velocity (C_p). A value of 3000 to 3300 ft/sec (915-1000 m/sec) was obtained by this method. The shear wave velocity could not be obtained by this approach.

The shear wave velocity can be estimated from the compression wave velocity from the following function of Poisson's ratio,

$$C_s = \sqrt{\frac{1-2\nu}{2(1-\nu)}} C_p \quad . \quad (2.1)$$

For dry granular soils, Poisson's ratio will be in the range of 0.25 to 0.40. An intermediate value of 0.333 can be used without introducing significant error (Richart, Hall, and Woods, 1970) and results in a ratio of C_s/C_p of 0.5. Therefore, the shear wave velocity, at the site, was estimated to have a value of 1500 to 1650 ft/sec (460-500 m/sec). An average value of 1575 ft/sec (480 m/sec) was used for the preliminary analysis.

2.5. REQUIREMENTS AND CHARACTERISTICS OF VIBRATION GENERATORS.

Construction cost constraints dictated that the specimen structure could have maximum plan dimensions of 10 to 12 ft (3-3.7 m). These dimensions correspond to a length scale of approximately 8 to 10 for a typical prototype building. To satisfy dynamic scaling, the range of excitation frequencies have to be increased from the prototype condition by a similar factor.

Housner (1970) reported that in the United States, velocity response spectra for large earthquakes indicated that most of the strong shaking had periods between 0.4 to 5.0 seconds. For smaller earthquakes ($M < 5.5$) most of the strong shaking had periods between 0.2 and 0.5 seconds. These observations were made at distances not far from the causative fault. The shorter period motions attenuate more rapidly with distance, and hence, at greater distances, the periods of the strong motion are greater. Therefore, the prototype excitation frequencies are between 0.2 to 5 Hertz. An experimental frequency range of 2 to 50 Hertz would be required to simulate prototype conditions.

Because of the high shear wave velocity, even higher test frequencies might be necessary to achieve the full dimensionless frequency range, particularly if the structure was kept small. The required high frequencies eliminated the use of the Caltech-designed VG-1 vibration generators which have a maximum operating speed of 9 Hertz and maximum force output of 5000 lbs (22.4 kN). A pair of high frequency shakers was obtained from the University of California, Los Angeles. These shakers had a theoretical maximum operating speed of 100 Hertz, and could generate up to 12,000 lbs (54 kN) each. At low frequencies, however, the force output of these shakers was small. Therefore, it was originally believed that both shakers would have to be run synchronously. This would have been difficult at the higher frequencies because the phase control of the amplidyne control system was not of sufficient accuracy at these higher frequencies.

Several attempts were made to operate the high frequency shakers with the motors and solid-state controllers from the Caltech system. The Caltech controllers, being of a newer design, would be able to operate the two shakers synchronously. The controllers, however, were of insufficient amperage capacity to drive the motors under full load. A pilot test was conducted to determine if the ground motion amplitude generated by one shaker was large enough to be measured readily by the transducers. Fortunately, it was. Therefore, only one shaker was required, and the original high frequency shaker, motor, and control

system were installed into the excitation structure. A maximum frequency of 80 Hertz was assumed for subsequent design purposes.

The shaker system will be discussed fully in subsection 3.1.1.

2.6. DESIGN OF THE SPECIMEN STRUCTURE.

The design of the specimen structure depended upon the site conditions, dimensionless parameter values, equipment capabilities, and construction cost. Several alternative designs were prepared and evaluated in terms of these criteria. In this section, the design of the specimen structure is summarized, with calculations to verify conformance with the design requirements.

2.6.1. Foundation Dimensions.

The foundation measured 10 ft (3.05 m) square in plan, and had a depth of 5 ft (1.52 m). The radius r_o of the circular foundation with the same contact area is 5.64 ft (1.72 m). At full embedment, the embedment ratio is,

$$\delta = \frac{d}{r_o} = 0.889 \quad . \quad (2.2)$$

For a maximum excitation frequency of 80 Hertz and shear wave velocity of 1575 ft/sec (480 m/sec), the dimensionless frequency a_o has a maximum value of,

$$a_o = \frac{2\pi f r_o}{C_s} = 1.8 \quad . \quad (2.3)$$

The foundation consisted of an open-topped concrete box with corner pilasters that encased the structural steel anchor frames to which the steel columns were welded. Reinforcing steel was provided for crack and shrinkage control.

2.6.2. Foundation and Superstructure Weight.

The superstructure weighed approximately 16,500 lbs (73.4 kN), while the foundation weighed 33,500 lbs (149 kN). Since the soil had a unit weight of approximately 100 lb/ft³ (15.7 kN/m³), and the total foundation volume was 500 ft³ (14.2 m³), the approximate weight of the excavated soil was 50,000 lbs (224 kN). The two weight, or mass, ratios, have the following values,

$$\mu_1 = \frac{M_s}{M_f} = 0.492 \quad (2.4)$$

$$\mu_2 = \frac{M_s + M_f}{M_e} = 1.0 \quad (2.5)$$

2.6.3. Superstructure Stiffness.

The columns were W12 × 22 (305 × 102 × 33 kg/m UB) steel sections, with a length of 5.0 ft (1.5 m). Welded moment-resisting connections were used at both ends. The total stiffness of the four columns in the primary (east-west) direction is

$$K_{sx} = \frac{12EI}{L^3} \times 4 = 1.2 \times 10^7 \text{ lb/ft} \quad (1.76 \times 10^8 \text{ N/m}) \quad (2.6)$$

The fixed base natural frequency of the superstructure in translation is

$$f_n = \frac{1}{2\pi} \sqrt{\frac{K_{sx}}{M_s}} = 24.4 \text{ Hz} \quad . \quad (2.7)$$

The fixed base natural frequency leads to a maximum frequency ratio of

$$\frac{f}{f_n} = 3.3 \quad . \quad (2.8)$$

The minimum frequency ratio is dependent upon the sensitivity of the transducers to the small amplitude motions generated at low frequencies. If a minimum frequency of 5 Hertz is assumed, the frequency ratio has a minimum value of

$$\frac{f}{f_n} = 0.20 \quad . \quad (2.9)$$

The steel columns were much more flexible about the minor axis, which corresponds to the north-south axis. Hence, diagonal bracing consisting of $2.5 \times 2.5 \times 5/16$ in ($64 \times 64 \times 7.9$ mm) angles was used to provide additional stiffness in that direction.

2.6.4. Miscellaneous details.

The foundation was constructed of poured-in-place concrete with 28-day design strength of 3000 psi (21 MP). Reinforcing steel, conforming to ASTM A615, grade 60 [$f_y = 60 \text{ ksi} = 420 \text{ MP}$], was used for crack and shrinkage control. All structural steel was ASTM A36 [$f_y = 36 \text{ ksi} = 250 \text{ MP}$], connected with shop and field welds. The superstructure

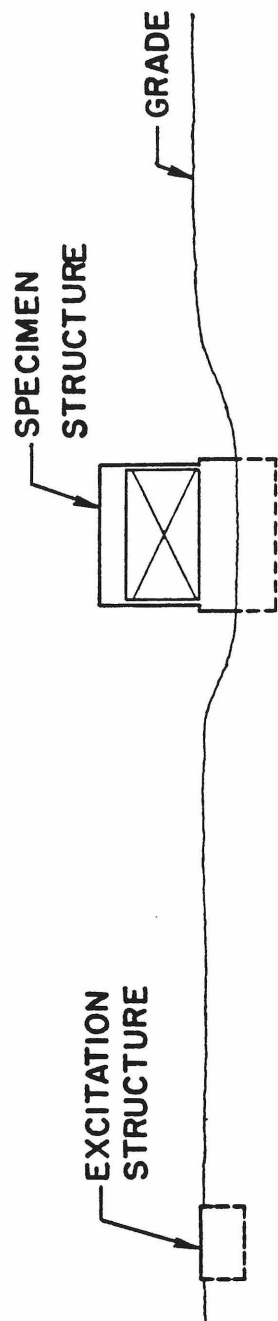
concrete was unreinforced, and placed directly into permanent corrugated metal forms.

The construction sequence was as follows,

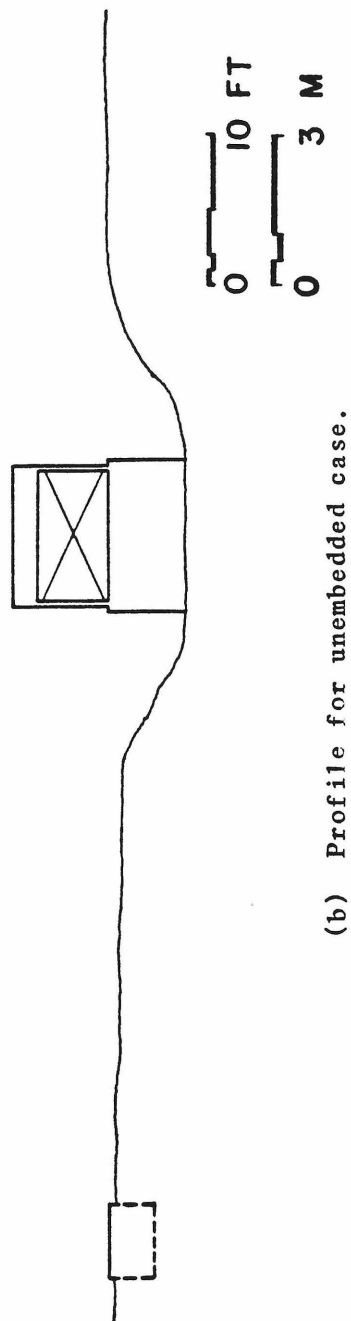
- Excavation for foundation,
- Construction of forms and placement of reinforcing steel,
- Pouring of foundation concrete,
- Stripping of foundation forms,
- Erection of superstructure steel frame and installation of metal deck and wall forms,
- Placement of superstructure concrete,
- Backfill of foundation excavation in 6 in (0.15 m) lifts with site materials. All cobbles larger than 3 in (0.08 m) diameter were removed from backfill material, and rock dust was used as replacement. Some water was used to facilitate compaction with an electrically driven pneumatic tamper.

After the tests were completed on the fully embedded foundation, the top 2.5 (0.76 m) feet of backfill were removed to provide half-embedment. The foundation was subsequently excavated to the unembedded case. Figures 2.4 (a) and (b) show the ground surface profiles along the north-south centerline for the two unembedded cases.

Unlike other tests that have considered foundation embedment, the foundation could not be cast directly against the sides of the excavation because of the size of the foundation and the nature of the soil.



(a) Profile for half-embedded case.



(b) Profile for unembedded case.

Figure 2.4. Ground surface profiles for unembedded foundation.

While the backfill was therefore not exactly the same as the undisturbed soil, it was believed that the variation would be inconsequential.

2.6.5. Comparison of Specimen Structure to Prototype Structures.

As stated in Section 2.2, a significant design requirement of the model structure was that it be representative of prototype structures. Table 2.1 compares the values of several measured, calculated, and parametric values for the Robert A. Millikan Memorial Library at the California Institute of Technology; Building No. 180 at the Jet Propulsion Laboratory; and for the specimen structure. The two prototype structures have been the object of several extensive experimental tests (Foutch, 1976; Jennings and Kuriowa, 1968; Nielsen, 1964; Wood, 1972). Several comments can be made about the calculations and results shown in Table 2.1.

1. The calculation of the equivalent radius is based on foundation contact area. This method may not be applicable to JPL 180, since the building is long and narrow, as compared to Millikan Library and the specimen structure, which are both nearly square.
2. The equivalent simple oscillator (ESO) has been calculated for both prototype structures. This model represents each mode of the structure as a single-degree-of-freedom system. In this case, only the fundamental mode has been modelled. Two such

TABLE 2.1. Comparison of Measured, Calculated and Parametric Values of Two Prototype Structures and the Specimen


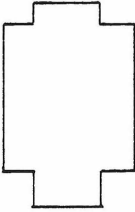

Value	JPL Building 180	Millikan Library	Specimen Structure
Plan shape and Dimensions	 220' X 40'	 69' X 75'	 10' X 10'
Structure Type	Concrete encased steel columns, and trussed floor and spandrel girders	Reinforced concrete frame and shear wall with central core	Structural steel frame
Overall height	153 ft (46.6 m)	158 ft (48.2 m)	11.4 ft (3.5 m)
Foundation embedment depth	16-32 ft (5.0-9.7 m)	14 ft (4.3 m)	5 ft (3.5 m)
Stories above ground	7 + roof	8 + roof	1
Average floor weight	1.3×10^6 lb (5.8 X 10 ⁶ N)	2.1×10^6 lb (9.3 X 10 ⁶ N)	1.65×10^4 lb (7.33 X 10 ⁴ N)

TABLE 2.1 (CONTINUED)

Value	JPL Building 180	Millikan Library	Specimen Structure
Total superstructure weight	1.04X10 ⁷ lb (4.67X10 ⁷ N)	2.1X10 ⁷ lb (9.3X10 ⁷ N)	1.65X10 ⁴ lb (7.33X10 ⁴ N)
Foundation weight	7.2X10 ⁶ lb (3.2X10 ⁷ N)	9.3X10 ⁶ lb (4.1X10 ⁷ N)	3.35X10 ⁴ lb (1.5X10 ⁵ N)
Weight of soil excavated for foundation	2.1X10 ⁷ lb (9.3X10 ⁷ N)	7.8X10 ⁶ lb (3.5X10 ⁷ N)	5.0X10 ⁴ lb (2.22X10 ⁵ N)
Fundamental Mode Frequency	N-S 0.97 Hz E-W 1.01 Hz	N-S 1.8 Hz	E-W 24.5 Hz
Excitation Frequency [Source]	0.2 < f < 8 Hz [San Fernando Earthquake, M = 6.3, 1971]	0.2 < f < 8 Hz [San Fernando Earthquake]	5 < f < 80 Hz [Forced Vibration]
Shear Wave Speed	910 ft/sec (280 m/sec)	1650 ft/sec (500 m/sec)	1575 ft/sec (480 m/sec)
Equivalent radius [by area]	52.9 ft (16.1 m)	40.6 ft (12.4 m)	5.64 ft (1.71 m)

TABLE 2.1 (CONCLUDED)

Value	JPL Building 180		Millikan Library	Specimen Structure
Weight of Equivalent SDF Oscillator	N-S 7.0×10^6 lb (3.1×10^7 N)	E-W 7.6×10^6 lb (3.4×10^7 N)	1.5×10^7 lb (6.7×10^7 N)	1.65×10^4 lb (7.34×10^4 N)
Stiffness of Equivalent SDF Oscillator	8.1×10^6 lb/ft (1.2×10^8 N/m)	9.5×10^6 lb/ft (1.4×10^8 N/m)	6.0×10^7 lb/ft (8.7×10^8 N/m)	1.2×10^7 lb/ft (1.8×10^8 N/m)
Frequency ratios	$0.21 < \frac{f}{f_n} < 8.2$	$0.20 \leq \frac{f}{f_n} < 7.9$	$0.11 \leq \frac{f}{f_n} \leq 4.44$	$0.20 \leq \frac{f}{f_n} \leq 3.3$
Mass Ratio $\mu_1 = \frac{M_{so}}{M_f}$	0.97	1.05	6.45	0.5
Mass Ratio $\mu_2 = \frac{M_{so} + M_f}{M_e}$	0.67	0.70	3.11	1.0
Maximum Dimensionless Frequency	2.92		1.24	1.8
Embedment ratio	$0.3 \leq \delta \leq 0.6$		0.34	$0 \leq \delta \leq .889$

models have been determined for JPL 180, one each for the long and short axes.

3. The ESO is determined by two parameters, the equivalent mass, M_{so} , and the equivalent stiffness K_{so} . These parameters are found from the lumped masses m_i and corresponding displacement x_i in the following way,

$$M_{so} = \frac{\left[\sum_{i=1}^n m_i x_i \right]^2}{\sum_{i=1}^n m_i x_i^2} \quad (2.10)$$

$$K_{so} = (2\pi f_n)^2 M_{so} \quad , \quad (2.11)$$

4. The superstructure mass used in the calculation of the two mass ratios μ_1 and μ_2 for the prototype structures is the equivalent mass for the ESO. In this way, the fundamental mode of the prototype structures is represented by the single-degree-of-freedom specimen superstructure.
5. The dimensionless parameter values of all three structures are generally close. The key exceptions are the maximum frequency ratio f/f_n , and the first mass ratio μ_1 . In both cases, these differences were thought to be unimportant. The higher excitation frequencies will not affect the fundamental mode response, which is of interest in this study. The different mass ratios do not pose a problem because the mass can be easily accounted for in analytical studies.

The comparison of parametric values of the specimen structure with those of the two prototype structures supports the conclusion that the specimen structure is representative of nominal prototype structures.

It should be noted that the vibrational properties of the specimen structure were discussed in terms of the fundamental translatory mode, which, in most prototype structures, is most important for seismic response. There are other vibrational modes of the specimen structure. All of these modes, however, are dependent on the structure's mass, stiffness, and geometry. Thus, it is not possible to specify the properties that determine the frequencies and mode shapes independently of one another. Selecting foundation dimensions, for example, to satisfy the dimensionless frequency requirement also specifies, implicitly, the behavior of the foundation in other modes as well.

2.6.6. Characteristics of the Specimen Structure "As-Built".

After the specimen structure was constructed, a more accurate determination of the masses and rotatory inertias of the superstructure and foundation was made, based on field measurements and observed conditions. This step is more important for smaller structures such as the specimen than it is for prototype structures, since the allowable dimensional tolerances are almost independent of the size of the structure. In the small structure, therefore, the variation between the as-built and designed conditions is proportionally larger than would be encountered in prototypes. The results of the calculations based on the as-built conditions are shown in Figure 2.5.

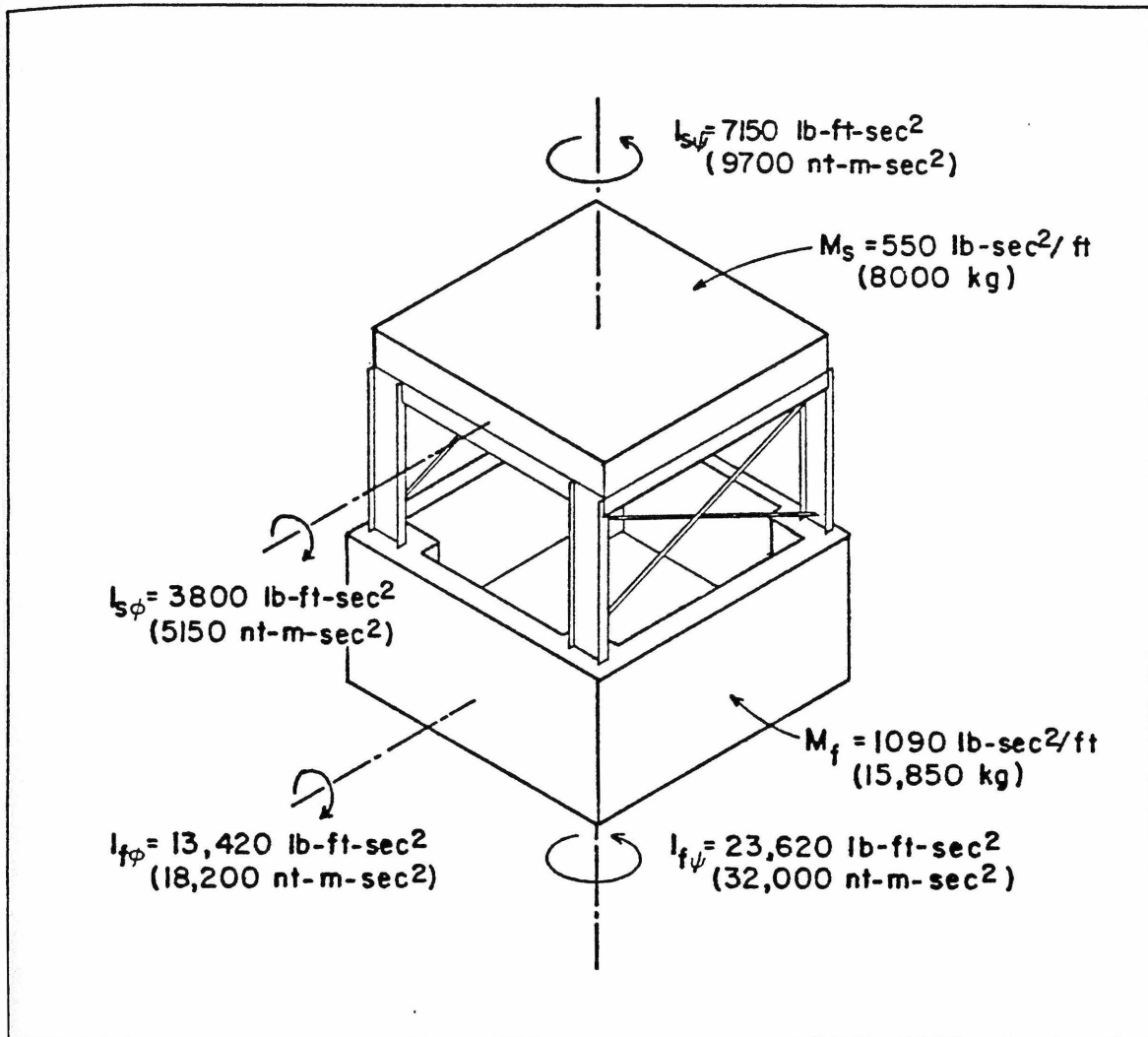


Figure 2.5. Specimen structure masses and moments of inertia under 'as-built' condition.

2.7. DESIGN OF THE EXCITATION STRUCTURE.

The excitation structure served primarily as a support for the shaker. Therefore, it had to be large enough to contain the shaking machine and driving motor and also provide enough space to permit access to all components for necessary repairs. Since the force resultant of the shaker was about 6 in (0.15 m) above the base, the shaker had to be

placed below grade to reduce rocking. The excitation structure is shown in Figure 2.6.

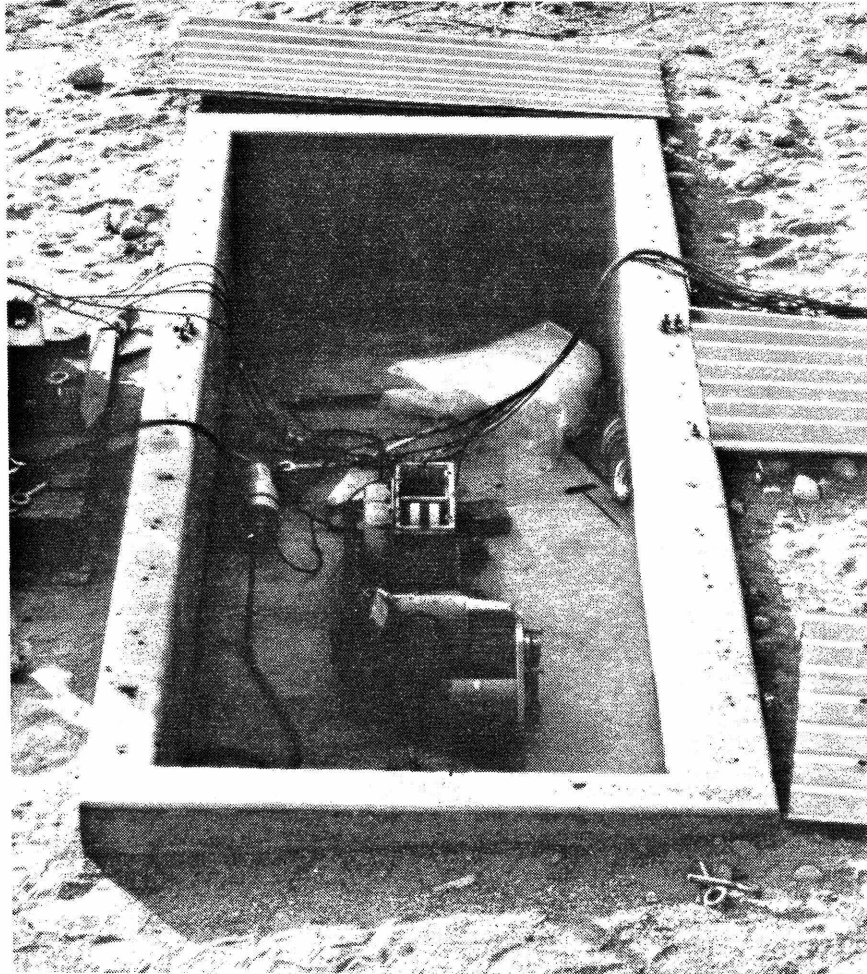


Figure 2.6. Excitation structure.

The separation between the excitation and specimen structures was another important dimension. Several factors had to be considered,

1. There had to be sufficient distance to permit measurement of structurally induced ground motion without interference from near-field effects of the excitation structure.

2. Adequate clearance had to be provided to allow maneuvering of construction equipment during re-excavation of specimen structure.
3. The wavefronts at the specimen structure had to be parallel and planar.
4. The excitation amplitude at the specimen structure had to be sufficiently large to be picked up by the motion transducers.

These considerations led to a distance of 47.5 ft (14.5 m) between the centers of the specimen and excitation structures. This provided for four building lengths [40 ft (12 m)] between the structures to allow the measurement of ground motion without interference from the excitation structure.

The existence of parallel wavefronts was verified by comparison of the ray lengths from the center of the excitation structure to the center, and sides, of the specimen structure. The difference in ray length was 0.31 ft (0.10 m). At a shear wave velocity of 1575 ft/sec (480 m/sec), this difference represented a time delay of 0.00002 seconds. The highest frequency excitation had a period of 0.0125 seconds. Therefore, the time delay represented by the difference in ray length was negligible.

CHAPTER REFERENCES.

Converse, Ward, Davis, and Dixon, Geotechnical Consultants, Inc. personal communications, April, 1981.

Foutch, D.A., A Study of the Vibrational Characteristics of Two Multi-Story Buildings, EERL 76-03, Caltech, Pasadena, California, Sept. 1976.

Housner, G.W., "Design Spectrum", Earthquake Engineering, R.L. Wiegel, Coordinating Editor, Prentice-Hall, Inc. Englewood Cliffs, N.J., 1970.

Jennings, P.C., and Kuriowa, J.H., "Vibration and soil-structure interaction tests of a nine-story reinforced concrete building," Bulletin of the Seismological Society of America, Vol. 58, No. 3, June 1968, pp. 891-916.

Nielsen, N.N., Dynamic Response of Multi-Story Building, Caltech, Pasadena, California, June, 1964.

Richart, F.E., Jr., Hall, J.R., Jr., and Woods, R.D., Vibrations of Soils and Foundations, Prentice-Hall, Englewood Cliffs, N.J., 1970.

Wood, J.H., Analysis of the Earthquake Response of a Nine-story Steel Frame Building During the San Fernando Earthquake, EERL 72-04 Caltech, Pasadena, California, Oct. 1972.

CHAPTER THREE

EQUIPMENT AND PROCEDURE

This chapter describes the equipment and procedures used during the field and laboratory phases of the experiment.

3.1. DESCRIPTION OF EQUIPMENT.

The equipment used in this experiment can be classified into three systems,

- Force generation,
- Data acquisition, and
- Data processing.

The following subsections will discuss the major components of each system.

3.1.1. Force Generation.

The force generating system consisted of a vibration generator, a variable speed direct current motor, and an amplidyne control unit. The motor and control units, originally designed and constructed at the California Institute of Technology, are described by Hudson (1961 and 1962). Theoretically, up to four shaking machines can be operated synchronously by the control system, although in this experiment, only one shaking machine was used.

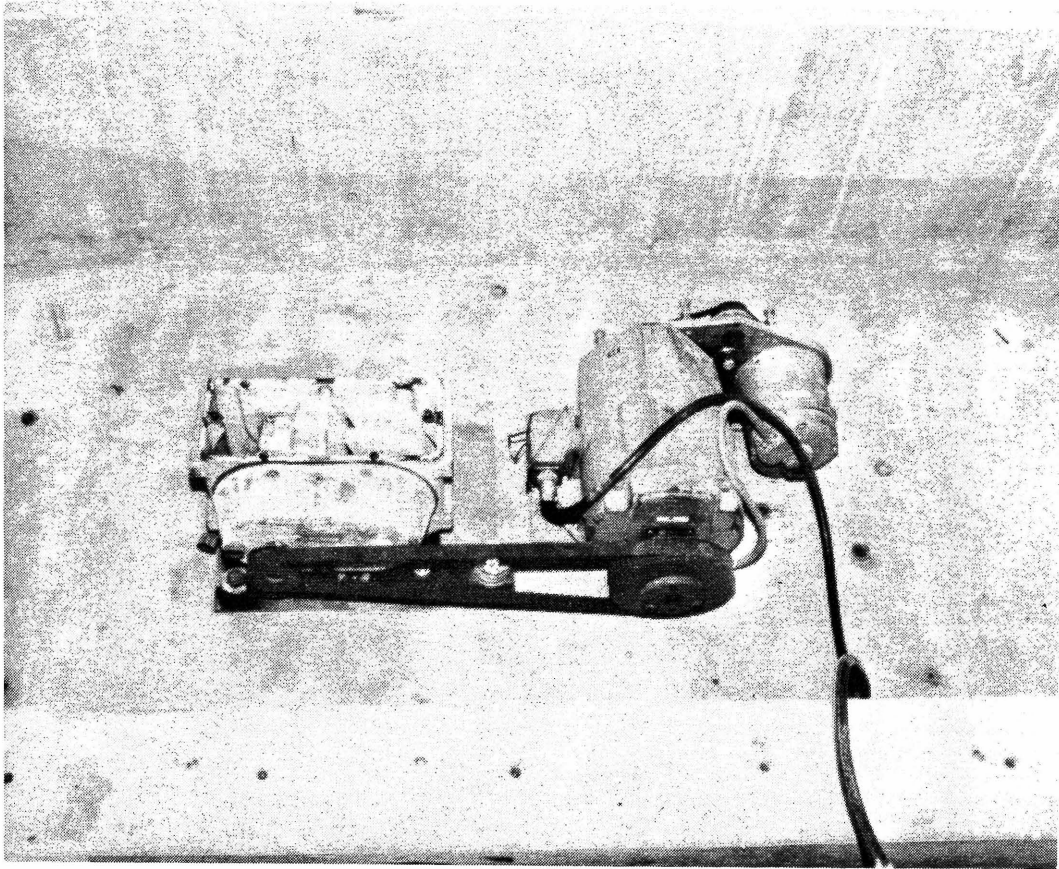


Figure 3.1. Vibration generator installed in the excitation structure.

The LAB vibration generator, shown installed in the excitation structure in Figure 3.1, was manufactured by LAB Corporation of Skaneateles, New York. The vibration generator has a maximum design operating speed of 100 Hertz, and can generate up to 12,000 lbs (53.4 kN) in continuous operation. The vibration generator has two sets of semicircular weights attached to counter-rotating horizontal shafts. The eccentricity of the weights can be varied by rotating the movable

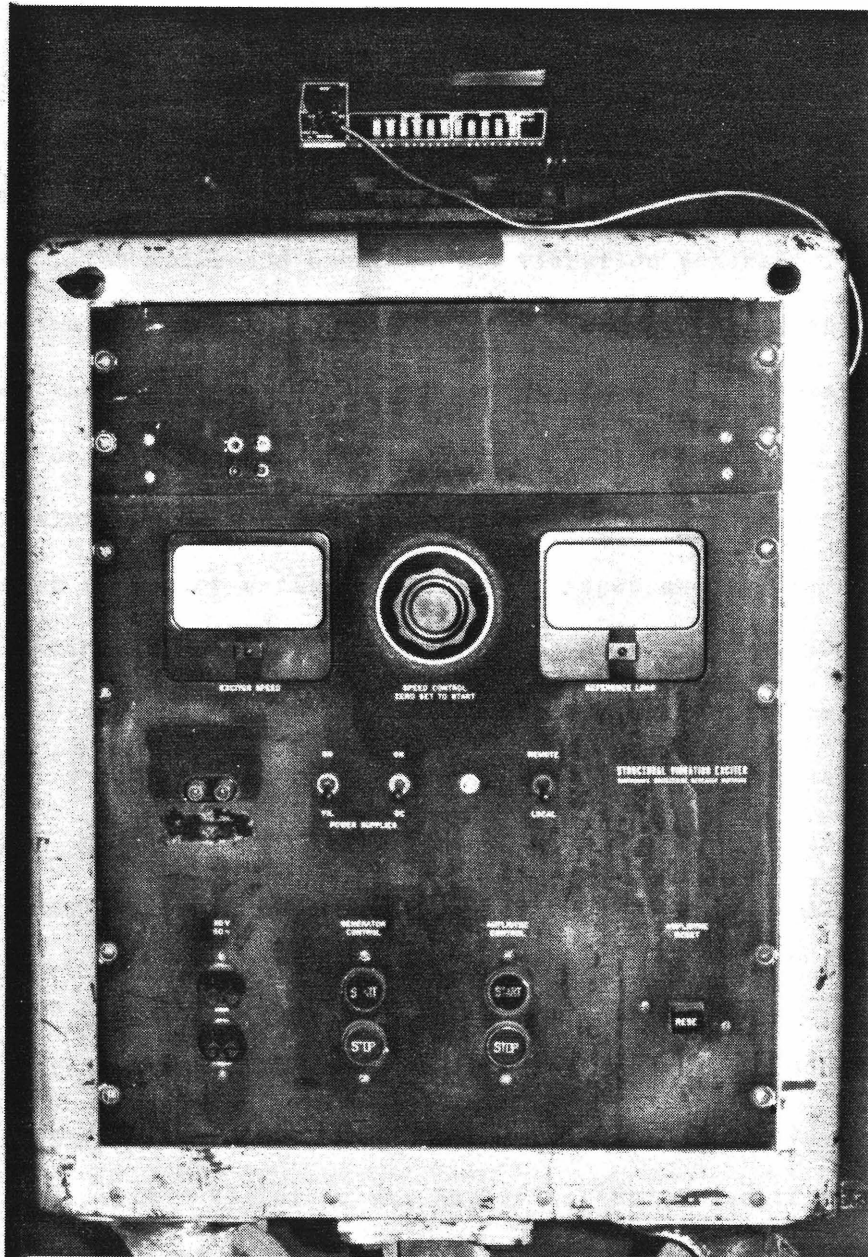


Figure 3.2. Amplidyne controller front panel.

set of weights with respect to the fixed set. The force output of the shaking machine can then be adjusted independently of the speed.

The drive motor was a 1.5 hp (1.1 kW) variable speed, direct current motor manufactured by General Electric. The motor was connected by belts to the vibration generator and to the speed control tachometer.

A servo-controlled electronic amplidyne system was used to control the speed of the motor and hence of the vibration generator. It is shown in Figure 3.2. The motor is controlled by setting the output voltage of the amplidyne. The voltage output of the tachometer, which is proportional to the speed of the vibration generator, is compared by the controller to the amplidyne output. A feedback system then adjusts the speed of the motor until the output voltages are the same.

The maximum speed of the motor/controller system was 30 Hertz. To achieve a shaker speed of 70 Hertz, it was necessary to increase the diameter of the motor output pulley to 2.5 times the diameter of the shaker input pulley. The resulting decrease in torque reduced the maximum force output to about 3000 lbs (13.3 kN).

3.1.2. Data Acquisition:

The data acquisition system consists of motion transducers, which convert ground motions into electrical signals; signal conditioners, which provide either filtering and amplification of the transducer output or carrier voltages; and data recorders.

3.1.2.1. Motion transducers.

Two motion transducers were used in the experiment; the Statham Accelerometer, and the Kinematics Ranger Seismometer. The Statham Model A4-0.25-350 Accelerometer, manufactured by Statham Instruments, has a natural frequency of 100 Hertz, and a maximum range of $\pm 0.25g$. The accelerometer consists of a mass connected to four strain-sensitive wires arranged as a Wheatstone Bridge. As the mass moves, the wires strain and change in resistance. The change in resistance alters the electrical balance of the bridge, which then affects the output voltage. Thus, the electrical output of the instrument is proportional to the acceleration.

Originally developed for the early unmanned lunar landings, the Model SS-1 Ranger Seismometer was manufactured by Kinematics, Inc. The nominal natural frequency of the instrument is one Hertz. The instrument consists of a spring-mounted magnetic mass suspended within a coil. The motion of the magnet with respect to the coil induces a voltage proportional to the relative velocity between the coil and the magnet. Since, in this experiment, the forcing frequency was much larger than the natural frequency of the instrument, the displacement of the mass is proportional to the displacement of the seismometer system. Hence, the output voltage was proportional to the velocity of base motion. Two Ranger Seismometers, deployed on the specimen superstructure, are shown in Figure 3.3.

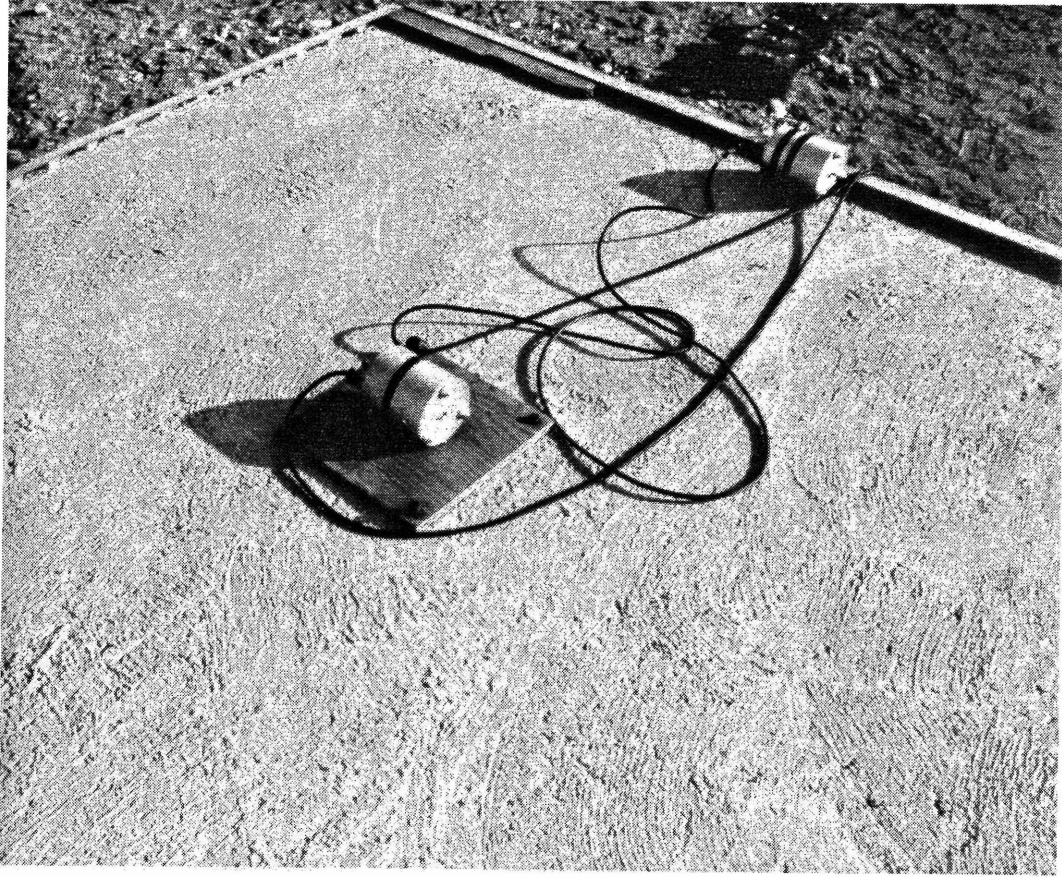


Figure 3.3. Ranger seismometers deployed on specimen superstructure.

Both types of transducers had to be used during the experiment to overcome limitations inherent in the design or operation of each instrument. The accelerometer responds accurately to static accelerations, and can be calibrated by tilting the instrument a known amount with respect to the earth's gravitational field. The sensitivity and signal-to-noise ratio, however, are not high enough to measure the small amplitude motions of this experiment. A longer set-up procedure is also required each time the instrument is relocated.

The seismometer is a sensitive and accurate transducer. It is difficult to calibrate absolutely, however, and therefore is most useful for determining relative amplitudes and phases. Also, because of small variations in the natural frequency and damping of the individual units, the amplification functions are not identical. Hence it is necessary to conduct relative calibrations throughout the frequency range. The seismometer was the principal motion transducer used during the experiment. The accelerometer was used only occasionally to provide information about absolute displacements.

3.1.2.2. Signal conditioners.

Because it was not possible to record the electrical output of the transducers directly, it was necessary to filter the signal before it was recorded on magnetic tape.

The two-channel Brush Model 13-4212-02 Carrier Preamplifier, manufactured by Gould Instruments, was used as a signal conditioner for the accelerometer. The preamplifier provided a 2 kHz alternating current across the accelerometer. The output signal consisted of the change in the current due to the change of balance of the Wheatstone Bridge. The preamplifier also provided user-variable amplification of the signal. Direct current offset was also provided to correct for the constant acceleration from the tilting of the accelerometer base.

The Kinometrics SC-1 four-channel signal conditioner was used with the seismometers. Each channel has two amplifiers in series with a total gain of 100,000. The gain can be adjusted by use of a nine-step,

54 decibel (dB) attenuator. A separate outboard attenuator was also available to reduce the gain by a factor of 100. The combination of the step and outboard attenuators resulted in an available range of gain of approximately 2 to 100,000. The signal conditioner also has a low-pass filter that can be set for any frequency between 1 and 100 Hertz. Without the filter, the signal conditioner responds to signals from 0.03 Hertz to 400 Hertz. Each input channel also has a variable potentiometer to provide electrical damping of the transducer's magnet/coil system. By setting the potentiometer to a resistance corresponding to 70% of the seismometer critical damping, the transducer has a nearly constant amplification factor over its frequency range. The signal conditioner was designed primarily for use with the Ranger, although other transducers can also be used.

3.1.2.3. Data recorders.

Three different data recorders were used in the experimental program. The two-channel Gould Brush Mark 220 Chart Recorder was used to monitor the output of the signal conditioners to allow for the adjustment of the attenuators. The chart recorder was also used to calibrate the accelerometer.

An eight-channel Hewlett-Packard Model 7758A thermal tip recorder was used for the in-situ determination of wave velocity and, in the lab, for the visual determination of relative phase between several stations.

A four-channel Hewlett-Packard Model 3960A magnetic tape recorder was used to as the main data recorder. The recorder has an internal

recording and playback calibration signal generator for four different peak-to-peak voltage levels. This calibration assured that the amplitude of the input signal was accurately recorded, and that the correct amplitude was reproduced when the signal was played back.

Figure 3.4 shows the signal conditioner, instrument tape recorder, and two chart recorders set up in the field for recording of data. This configuration was used in the majority of tests.

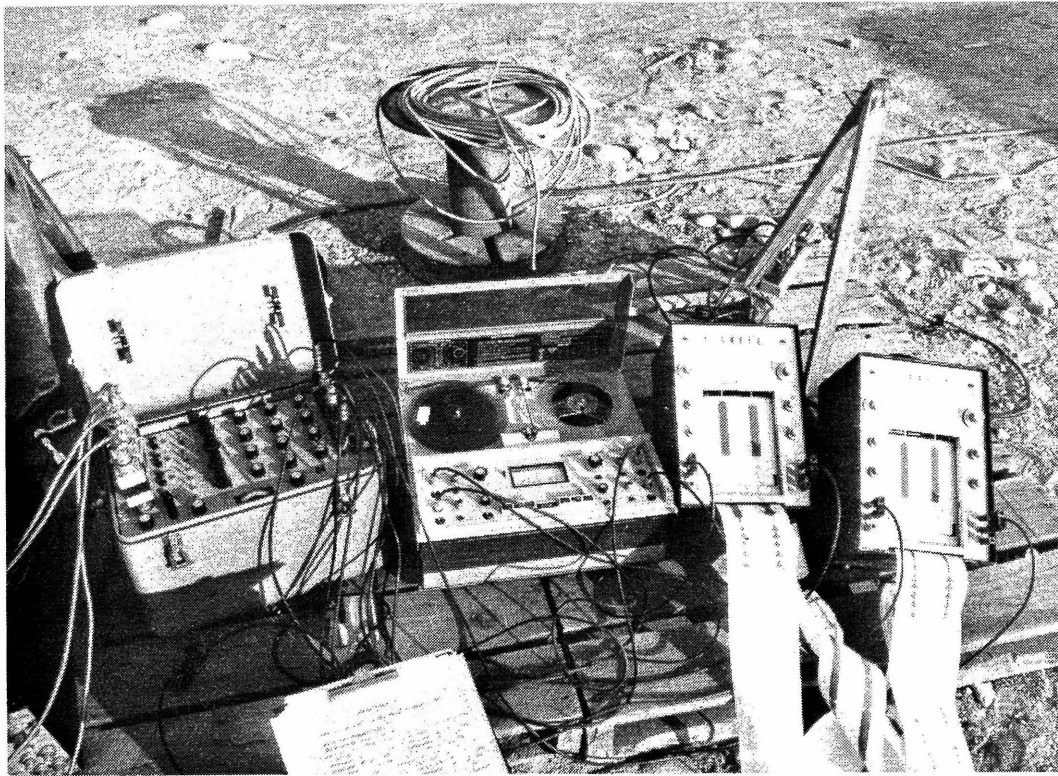


Figure 3.4. Field arrangement of signal conditioner, instrument tape recorder and chart recorders to record test data.

3.1.3. Data Reduction.

Data recorded in the field on magnetic tape had to be processed to determine signal amplitudes and frequencies, as well as the relative phase between various responses. For this purpose, two methods were used.

One method used a two-channel Model SD360 Digital Signal Processor manufactured by the Spectral Dynamics Corporation, shown in Figure 3.5 in the Vibrations Laboratory. The processor amplifies, filters, and digitizes the input, and then calculates and displays the Fourier amplitude spectrum. While the signal processor has many functions and controls, only those features which were used to process experimental data are discussed here.

The input signal strength can be modified over a range of 69 dB, in one-dB steps. A setting of less than 34 dB amplifies the input signal, while a setting greater than 34 dB attenuates the input signal. The input signal amplitude must be less than 12.6 volts to prevent distortion. After amplification, the signal is filtered by a switchable low-pass anti-aliasing filter. The filter cut-off frequency is set by default at 0.8 of the maximum analysis frequency. Other cut-off frequencies can also be specified.

The analysis frequency also determined the sampling frequency of the 12-bit analog-digital (a/d) converter. The a/d converter samples at twice the maximum analysis frequency. Each spectrum is calculated from 1024 data words, therefore, the length of each record used for the calculation depends on the range of analysis frequency. Because there

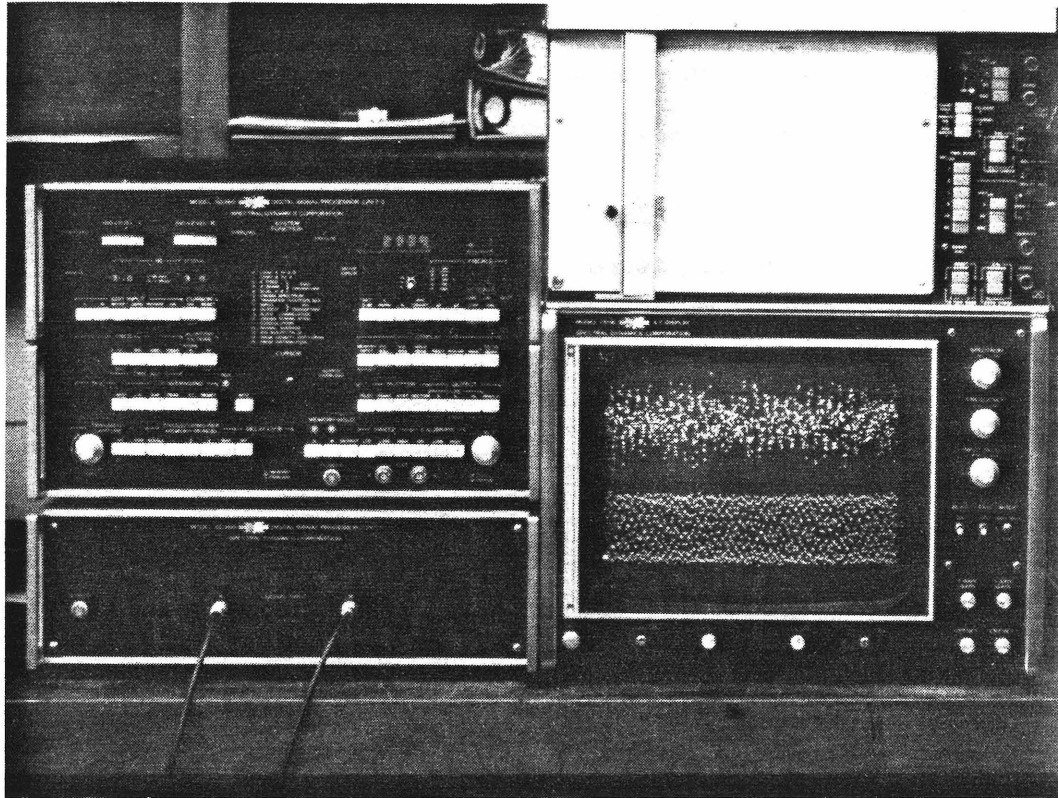


Figure 3.5. Digital signal processor in Vibrations Laboratory.

is only a finite number of frequency ordinate points, the maximum analysis frequency has to be chosen to maximize resolution while still including all of the significant frequencies. The amplified, filtered, and digitized input is next analyzed by use of the fast Fourier transform. Averaging can be used to reduce random noise. The transforms of both channels can be calculated simultaneously and displayed on the video screen, or plotted. Both output devices can also be used to display the input in real time. Log-log, semi-log, and linear scales can be used for the spectral displays.

The signal processor was also used to calculate transfer functions between two simultaneously recorded channels of data. The output could be expressed in terms of the real and imaginary components of the cross spectrum or in terms of the magnitude and phase.

A second method of amplitude determination, which will be described in paragraph 3.2.2.2, utilized a band-pass filter, true RMS voltmeter, and the input display mode of the digital signal processor. The Model 3750 Solid-State Variable Filter, manufactured by the Krohn-Hite Corporation, consists of variable high- and low-pass filters. The attenuation rate is also variable, and for this experiment was set at 24 dB per octave. The True RMS voltmeter was a Hewlett-Packard Model 3403A.

3.2. PROCEDURE.

The experimental procedure used in this study consisted of data acquisition in the field, and data reduction and analysis in the laboratory.

There were two phases of data acquisition. The preliminary phase, completed prior to the construction of the specimen structure, consisted of the measurement of the ground motion caused by the vibration of the excitation structure. The results of this phase will be known as the free-field ground motion. The major phase involved the measurement of the response of the specimen structure to ambient and forced vibration. These measurements were conducted for the full-, half-, and zero-

foundation embedment cases. The ground motion and mode shape of the specimen structure at the fundamental frequency were also measured.

Data reduction for the ambient vibration tests consisted of the calculation of the Fourier amplitude spectra. Excitation frequency, root-mean-square (RMS) amplitude of the recorded signal, and sometimes, the relative phase of two responses were determined from the data recorded during the forced vibration tests. The RMS voltages had to be corrected to account for the amplifier and filter settings, shaker eccentricity, excitation frequency, and seismometer characteristics to obtain the final response curves. This last calculation was completed during the data analysis.

The following subsections will discuss each part of the experiment in further detail.

3.2.1. Data Acquisition.

3.2.1.1. Preliminary phase: free-field motion.

The free-field motion caused by the vibration of the excitation structure was measured to achieve three principal objectives:

- To determine the amplitude of ground motion at the future site of the specimen structure,
- To establish base-line free-field ground motion amplitudes to permit future measurement and determination of any effects of structural response on ground motion amplitudes, and

- To obtain a more accurate estimate of the shear wave velocity in the soil.

Free-field motion was measured at 10 ft (3 m) centers along the north-south centerline of the excitation structure. Additional measurements were made at the site of the specimen structure. Since four channels of data could be recorded simultaneously, it was possible to record data at three measurement stations while using one seismometer to monitor the excitation structure. The amplitudes measured at each point in the free-field were normalized to the amplitude of the excitation structure floor at the same frequency. This procedure accounted for variations in the response of the excitation structure due to changes in excitation levels, frequencies, or other factors.

The typical procedure followed for each set of data records was;

1. The seismometers were deployed on the site and balanced.
2. The eccentricity of the vibration generator was adjusted to provide the required force level.
3. The vibration generator was brought up to the required speed.
4. The seismometer output was observed on both the chart recorder and on the input signal strength monitor of the tape recorder.
5. The signal conditioner gain was adjusted to provide the largest signal that could be accommodated by the tape recorder. If the signal amplitude was too large, the record would be distorted in amplitude and shape.

6. If high frequency noise interfered with the signal, the signal conditioner's low-pass filter was used. Noise was usually a problem only at the lower frequencies, where the excitation level was not high enough to overcome ambient ground noise.
7. Sixty to 90 seconds of data were recorded for each set.
8. All attenuation and filter settings, as well as the test frequency and shaker eccentricity, were recorded on the data form reproduced in Figure 3.6.
9. The speed of the vibration generator was then changed to the next test frequency, and steps 4 through 8 were repeated. During each frequency sweep, it was necessary to bring the vibration generator to a complete stop, and reset the eccentricity two or three times to keep the force output within usable levels.

The preliminary phase was also used to check the equipment and procedure. During these tests, several characteristics of the seismometer/signal conditioner system were discovered that could have significantly affected the accuracy of the final results if these characteristics had not been accounted for during the data reduction.

The four seismometers used in the experiment had the individual characteristics shown in Table 3.1. These values were provided by the manufacturer. During the tests, each seismometer was always connected to the same signal conditioner and recorder channels. In this way, the

DATA FORM 1

Date _____ Series _____ Sheet _____ of _____

Excitation Frequency _____

Eccentricity _____

<p>CHANNEL 1</p> <p>Attenuator A $\frac{1}{1}$ $\frac{1}{100}$</p> <p>Attenuator B _____ dB</p> <p>L.P. Filter _____ Hz</p>	<p>CHANNEL 2</p> <p>Attenuator A $\frac{1}{1}$ $\frac{1}{100}$</p> <p>Attenuator B _____ dB</p> <p>L.P. Filter _____ Hz</p>
<p>CHANNEL 3</p> <p>Attenuator A $\frac{1}{1}$ $\frac{1}{100}$</p> <p>Attenuator B _____ dB</p> <p>L.P. Filter _____ Hz</p>	<p>CHANNEL 4</p> <p>Attenuator A $\frac{1}{1}$ $\frac{1}{100}$</p> <p>Attenuator B _____ dB</p> <p>L.P. Filter _____ Hz.</p>

ACCELEROMETER

Accelerometer range _____ g

Carrier Pre-Amp _____ $\mu\text{in/in/div}$

Brush Recorder _____ volts/in.

Calibration info

_____ div = _____ g

H.P. RECORDER

Start Address _____

Finish Address _____

Figure 3.6. Form used to record field settings.

variation between channels of any of the components could be consistently accounted for in the data analysis.

TABLE 3.1. Characteristics of Ranger Seismometers used during experiment

Channel Assignment	Manufacturer's Serial Number	Natural Frequency In Hertz	Damping Resistance in Ohms for 0.7 of Critical
1	270	1.049	4300
2	271	0.982	4780
3	267	1.028	5090
4	274	1.000	5630

The Ranger seismometer is normally used to measure motions having frequencies of less than 10 Hertz. To minimize the frequency dependent variation of the seismometer, the resistance of the signal conditioner is normally set to provide 70% of the critical damping for each seismometer. Furthermore, in earthquake engineering experiments, these seismometers have normally been used to measure structural response; primarily to identify natural frequencies, and less frequently, to determine mode shapes. In these cases, the difference in the amplitude of motion between two recording stations was usually less than a factor of five or ten. Also, hard copy records were usually obtained in the field for determination of displacement amplitudes, and magnetic tape records were used for laboratory analysis in the frequency domain.

In this experiment, however, the conditions were different. The maximum test frequency was 70 Hertz. The amplitude ratio between two records could be 40 or more. Data would be recorded almost entirely on

magnetic tape which would then be used for both magnitude and frequency determination. These conditions required a more thorough characterization of the entire data acquisition system.

The inboard 54 dB step attenuator of the signal conditioner was described in paragraph 3.1.2.2. Because dB units cannot be used directly in the calculations, it is necessary to express attenuation in terms of voltage ratios. The following relation was used,

$$\frac{V_1}{V_2} = 10^{a/20} \quad . \quad (3.1)$$

where a is the attenuation, in dB, between V_1 and V_2 . Therefore, a 6 dB attenuation corresponds to a input/output voltage ratio of 1.9953.

Laboratory measurements of the output voltages at various gain settings, however, showed that the actual attenuation for each 6 dB step was not exactly 1.9953. The manufacturer may have used ready-made resistors with impedances close to, but not exactly, the values required to produce exact 6 dB attenuations. The attenuation values were also found to depend on the potentiometer resistance. Therefore, a damping resistance of 5000 ohms was used for all channels. In this way, all channels would have the same gain for each setting. The results of the lab tests on the signal conditioner resulted in the actual attenuation represented by each gain setting. Both the cumulative attenuation, and the incremental attenuation are listed in Table 3.2. The effect of the outboard attenuators is also listed in the table.

TABLE 3.2. Cumulative and incremental attenuations for signal conditioner dial settings, with and without outboard attenuator.

Dial Setting in dB	Without Outboard Attenuator		With Outboard Attenuator	
	Cumulative Attenuation	Incremental Attenuation	Cumulative Attenuation	Incremental Attenuation
0	1		83.48	
6	1.964	1.964	163.8	1.962
12	3.856	1.964	329.4	2.011
18	7.571	1.964	660.9	2.006
24	19.87	1.964	1334	2.018
30	28.50	1.916	2715	2.035
36	54.50	1.912	5362	1.975
42	108.4	1.989	10220	1.906
48	217.4	2.006	20440	2.000
54	433.6	1.994	39860	1.950

The selection of a damping resistance other than 70% of critical damping for each seismometer increased the frequency dependence of the amplification factor. These differences, however, were included in the dynamic calibration. The Rangers were calibrated by measuring their response to the vibration of the excitation structure, at discrete frequency intervals. Because the concrete excitation structure responds to the vibration generator essentially as a rigid body, there would be very little difference in the motion input to the four seismometers. Any difference in output could then be attributed to variations between the instruments. The response of each seismometer was normalized to the

response of the Channel 1 Ranger. A least squares fit of the normalized amplitudes was used to determine a second order calibration function that could be evaluated at any frequency in the test range. The results of the dynamic calibration, as well as the fitted function, are shown in Figure 3.7. The dynamic calibration functions for each seismometer are given by:

$$C_1 = 1.0 \quad (3.2)$$

$$C_2 = 0.875 + .00483f - .0000279f^2 \quad (3.3)$$

$$C_3 = 0.996 + .00180f + .0000093f^2 \quad (3.4)$$

$$C_4 = 0.894 + .00473f - .0000311f^2 \quad (3.5)$$

During the free-field motion determination, it was found that the reproducibility and stability of the results were sometimes poor. The recorded amplitude of motion during one trial, or between different trials could change substantially, especially at higher frequencies. Plywood boards, measuring 8 in (0.20 m) square, had been used to keep the seismometers from settling into the loose surface soil and becoming unbalanced. This support system would occasionally resonate. The next attempt used partially buried concrete masonry units, but because the soil had many cobbles and rocks, it was difficult to install these blocks so that they were level and stable. Finally, concrete pads, measuring approximately 12 in (0.3 m) square, and 2 in (0.05 m) thick were poured directly against the soil. These concrete pads were stable

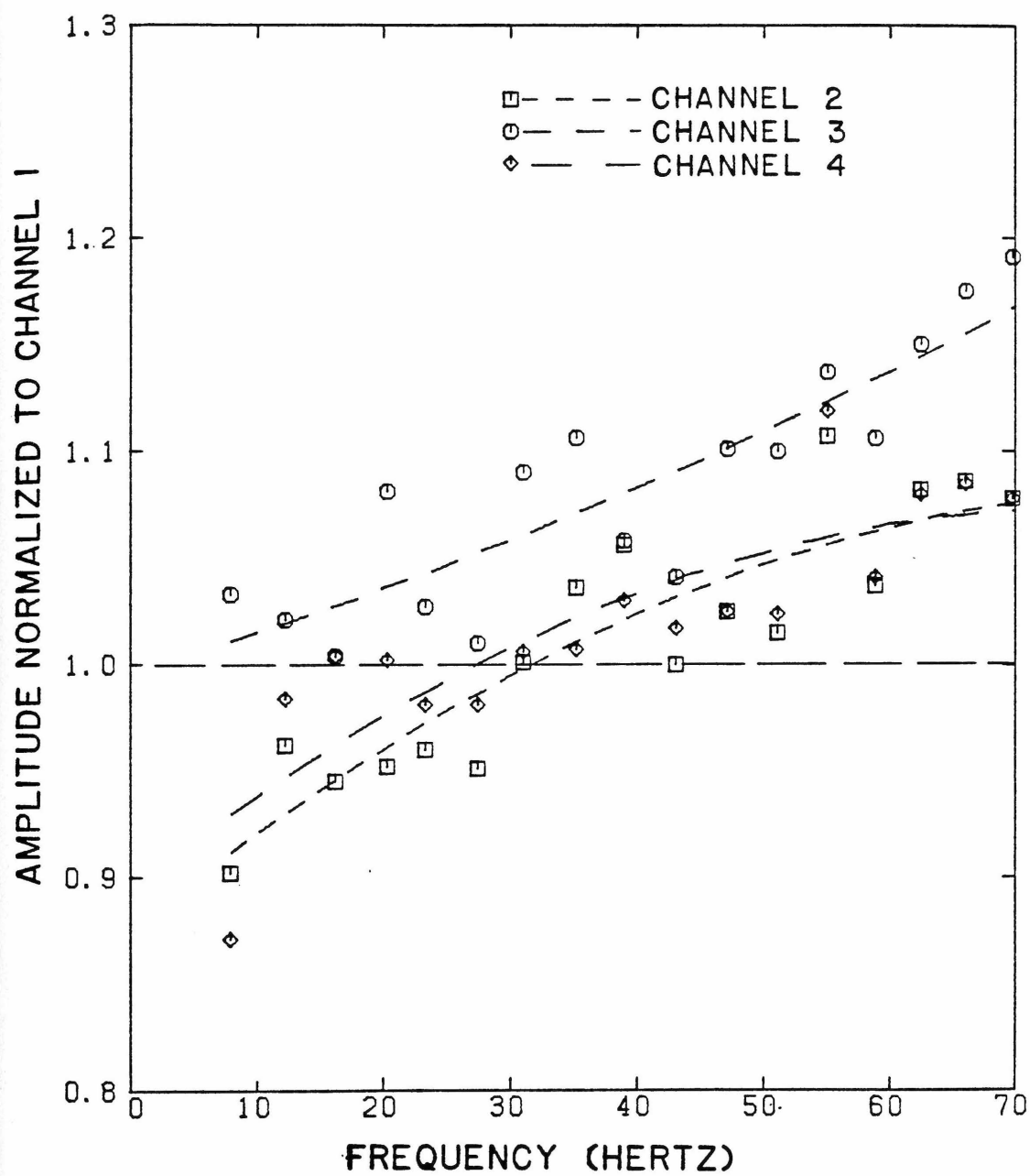


Figure 3.7. Results of dynamic calibration. Seismometer Channels 2, 3, and 4 have been normalized to Channel 1.

and bonded to the soil. Furthermore, the density of the pads was close to the density of the soil, and no resonances developed.

The field testing required the exposure of sensitive laboratory equipment to the adverse field conditions of heat, wind, and dust. Even though most tests were conducted during the morning and evening hours, the air temperature could still reach the mid 90's F (35° C). Under these conditions, the data recording system could overheat and not function properly.

Therefore, the equipment was elevated from the ground surface to permit the free circulation of air and shaded from direct sunlight. During extremely hot weather, the equipment was periodically turned off and allowed to cool. Dust also caused problems. All cable connectors, button contacts, tape recorder heads, etc., were frequently blown clean with dry fluorocarbon gas.

The importance of properly maintained equipment cannot be overemphasized. Since approximately 30 to 45 minutes were required to set up the equipment each day, much time could be lost if any element of the system failed to operate. Such failures occurred with surprising frequency. Fortunately, spare recorders, signal conditioners, and other pieces of equipment were available for substitution.

3.2.1.2. Major phase: response of the specimen structure.

This subsection describes the procedure used to measure the response of the specimen structure and the mode shape and ground motion

induced by the response of the structure in the fundamental mode. The measurements were repeated for each embedment case.

3.2.1.2.a. Ambient vibration. Ambient vibration testing is a simple and fast way to obtain estimates of resonant frequencies, and under favorable conditions, mode shapes. The method is attractive because it does not require the installation of structural vibration equipment, and depends solely on excitation due to ground noise, wind, and in the case of occupied structures, even the occupants. The following procedure was used for these tests:

1. The seismometers were deployed and balanced. Since normalization was not necessary, four channels of data could be obtained simultaneously. Ambient vibration measurements were taken at the locations shown in Figure 3.8.
2. The signal strength was monitored on the magnetic tape recorder while the signal conditioner gain was adjusted to prevent saturation of the tape or amplifiers.
3. The data were recorded for 10 minutes.

3.2.1.2.b. Ring-down test. The ring-down test is another simple method of determining the lowest natural frequency and corresponding damping for smaller structures. In this test, the seismometers were deployed on the superstructure, and the structure was struck sharply with a piece of lumber to provide an impulsive

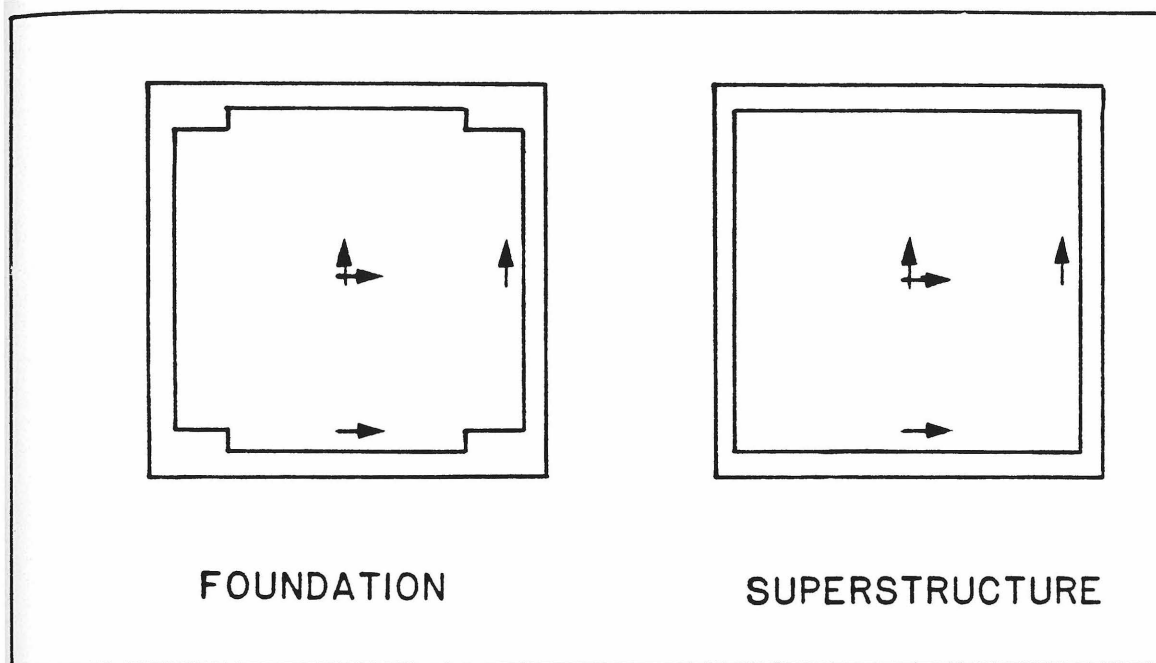


Figure 3.8. Ranger locations for ambient vibration tests. Arrow indicates seismometer orientation and location.

load. The following equation was used to determine damping from the free-vibration record

$$\zeta = \frac{1}{2\pi n} \ln \frac{X_0}{X_n} \quad (3.6)$$

where X_n is the amplitude n cycles after X_0 .

3.2.1.2.c. Forced vibration test. Forced vibration tests are often the preferred method to evaluate structural response in detail. The advantage of forced vibration tests, in comparison to ambient and ring-down tests, is that the input motion can be well-defined and controlled. Furthermore, higher excitation levels are possible with the larger structural vibrators. The principal

disadvantage of forced vibration is the effort required to obtain and install the shakers on prototype structures.

The basic procedure employed in the forced vibration test was very similar to that used during the free-field motion studies, except that records were taken primarily on the specimen structure, and at many more frequencies. In this way, accurate estimates of resonant frequencies, mode shapes, and dampings could be obtained. Initially, only three channels of data were taken simultaneously, with one channel placed on the excitation structure floor to provide data for normalization. In later tests, as confidence in the reproducibility of the test results increased, all four channels were used to collect data simultaneously. Figure 3.9 shows the seismometer locations that were used to measure the translational and torsional responses. In addition to these displacements, rocking and vertical response were also measured. These measurements were obtained at the seismometer locations shown in Figure 3.10.

From the standpoint of earthquake behavior, the response of prototype structures in the fundamental mode (consisting of foundation translation, interfloor displacement, and rigid body rocking) is the most significant. Therefore, careful attention was paid to determining the mode shape of the specimen structure at the fundamental resonance. The motion induced in the ground by the resonance of the structure was also measured. The mode shape at resonance was determined by making measurements at the locations shown

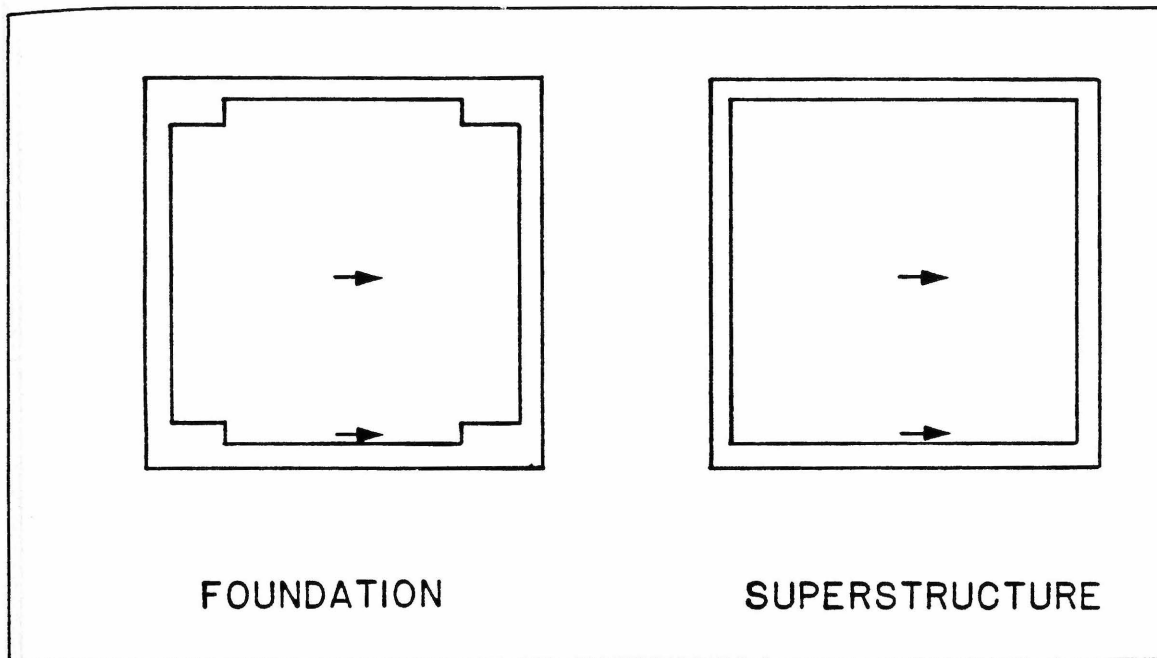


Figure 3.9. Ranger locations for forced vibration tests for translatory and torsional responses.

in Figure 3.11. Other seismometer locations were used for occasional specialized tests. These locations will be identified in subsequent discussion.

3.2.2. Data reduction.

The recorded data were analyzed in the Vibrations Laboratory on the Caltech campus. The procedures used to analyze data obtained from the free-field motion studies, as well as the ambient and forced vibration tests of the specimen structure, are discussed in the following paragraphs.

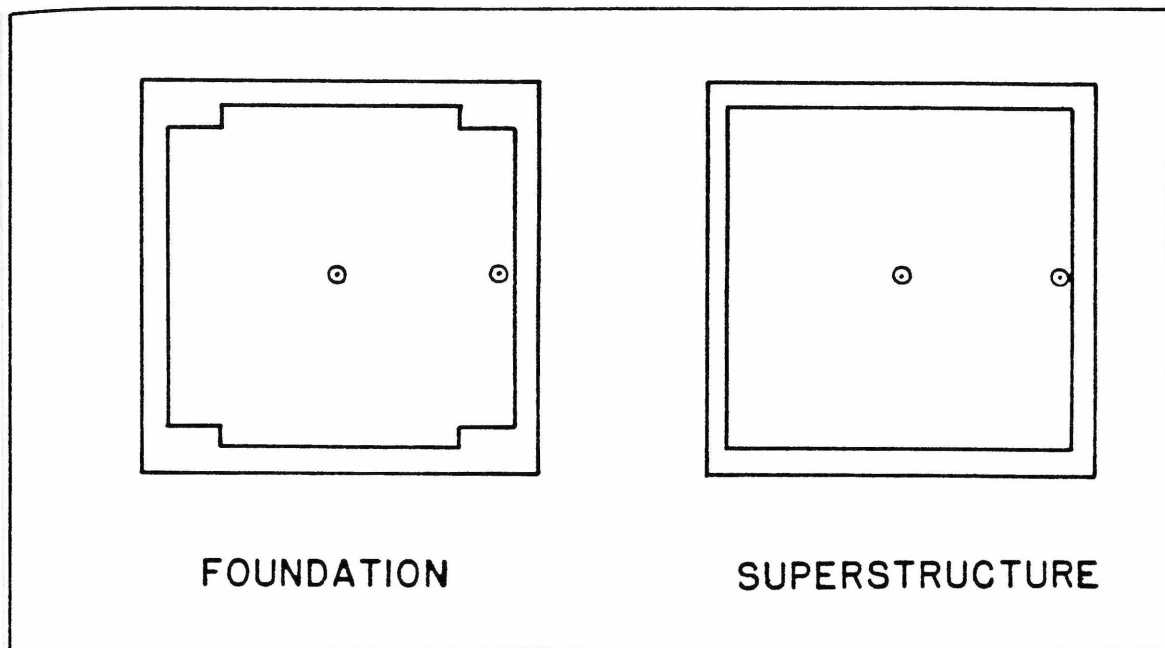


Figure 3.10. Ranger locations for forced vibration tests for vertical and rocking responses.

3.2.2.1. Ambient vibration.

Fourier amplitude spectra and transfer functions were calculated from ambient vibration tests by use of the digital signal processor. The Fourier amplitude spectra provided information for identification of resonant frequencies, while transfer functions were used to obtain relative phase, from which mode shapes could be determined. The procedures used in such analyses were in accordance with the instructions provided by the equipment manufacturer. Amplitude spectra were usually obtained in the frequency range of zero to 40 Hertz.

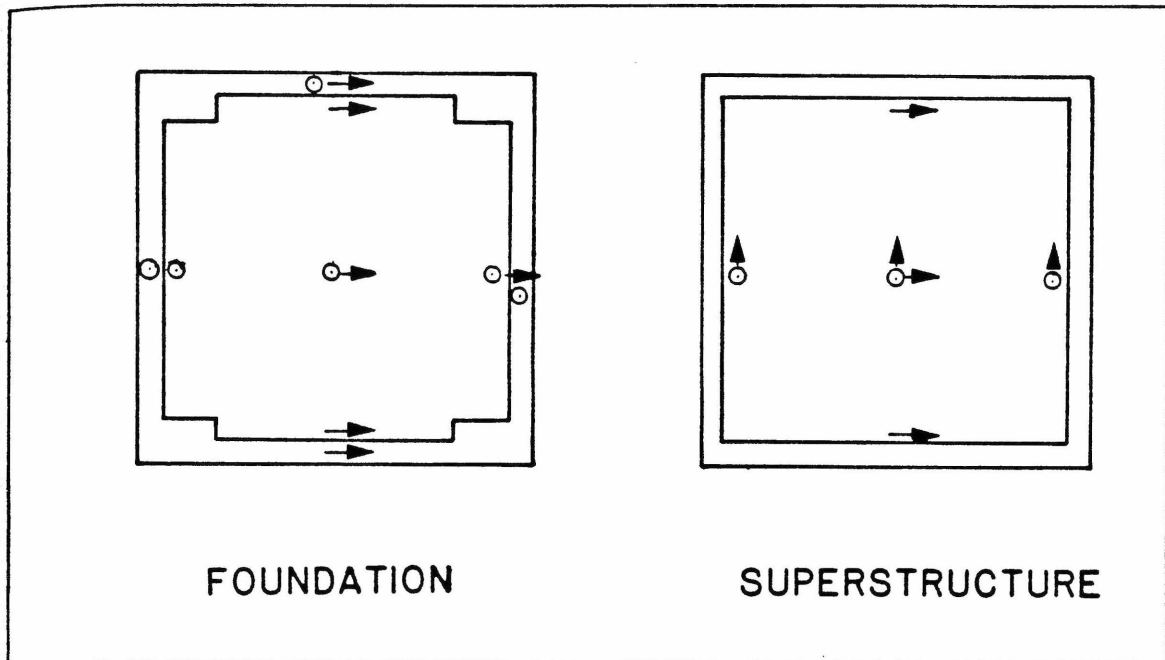


Figure 3.11. Ranger locations for fundamental mode shape measurement.

3.2.2.2. Forced Vibration.

Forced vibration tests comprised the bulk of the experimental program. Resonant frequency, mode shapes, and modal dampings were determined from these tests. It was necessary to devise a consistent and accurate method of reducing the raw data to a form that had significance. Several factors had to be considered:

1. While the signal-to-noise ratio was usually high, noise would sometimes be a problem, particularly at low frequencies where the excitation levels would not be much greater than the

ambient motions. The data analysis would have to permit the consistent separation and reduction of noise in the data.

2. Although the forced vibration tests were steady-state, some variation in response amplitude had to be expected, especially near the resonant frequencies where, because of the low damping of the system, small changes in frequency would cause large changes in the response. Furthermore, when the excitation frequency was near same resonant frequency, superposition of the free and forced vibration responses could give rise to some beating phenomenon. Enough data points would have to be examined to account for these variations.
3. The data reduction procedure had to be as streamlined and efficient as possible because many data points would be obtained.

The reduction of the forced vibration data required the determination of the frequency and amplitude of the response at a given location.

3.2.2.2.a. Determination of frequency. Unlike the newer controllers manufactured by Kinometrics for the Caltech-designed VG-1 shakers, the amplidyne controllers do not display frequency, but instead display the voltage input to the shaker motors. Although the voltage could be used to obtain an estimate of the frequency, it was still necessary to determine the exact frequency of excitation (and response) by use of the digital signal processor.

The excitation frequency was found by calculating the Fourier amplitude spectra of the forced vibration record. Where possible, the record from the excitation structure was used. When all four seismometers were placed on the specimen structure, the spectrum was computed from the record with the largest amplitude.

3.2.2.2.b. Determination of amplitude. Figure 3.12 shows, schematically, the apparatus set-up used to determine the signal amplitude. The band-pass filter was used to remove noise from the signal. The high-pass filter was set two octaves below the excitation frequency, and the low-pass filter was set two octaves above the excitation frequency. The attenuation was 24 dB per octave. The filtering window is shown in Figure 3.13.

The digital signal processor was used in the input display mode with the same attenuation settings for both channels. The outputs of the two channels were superimposed on the video screen and the output of the signal generator varied until the amplitudes of the two outputs were the same. The amplitude of the signal generator output, measured by the true RMS meter, corresponded to the signal strength. The two signals were matched over seven to eight seconds of data.

At frequencies of approximately 10 Hertz or less, the force output was too small to excite the forced vibration of the structure, particularly for the foundation. The response consisted

FOUR CHANNEL MAGNETIC TAPE RECORDER

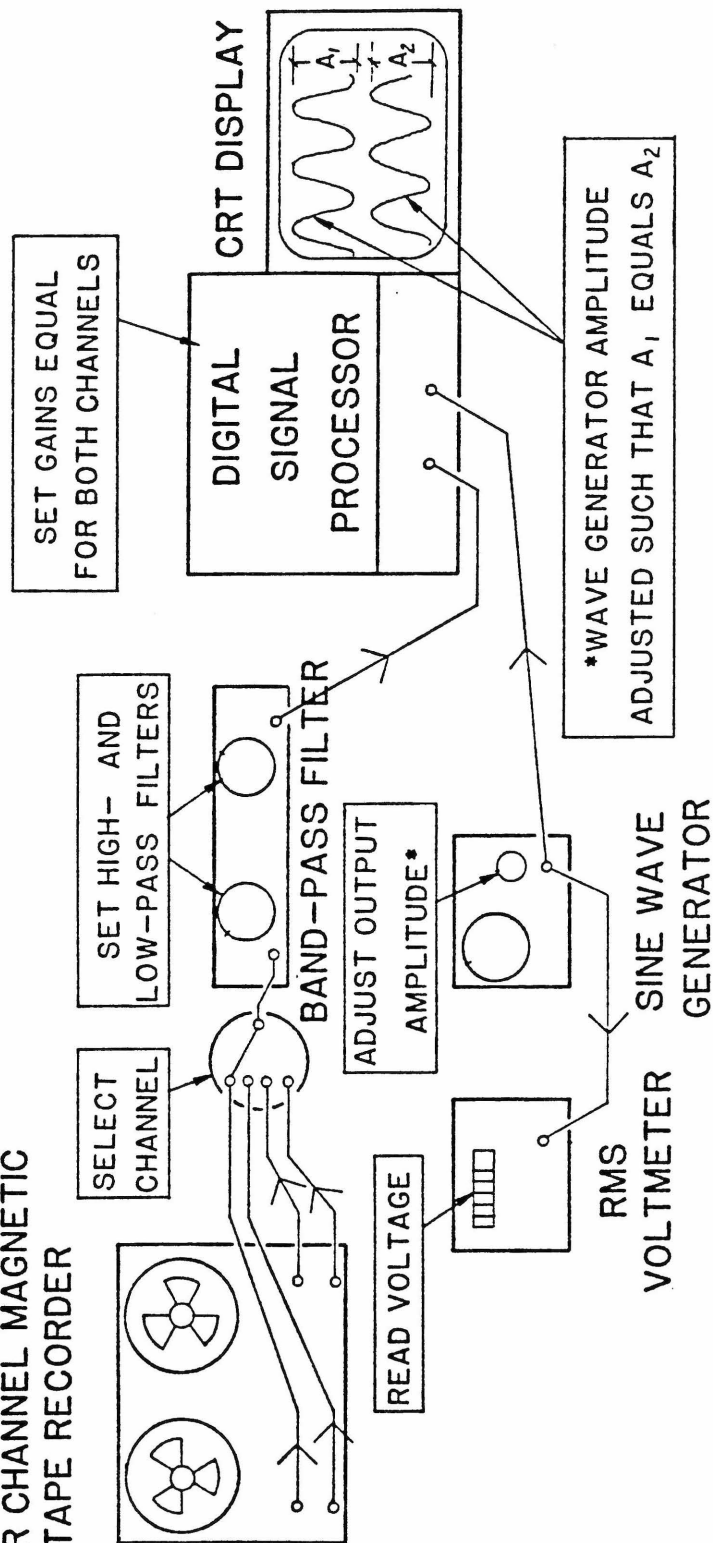


Figure 3.12. Schematic diagram for apparatus set-up used to determine signal amplitude from magnetic tape records.

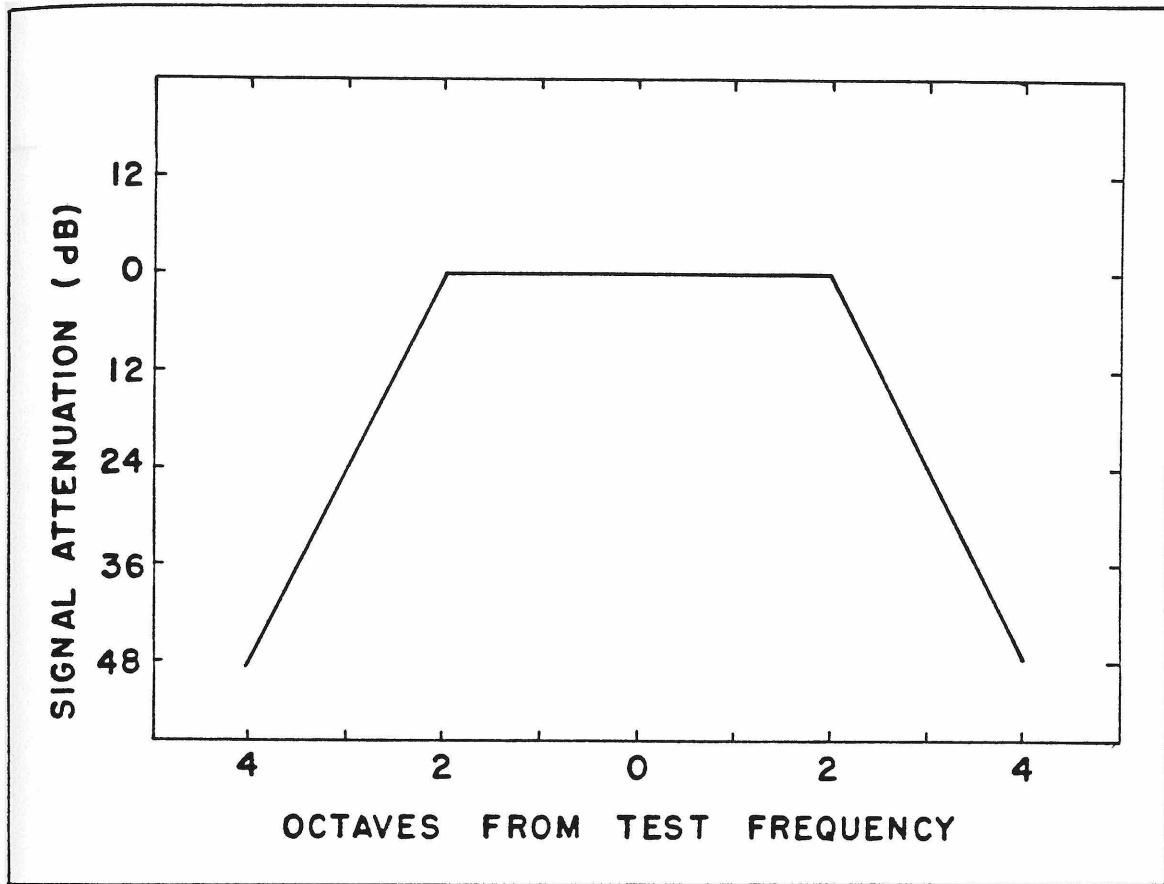


Figure 3.13. Band-pass filtering window for data reduction.

of a combination of the forced and free vibration. In this case, the amplitude could not be determined.

3.2.2.2.c. Determination of phase. The relative phase between the response of two locations was sometimes needed to determine the mode shape. The two channels of data were filtered and then recorded on the chart recorder. The relative position of the two records could then be used for phase determination. Greater accuracy was obtained if zero crossing points, as opposed

to maximum points, were used. A sample record is shown in Figure 3.14 to illustrate this method.

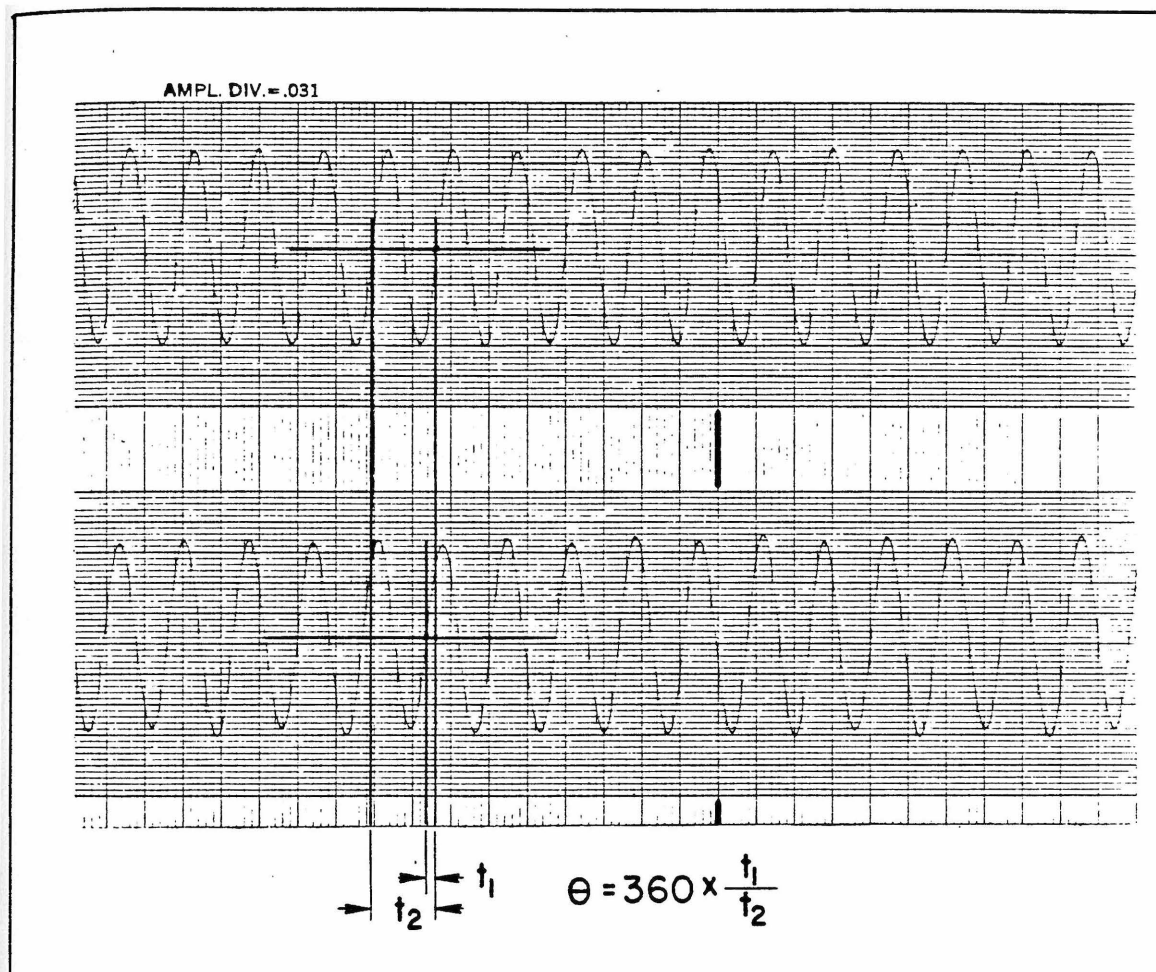


Figure 3.14. Phase angle calculation, sample record

3.2.3. Data Analysis.

The results of the data reduction did not directly provide the amplitude of response to forced vibration. Different attenuator settings, shaker eccentricities, excitation frequencies, and the frequency

dependence of the response of the seismometers had to be compensated for before the data could be interpreted. Therefore, a PRIME 500 computer was used to make all necessary corrections to obtain the amplitudes of response.

3.2.3.1. Free-field motion data.

The inputs to the program were:

1. Excitation frequency, FREQ.
2. Signal conditioner gain setting, IATTA. A simple code was devised to input this parameter. The attenuation of the inboard attenuator was entered in the dB setting from the dial. If the outboard attenuator was present, the two digit dB attenuation would be prefaced with a "1". Hence, if the dial setting was 24 dB, then IATTA=24, if the outboard attenuator was also used, then IATTA=124.
3. Voltage amplitude from voltmeter, RMS.

From these inputs, the program would determine the following values:

1. Frequency dependent dynamic calibration factor for each seismometer, CALIB(I) [from Equations (3.2), (3.3), (3.4), and (3.5)].

2. Amplifier gain, ATTA, corresponding to IATTA. Since the gain is not a simple function of the dial settings, the program locates the gain from the tabulated values of Table 3.2.

3. Corrected velocity proportional amplitude, CORAMP, defined by,

$$\text{CORAMP}(I) = \text{RMS} * \text{CALIB}(I) * \text{ATTA}.$$

4. Amplitude of each channel normalized to the amplitude of the first channel, NORAMP, where,

$$\text{NORAMP} = \text{CORAMP}(I) / \text{CORAMP}(1), I \neq 1.$$

The program then printed out all of the input values as well as the results, CORAMP and NORAMP.

3.2.3.2. Structural response data.

The analysis of the structural response data was more involved. The excitation force and the ground motion at the specimen structure had to be included so that displacement ratios could be obtained. All displacements could then be compared independently of the excitation force level.

The input, in addition to that required in the preceding calculation, now also included the shaker eccentricity, ECC. The following quantities were calculated by the program,

1. CALIB(I),
2. ATTA,
3. CORAMP,
4. NORAMP,

5. Excitation force, FORCE, developed by the shaker as a function of frequency and eccentricity, or

$$\text{FORCE} = 4.845 * \text{ECC} * \text{FREQ} ** 2.$$

6. Ground motion at the specimen structure, GROUND, a function of the excitation frequency.

7. The final corrected displacement amplitude, DISAMP, given by,

$$\text{DISAMP} = \text{CORAMP} / (\text{FORCE} * \text{GROUND} * \text{FREQ} * 2 * \text{PI}).$$

The printout of the program included all of the input parameters, as well as CORAMP, NORAMP and DISAMP. In an alternate form of the program, the output consisted only of FREQ and DISAMP to facilitate plotting of response curves. The data reduction program, as well as sample input and outputs are listed in the Appendix.

3.2.4. Errors Analysis for Forced Vibration Tests.

The procedure described above for the collection, reduction, and analysis of forced vibration data was carefully developed to minimize the systematic errors in the final result. The results of the forced vibration tests take several forms, and hence, are each susceptible to different types of inaccuracies. These various forms and corresponding errors, are:

1. Response curves show the variation, in amplitude, of a certain response, such as the translation of the foundation, with frequency. These curves permit identification of resonant

frequencies and the comparison of the amplitudes of response of various modes.

The test frequency range of 7 to 70 Hertz is much larger than normally encountered in earthquake engineering research experiments. Hence, non-linear or frequency-dependent variations of the equipment, particularly the motion transducers, must be determined. Higher resonant frequencies, for example, might not be identified from records taken with an instrument whose sensitivity decreases substantially with frequency.

2. Mode shape measurements require the simultaneous comparison of several response amplitudes at a given frequency. Because the structure is expected to have low damping, the determination of modal displacement ratios requires the normalization of the displacements at various locations to a single simultaneously obtained record, for example, of the superstructure. In this way, changes in the overall response amplitude due to small frequency shifts can be corrected for.

These measurements require consistency, or at least, quantifiable variations between the transducers. That is, if the amplitude measured at two locations by different transducers varies by a factor of two, for example, it must be known how much of the variation is due to the equipment, and how much of the variation is actually present in the response. The dependence of these relative variations on frequency must also be known.

3. Response amplitudes, especially near resonant frequencies, must be accurately obtained to permit the calculation of damping. Again, because damping is small, the resonant amplitudes will be significantly higher than non-resonant amplitudes. The system must be linear over a large range of amplitudes to permit accurate comparison.

Systematic errors can be reduced by careful procedures and accurate equipment. In a large test program such as this, random errors must also be examined. Most random errors, unfortunately, are human in origin, and are therefore difficult to eliminate. The effect of random error can often be determined by examining the reproducibility of the results. That is, within the noise of the system, do the measurements of a given response from two different test series agree. To provide information of this important aspect, certain key measurements, such as the peak response amplitude, were repeated and checked for repeatability.

The entire process of data collection, from the acquisition in the field to the final data analysis by computer, can be discussed as a sequence of events. Each event has a different probability and type of error. The significant events, from an errors analysis standpoint, are:

1. The Ranger seismometers, individually, are accurate transducers for converting input base motion to output electrical signals. The transducers have been designed to respond to a wide range of amplitudes and frequencies. Since the test frequencies will

always be significantly larger than the nominal natural frequency of the seismometer, the output of the transducer will always be proportional to the velocity.

The comparative outputs of the seismometers was determined during the dynamic calibration. In this way, the frequency dependent variation between individual seismometers was accounted for. The maximum variation between the individual data points and the fitted curves, as shown in Figure 3.7, is about 5%. This difference is not significant in comparison with the range of displacement amplitudes. That is, the maximum error is small enough that it will not be confused with a real phenomenon.

2. The accuracy of the signal conditioner is another important factor. Because there was a large range in response amplitude, it was necessary to use the variable gain of the signal conditioner to put the data in a recordable form. The bench tests of the signal conditioner, the results of which were shown in Table 3.2, permitted the accurate quantification of each dial setting. These results were used in the data analysis.
3. The magnetic tape recorder played an important role in the data collection system. Bench tests on the recorder showed that the output of the recorder accurately reproduced the input. The design accuracy of the recorder far exceeded the requirements of the experiment.

4. Since the frequencies of excitation response had to be calculated from the data, the accuracy of the digital signal processor was important. Unfortunately, there was no independent way of verifying the accuracy of the processor, and hence, the manufacturer's design values had to be accepted.

Because only a finite number (1024) frequency ordinate points are available for display, the lack of resolution was a possible error. The resolution can be maximized by selecting an analysis frequency as close to the test frequency as possible. At 20 Hertz, for example, the resolution of the display is 0.02 Hertz, while at 70 Hertz, the resolution is 0.07 Hertz. In comparison to the natural fluctuation of the specimen structure, however, these variations can be seen to have minor importance.

5. The determination of the RMS amplitude possible has the largest possibility for error. As shown in Figure 3.12, this step required the adjustment of the function generator output amplitude until it was the same as the amplitude of the magnetic tape record, as displayed on the video screen of the signal processor. For records containing very little noise, this matching was very easy. Records containing significant amounts of noise, such as the vertical response measurements, however, required considerable judgement to determine when the amplitudes did indeed match. Fortunately, this situation did not

arise very often, and was of minor consequence when it did occur.

In general, the accuracy of the results to be presented in the next chapter is satisfactory. Even if other test procedures are devised and applied to this experiment, the general qualitative aspects of the results should remain, although some specific details may vary. There are some results that contain considerable noise or uncertainty; these cases will be pointed out as they arise.

CHAPTER REFERENCES

Carrier Preamplifier Model-13-4212-02 Operating Instructions, Gould Incorporated, Brush Instruments Division, Cleveland, OH, 1969.

Hudson, D.E., A New Vibration Exciter for Dynamic Tests of Full Scale Structures, Caltech, 1961.

Hudson, D.E., Synchronous Vibration Generators for Dynamic Tests of Full Scale Structures, Caltech, 1962

Operating Instructions for Model SS-1 Ranger Seismometer, Kinometrics, Incorporated, Pasadena, CA, 1970.

Operating Instructions for Model SC-1 Signal Conditioner, Kinometrics, Incorporated, Pasadena, CA, 1974.

General Information for SD360-13 Digital Signal Processor, Spectral Dynamics Corporation, San Diego, CA, 1977.

CHAPTER FOUR

THE EXPERIMENTAL RESULTS

This chapter presents the results of the experimental program. The first section describes the free-field motion determination which was completed prior to the construction of the specimen structure. The results of the ambient vibration, ring-down, and forced vibration tests of the specimen structure are reported on in Section 4.2. These tests were conducted for each embedment case. In the third section, analyses of the experimental results are conducted to obtain accurate determinations of the resonant frequencies and modal dampings, as well as estimates of the structural and foundation impedances. Each section also contains a discussion of the results presented therein. The fourth section discusses the relative agreement of the vibrational characteristics determined by the ambient, ring-down, and forced vibration tests of the structure. The results are summarized in the last section.

4.1. FREE-FIELD MOTION DETERMINATION.

The ground motion amplitude caused by the vibration of the excitation structure was measured at the stations shown in Figure 4.1 along the north-south centerline of the site. These measurements were completed prior to the construction of the specimen structure. The results of these measurements are shown in Figures 4.2 to 4.10. The free-field displacements in each plot have been normalized to the displacement of the excitation structure measured at station 0+00.

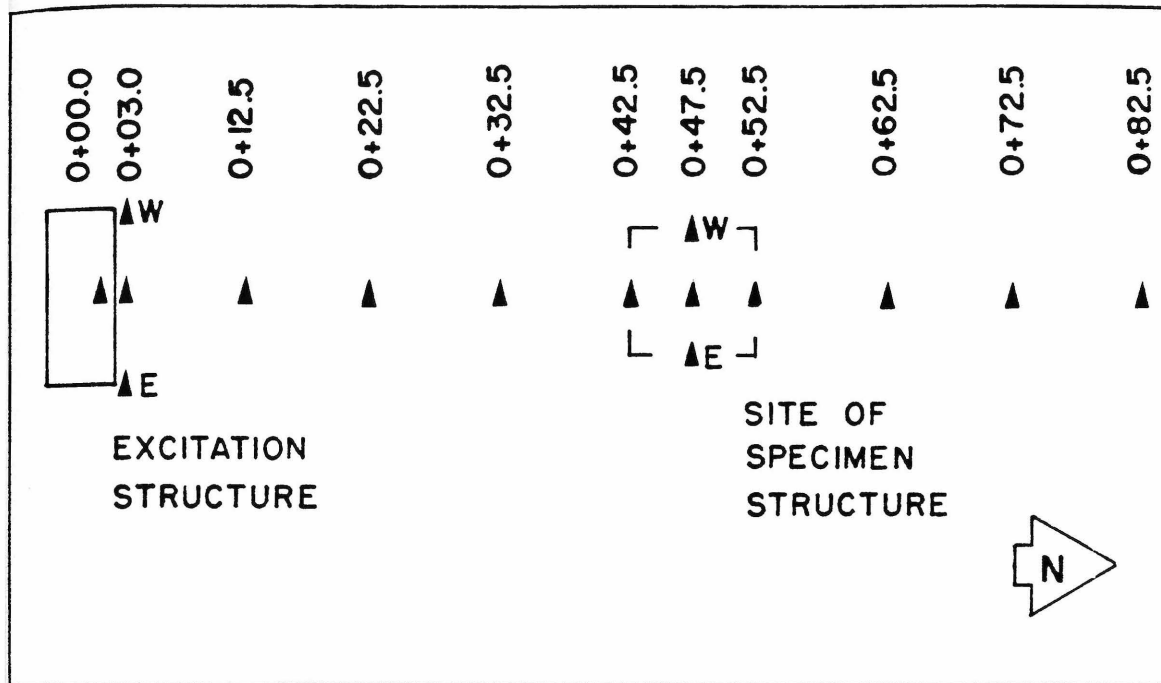


Figure 4.1. Free-field motion measurement stations.

Several interesting aspects of these results are described here:

1. The reproducibility of the data at higher frequencies (i.e. above 50 Hertz) is poor. For clarity, not all of the measured points have been plotted.
2. The attenuation of ground motion does not appear to be a smooth function of distance and excitation frequency. This may be due to scatter in the experimental data.
3. The amplitude of ground motion immediately outside of the excitation structure can be larger than the displacement of the excitation structure. This ground motion, normalized to the excitation structure displacement, increases from a factor of

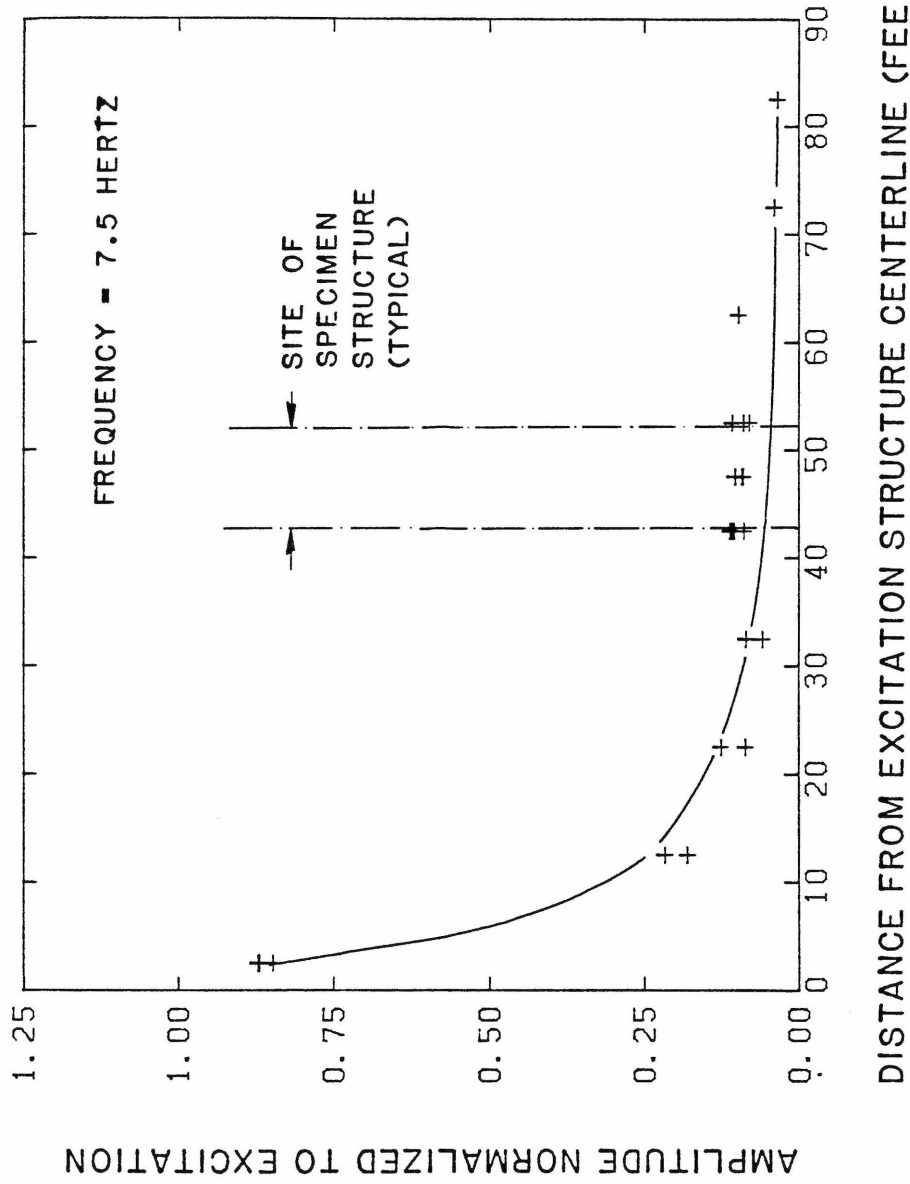


Figure 4.2. Free-field ground motion at 7.5 Hertz. Location of specimen structure site typical for Figures 4.2 to 4.10. Ground motion amplitudes have been normalized to excitation structure displacement at station 0+00.

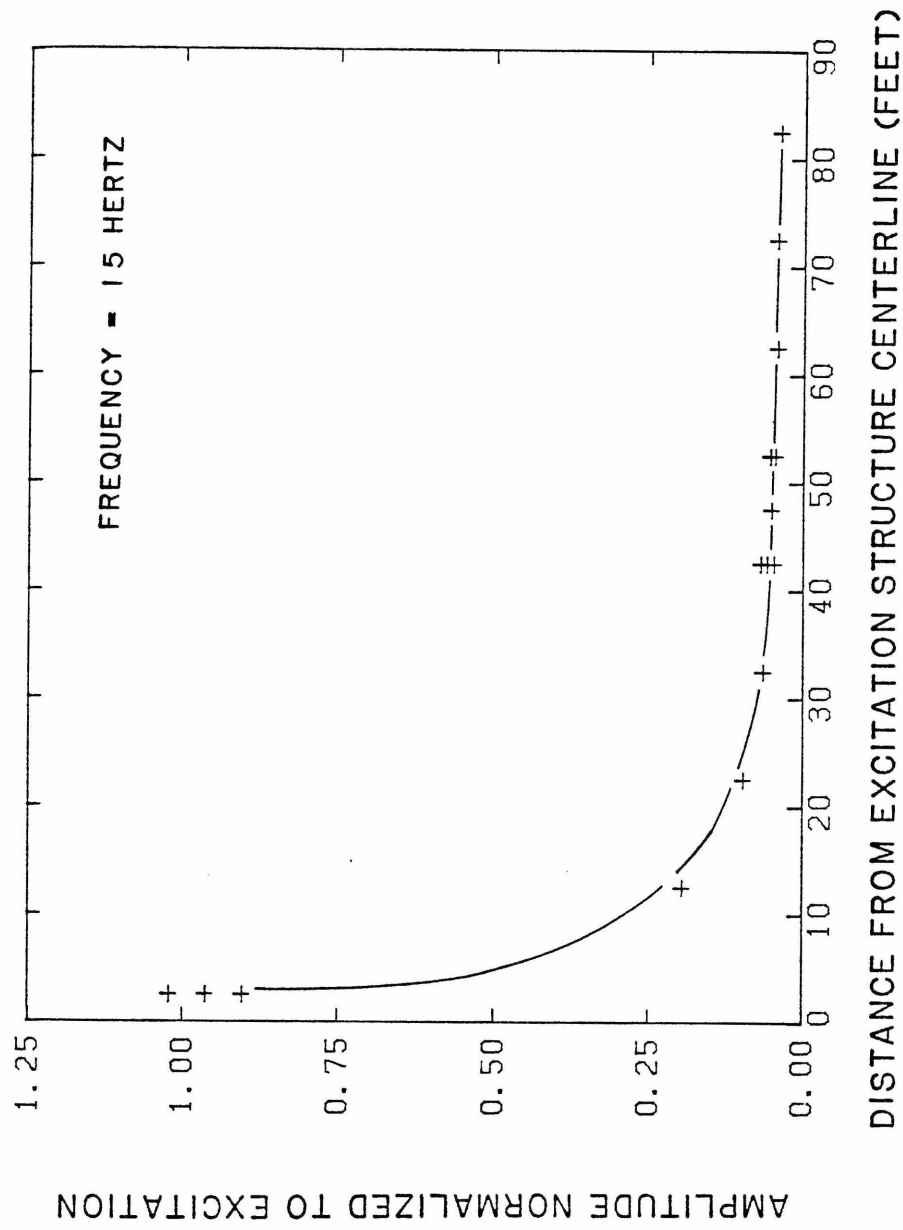


Figure 4.3. Free-field ground motion at 15 Hertz.

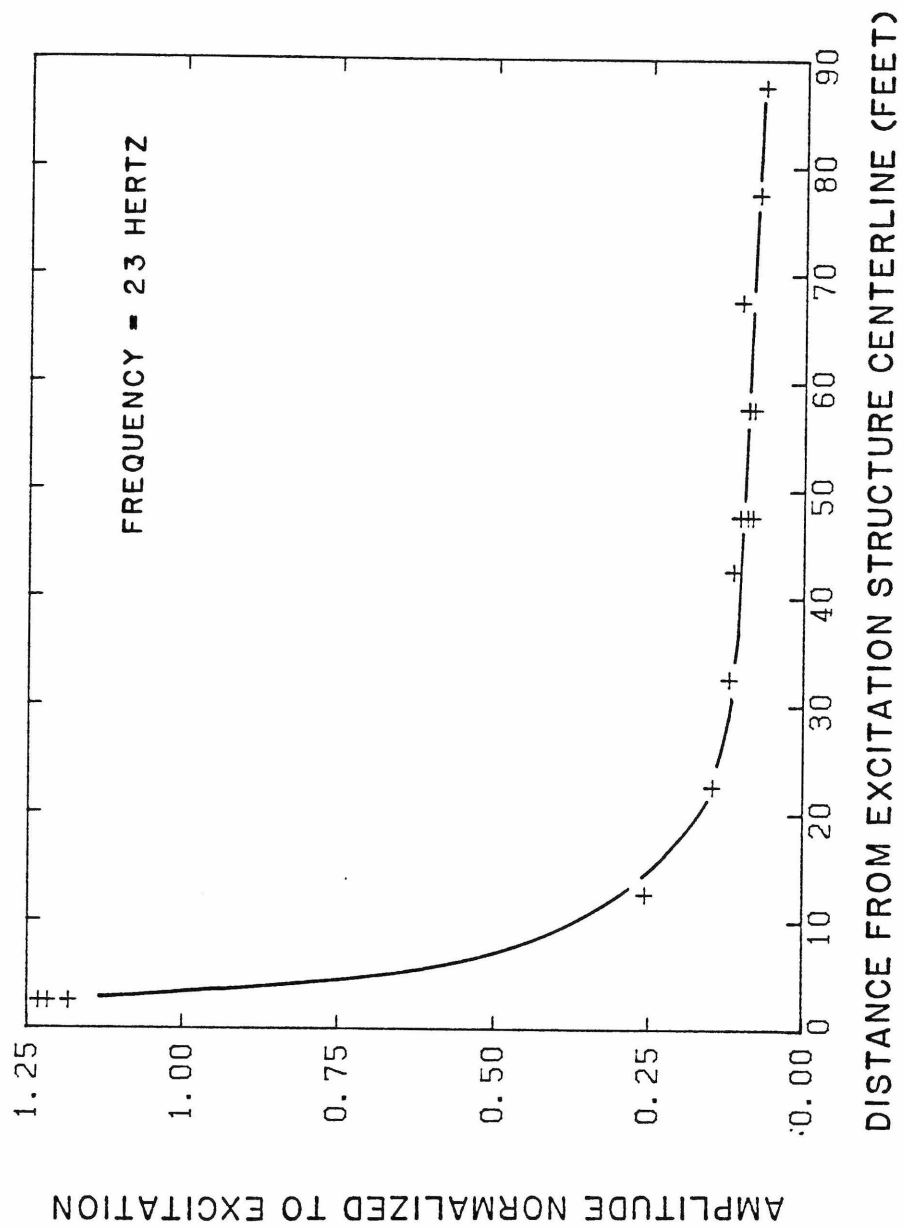


Figure 4.4. Free-field ground motion at 23 Hertz.

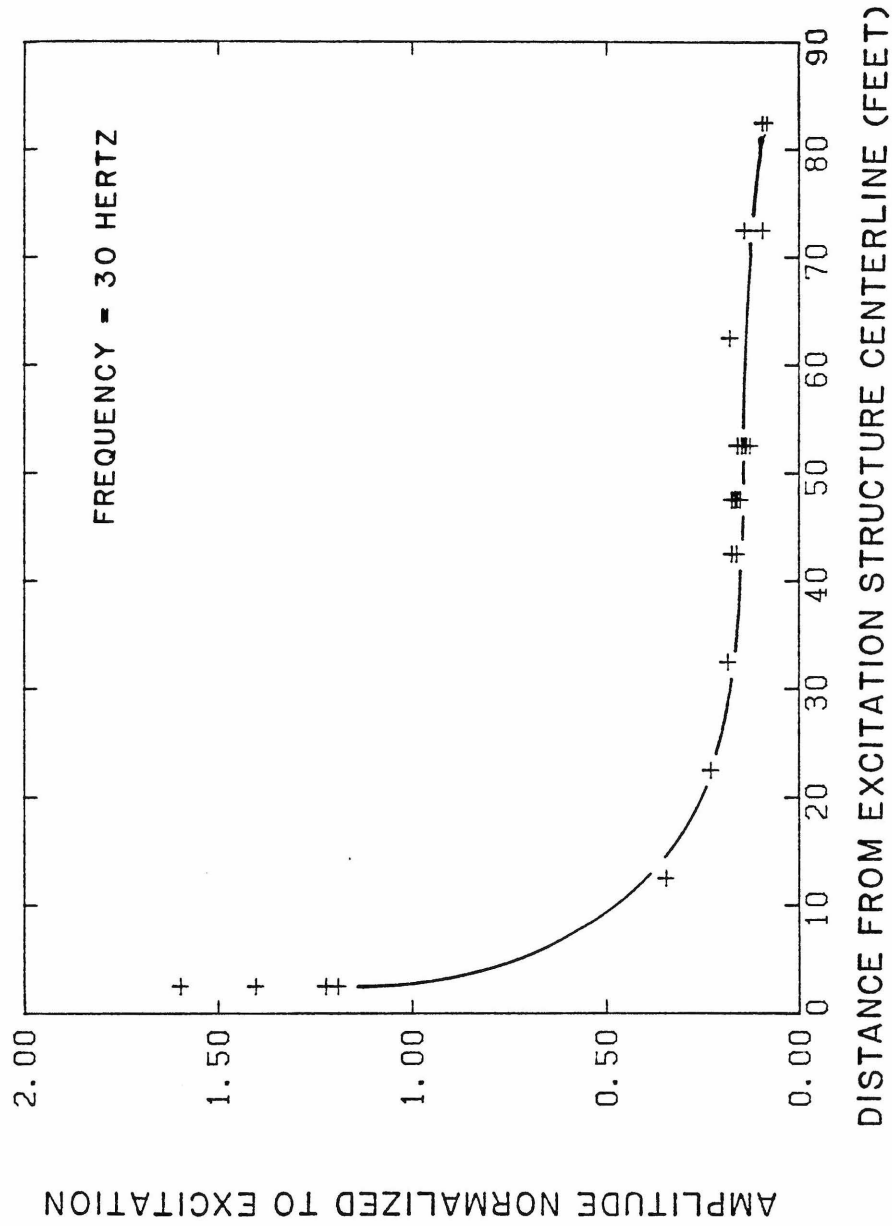


Figure 4.5. Free-field ground motion at 30 Hertz.

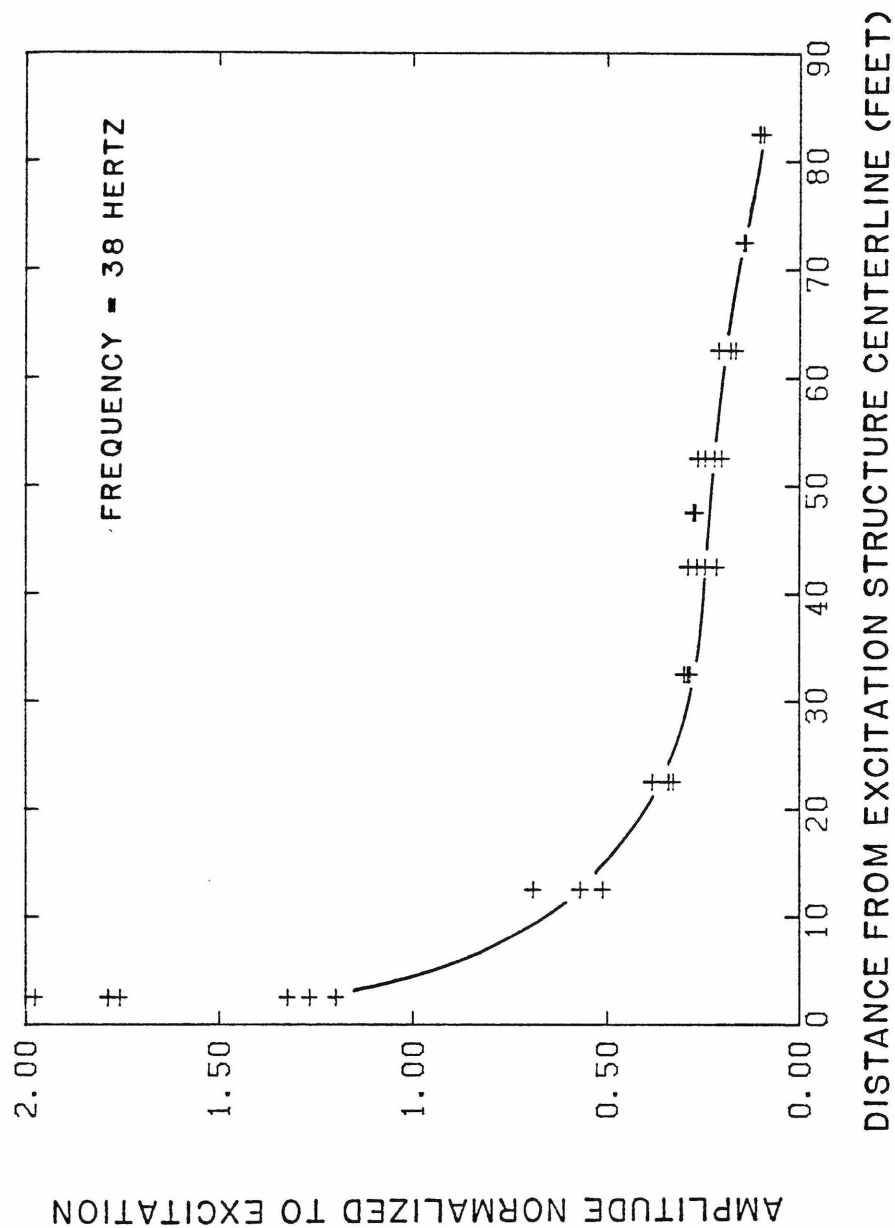


Figure 4.6. Free-field ground motion at 38 Hertz.

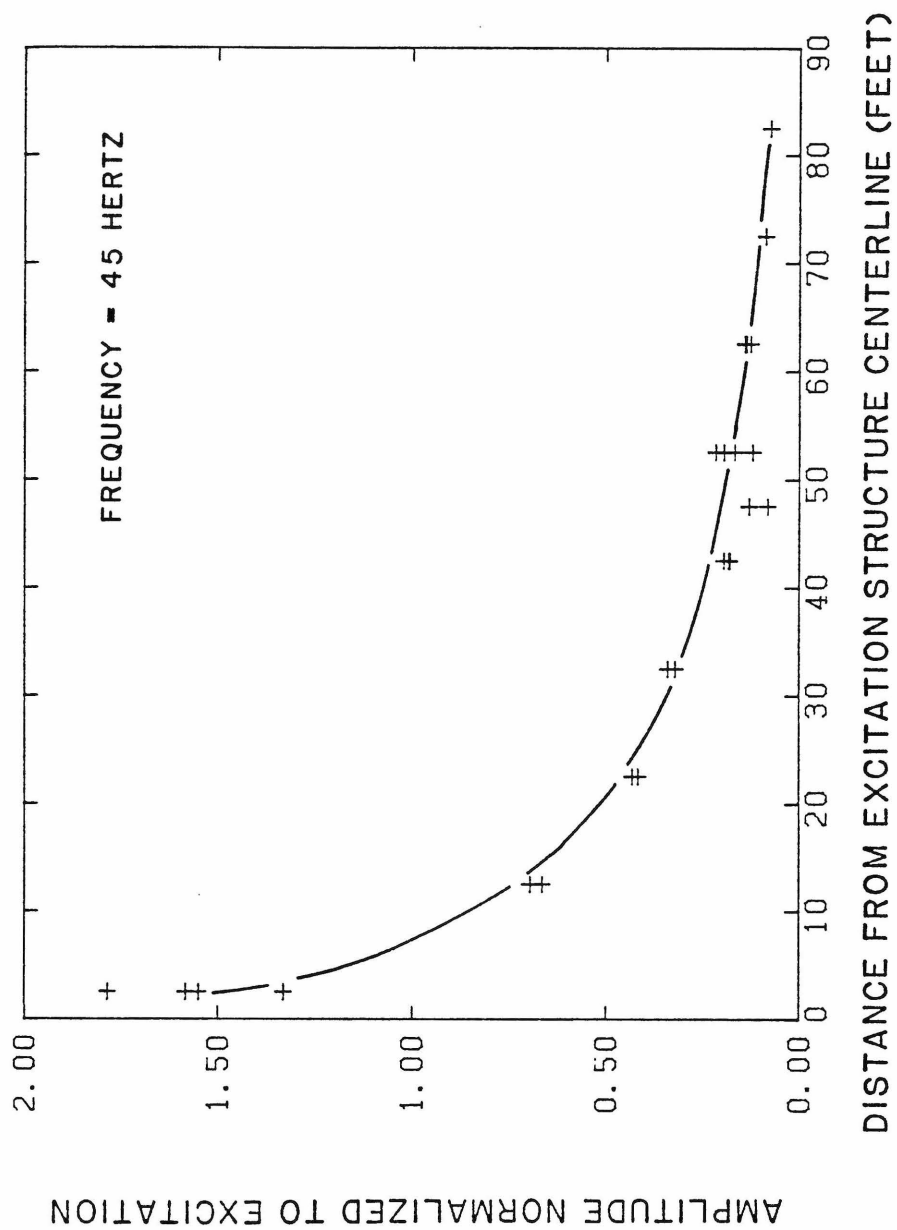


Figure 4.7. Free-field ground motion at 45 Hertz.

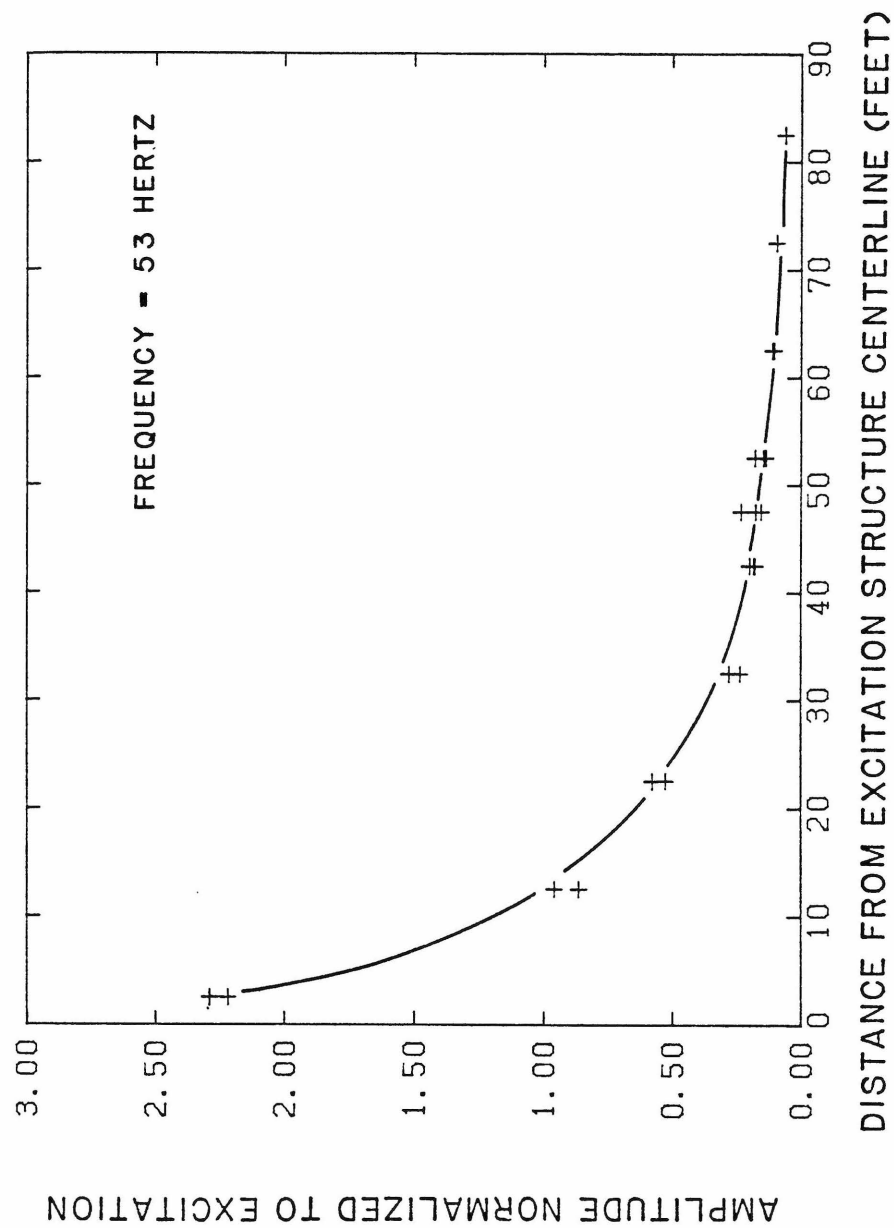


Figure 4.8. Free-field ground motion at 53 Hertz.

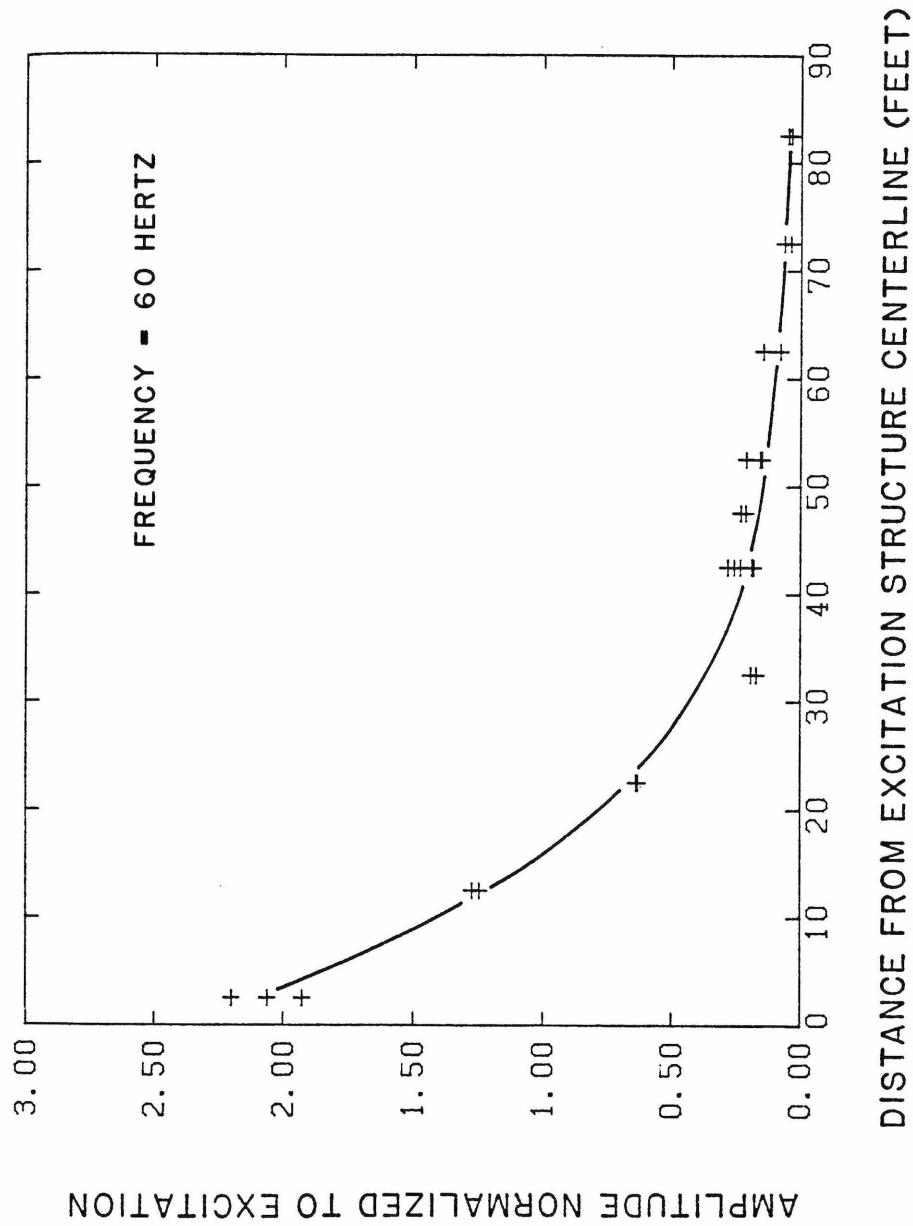


Figure 4.9. Free-field ground motion at 60 Hertz.

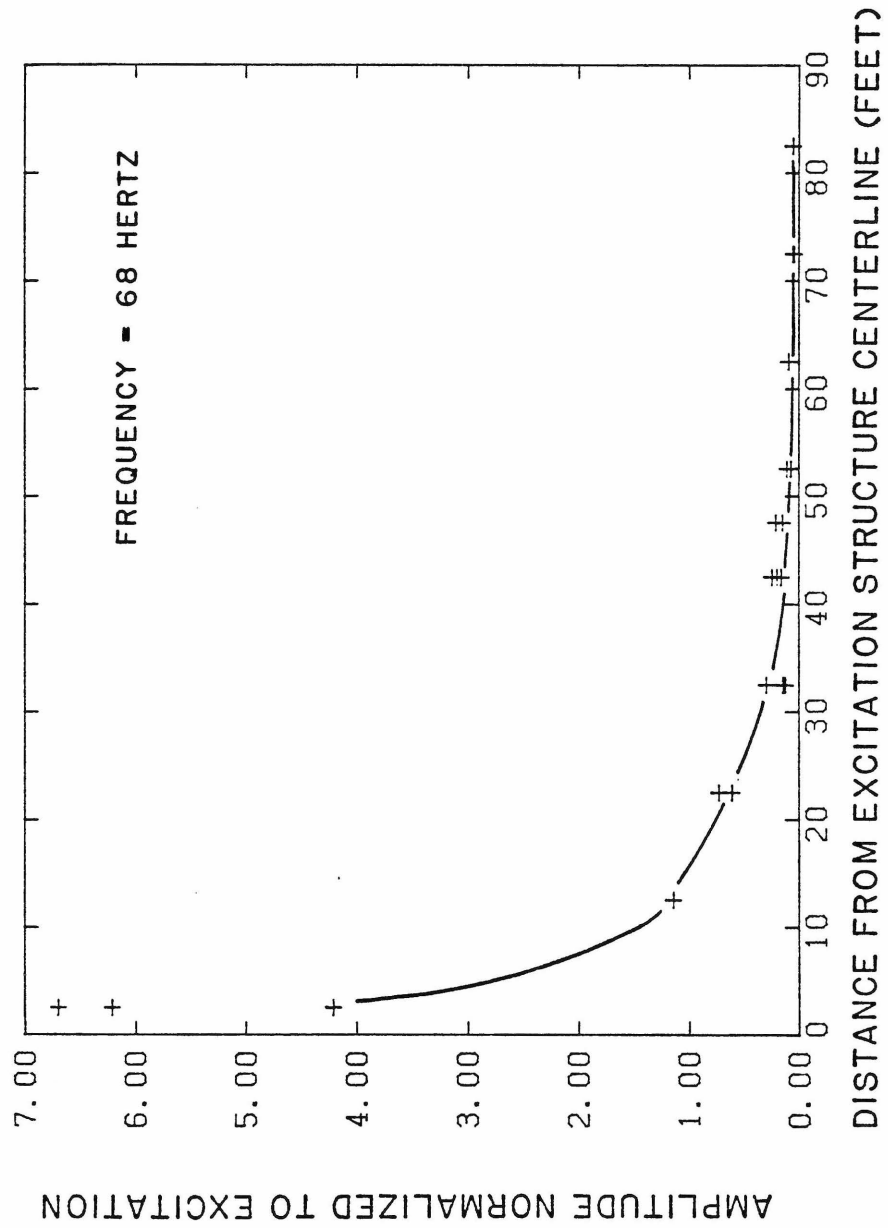


Figure 4.10. Free-field ground motion at 68 Hertz.

0.85 at the lowest test frequency of 7.5 Hertz, to a factor of approximately 5 at the highest frequency of 67.5 Hertz. At 67.5 Hertz, the amplitude of ground motion 10 ft (3 m) away from the excitation structure is comparable to the excitation structure displacement.

4. At a distance of 45 ft (14 m) from the excitation structure, the ground motion is about 20% of the excitation structure displacement for all but the lowest excitation frequencies.
5. Relative to the excitation structure displacement amplitude, free-field amplitudes, in general, increase with frequency. A notable exception occurs between 7.5 and 15 Hertz. At a given location, the ground motion measured at 7.5 Hertz is generally greater than that measured at 15 Hertz. This is attributable to the low force levels produced at 7.5 Hertz. At this frequency, the ambient ground noise is comparable, or even larger than, the displacements produced by the excitation structure. Thus, there is a constant amplitude of motion at all measurement points, to which is added the distance-dependent amplitude caused by the vibration of the excitation structure. It was not possible to separate the contributions to ground displacement from the two sources.
6. If the ground motion at each measurement point is normalized to the ground motion immediately outside the excitation structure, the amount of attenuation with distance increases with frequency. Qualitatively, this is supported by theory, since

there are more wavelengths between any two points at a higher frequency than at a lower frequency, resulting in greater losses due to material damping. Radiation damping should be independent of the vibrational frequency.

Since the specimen structure would be located 45 ft (14 m) from the excitation structure and have a fundamental resonant frequency less than 20 Hertz, any peculiarities in the high frequency behavior were not expected to have serious impact on the experimental program.

As stated in the previous chapter, there were three principal objectives of this phase of experimentation.

- Establishment of a base-line, free-field ground motion amplitude,
- Determination of the frequency dependence of free-field ground motion at the site of the specimen structure, and
- Estimation of the in situ shear wave velocity.

The first objective was satisfied by the data shown in Figures 4.2 to 4.10. These figures show the attenuation of ground motion with distance from the excitation structure over the test frequency range. Subsequent measurements of ground motion can be directly compared to these results. The latter two objectives will be discussed in the following subsections.

4.1.1. Ground Motion at Specimen Structure.

Figure 4.11 is a plot of the ground motion amplitude at the site of the specimen structure, as a function of frequency. The ordinal points are averaged values of amplitudes measured at stations 0+42.5, 0+47.5, 0+47.5E, 0+47.5W, and 0+52.5 of Figure 4.1. As discussed in subsection 3.2.3, the ground motion at the specimen structure site must be expressed as a function of the excitation frequency. This will permit the calculation of the ground motion input to the specimen structure for any excitation frequency. A least squares fit of the points plotted in Figure 4.11 leads to the following second-order equation,

$$X_g/X_e = -.03 + .0089f - .0000878f^2 \quad 7 < f < 70 \text{ Hz} \quad (4.1)$$

where X_g is the ground motion at the specimen structure site, and X_e is the displacement of the excitation structure. Because of uncertainty and possible error in the measured ground motion at 7.5 Hertz, this point was given one-half the weight of the other points in the least squares fit.

4.1.2. Shear Wave Velocity.

The last objective of the free-field motion studies was the determination of the in situ shear wave velocity, C_s . As discussed in Chapter 2, only the compression wave velocity was obtained directly from the preliminary investigations because of the difficulty involved in creating a sufficiently large surface shear disturbance.

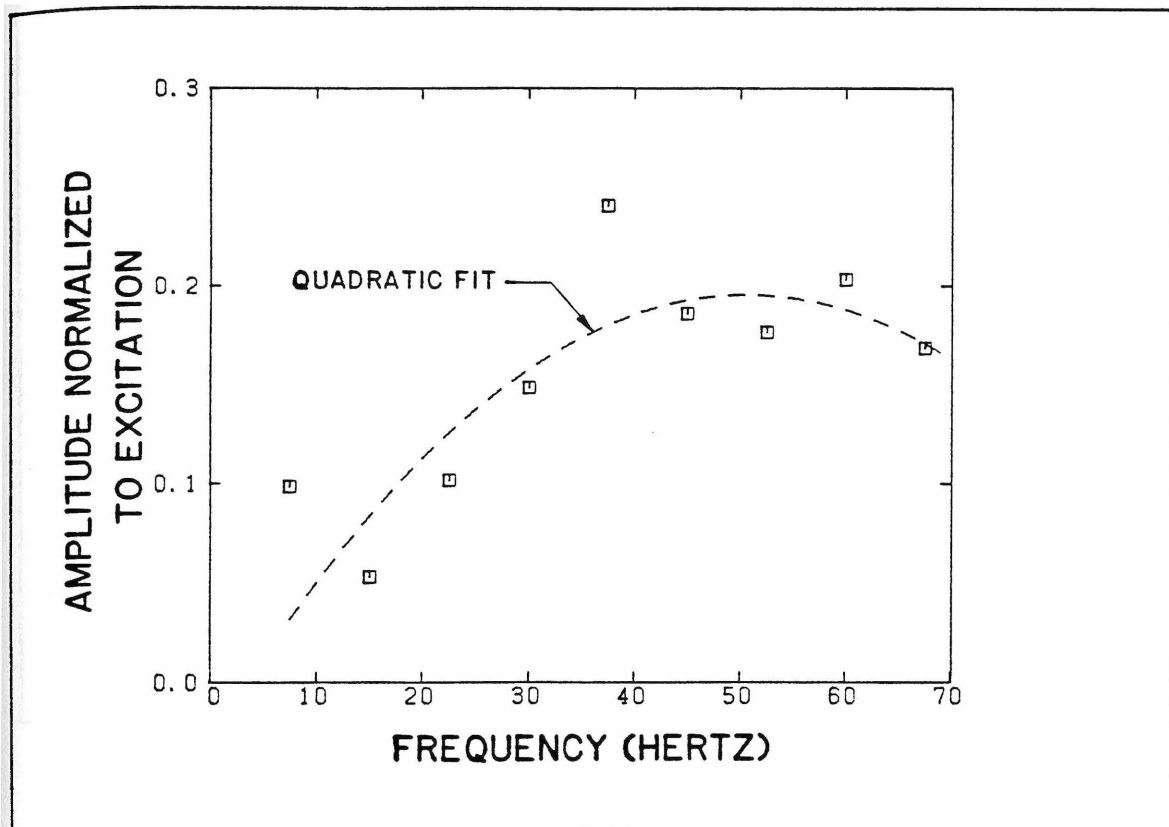


Figure 4.11. Free-field ground motion at specimen structure site.

Two methods were used to determine C_s . In the first method, the shear wave velocity was calculated from the interval of time required for the wave to travel from the excitation structure to the seismometer. The velocity is then calculated from the elapsed time and separation distance. Figure 4.12 shows a typical record that was used for this method.

Line A-A is drawn through all records at time $t=0$, when the motion of the excitation structure is at an extremum. Line B-B is drawn through the corresponding peaks in the free-field records. Note that

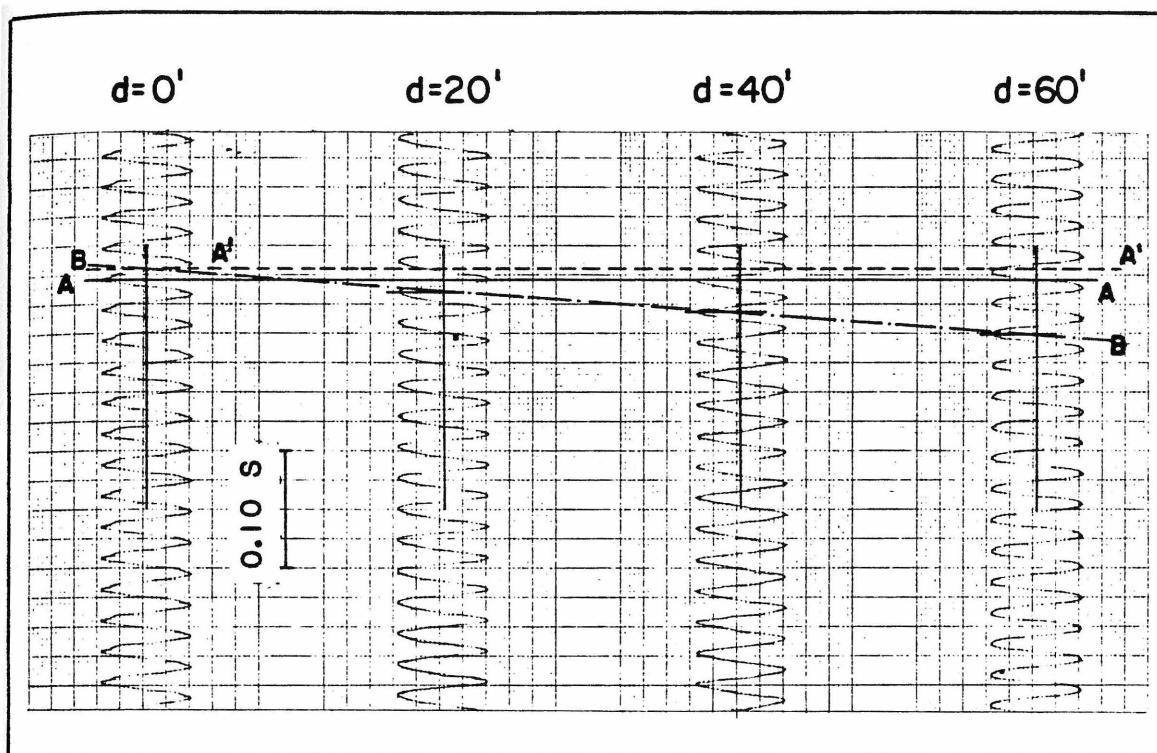


Figure 4.12. Sample record for determination of shear wave velocity

B-B does not intersect A-A at the center of the first record. Hence, a new $t=0$, corresponding to the ground motion outside the excitation structure, is indicated by the line A'-A'. Since the recording chart speed is known, the distance between lines A'-A' and B-B for each record can be used to calculate the elapsed time required for the wave to travel the distance between the excitation structure and the recording station. The velocity of the wave can be found since both the time and distance of travel are known.

In the second method, the relation $C_s = f \times L$ was used to calculate the wave velocity from the wavelength, L , and frequency, f . At each frequency, the relative phase of each recording station with respect to the excitation is determined. The first station moving in phase with the excitation structure is located one wavelength from the excitation structure. Because the recording stations were located at discrete intervals, interpolation was usually required to find the wavelength.

Table 4.1 lists the values of C_s obtained as a function of the excitation frequency and source-receiver separation distance by the first method, and also the values of wavelength and wave velocity found by the second method. Note that the results of the two methods, in general, agree with each other. In this application, less effort is required for the second method, although the results of the first method appear to be more consistent.

Steady state vibration tests have been used in geotechnical studies to determine the subsurface soil properties (Richart, Hall, and Woods, 1970). Most commonly, Rayleigh waves, a radially-polarized surface wave, are used. In the case of the Rayleigh wave, most of the energy travels through a layer whose thickness is approximately equal to the wavelength. Several field studies (Heukelom and Foster, 1960; Fry, 1963; and Ballard, 1964) have shown that the properties of the soil within this layer can be approximated by the soil properties at a depth equal to one-half of the wavelength.

TABLE 4.1. Results of in situ shear wave speed determination by two methods (in feet per second.)

Distance from source in feet	Excitation Frequency in Hertz							
	15	23	30	38	45	53	60	68
10	1330	1100	1430	1180	1250	1000	1030	1180
20	1330	1080	1030	1180	1140	1050	1000	1080
30	1330	1130	1360	1130	1090	1030	1050	940
40	1600	1360	1330	1140	1000	—	1040	940
50	—	1390	1370	1270	1250	—	970	910
60	—	1460	1210	1200	1200	—	900	890
Average value	1400	1250	1290	1180	1160	1060	1000	970
Wavelength in feet	90	55	45	35	25	20	15	15
$C_s = f \times L$	1350	1240	1350	1310	1130	1050	900	1010

In this experiment, the surface generated anti-plane SH-waves (Fung, 1965) can be assumed to have behavior similar to that of the Rayleigh wave. Hence, the depth of sampling can be expected to be proportional to the wavelength, and thus inversely proportional to the frequency. Higher frequencies give rise to shorter wavelengths, which, in turn, sample closer to the surface of the soil.

Figure 4.13 is a plot of the measured wave velocity as a function of wavelength. If the sampled depth is on the order of the wavelength, then the sampled depths vary from approximately 15 to 90 ft (14 to 27 m). The specimen structure, which is founded at a depth of

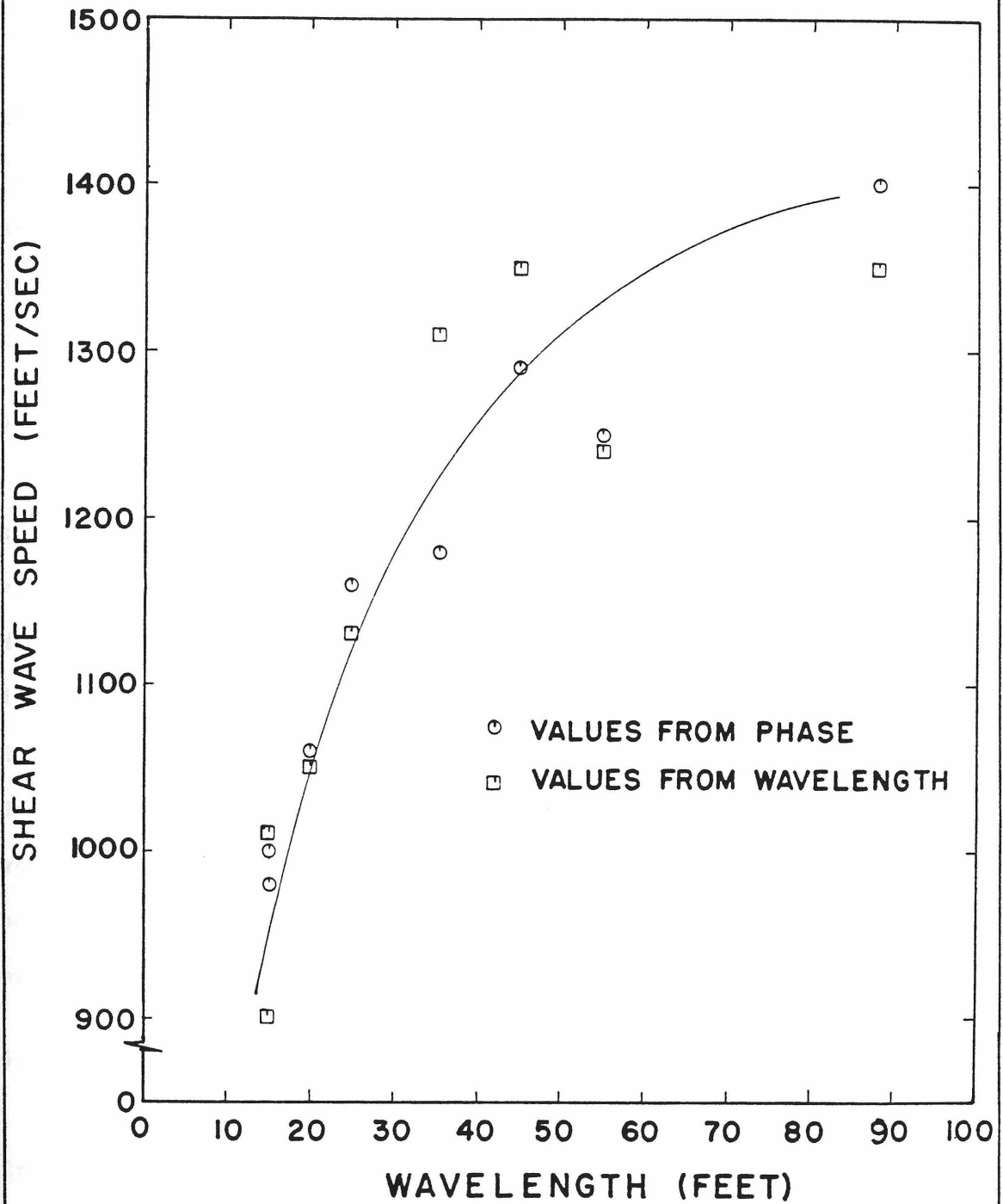


Figure 4.13. Shear wave speed vs. wavelength.

5 ft (1.5 m), will interact significantly only with soil that extends a few feet deeper than the foundation. In other words, the behavior of the foundation is not measurably affected by the properties of the soil, for example, 30 ft (9 m) below the surface; the soil closer to the structure controls the interaction of the foundation. Therefore, the shear wave velocity corresponding to shallow depth [1000 ft/sec (305 m/sec)], will be used in subsequent analysis.

4.2. SPECIMEN STRUCTURE RESPONSE.

The specimen structure, previously described in Section 2.6, was constructed after completion of the free-field motion tests. Ambient vibration, ring-down, and forced vibration tests were conducted to determine the natural frequencies and dampings of the excitable modes. In keeping with the basic intent of the experiment, more thorough determinations of the mode shape and ground motion were made at the fundamental resonant frequency in the principal test direction. The tests were conducted for each embedment case. The results of these tests will be presented and discussed in the following subsections. A comparison of the results is contained in Section 4.4.

4.2.1. Ambient Vibration Test Results.

Ambient vibration tests were used to obtain estimates of resonant frequencies. The seismometers were located on the specimen structure as shown in Figure 3.8. Four modes of response were identified from the resulting Fourier amplitude spectra. A shorthand notation was developed

to describe the response measured by each seismometer. The following list gives the abbreviated name and corresponding measurement:

- SCT - Superstructure Center Translation
- SET - Superstructure Edge Translation
- FCT - Foundation Center Translation
- FET - Foundation Edge Translation.

In addition, a single number is appended to each acronym to represent the degree of embedment; 0 for the unembedded case, 5 for half-embedment, and 1 for full-embedment. The direction of measurement is given by an additional suffix, N, for measurements in the north-south direction. An unsuffixed name indicates measurement in the principal, east-west, direction. This notation will be used throughout the remainder of this report.

A set of Fourier amplitude spectra for the full embedment case is shown in Figures 4.14 to 4.21. These spectra were calculated by the digital signal processor described in subsection 3.1.3 over a range in analysis frequency of 0 to 40 Hertz (sampling frequency of 80 Hertz). Each spectrum was calculated from 1024 data points, recorded over 12 seconds. Two transforms were calculated from each record (moving average), with a total of 16 transforms calculated and averaged for each spectrum. Therefore, a total of 100 seconds of data were used for each output spectrum. The spectra for the half- and non-embedment cases are similar to the corresponding spectra of the full-embedment case.

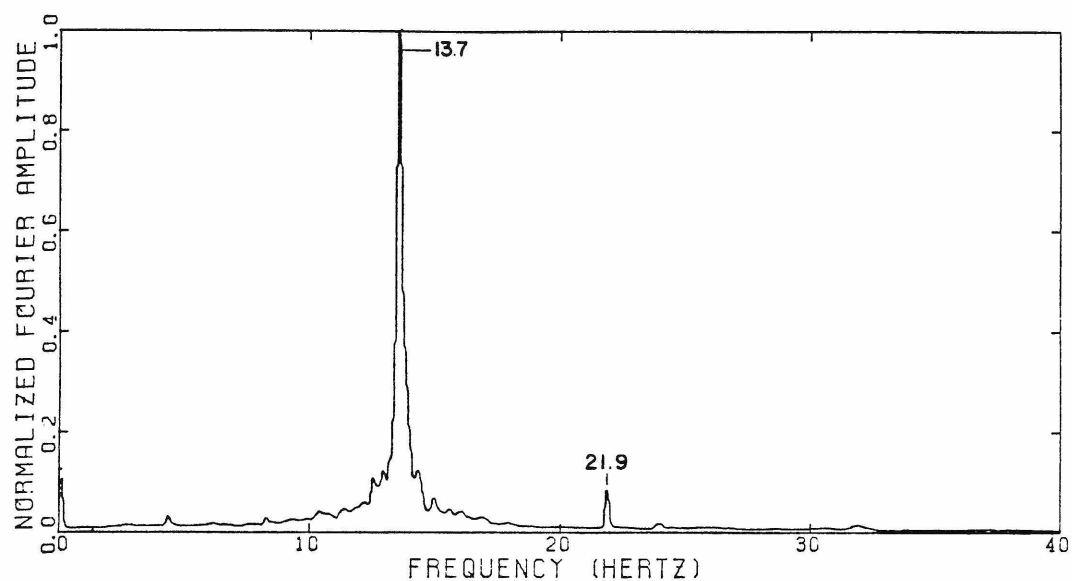


Figure 4.14. Fourier amplitude spectrum for superstructure center translation in principal direction (SCT-1), from ambient vibration test.

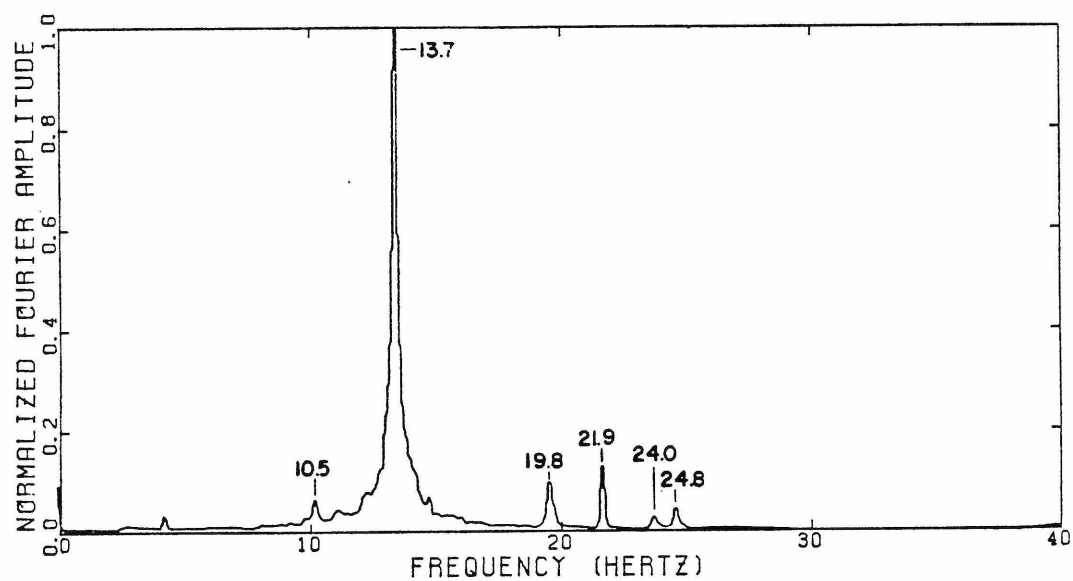


Figure 4.15. Fourier amplitude spectrum for superstructure edge translation in principal direction (SET-1), from ambient vibration test.

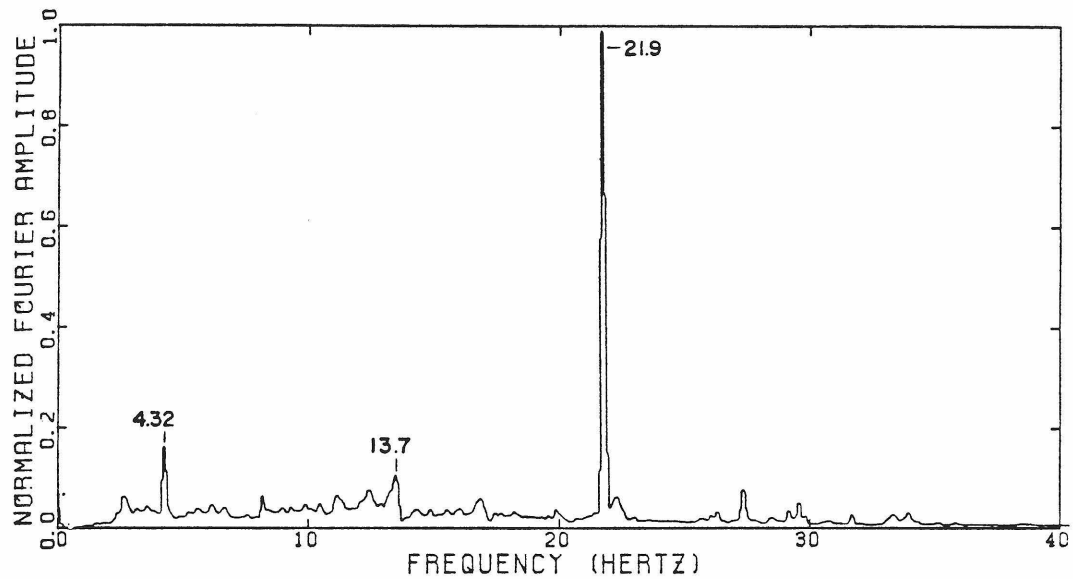


Figure 4.16. Fourier amplitude spectrum for foundation center translation in principal direction (FCT-1), from ambient vibration test.

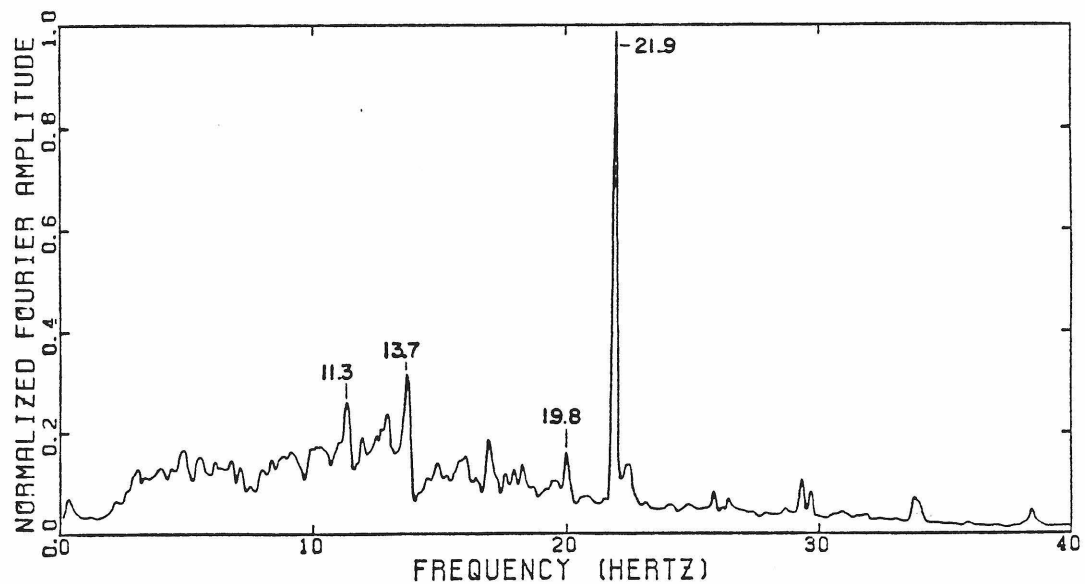


Figure 4.17. Fourier amplitude spectrum for foundation edge translation in principal direction (FET-1), from ambient vibration test.

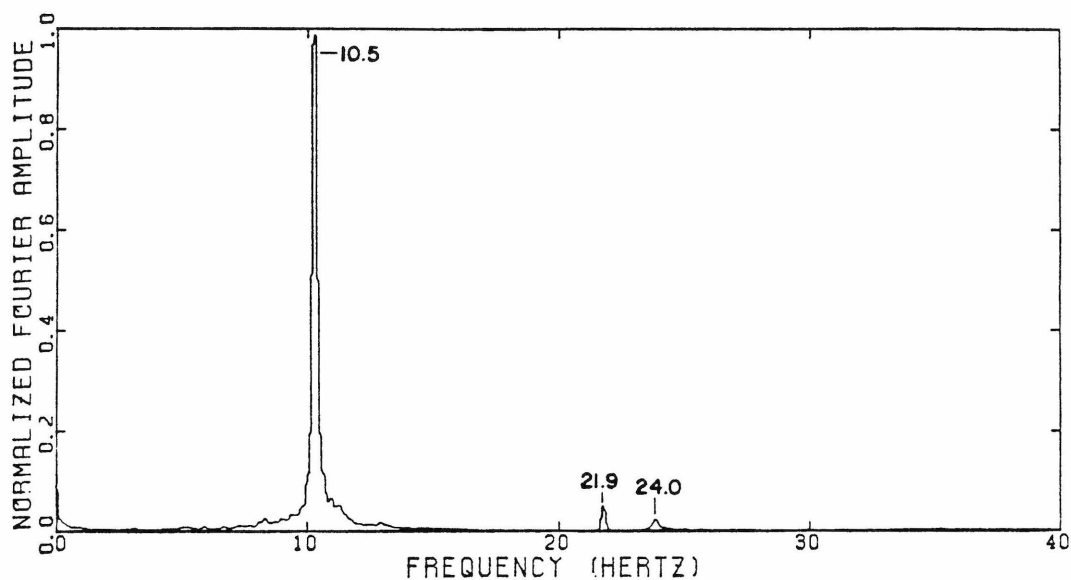


Figure 4.18. Fourier amplitude spectrum for superstructure center translation in north-south direction (SCT-1N), from ambient vibration test.

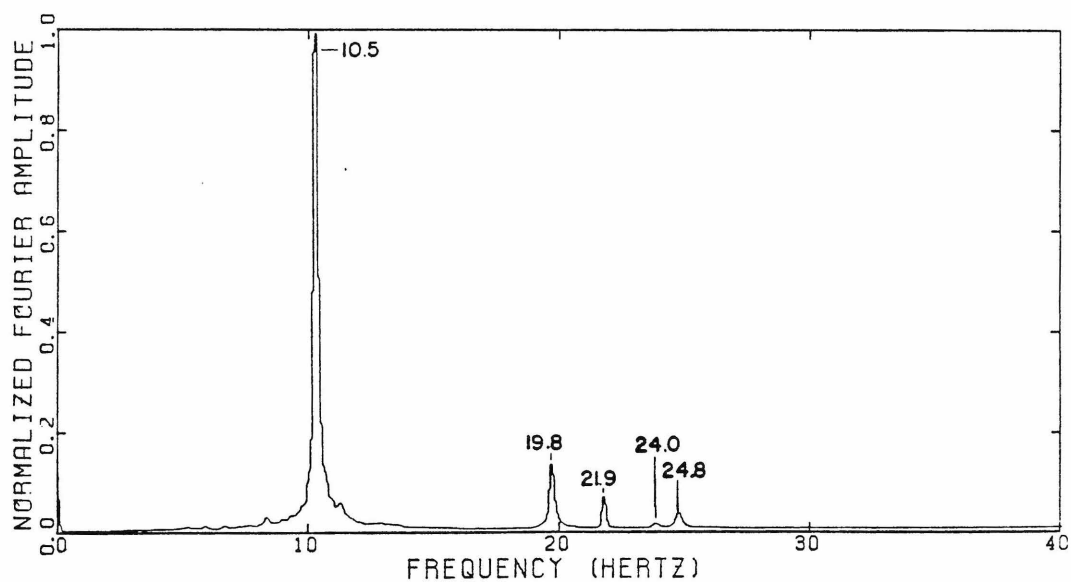


Figure 4.19. Fourier amplitude spectrum for superstructure edge translation in north-south direction (SET-1N), from ambient vibration test.

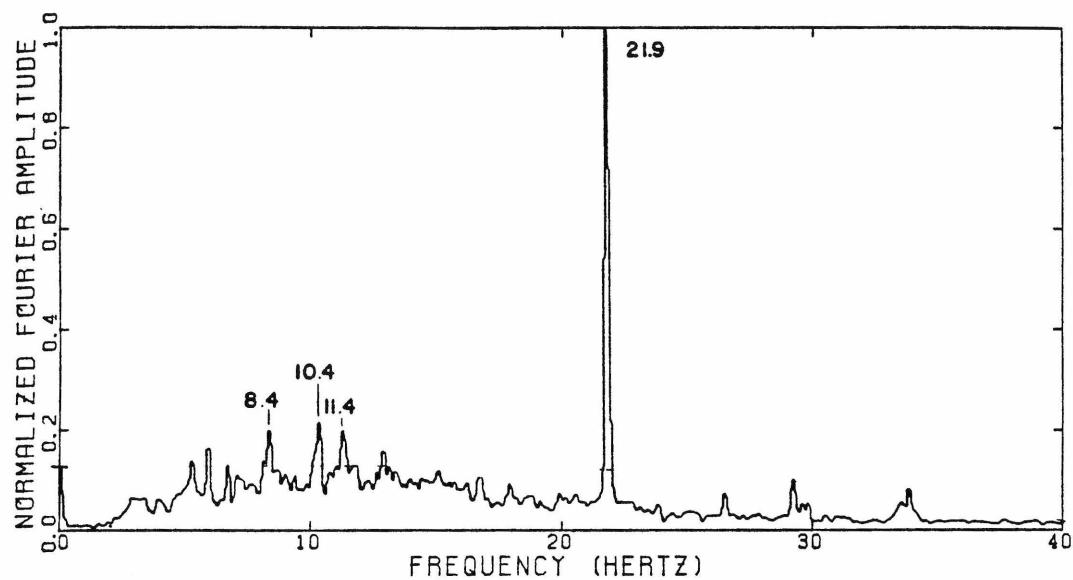


Figure 4.20. Fourier amplitude spectrum for foundation center translation in north-south direction (FCT-1N), from ambient vibration test.

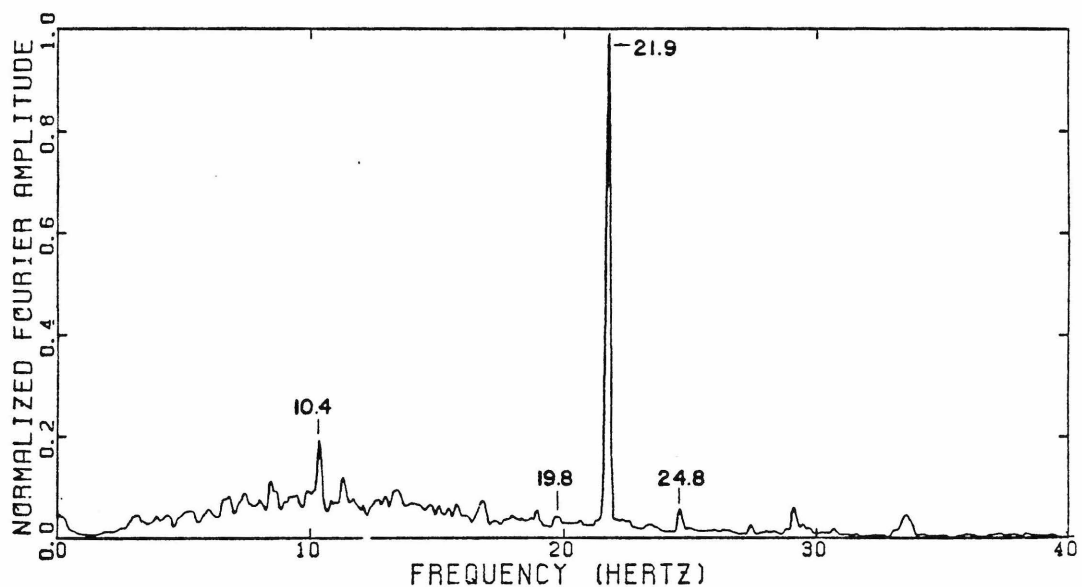


Figure 4.21. Fourier amplitude spectrum for foundation edge translation in north-south direction (FET-1N), from ambient vibration test.

Resonant peaks occur at 13.7 and 21.9 Hertz in both SET-1 and SCT-1. Two additional peaks appear in SET-1 at 19.8 and 24.8 Hertz that do not appear in SCT-1. The spectral peaks at 19.8 and 24.8 Hertz also appear in SET-1N but not in SCT-1N. Peaks at 10.5 and 21.9 Hertz, however, do occur in both of the latter spectra. The foundation spectra (FCT-1 and FCT-1N) both contain a predominant peak at 21.9 Hertz.

Comparison of these spectra permits the identification of the principal modes. The fundamental translatory mode in the east-west direction occurs at 13.7 Hertz. The spectral amplitude is approximately the same in both the center and the edge spectra. Hence, both points are moving with about the same amplitude. A similar argument identifies 10.5 Hertz as the translational frequency in the north-south direction.

Smaller torsional resonances occur at 19.8 and 24.8 Hertz. Fourier peaks occur at these frequencies in both SET-1N and SET-1, but not at SCT-1 and SCT-1N. This indicates that the edges are moving at the same frequency, but there is little motion at the center. Therefore, the center of the structure is a center of rotation, and thus, these two frequencies correspond to torsional resonances. The first peak indicates an amplitude of response two to three times greater than that of the higher peak.

As intended in the original design, the vibrational properties of the superstructure are different in the east-west and north-south directions. However, the foundation is square and has the same properties in both directions. Therefore, the peak at 21.9 Hertz which occurs in all spectra may possibly be indicative of motion which is primarily due to

foundation translation in both directions. However, the lack of dependence of this resonant frequency upon foundation embedment suggests that this interpretation is not correct. (This frequency will be seen not to occur in the forced vibration tests, and therefore, can be attributed to the ambient input).

The nature of the ambient excitation can affect the response of the structure. The Fourier spectra for SCT-5, SCT-5N, FCT-5, and FCT-5N that are shown in Figures 4.22 to 4.25 contain large peaks at 3.6, 4.4, and 5.1 Hertz in both directions. Similar peaks occur in the spectra for the unembedded case, but were not present, as shown in Figures 4.14 to 4.21, in the full-embedment spectra. These three peaks may be due to vibrations generated by the operation of an adjacent sand and gravel quarry. The ambient vibration tests for the full-embedment case were conducted during the early evening, when the quarry was not in operation. The tests for the other embedment cases, however, were conducted during the day, when many artificial and non-random vibrations are present. Therefore, the structural response indicated by these peaks is one of low amplitude forced vibration, and not of resonance. The presence of non-random ambient vibration can lead to erroneous conclusions about the vibrational properties of structures.

A detailed discussion of possible errors that could affect the interpretation of Fourier amplitude spectra resulting from ambient vibration tests was presented by Foutch (1976). In that report, Foutch found that the non-stationary response of structures had a significant effect on the Fourier amplitude spectra. As the resonant frequency

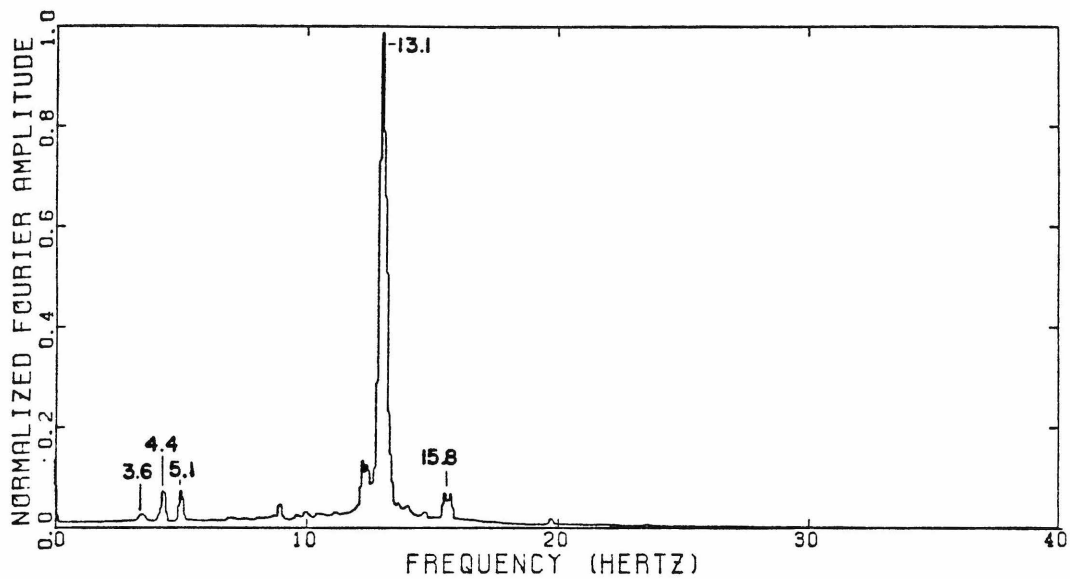


Figure 4.22. Fourier amplitude spectrum for superstructure center translation in principal direction (SCT-5), from ambient vibration test.

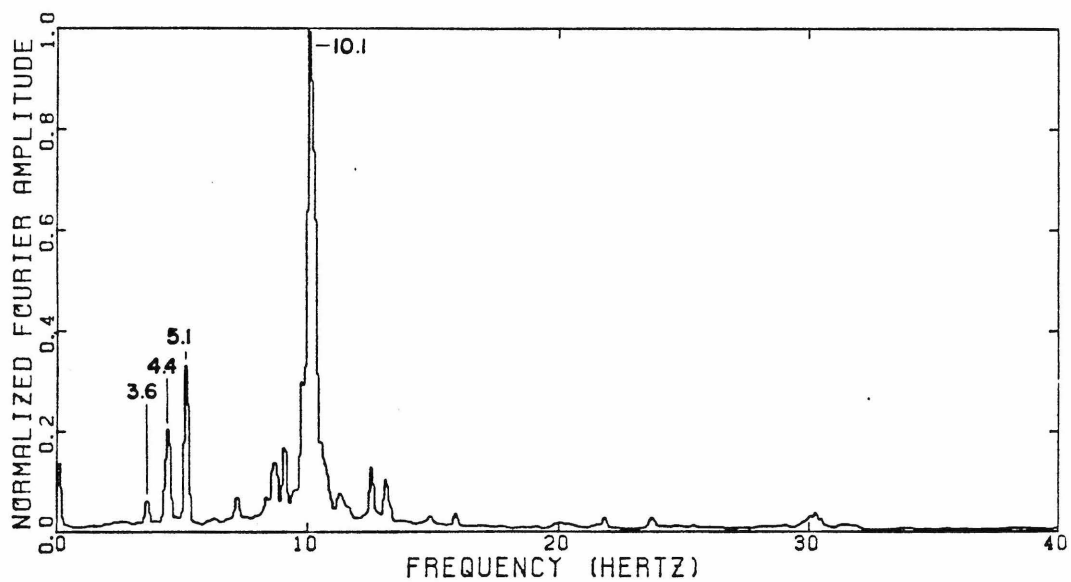


Figure 4.23. Fourier amplitude spectrum for superstructure center translation in north-south direction (SCT-5N), from ambient vibration test.

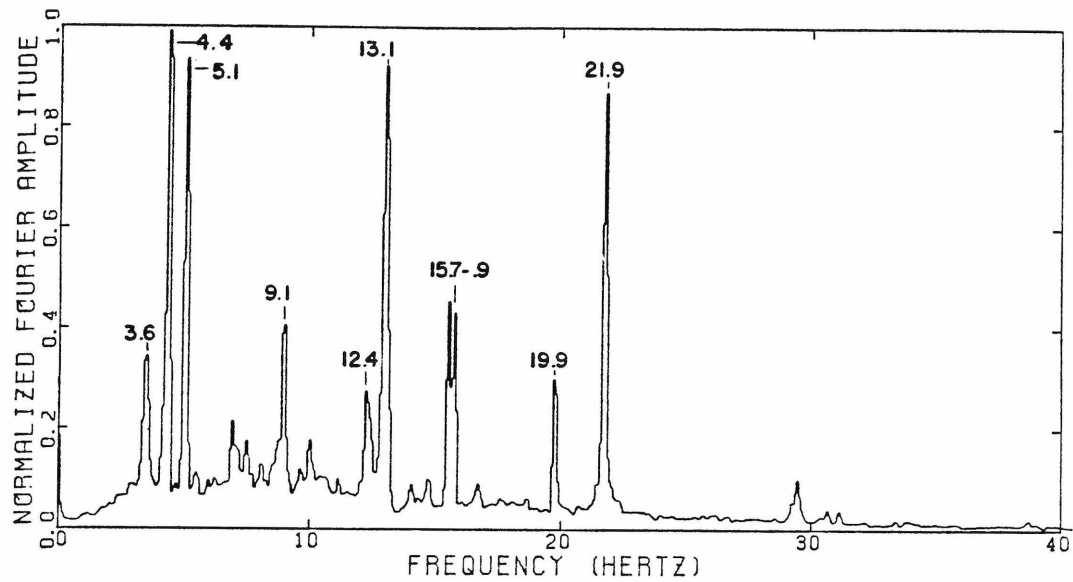


Figure 4.24. Fourier amplitude spectrum for foundation center translation in principal direction (FCT-5), from ambient vibration test.

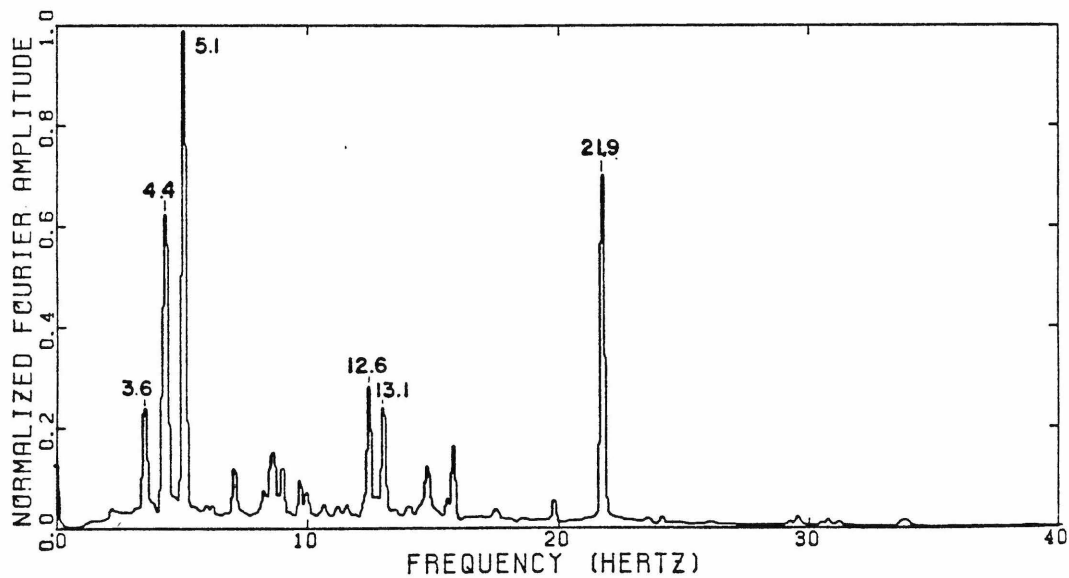


Figure 4.25. Fourier amplitude spectrum for foundation center translation in principal north-south direction (FCT-5N), from ambient vibration test.

shifted, the quality of the response peaks decreased. The appearance of double peaks (such as that occurring at 15.7 and 15.9 Hertz in Figure 4.24) was one effect of such shifting.

To aid interpretation, Fourier spectra are often filtered and smoothed. This procedure eliminates side lobes and improves the accuracy of the spectral peaks. Unfortunately, the digital signal processor does not possess such a capability, hence, the spectra presented in Figures 4.14 to 4.25 are unfiltered and unsmoothed, except by averaging, as noted above. As a result, some of the spectral peaks are not well defined, and must be interpreted with care.

The absence of smoothing and the limited resolution of the output contributes to the presence of "lumps" along the sides of the spectral peaks. These lumps are not indicative of any real phenomenon. The appearance of the spectra can be improved somewhat by operation of the plotter under manual control. In this mode, the plotting speed can be increased and the spectra will not be reproduced quite as faithfully, resulting in a crude type of smoothing. If not done carefully, however, significant errors can be introduced by this method.

TABLE 4.2. Resonant frequencies from ambient vibration tests in Hertz.

Embedment in feet	Fundamental Translation		Torsion	
	East-West	North-South	1	2
0	12.0	9.6	19.4	24.5
2.5	13.1	10.1	19.7	24.7
5.0	13.7	10.5	19.8	24.8

Table 4.2 shows the resonant frequencies of the structure that were identified from the ambient vibration tests. These results indicate that the resonant frequencies of the fundamental translatory and the two torsional modes increase with embedment. This indicates an expected increase in the overall stiffness of the system. Since, for a simple system, resonant frequency is proportional to the square root of the stiffness, a description of the effect of embedment on the overall stiffness of the system can be obtained by squaring the ratio of the embedded to unembedded resonant frequency. The stiffness ratios obtained for the four modes are plotted in Figure 4.26 as functions of embedment depth.

These stiffness ratios reflect the change in the overall stiffness of the system, that is, the combined effects of the superstructure and foundation stiffnesses. Since the superstructure stiffness is independent of embedment, the variation in the foundation-soil stiffness will be greater than that indicated in Figure 4.26.

It should be noted that there is a larger change in resonant frequency between the half- and non-embedment cases, compared to the change from the full- to half-embedment cases. It should also be realized that the foundation motions are coupled. That is, in the fundamental mode, the foundation will both rock and move laterally. The foundation impedances involved for these motions may not have the same dependence on embedment.

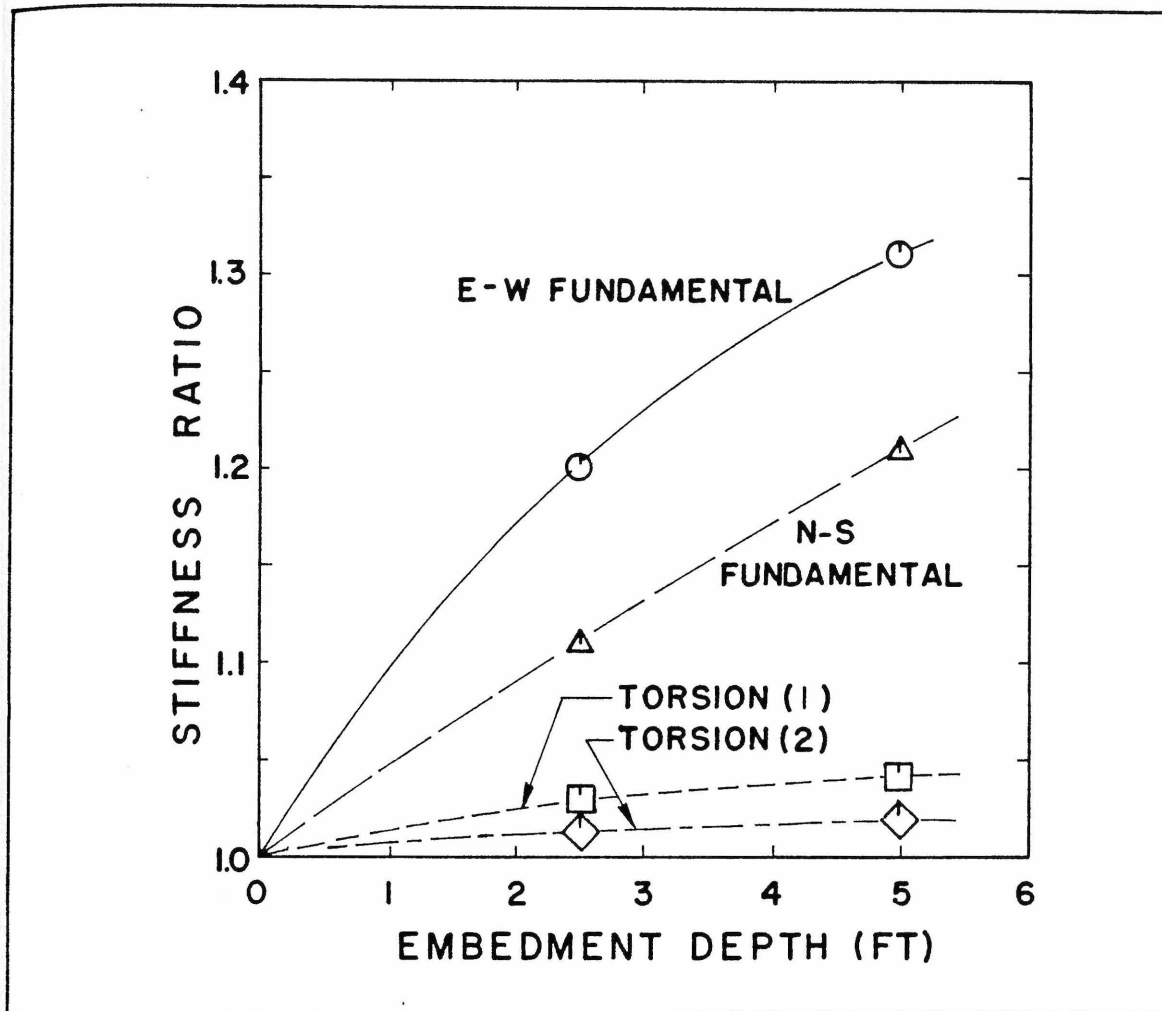


Figure 4.26. Effect of embedment on stiffness of specimen structure system from ambient vibration tests.

4.2.2. Ring-down Results.

It is normally difficult to conduct ring-down tests on prototype structures. For smaller structures, however, ring-down tests are a fast and simple way of obtaining approximate estimates of fundamental natural frequencies and dampings. A typical ring-down time history, in this case, for the east-west vibration of the superstructure in the

unembedded case, is shown in Figure 4.27. The upper trace was recorded at the center, and the lower trace recorded at the edge of the superstructure.

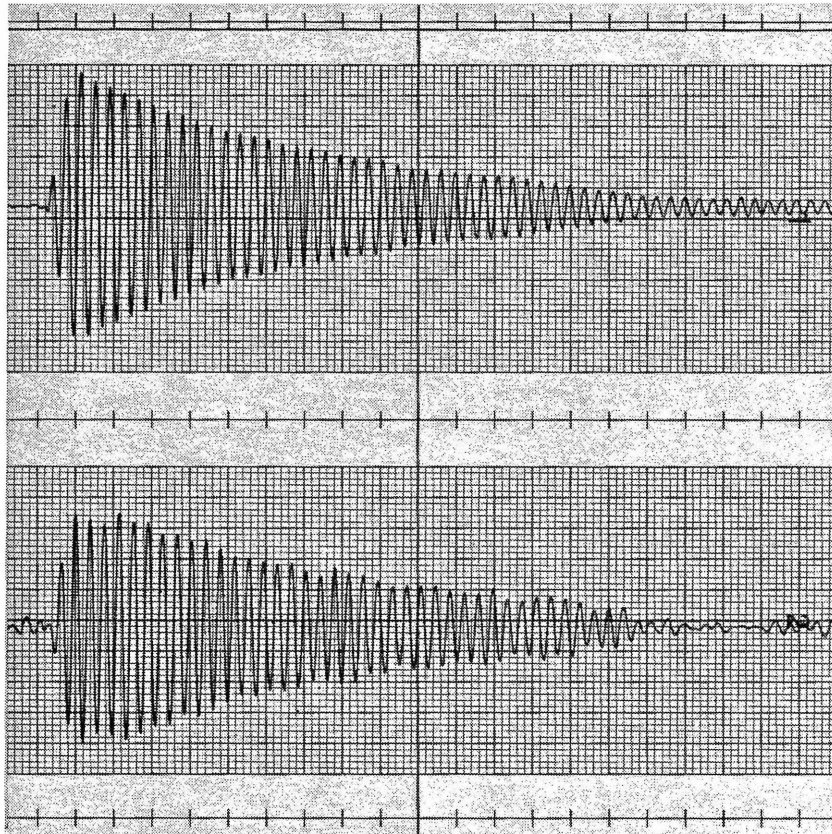


Figure 4.27. Typical ringdown record; Top SCT-5, Bottom, SET-5.

Table 4.3 summarizes the natural frequencies and dampings of the fundamental translational mode in the north-south direction for the three embedment cases, and the east-west direction for two embedment

TABLE 4.3. Resonant frequencies and damping factors for fundamental mode in east-west and north-south directions from ring-down tests.

Embedment in feet	East-west translation		North-south translation	
	Resonant frequency in Hertz	Damping factor as percent of critical	Resonant frequency in Hertz	Damping factor as percent of critical
0	11.9	0.94	9.6	0.54
2.5	13.2	0.88	10.4	0.24
5.0	*	*	10.4	0.23

*Not available, east-west direction at full embedment was not an original part of the test program.

cases. Several conclusions can be drawn from these results. First, the resonant frequencies in both directions generally increase with embedment. In the north-south direction, however, there is only a very small difference between the half- and full-embedment cases. Second, damping in the north-south mode is significantly lower than for the east-west direction. Since the foundation is square, and hence should have the same properties in both directions, this difference is attributed to the superstructure. Third, the two damping values in the east-west mode appear to be almost independent of the embedment. The damping in the north-south direction, however, is reduced by a factor of two from the unembedded cases for the half- and full-embedment conditions.

4.2.3. Forced Vibration Test Results.

The thorough dynamic characterization of a structure made possible by the results of forced vibration tests will, in most cases, compensate for the additional difficulty and expense required by these tests. Because the excitation frequency and force level can be controlled, various aspects of the dynamic behavior of a structure can be studied in detail. Resonant frequencies, mode shapes, damping, and even non-linear effects can be measured carefully to characterize a model or prototype structure.

4.2.3.1. Determination of response modes.

Response to forced vibration was measured at the locations shown in Figures 3.9 and 3.10. The responses were assigned the following acronyms:

- SCT - Superstructure Center Translation,
- SET - Superstructure Edge Translation,
- FCT - Foundation Center Translation,
- FET - Foundation Edge Translation,
- SCV - Superstructure Center Vertical,
- SEV - Superstructure Edge Vertical,
- FCV - Foundation Center Vertical,
- FEV - Foundation Edge Vertical.

As in the ambient vibration test results, a single number, 0, 5, or 1, will be appended to each acronym to indicate the zero-, half-, and full-

embedment conditions. Since the forced vibration tests were conducted for east-west vibration, there is no need for an additional suffix to indicate the direction of the response; all translatory motions are in the east-west direction.

In addition to these measured quantities, two calculated quantities were also determined,

- STR - Superstructure Translation Ratio, SET/SCT ,
- CTR - Center Translation Ratio, SCT/FCT

These two ratios can be used to help identify response modes. More specifically, torsional response will be more clearly seen in the quotient STR, which compares the translation of the edge to that of the center of the superstructure. CTR, on the other hand, will emphasize differences between the superstructure and foundation translations, thereby aiding in the identification of modes with large interfloor displacements.

It should be noted that the calculation of STR and CTR may be ill-conditioned; a small value in the denominator can make the quotient artificially large and therefore appear to be significant. Because the amplitude of the vertical vibrations were, in most instances, not much larger than the noise, similar displacement ratios were not calculated for the vertical motions.

Figures 4.28 to 4.56 plot these ten measured and calculated quantities for the three embedment cases. For the four quantities related to superstructure translation, SCT, SET, STR, and CTR, two plots

have been provided. The first, (a), shows the response over the entire frequency range of 0 to 70 Hertz. The second, (b), shows the response over the range of 5 to 30 Hertz, to provide better detail. The individual data points are indicated by the symbol (X).

Several remarks should be made to aid in the interpretation of the results,

1. The y-axis scale is expressed in terms of displacement per unit force, in arbitrary units. The same scale has been used for all of the response curves. Hence, the peak amplitude of 6300 in SCT-1 (Figure 4.40) is indeed over 30 times greater than the peak amplitude of 180 in FCT-1 (Figure 4.44). In terms of absolute units, the relative scale is approximately 1 to 2.0×10^{-10} inch/lb or 0.20 μ inch/kip (1.15×10^{-6} mm/kN). The scaling is only approximate because of the difficulty in comparing the outputs of the accelerometer and the seismometer over the large frequency range. The arbitrary units used for the plots are, however, sufficient for the purposes of this study.
2. Not all data points have been plotted. Although the response curve obtained from any one test was smooth and well-defined, there were small day-to-day variations in the specimen that prevented the total agreement between the results of several tests. These variations are not significant in terms of the experiment, but resulted in some scatter of the data. If all

of the data were plotted on each response curve, the plots would be confusing and would also indicate a lower degree of accuracy than actually obtained in a particular test.

3. Table 4.4 shows the number of points recorded and plotted in the response curves. A subjective five-point scale of "quality" of the results is also shown. The quality is indicative of the noise and relative scatter in the data. A rating of 5 means that the excluded points were very close to the included points. The lowest rating of 1, on the other hand, indicates considerable scatter in the data. In some cases, only a small number of points were recorded, and a large percentage of these points had to be plotted just to show the approximate behavior, even if there was considerable scatter in the results (e.g. SEV-1). The test program started with the full-embedment case. As shown in Table 4.4, the number of data points recorded at each station increased during the test program, a key example is SET; for which 48 points were recorded for the first case of full embedment, and 114 points recorded for the final unembedded case. The increased number of data points is reflected in the assigned "quality" of the plots, as well as by visual comparison of the plots themselves.
4. The measurement of the vertical motion of the superstructure was not an original part of the test program. Hence, there is no plot for SCV-1, and only a few points in SEV-1.

TABLE 4.4. Number of data points recorded and plotted in Figures 4.28-4.56, with five-point scale estimate of 'quality'.

Plot name	Full-embedment			Half-embedment			Zero-embedment		
	No. of points		Q	No. of points		Q	No. of points		Q
	R	P		R	P		R	P	
SCT	83	60	5	117	58	5	114	70	5
SET	48	45	4	85	58	5	114	73	5
STR	48	41	4	86	56	5	114	66	4
FCT	106	61	3	67	43	3	114	62	4
FET	63	49	2	119	62	3	114	69	4
CTR	80	51	5	68	45	5	114	62	4
SCV	0	0	0	68	59	1	50	45	2
SEV	11	11	1	68	51	2	49	49	2
FCV	37	27	1	66	48	1	48	46	2
FEV	37	32	2	67	52	2	49	47	2

R - Total number of points recorded.

P - Total number of points plotted.

Q - 'Quality' of plot.

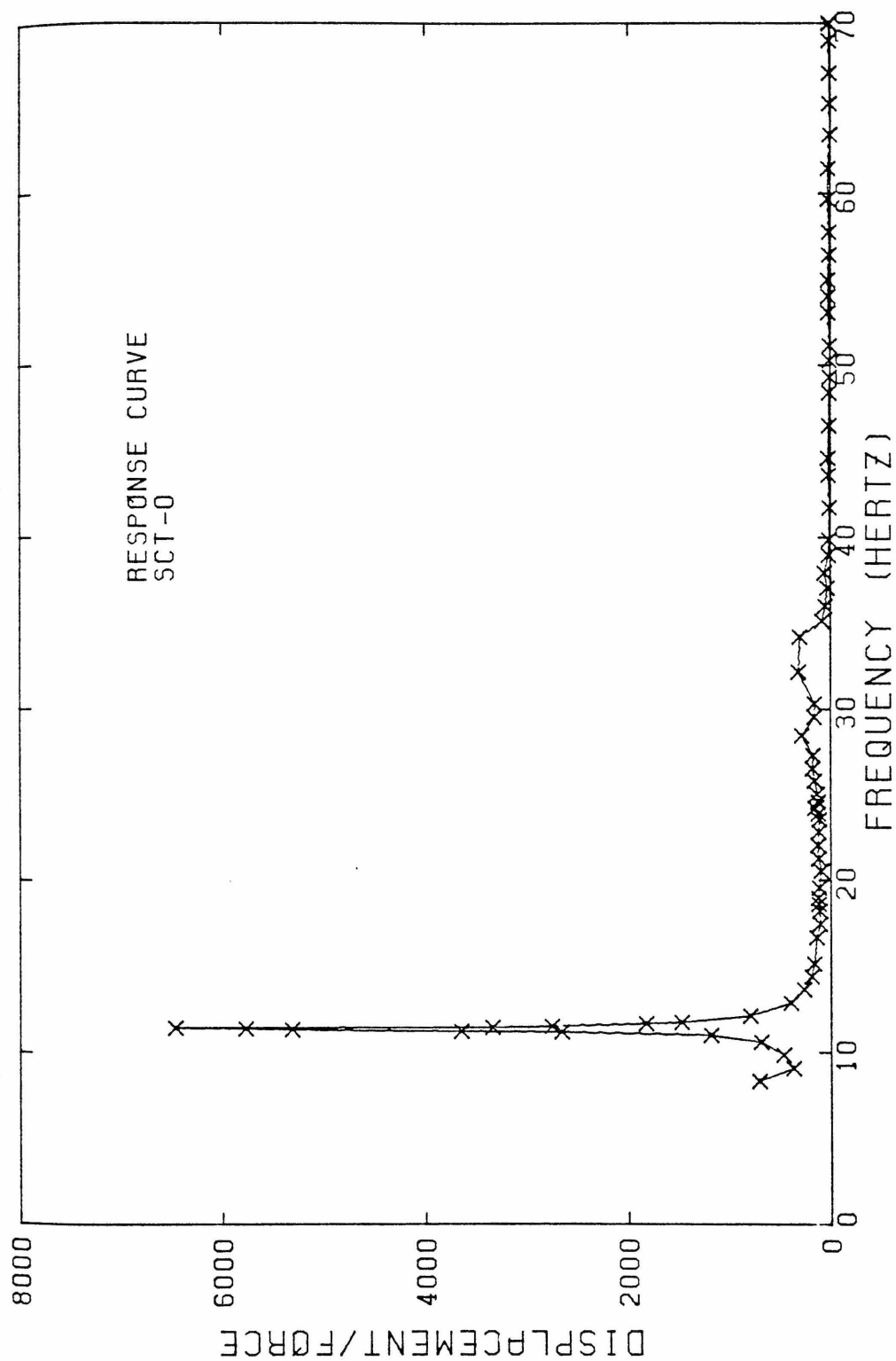


Figure 4.28(a). Response curve for superstructure center translation (SCT-0). Full frequency range, 0-70 Hz.

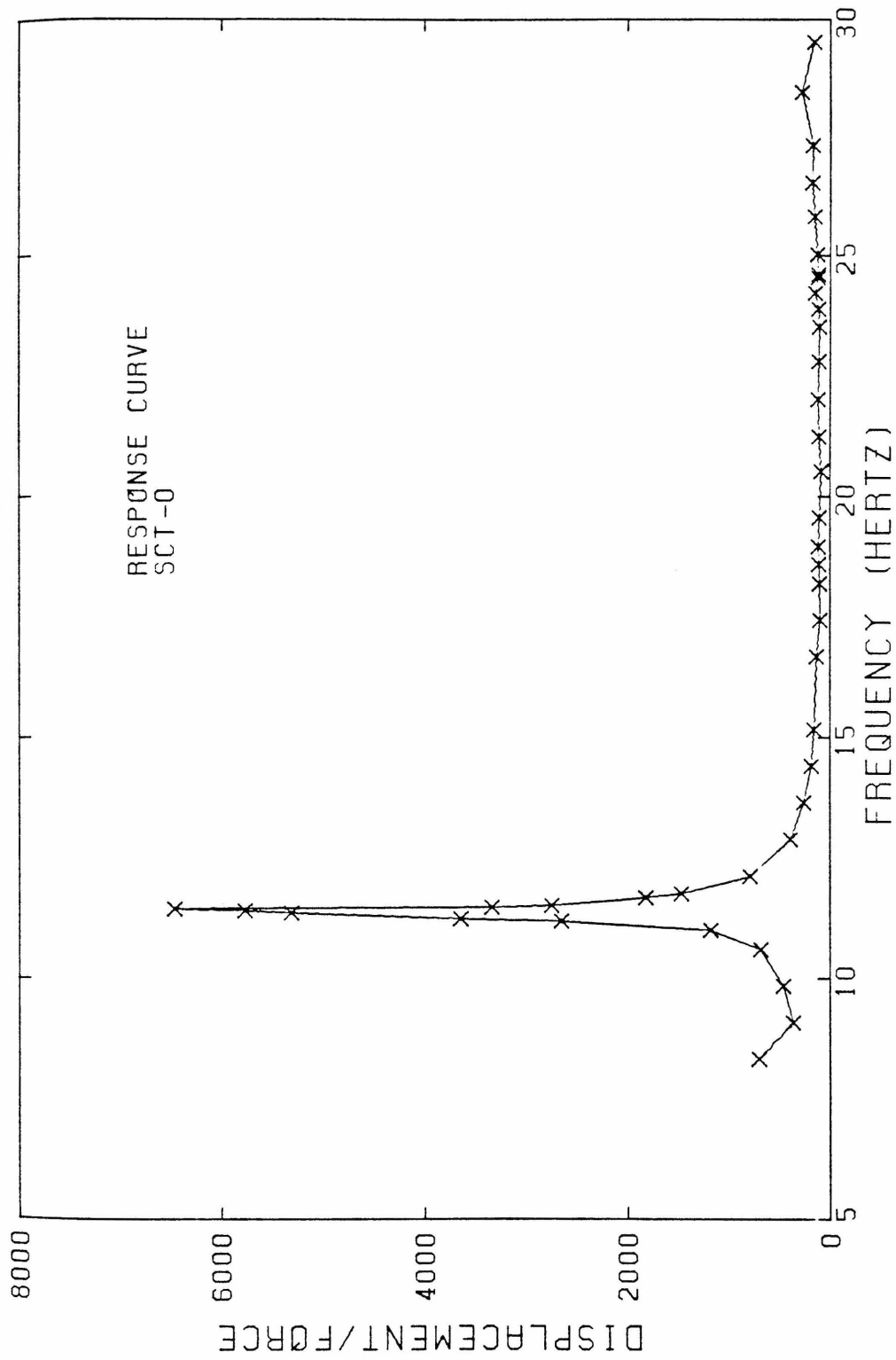


Figure 4.28(b). Response curve for superstructure center translation (SCT-0). Partial frequency range, 5-30 Hz.

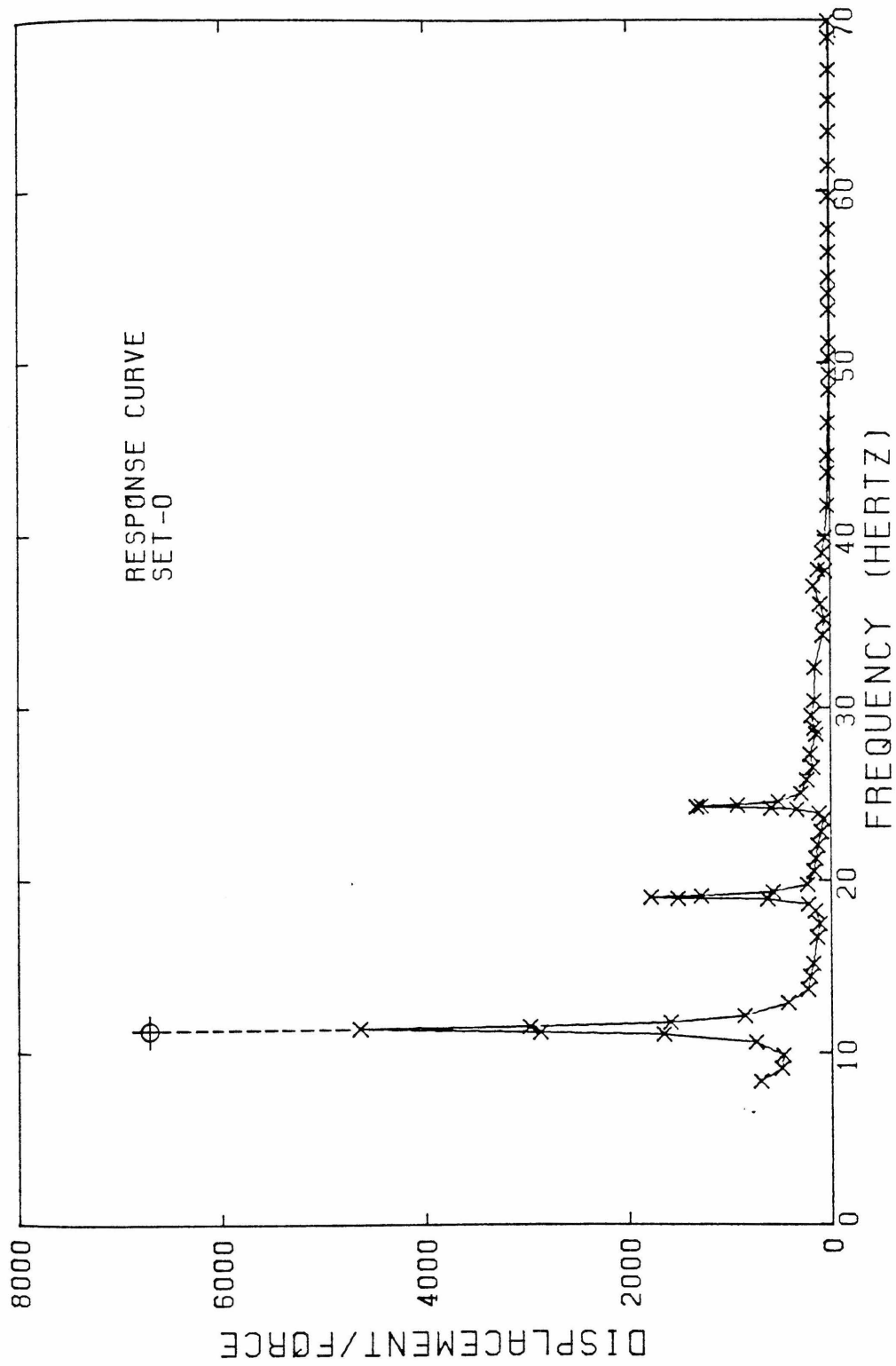


Figure 4.29(a). Response curve for superstructure edge translation (SET-0). Full frequency range, 0-70 Hz.

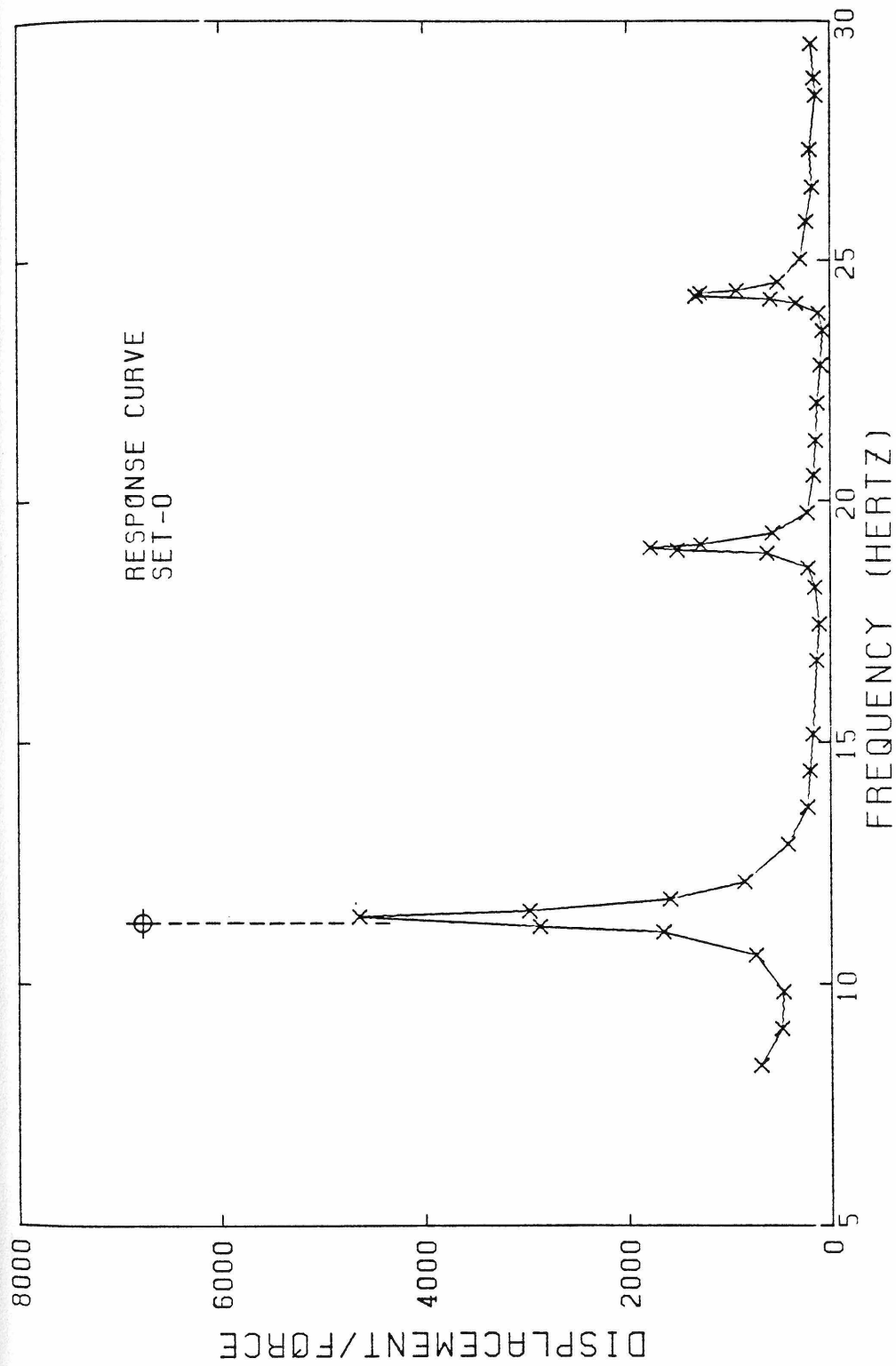


Figure 4.29(b). Response curve for superstructure edge translation (SET-0). Partial frequency range, 5-30 Hz.

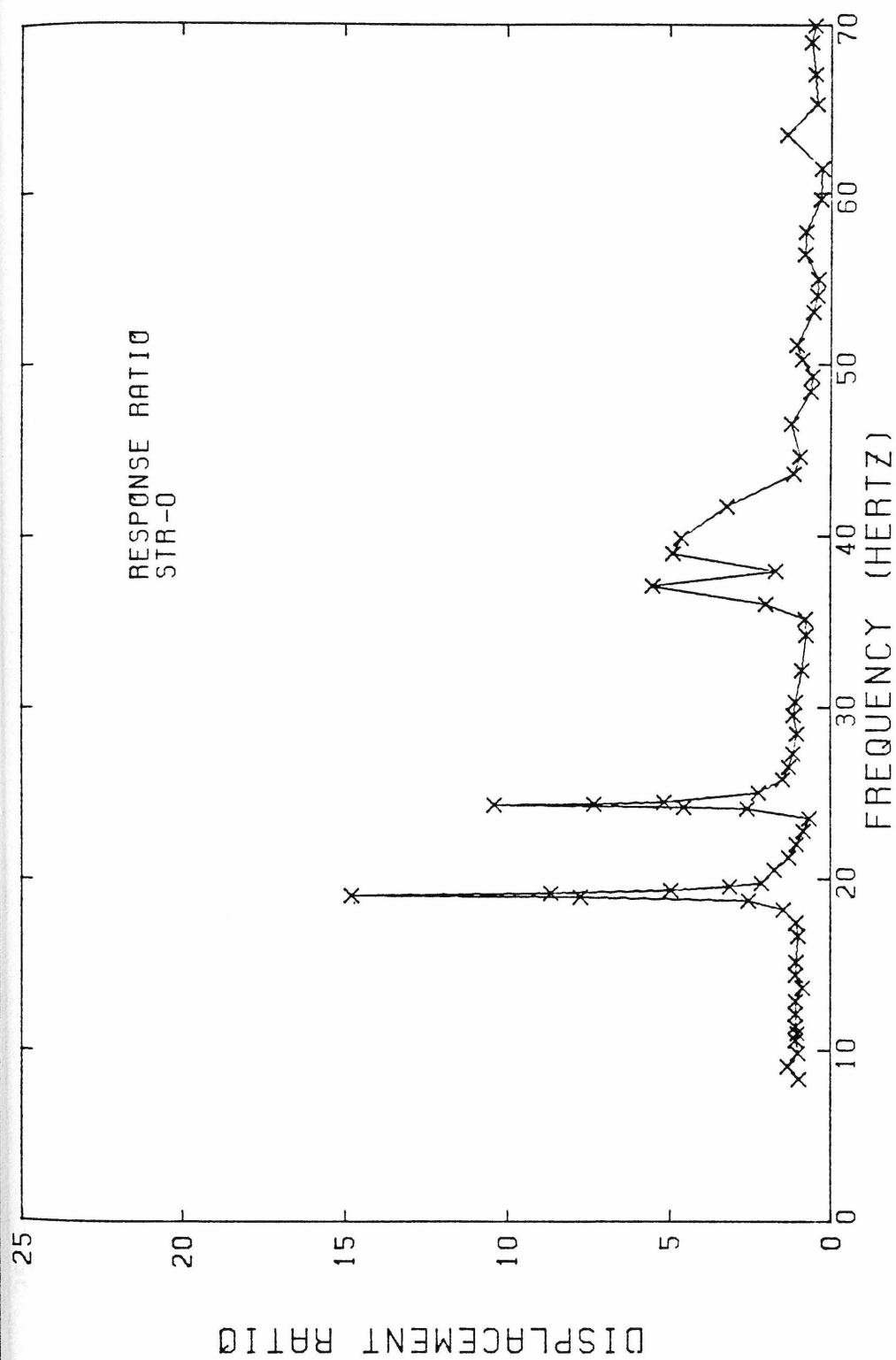


Figure 4.30(a). Calculated response ratio for superstructure translation (STR-0). Full frequency range, 0-70 Hz.

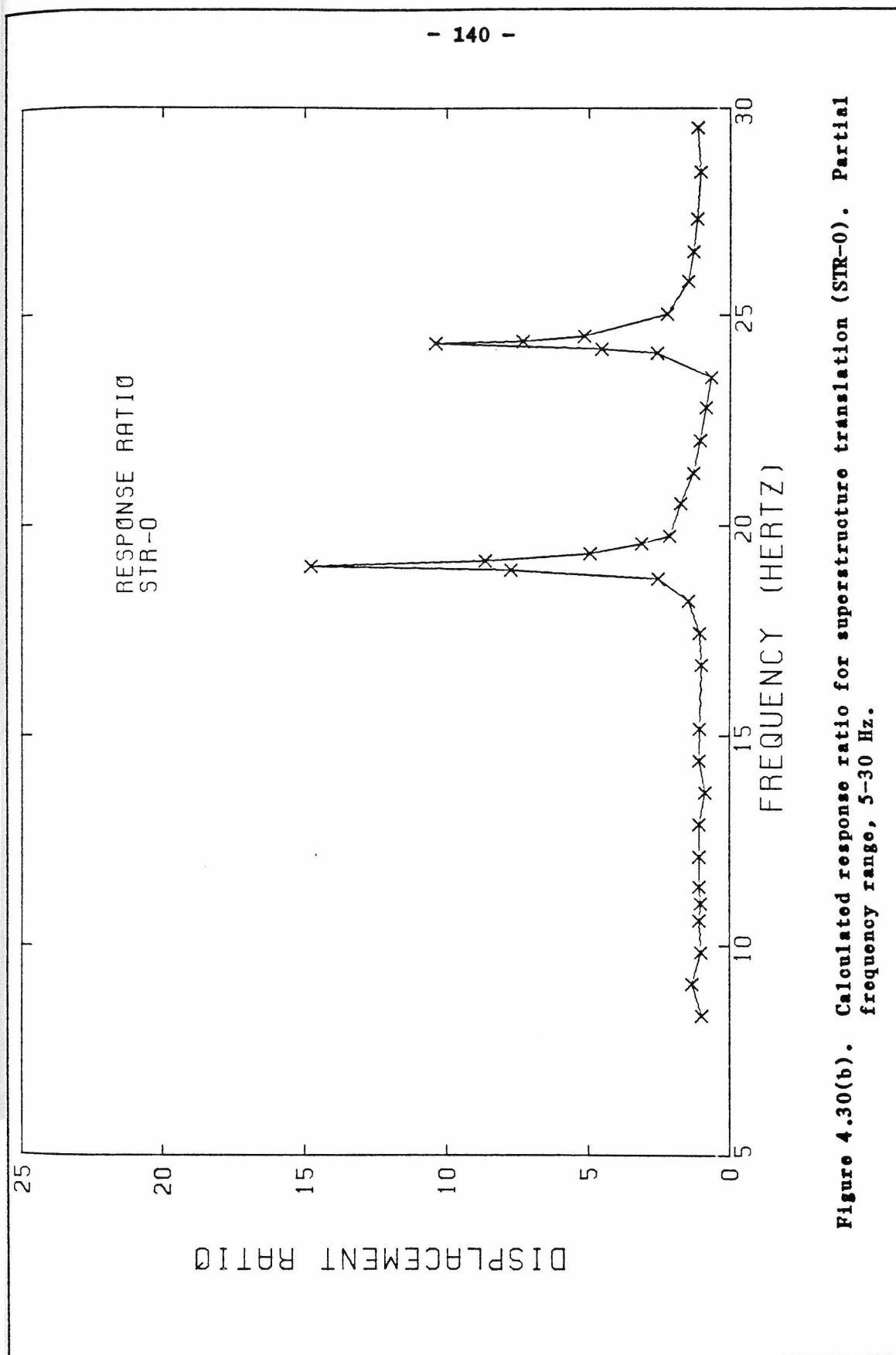


Figure 4.30(b). Calculated response ratio for superstructure translation (STR-0). Partial frequency range, 5-30 Hz.

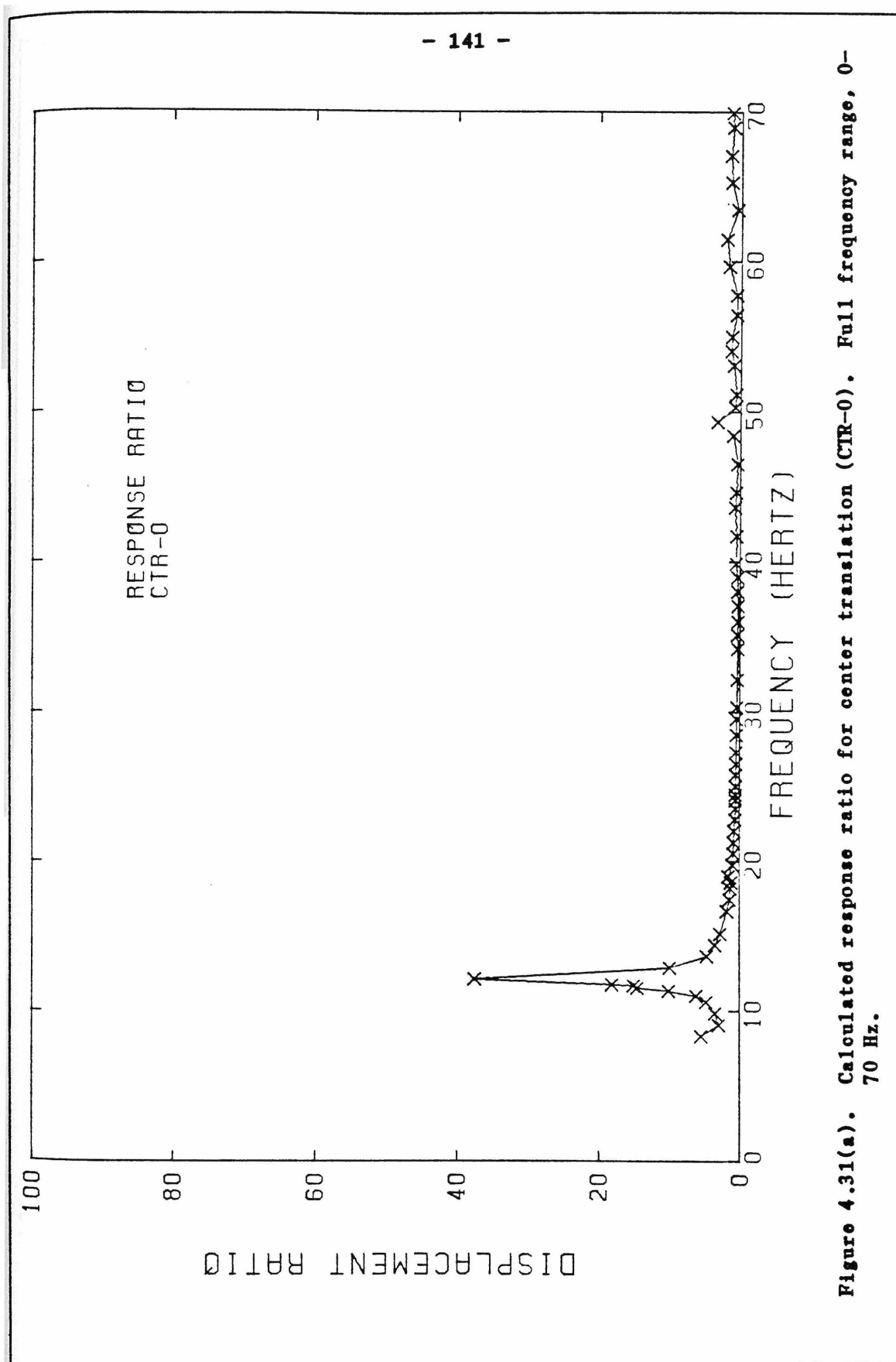


Figure 4.31(a). Calculated response ratio for center translation (CTR-0). Full frequency range, 0-70 Hz.

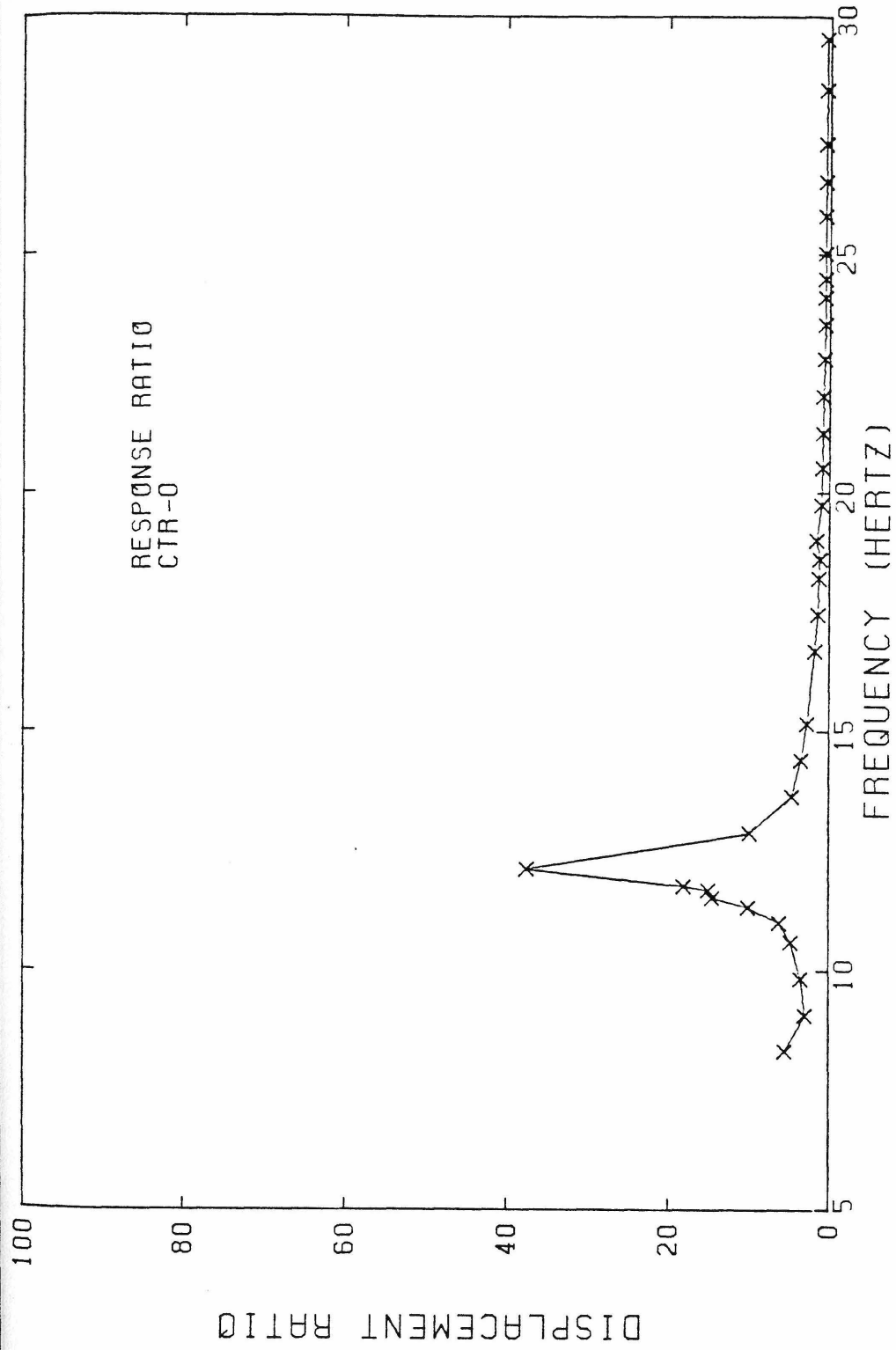


Figure 4.31(b). Calculated response ratio for center translation (CTR-0). Partial frequency range, 5-30 Hz.

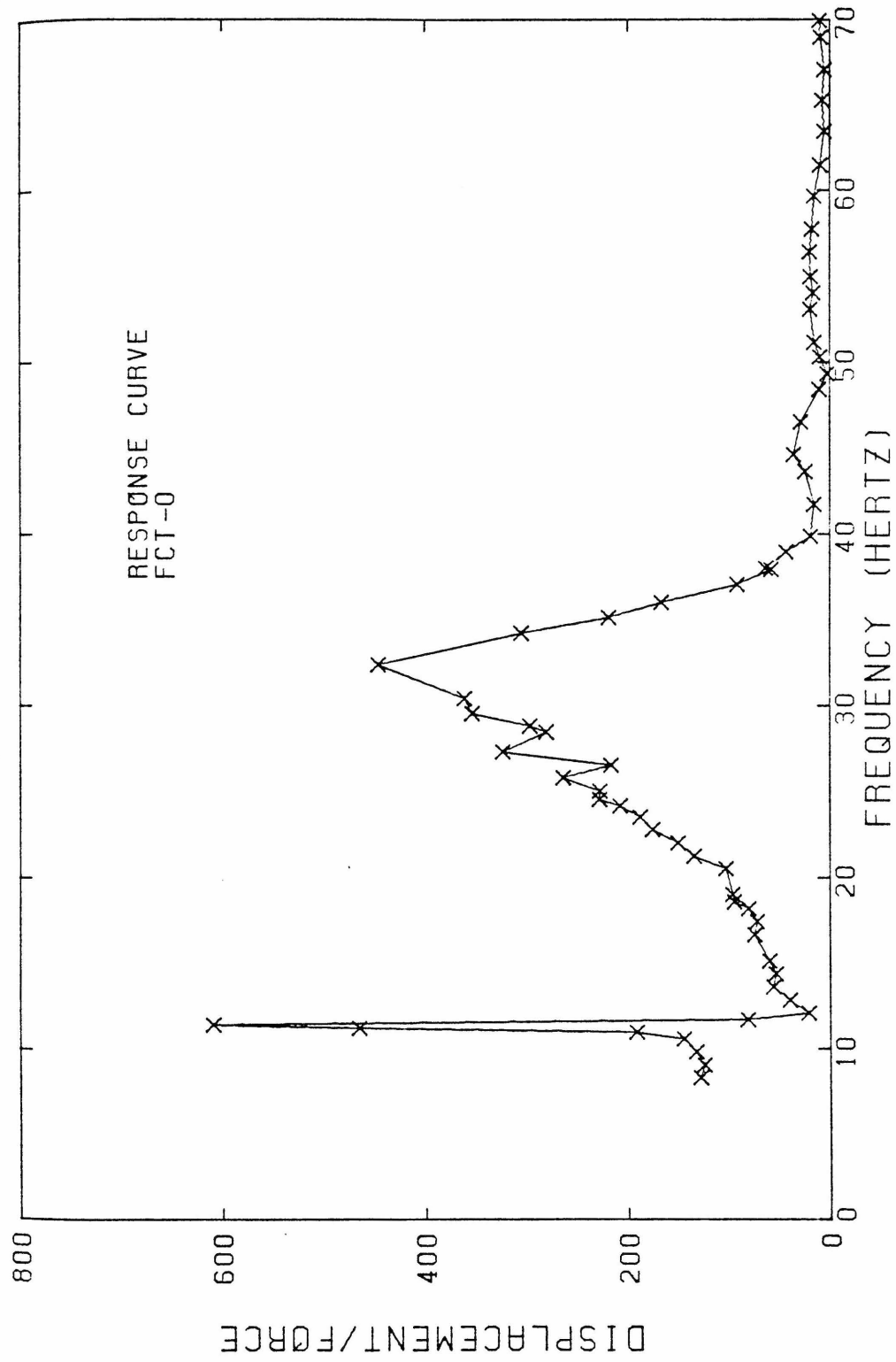


Figure 4.32. Response curve for foundation center translation (FCT-0).

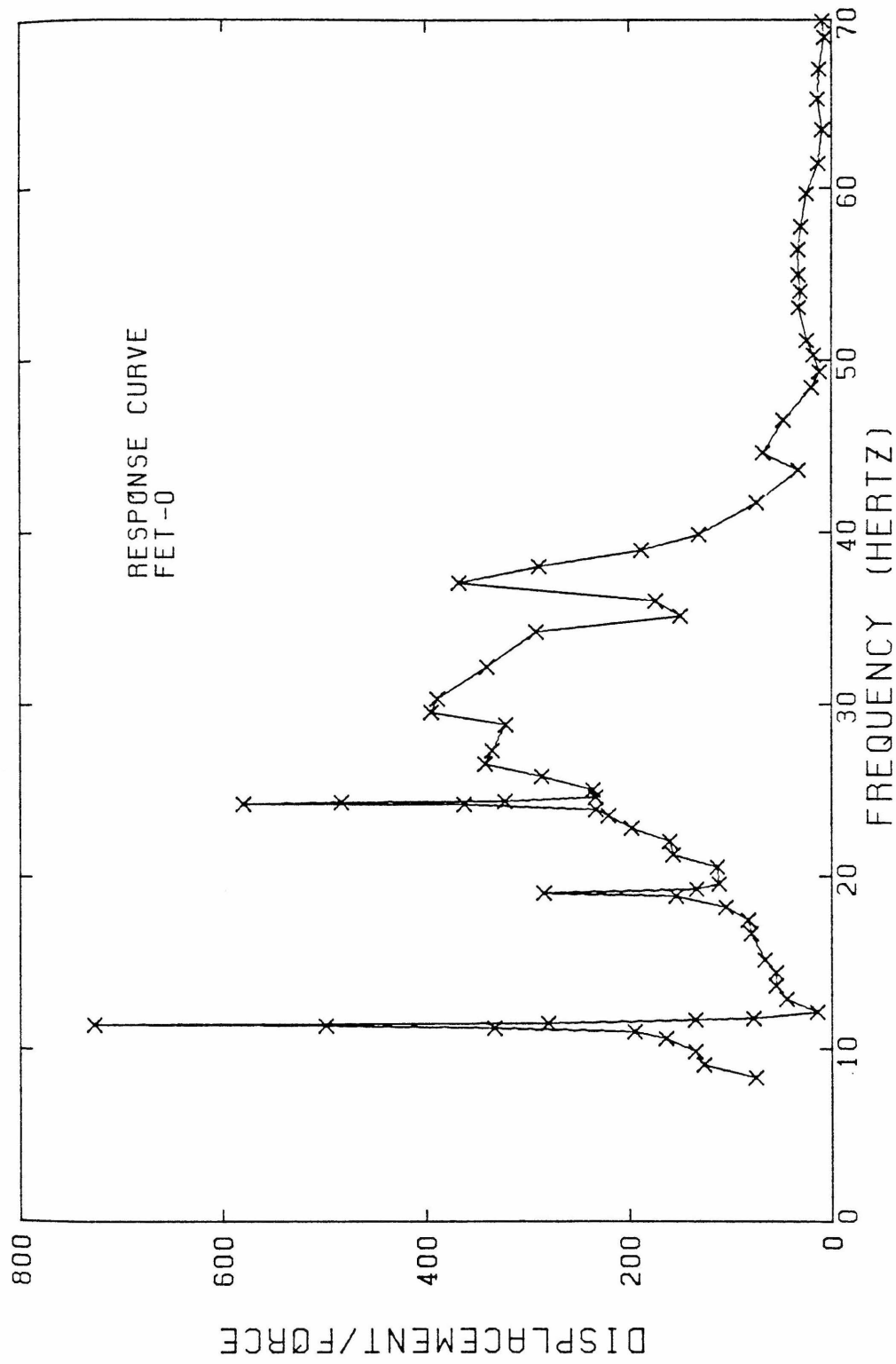


Figure 4.33. Response curve for foundation edge translation (FET-0).

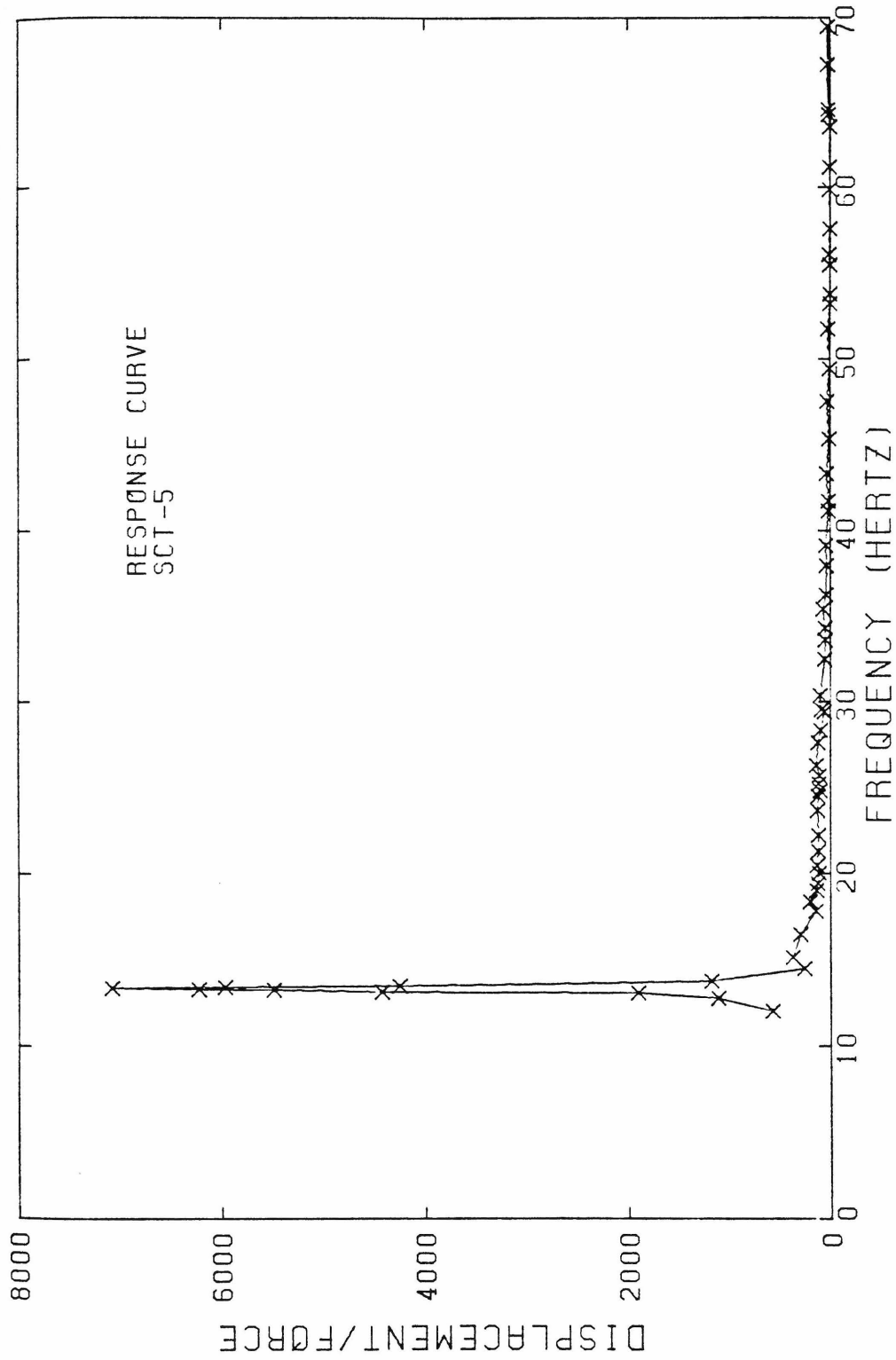


Figure 4.34(a). Response curve for superstructure center translation (SCT-5). Full frequency range, 0-70 Hz.

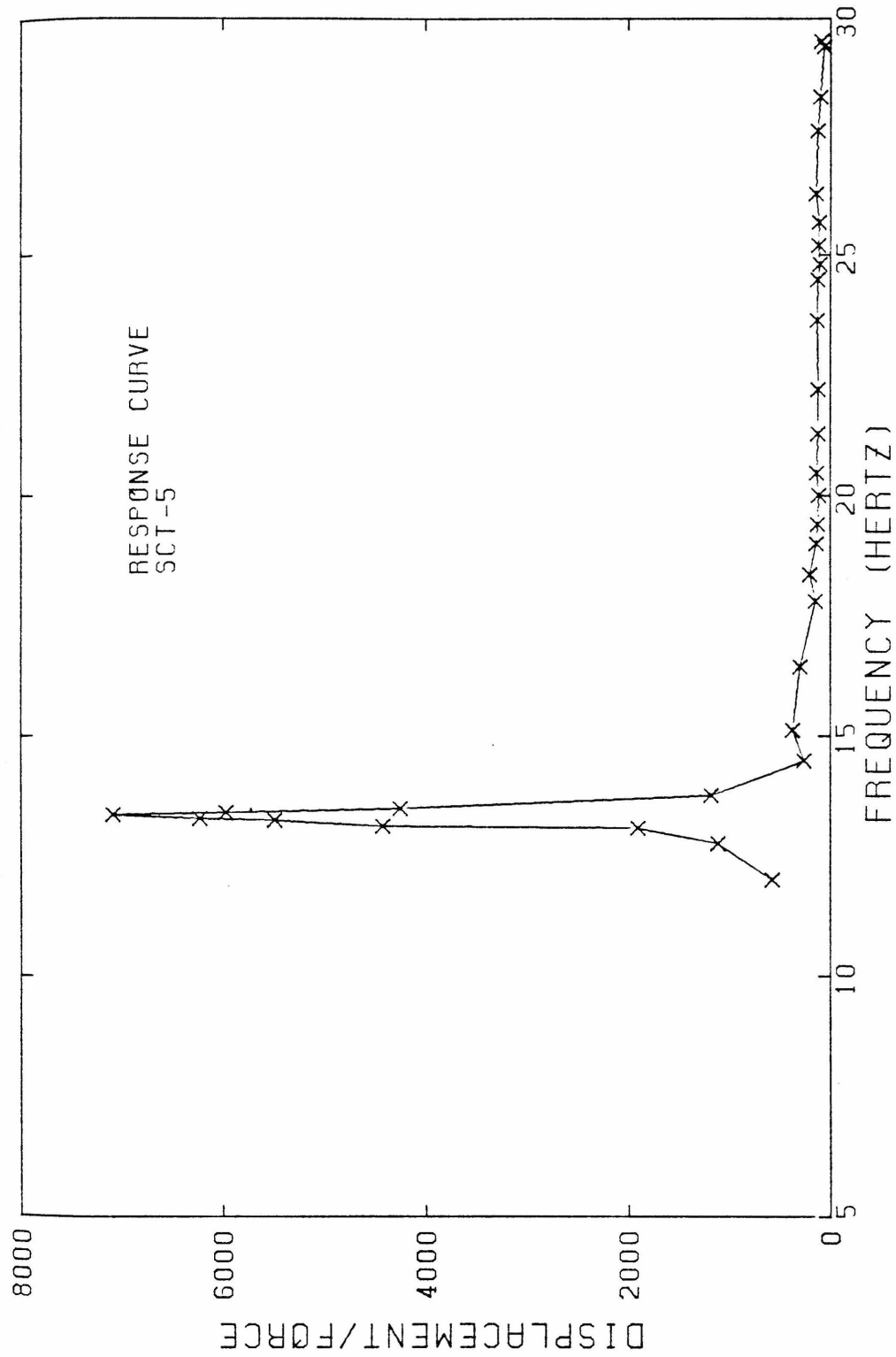


Figure 4.34(b). Response curve for superstructure center translation (SCT-5). Partial frequency range, 5-30 Hz.

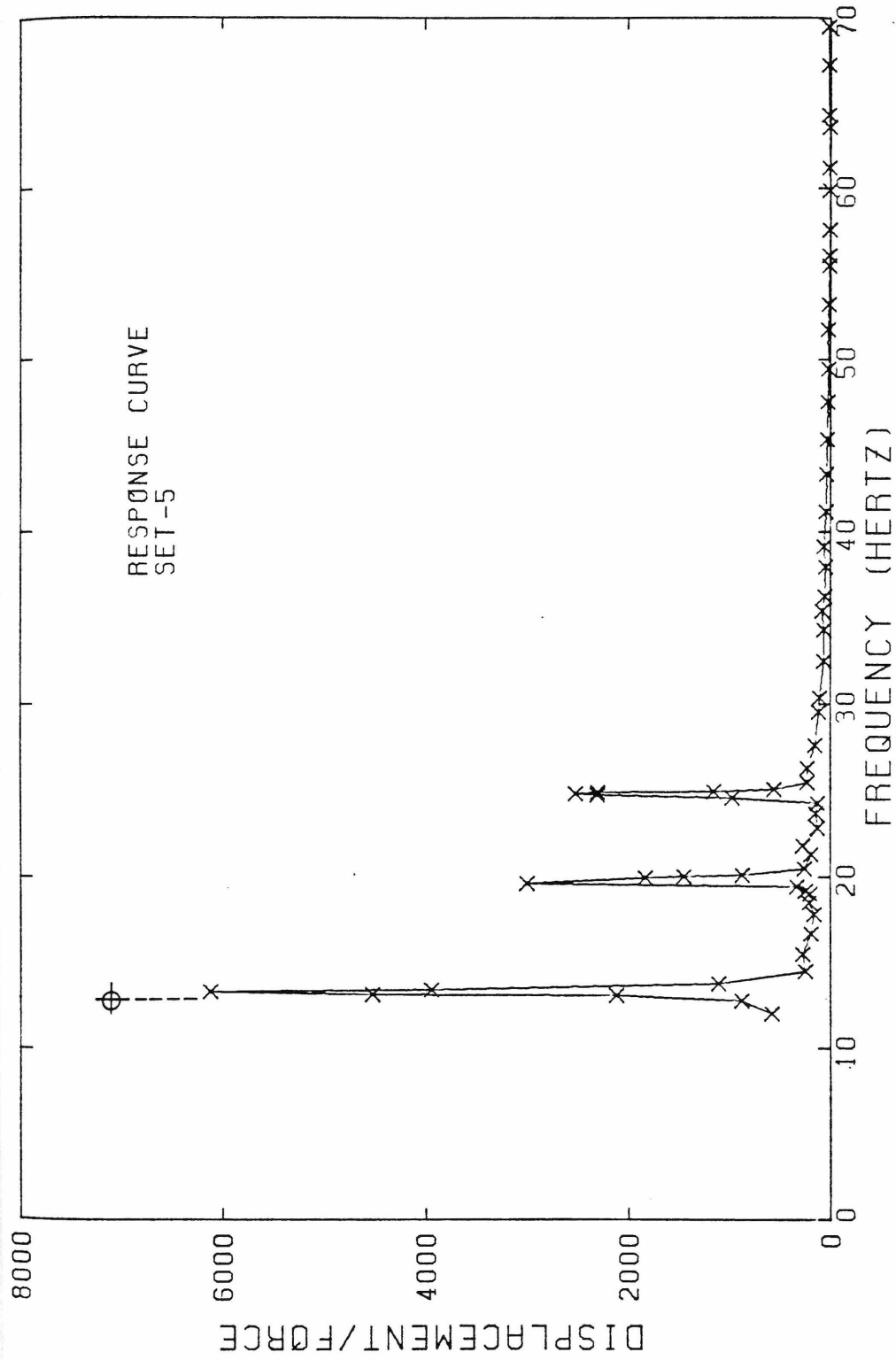


Figure 4.35(a). Response curve for superstructure edge translation (SET-5). Full frequency range, 0-70 Hz.

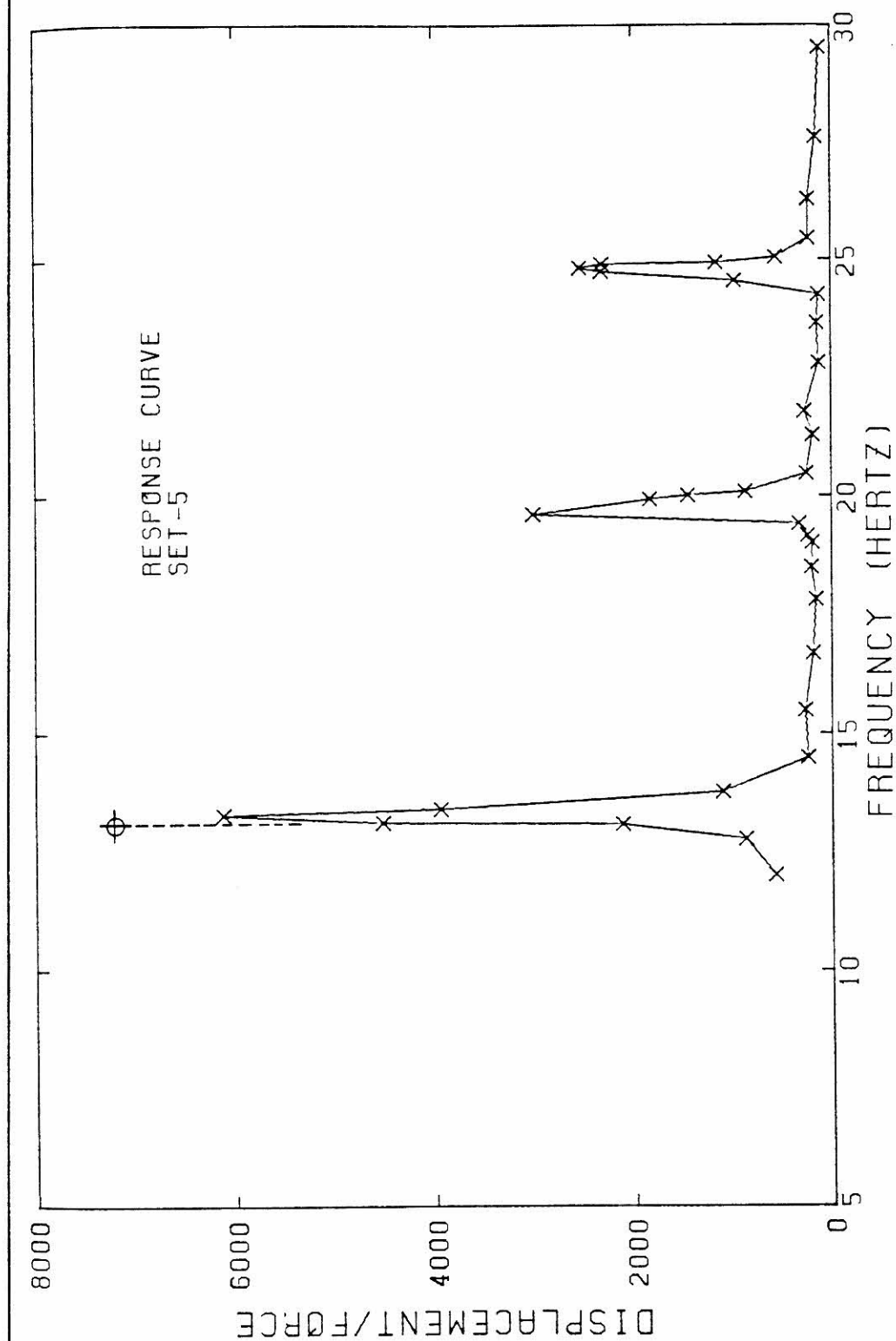


Figure 4.35(b). Response curve for superstructure edge translation (SET-5). Partial frequency range, 5-30 Hz.

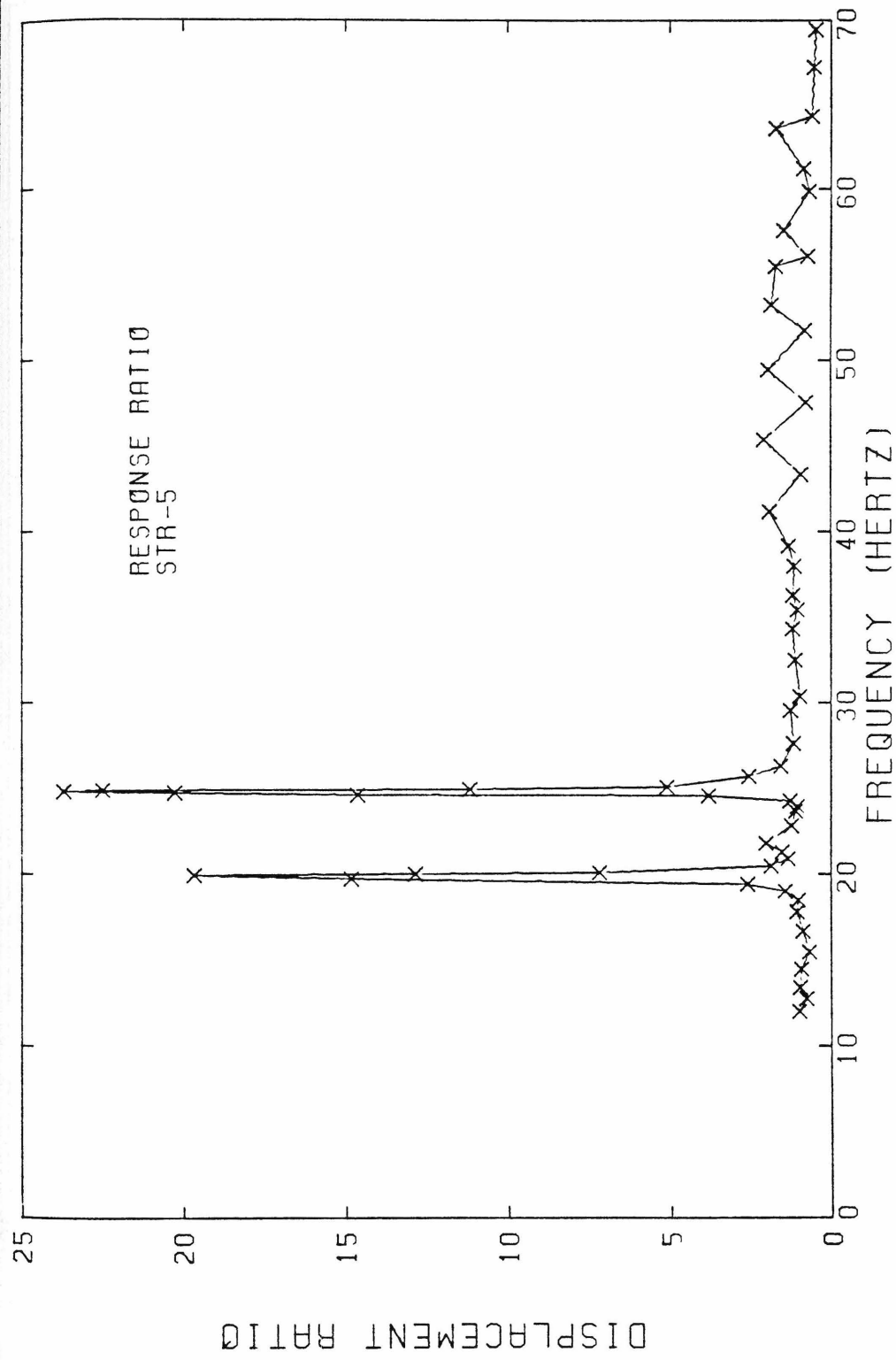


Figure 4.36(a). Calculated response ratio for superstructure translation (STR-5). Full frequency range, 0-70 Hz.

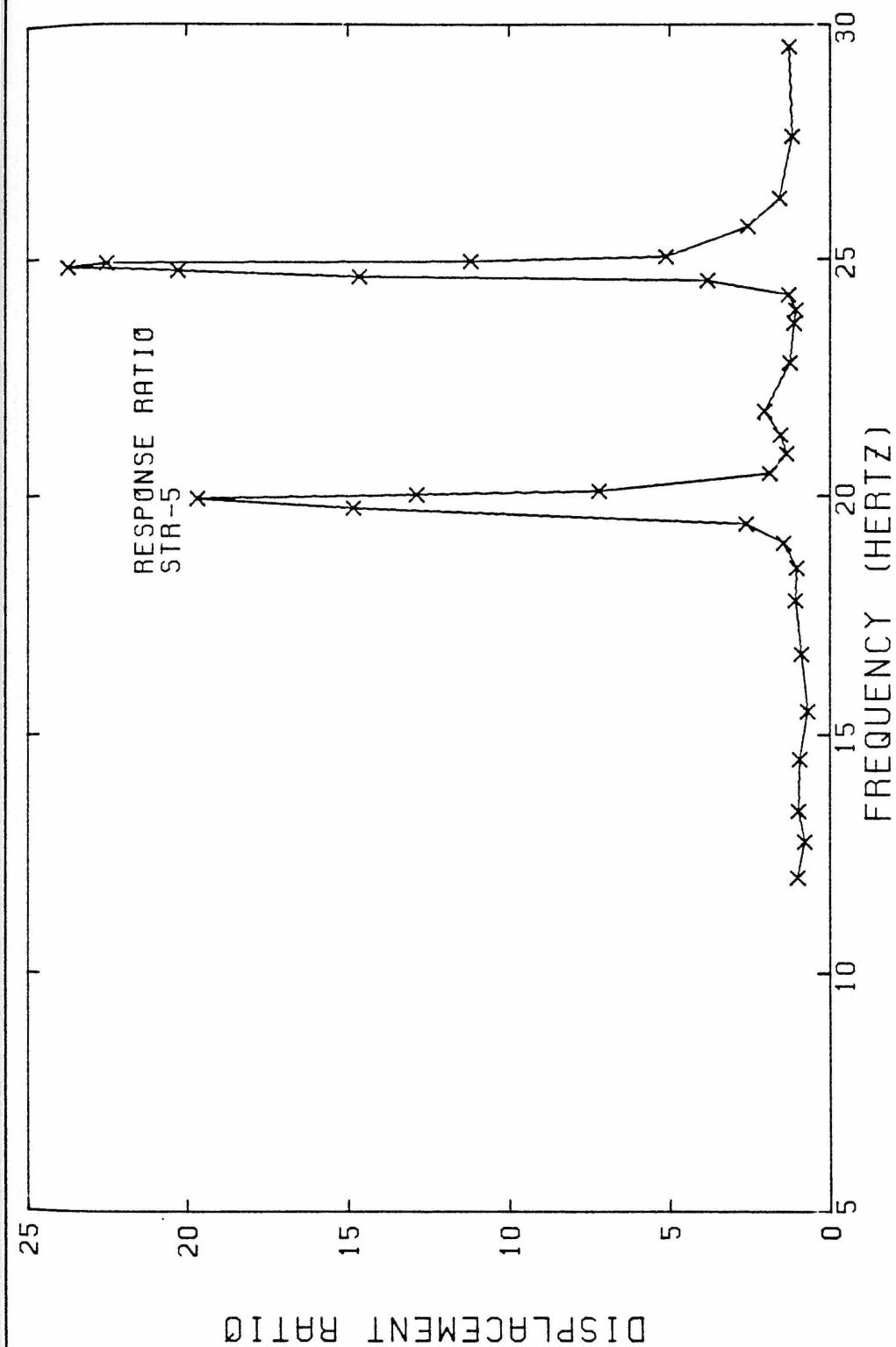


Figure 4.36(b). Calculated response ratio for superstructure translation (STR-5). Partial frequency range, 5-30 Hz.

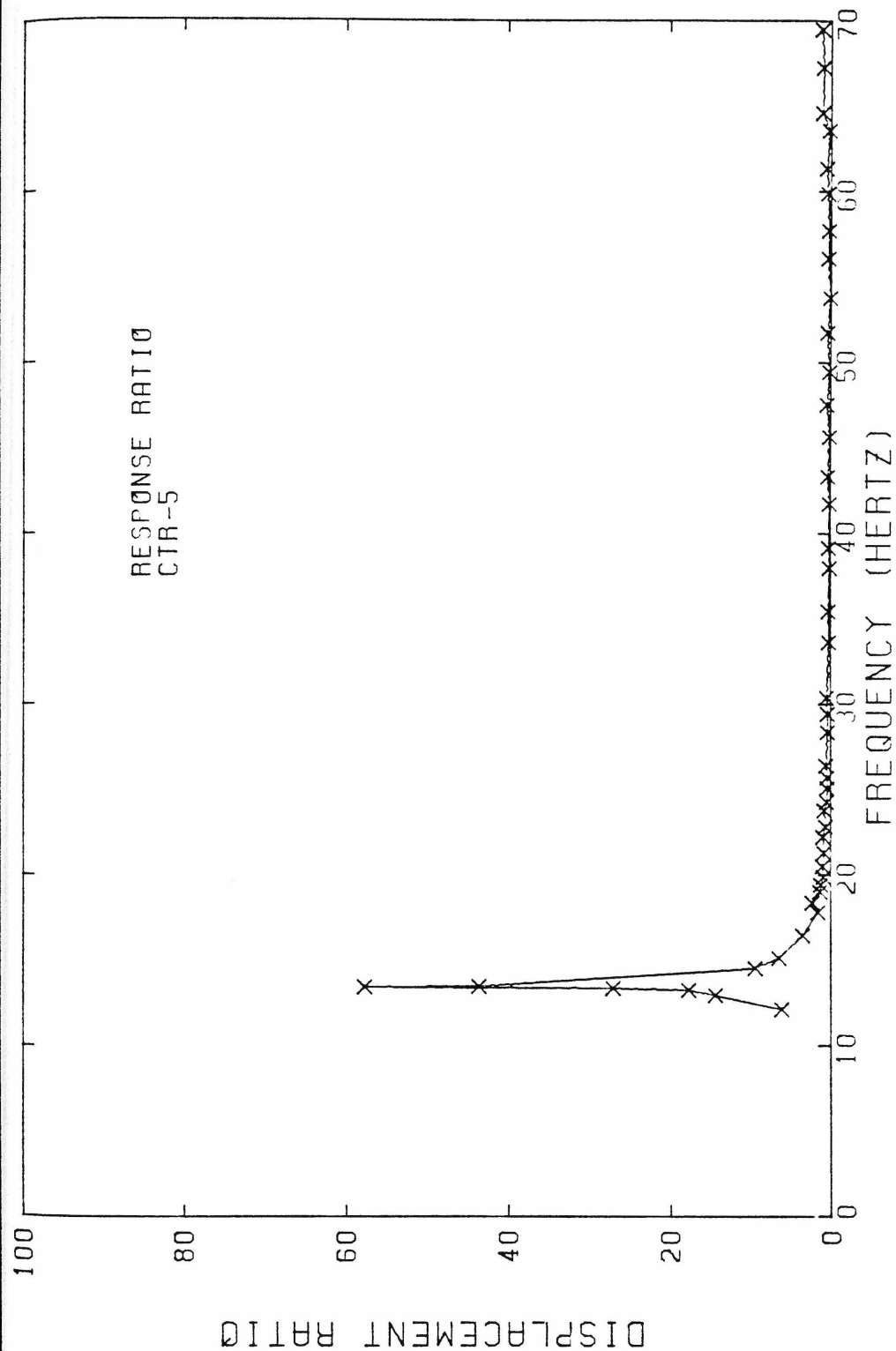


Figure 4.37(a). Calculated response ratio for center translation (CTR-5). Full frequency range, 0-70 Hz.

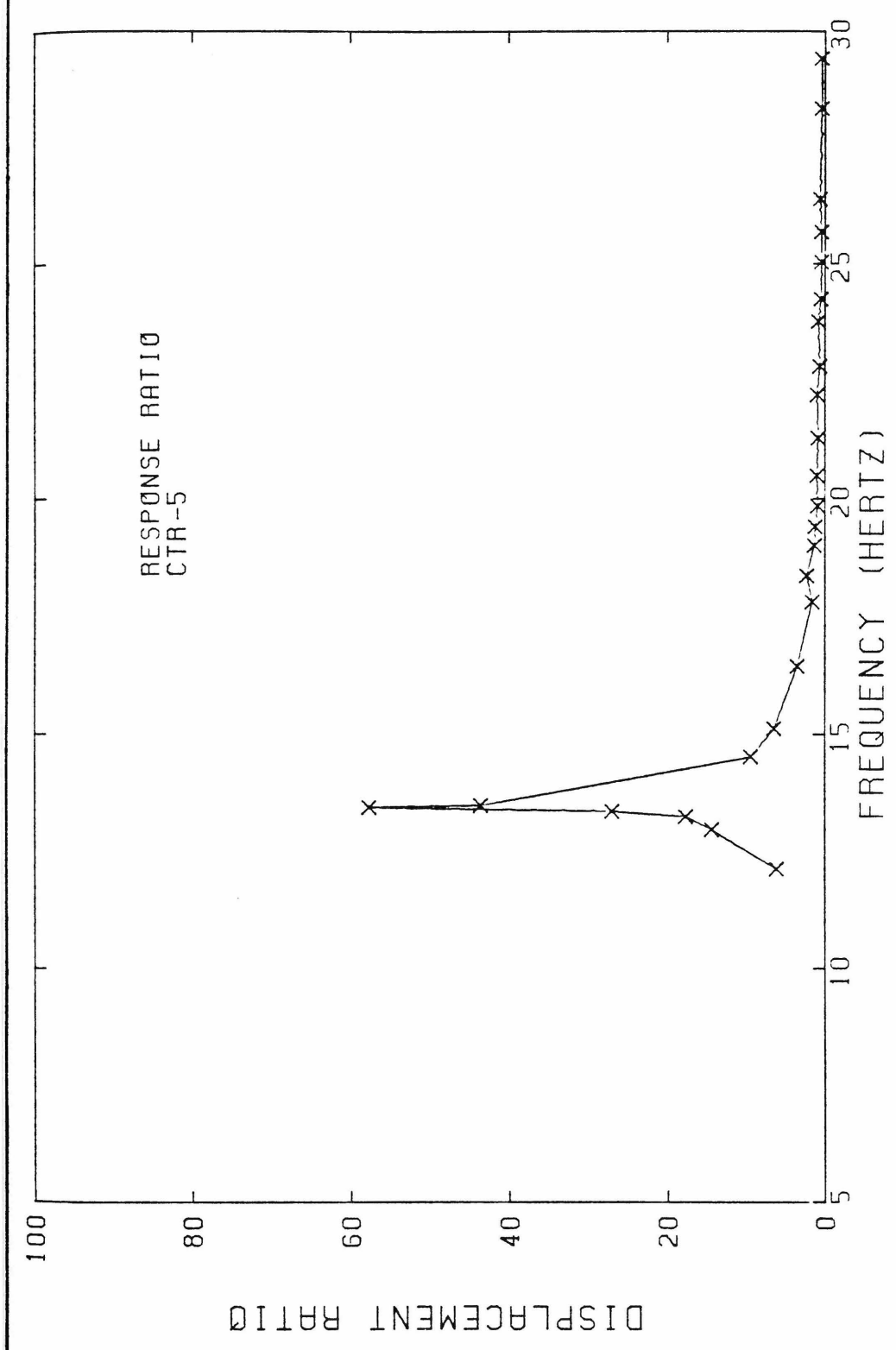


Figure 4.37(b). Calculated response ratio for center translation (CTR-5). Partial frequency range, 5-30 Hz.

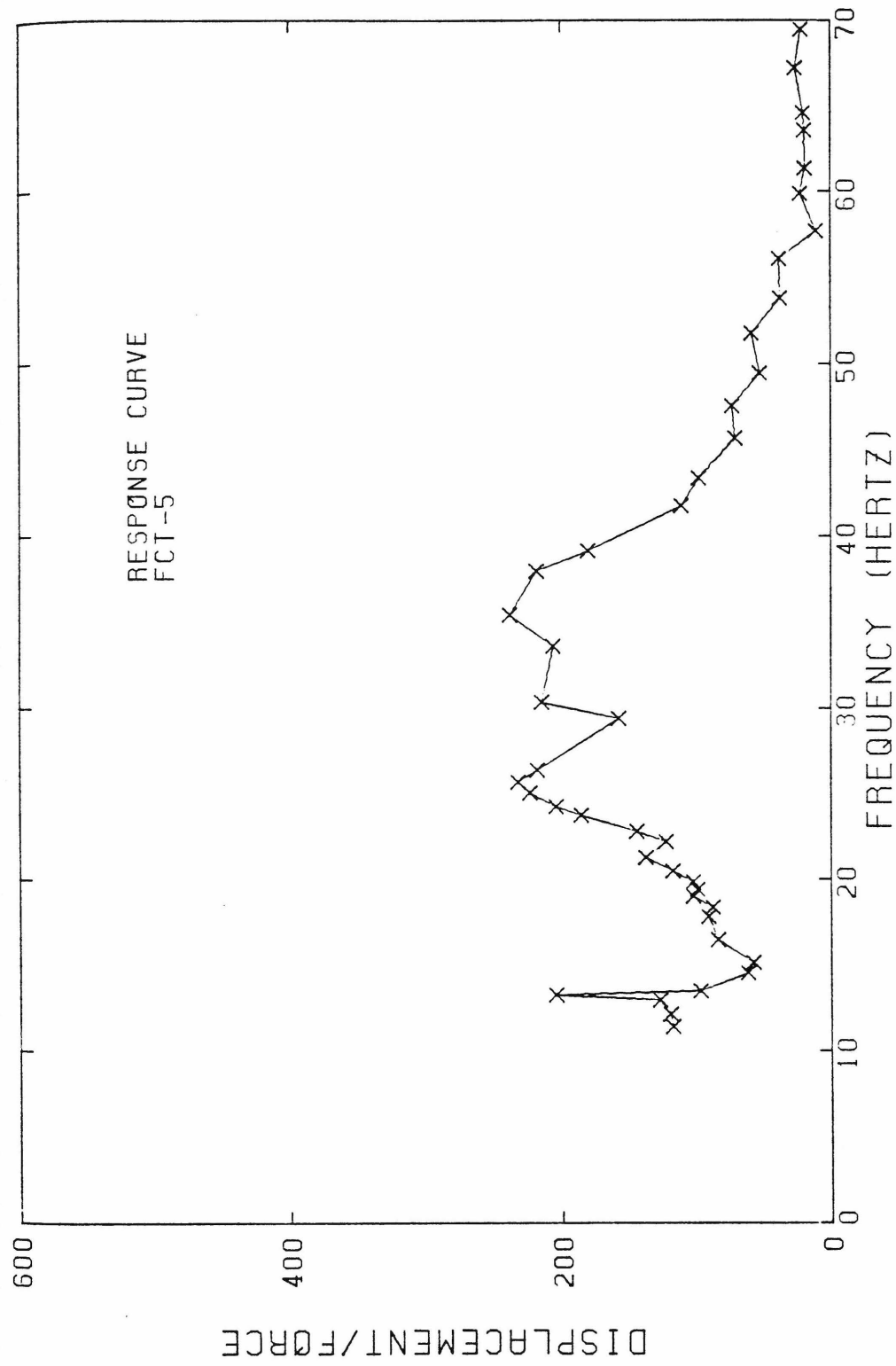


Figure 4.38. Response curve for foundation center translation (FCT-5).

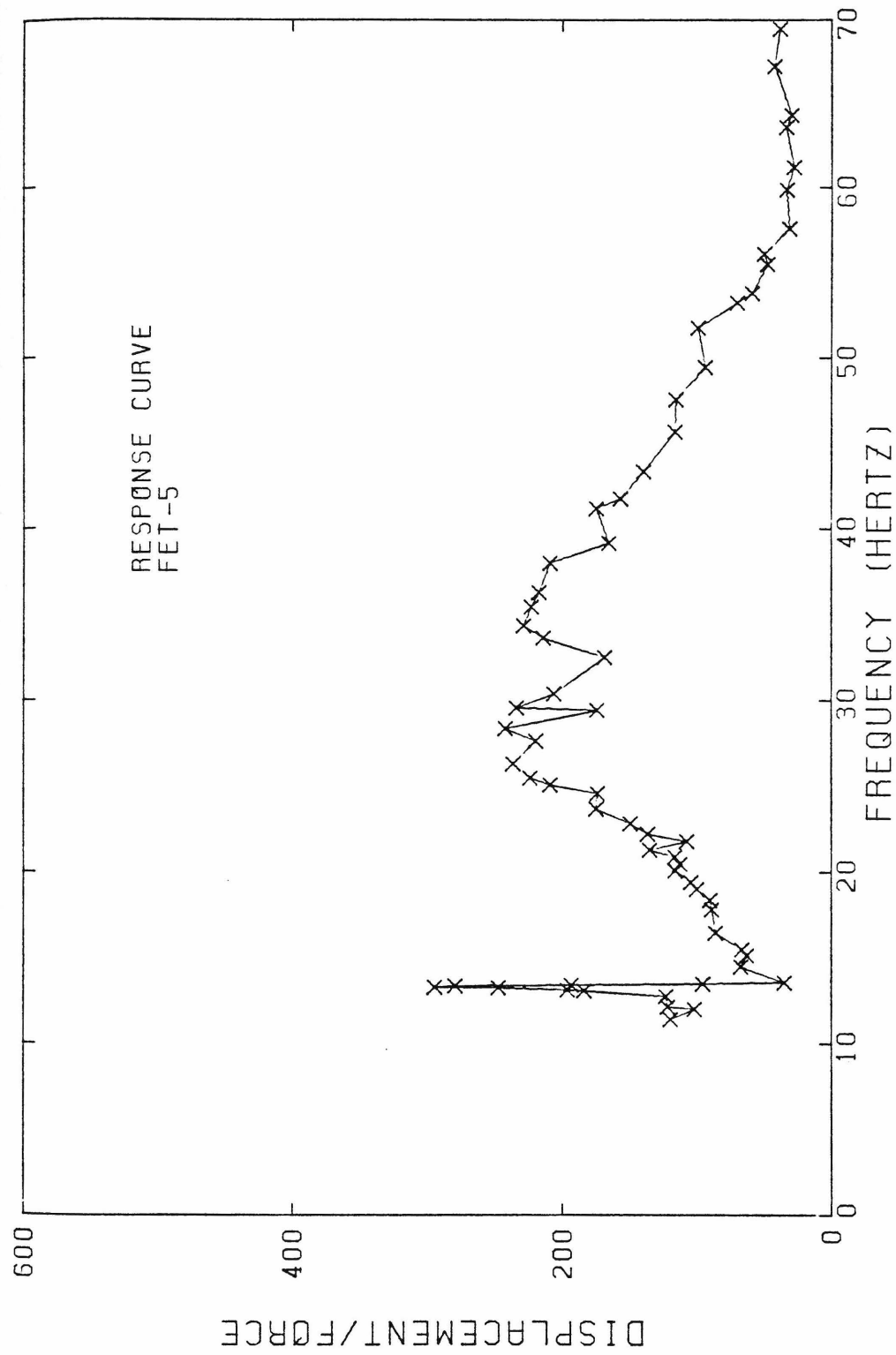


Figure 4.39. Response curve for foundation edge translation (FET-5).

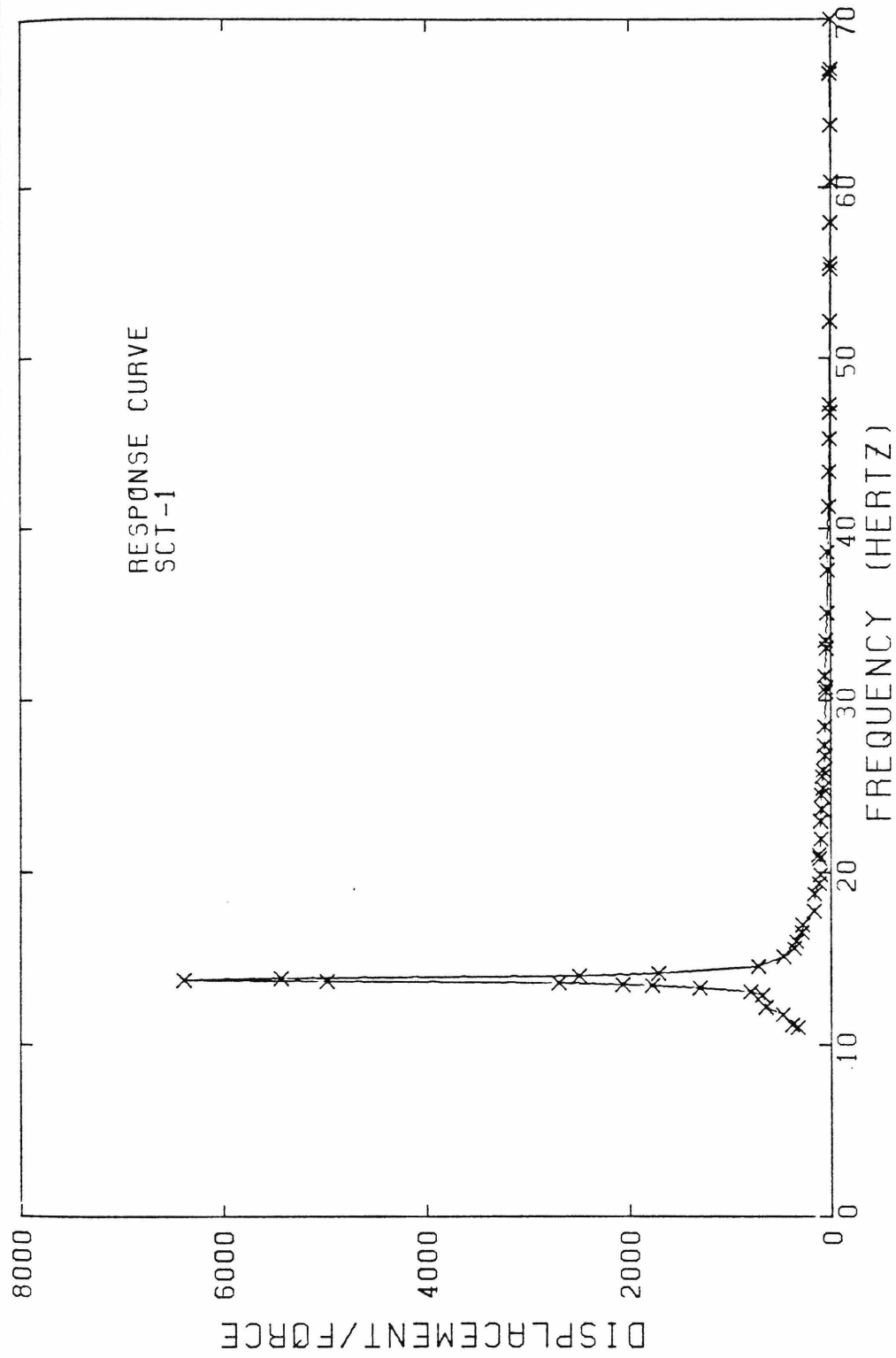


Figure 4.40(a). Response curve for superstructure center translation (SCT-1). Full frequency range, 0-70 Hz.

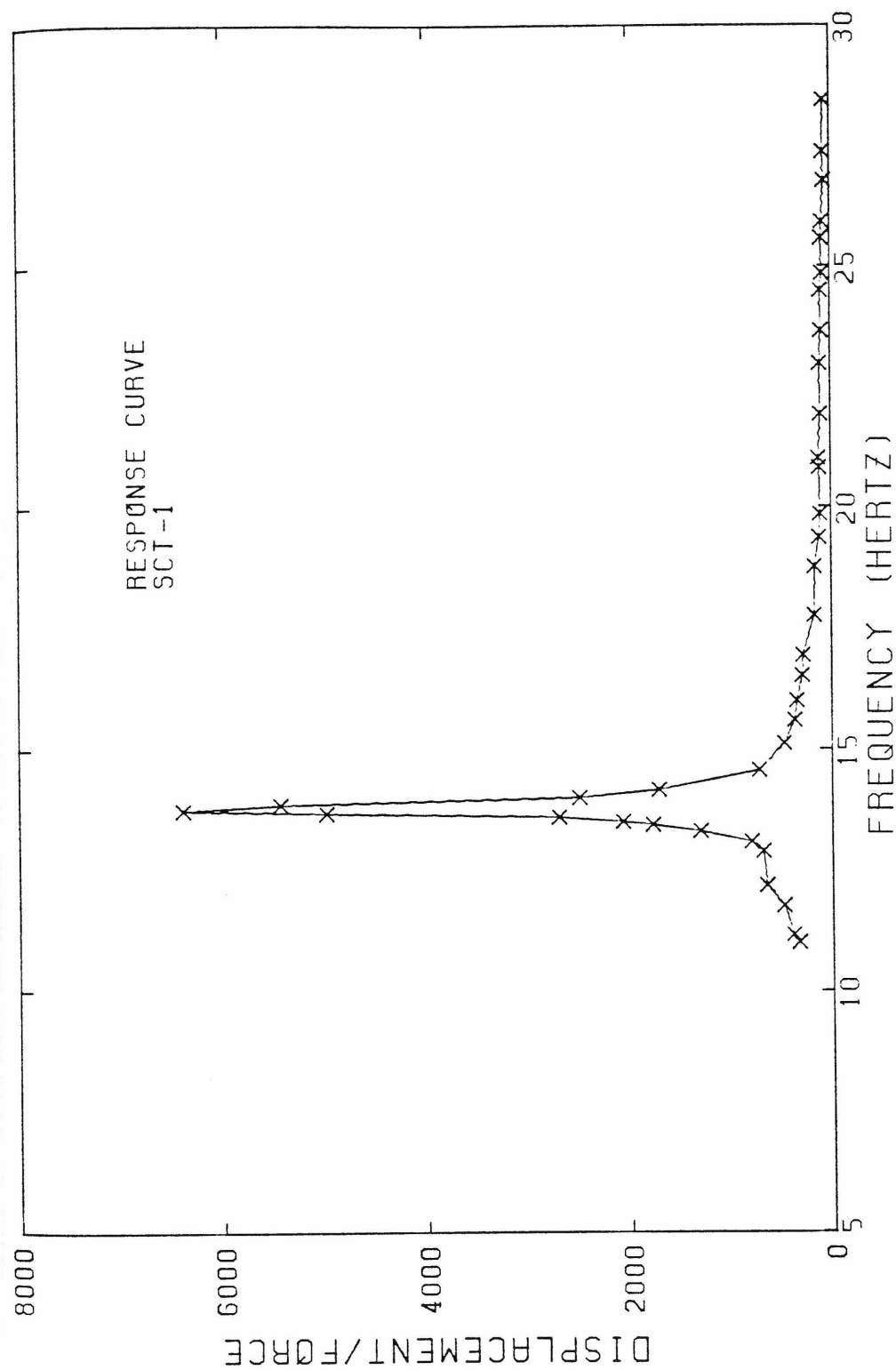


Figure 4.40(b). Response curve for superstructure center translation (SCT-1). Partial frequency range, 5-30 Hz.

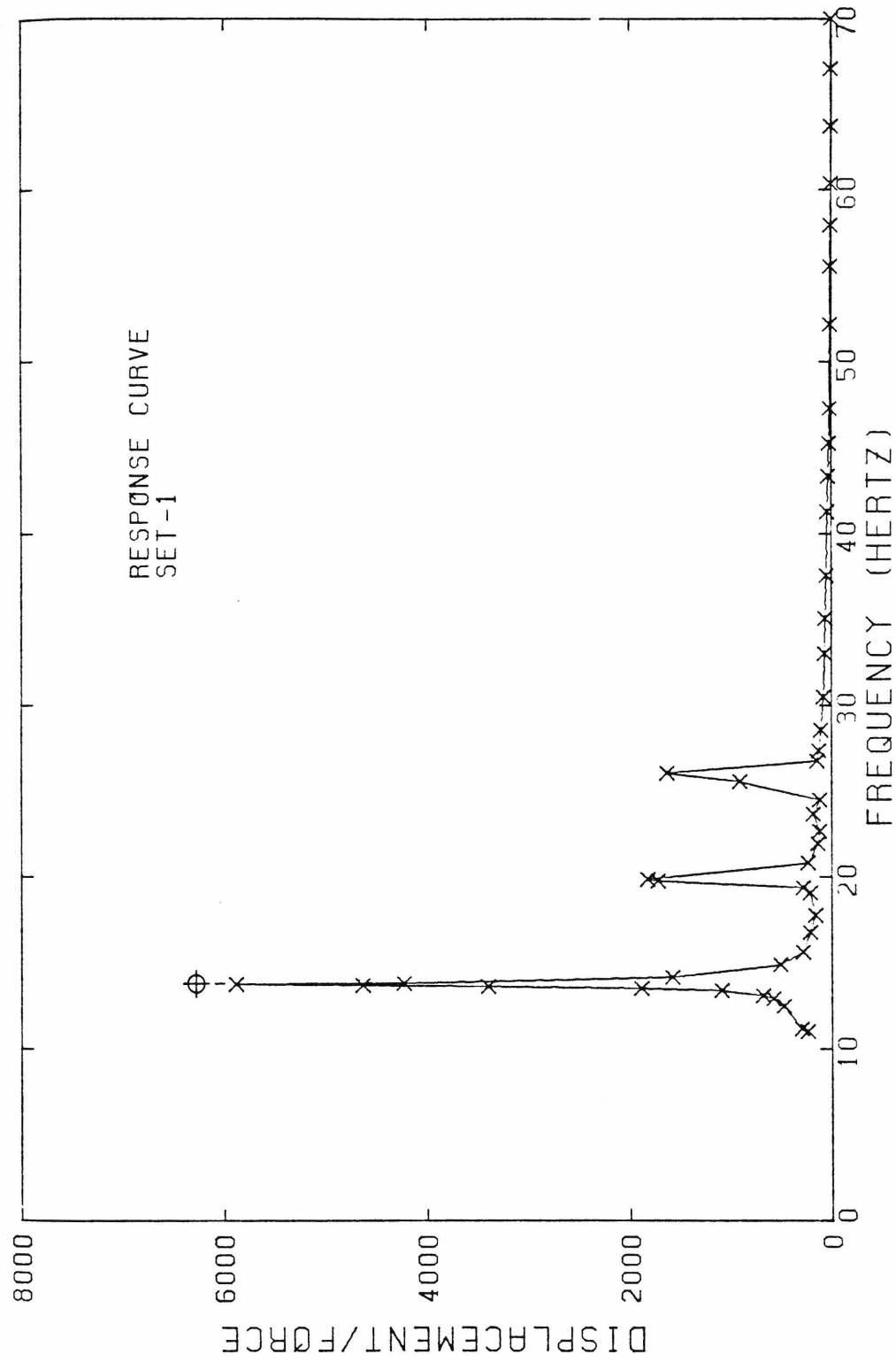


Figure 4.41(a). Response curve for superstructure edge translation (SET-1). Full frequency range, 0-70 Hz.

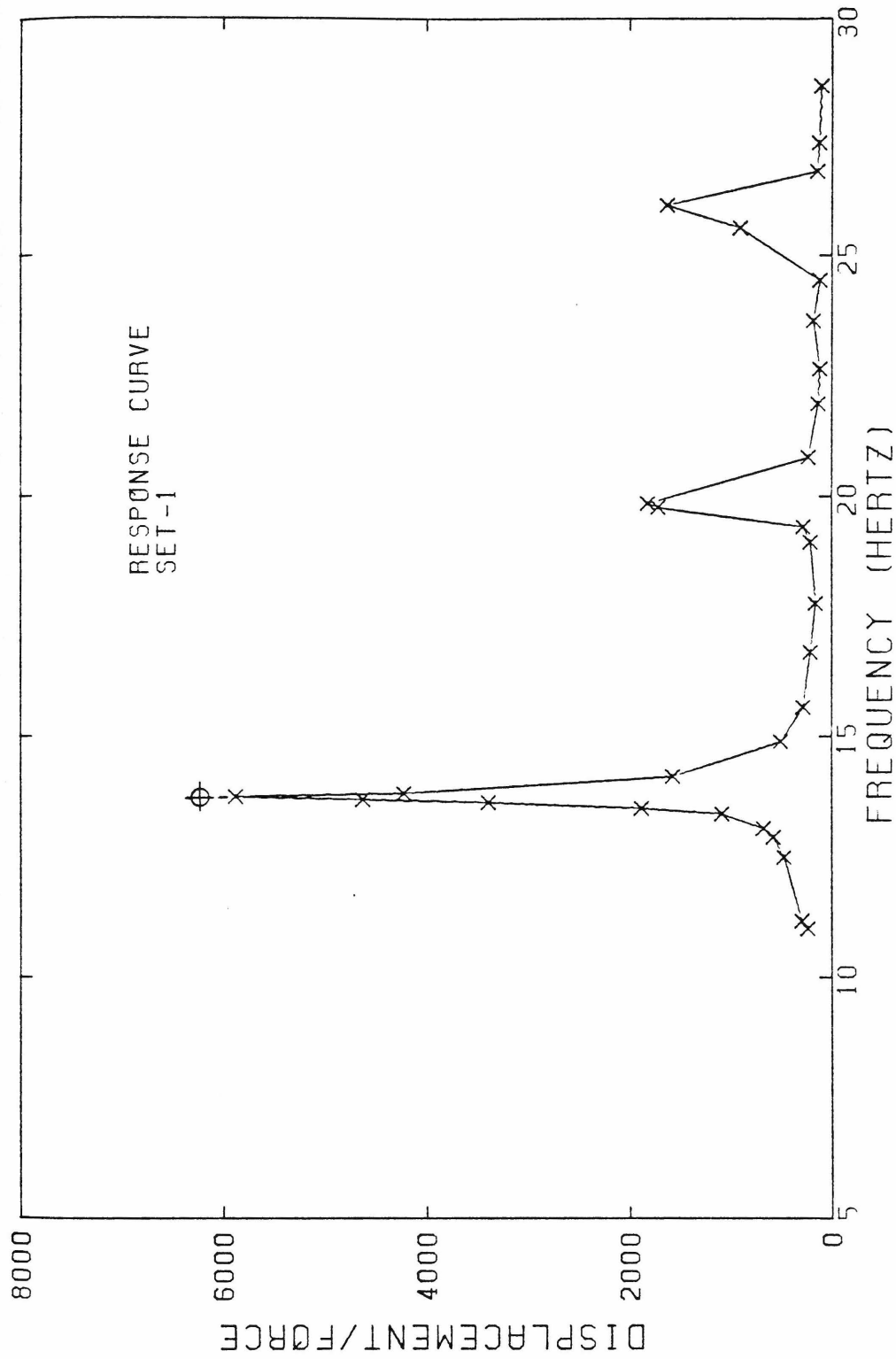


Figure 4.41(b). Response curve for superstructure edge translation (SET-1). Partial frequency range, 5-30 Hz.

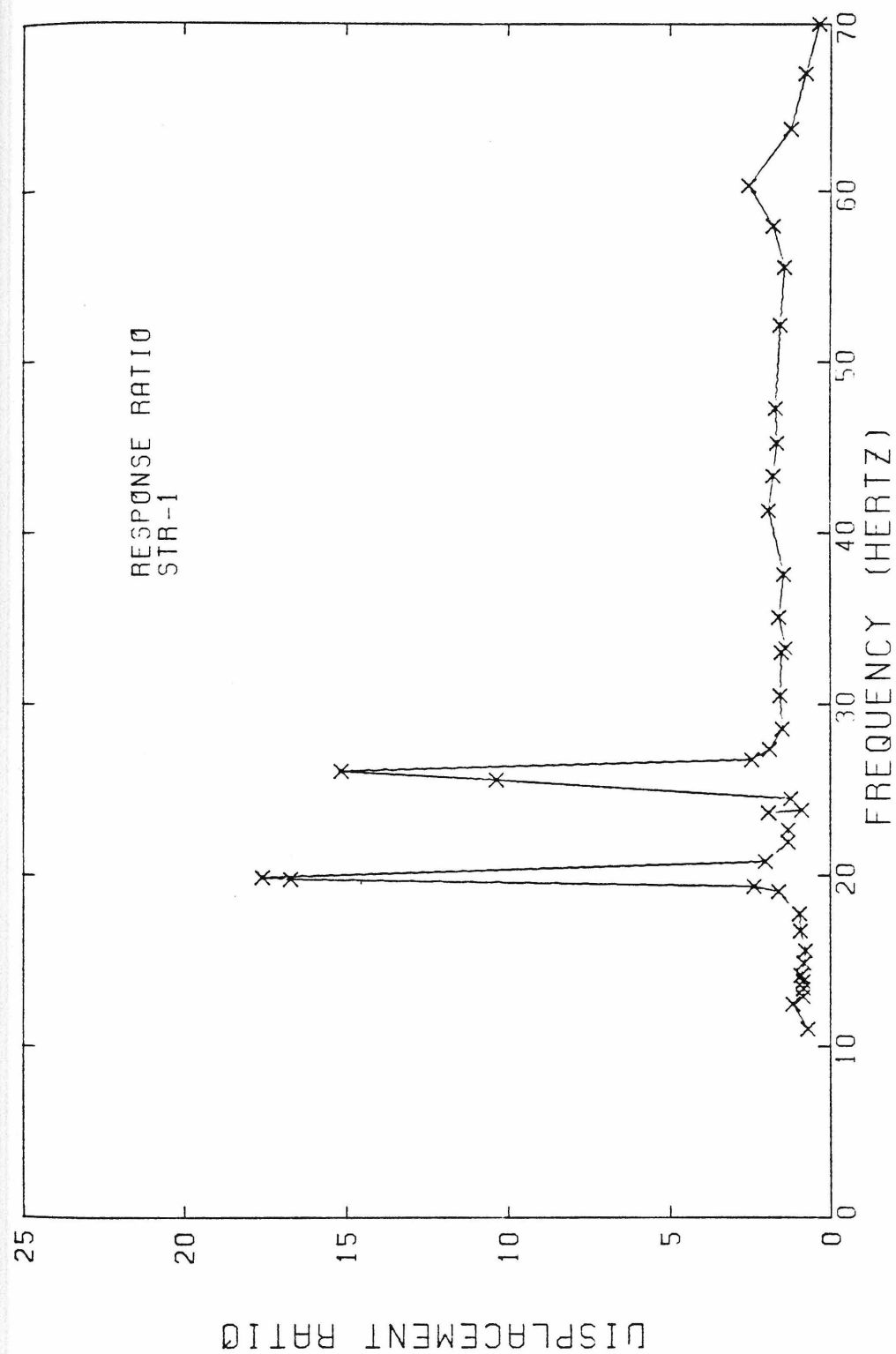


Figure 4.42(a). Calculated response ratio for superstructure translation (STR-1). Full frequency range, 0-70 Hz.

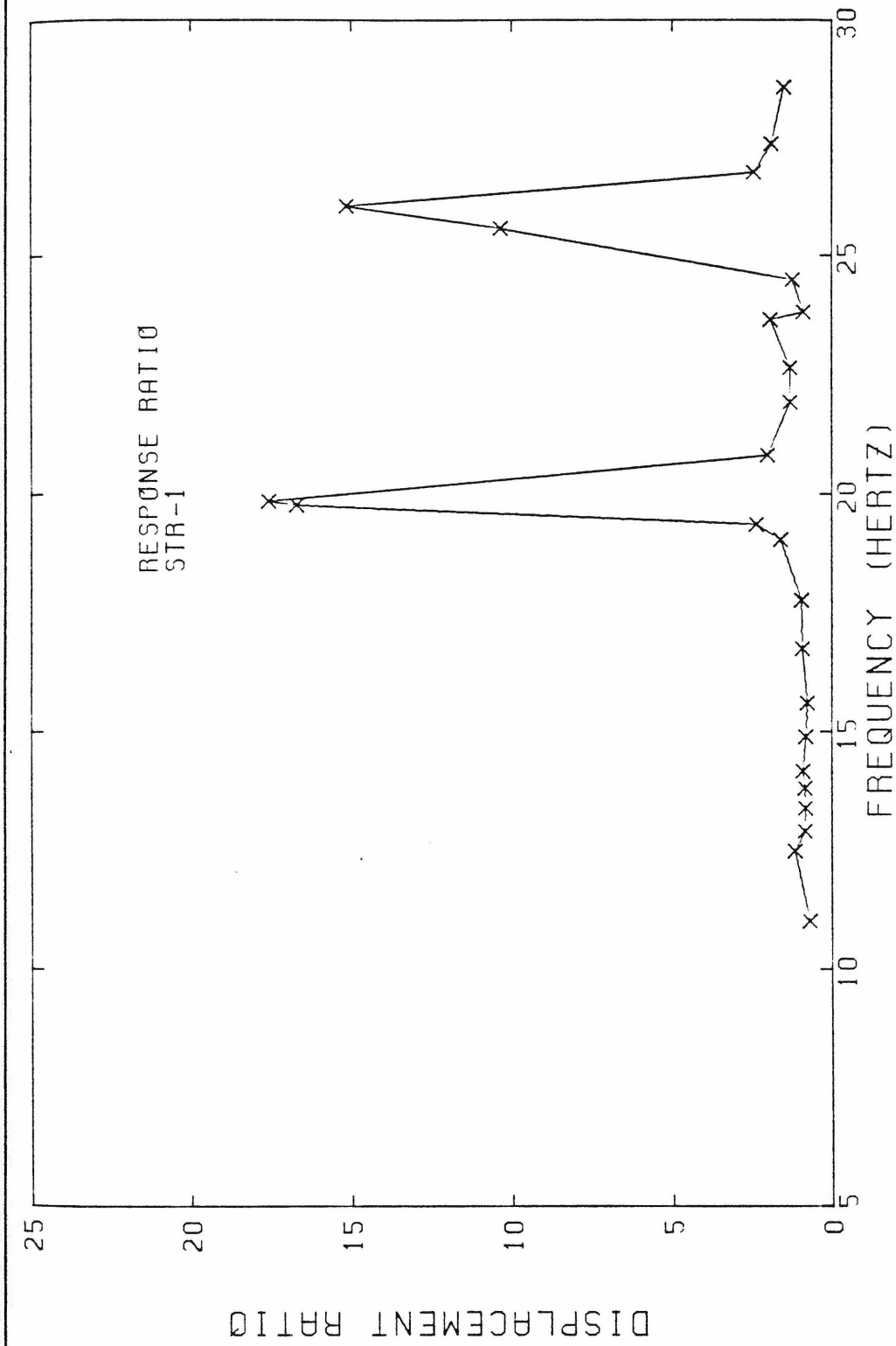


Figure 4.42(b). Calculated response ratio for superstructure translation (STR-1). Partial frequency range, 5-30 Hz.

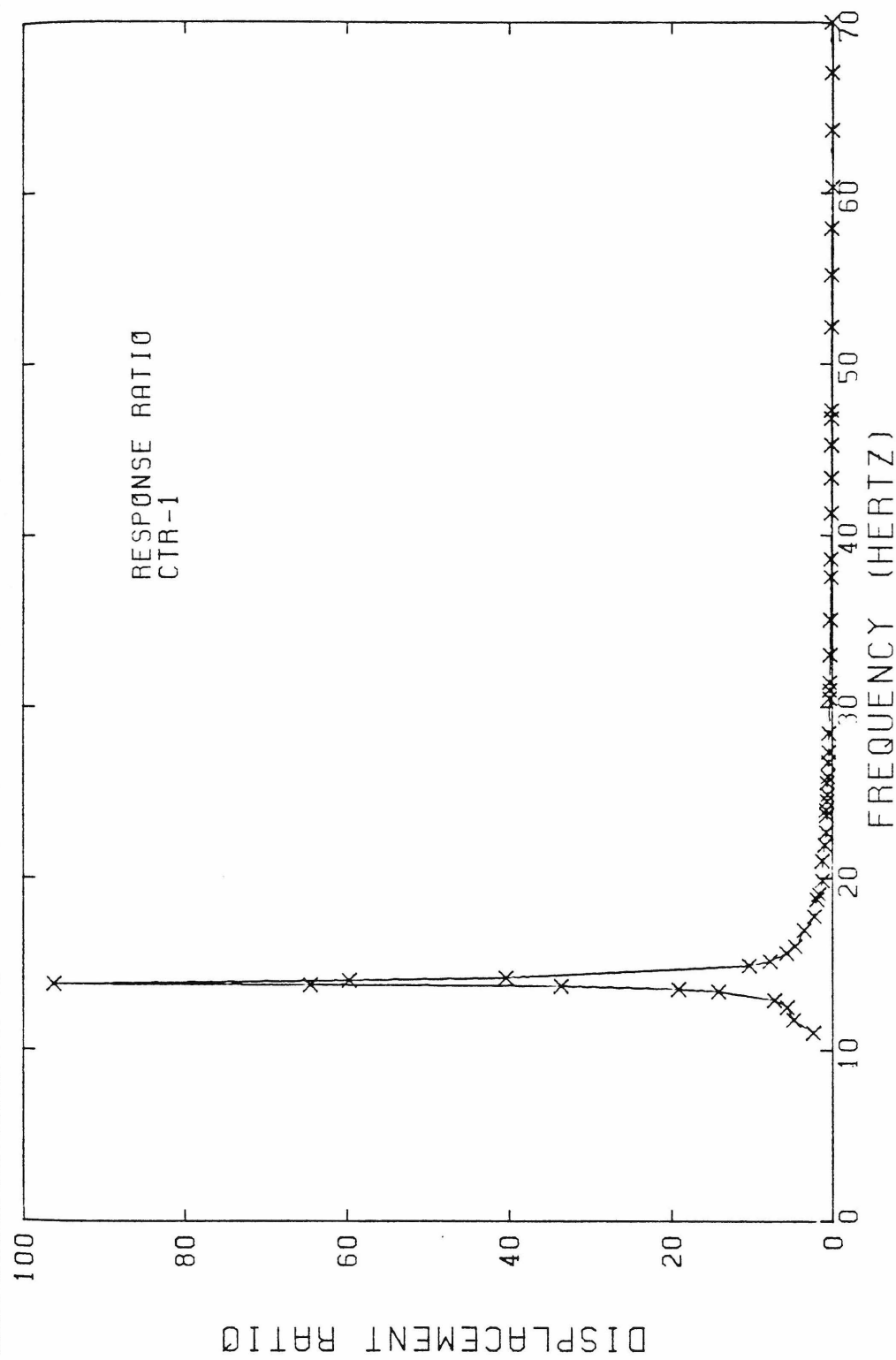


Figure 4.43(a). Calculated response ratio for center translation (CTR-1). Full frequency range, 0-70 Hz.

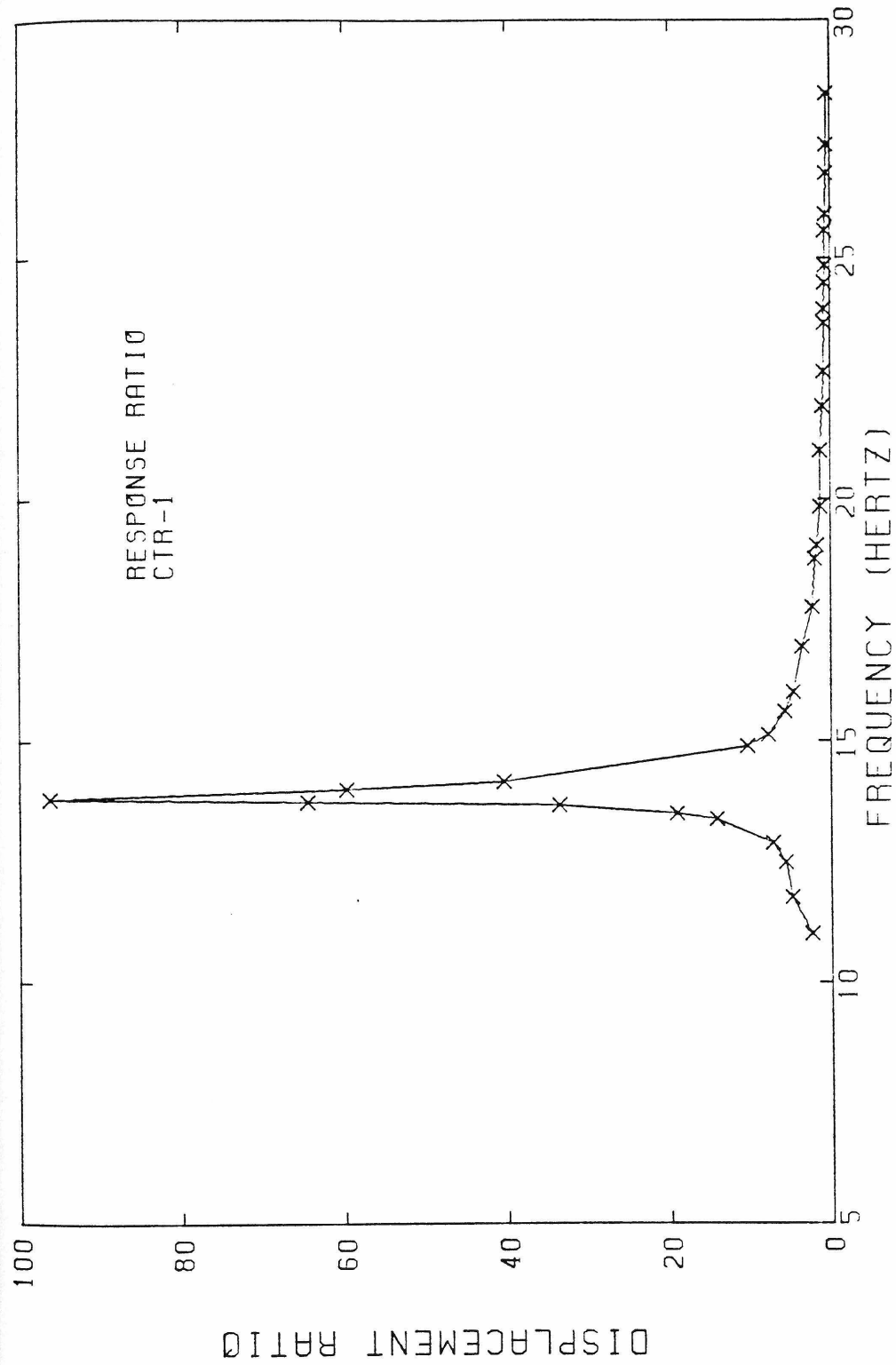


Figure 4.43(b). Calculated response ratio for center translation (CTR-1). Partial frequency range, 5-30 Hz.

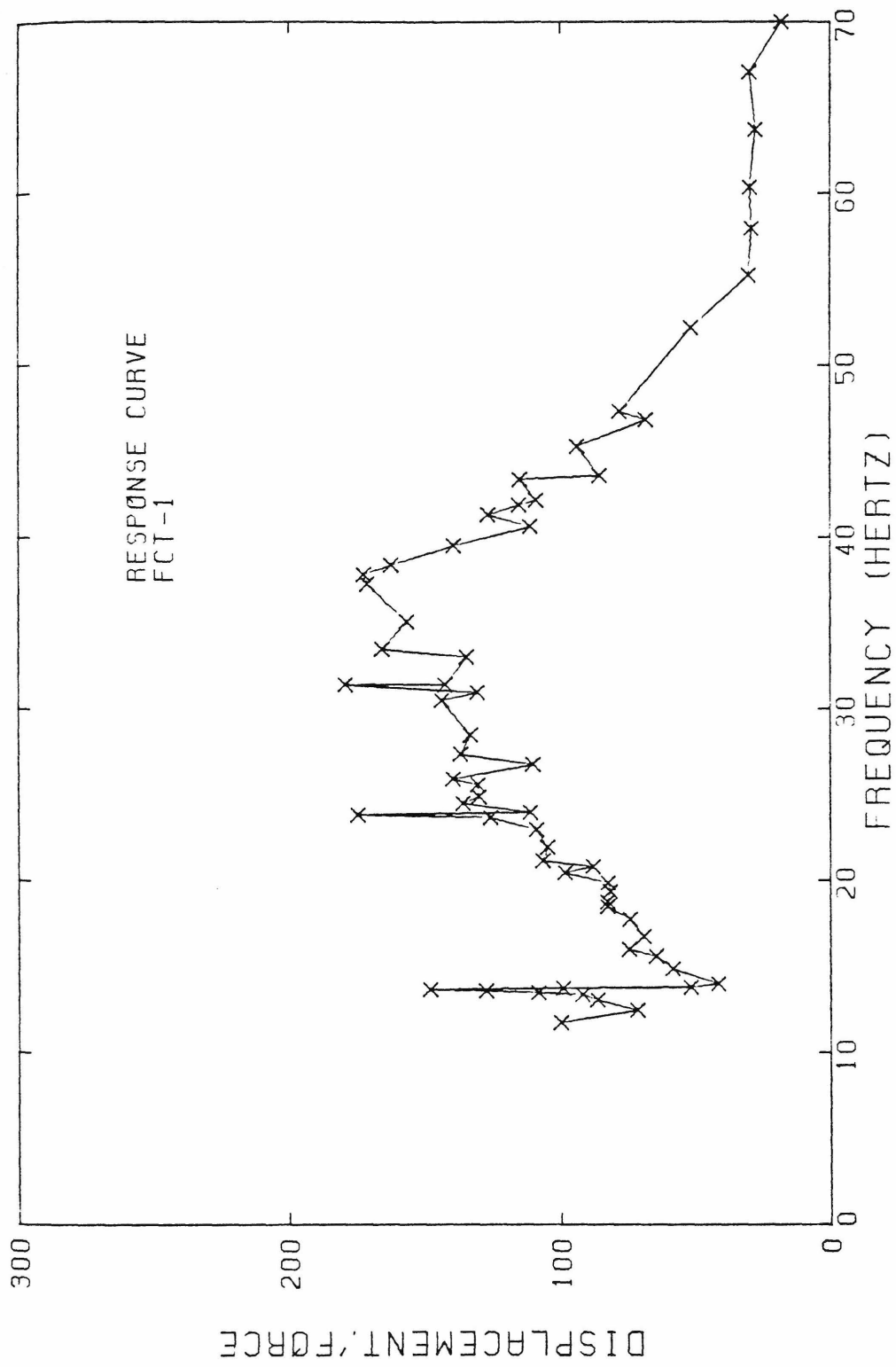


Figure 4.44. Response curve for foundation center translation (FCT-1).

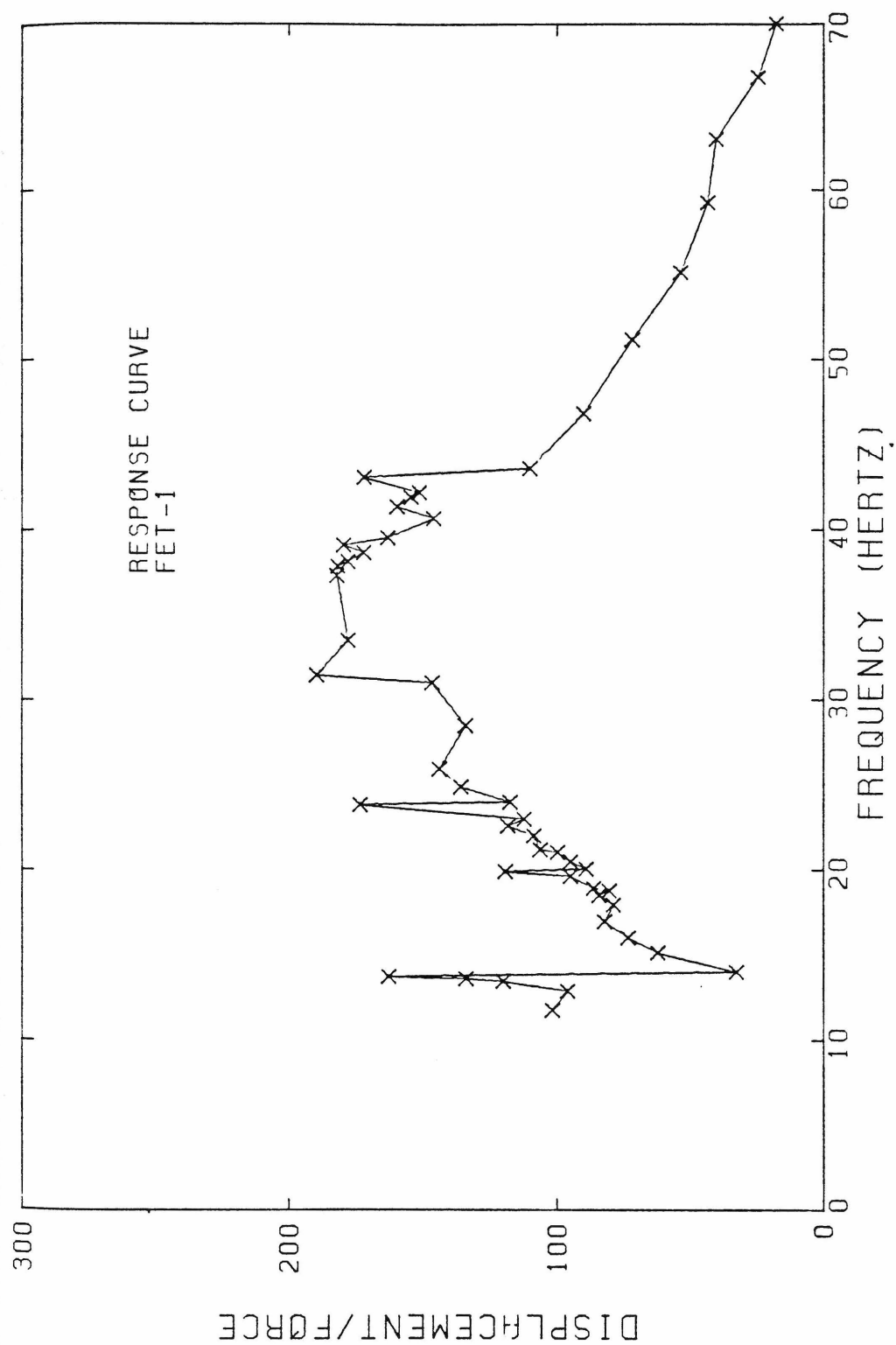


Figure 4.45. Response curve for foundation edge translation (FET-1).

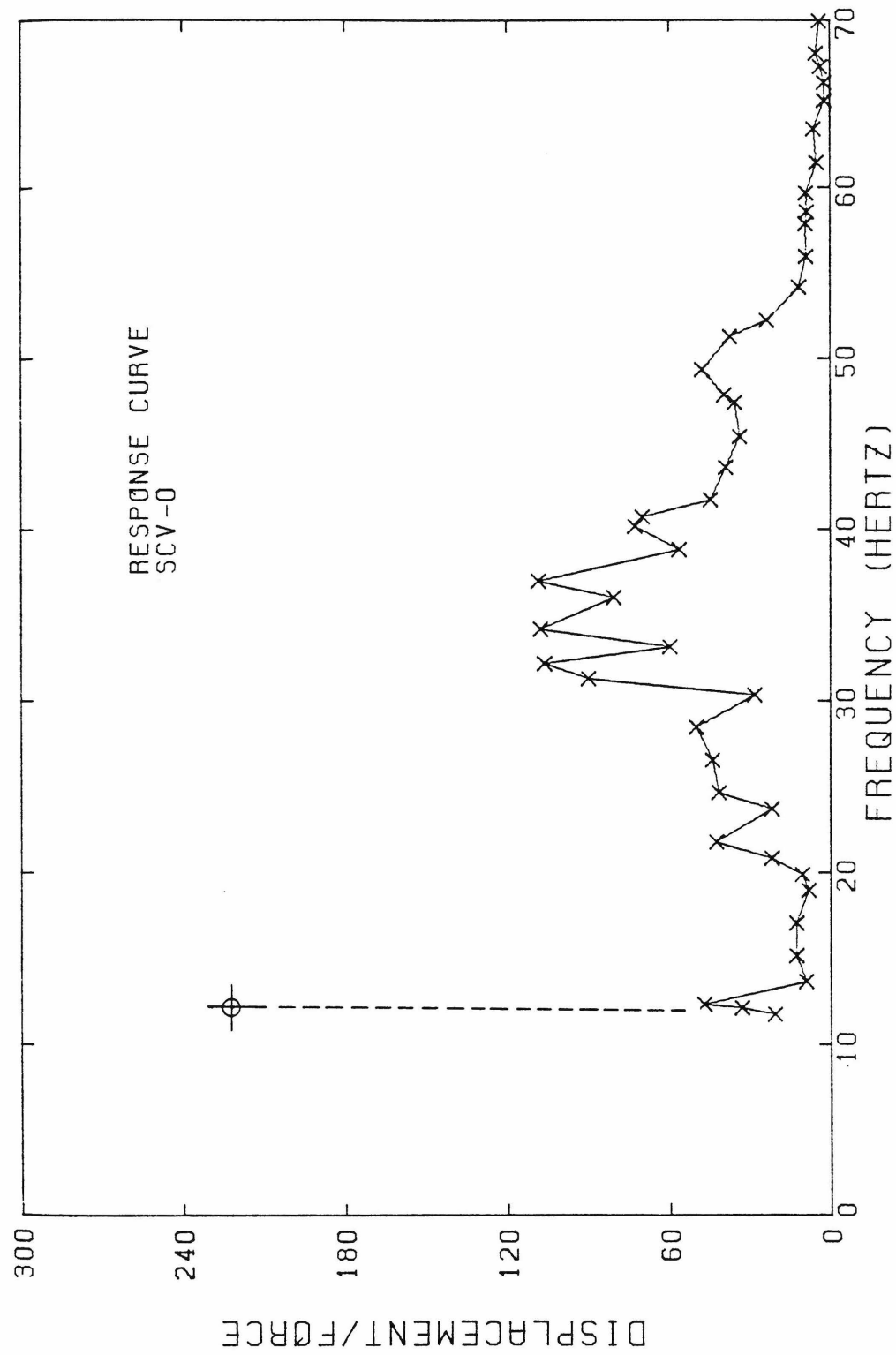


Figure 4.46. Response curve for superstructure center vertical (SCV-0).

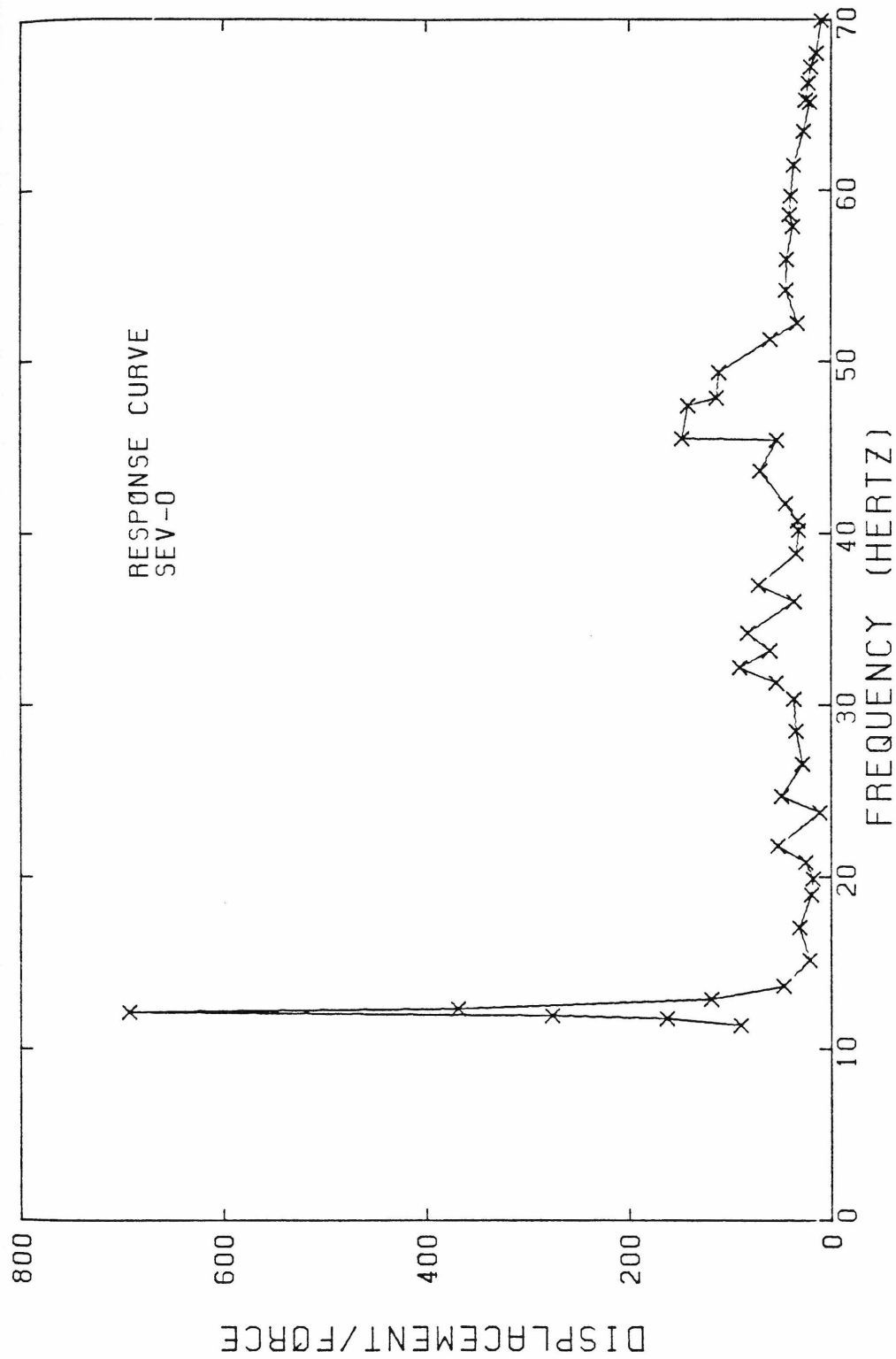


Figure 4.47. Response curve for superstructure edge vertical (SEV-0).

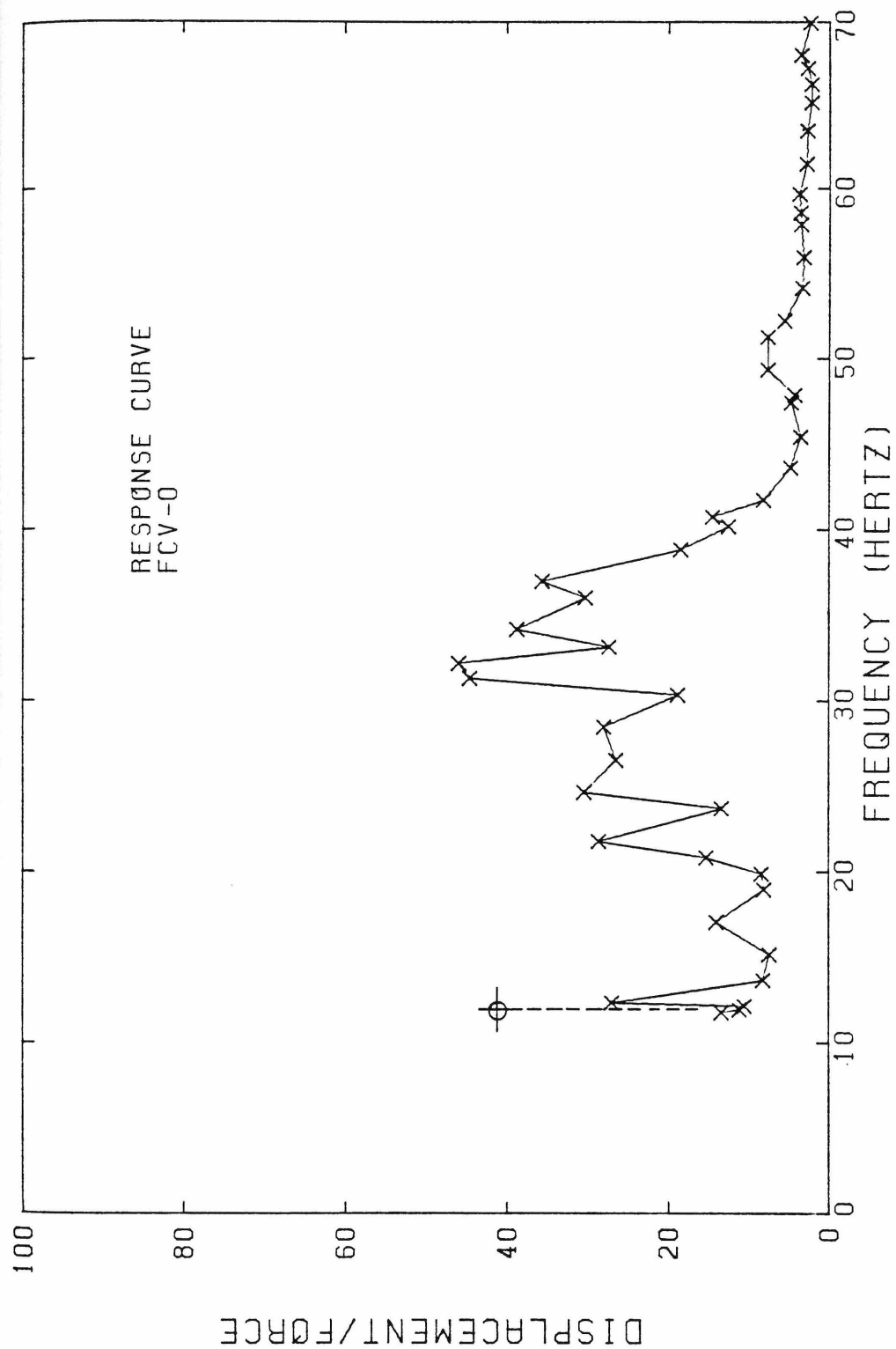


Figure 4.48. Response curve for foundation center vertical (FCV-0).

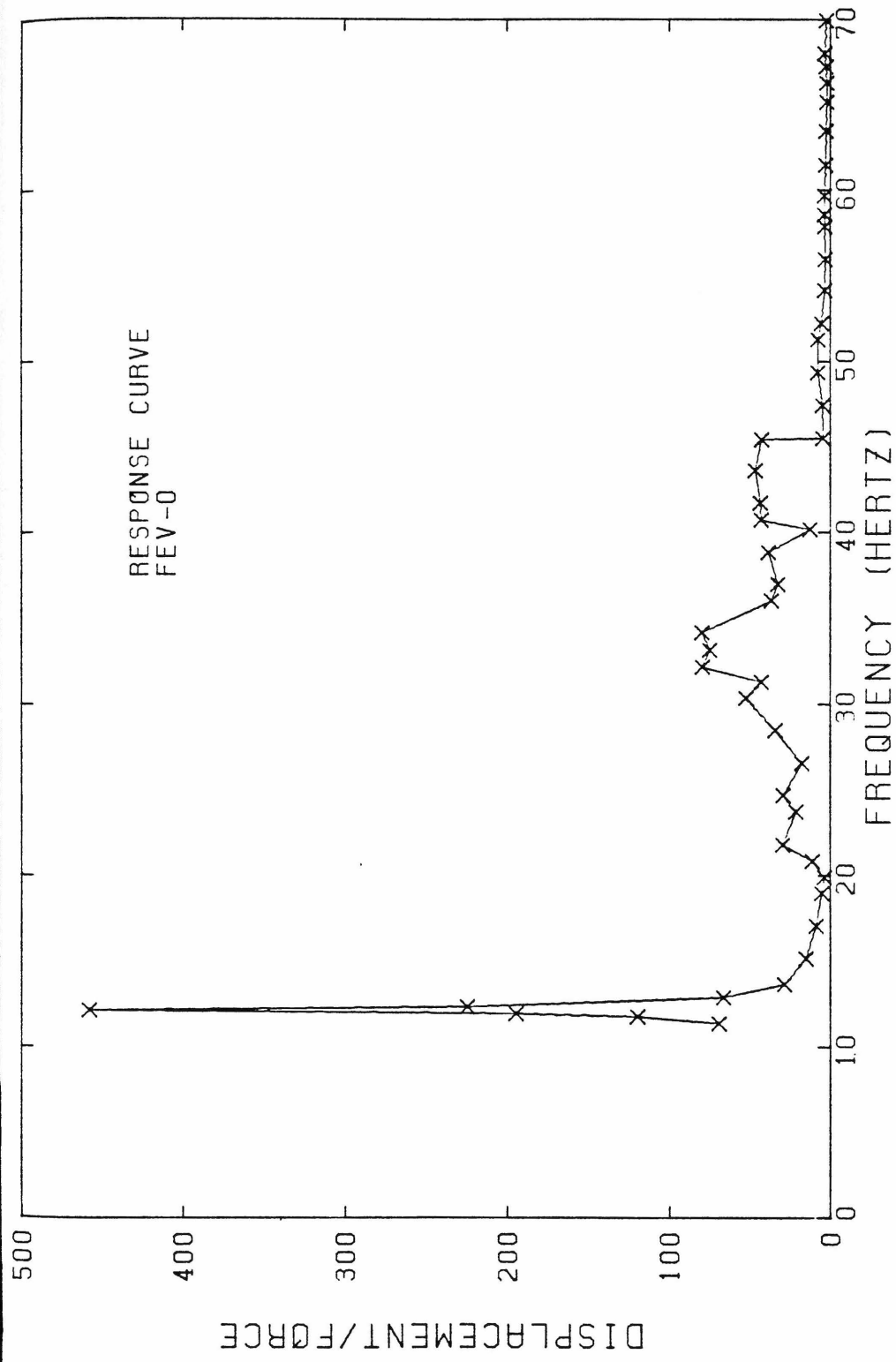


Figure 4.49. Response curve for foundation edge vertical (FEV-0).

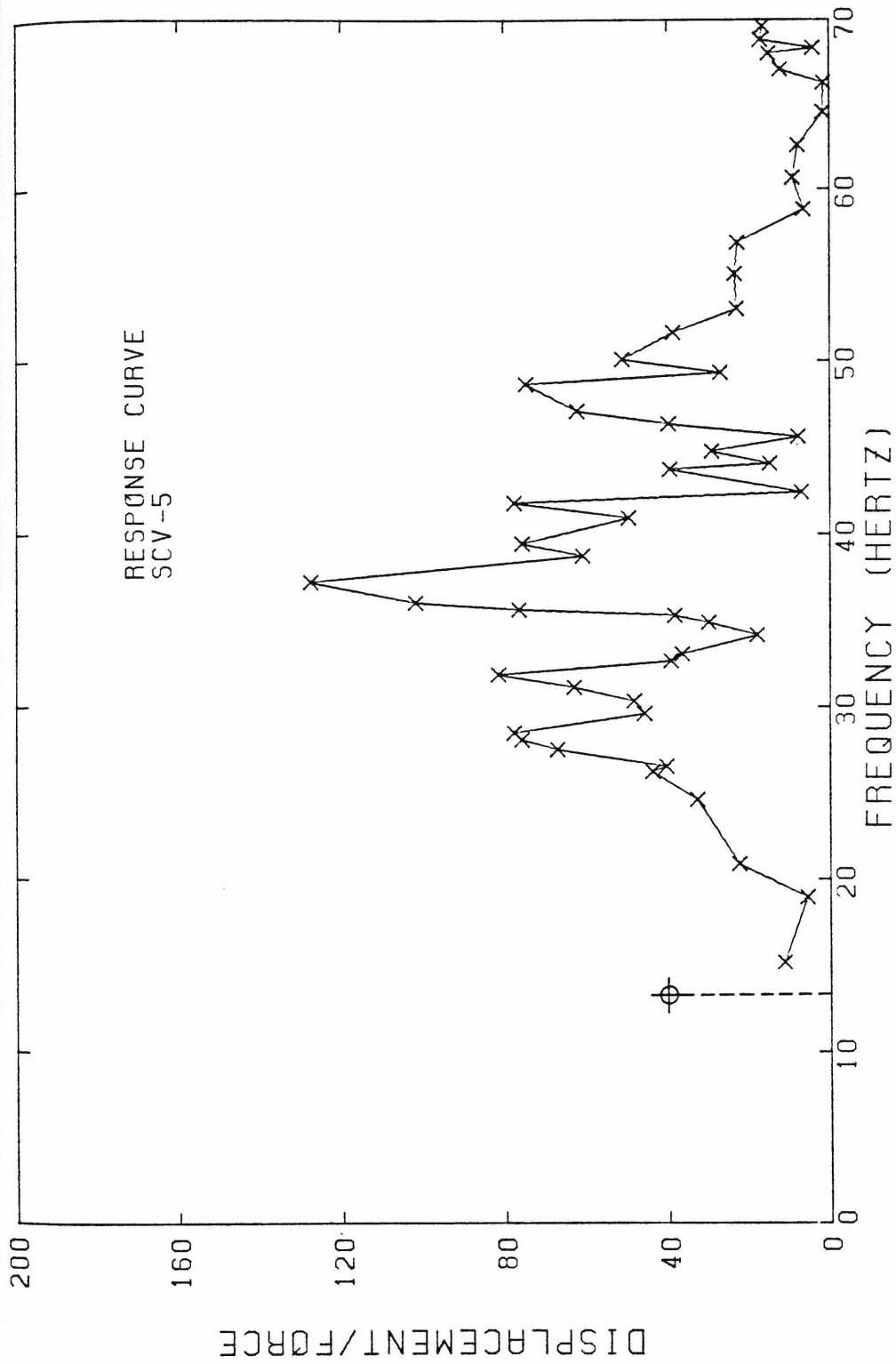


Figure 4.50. Response curve for superstructure center vertical (SCV-5).

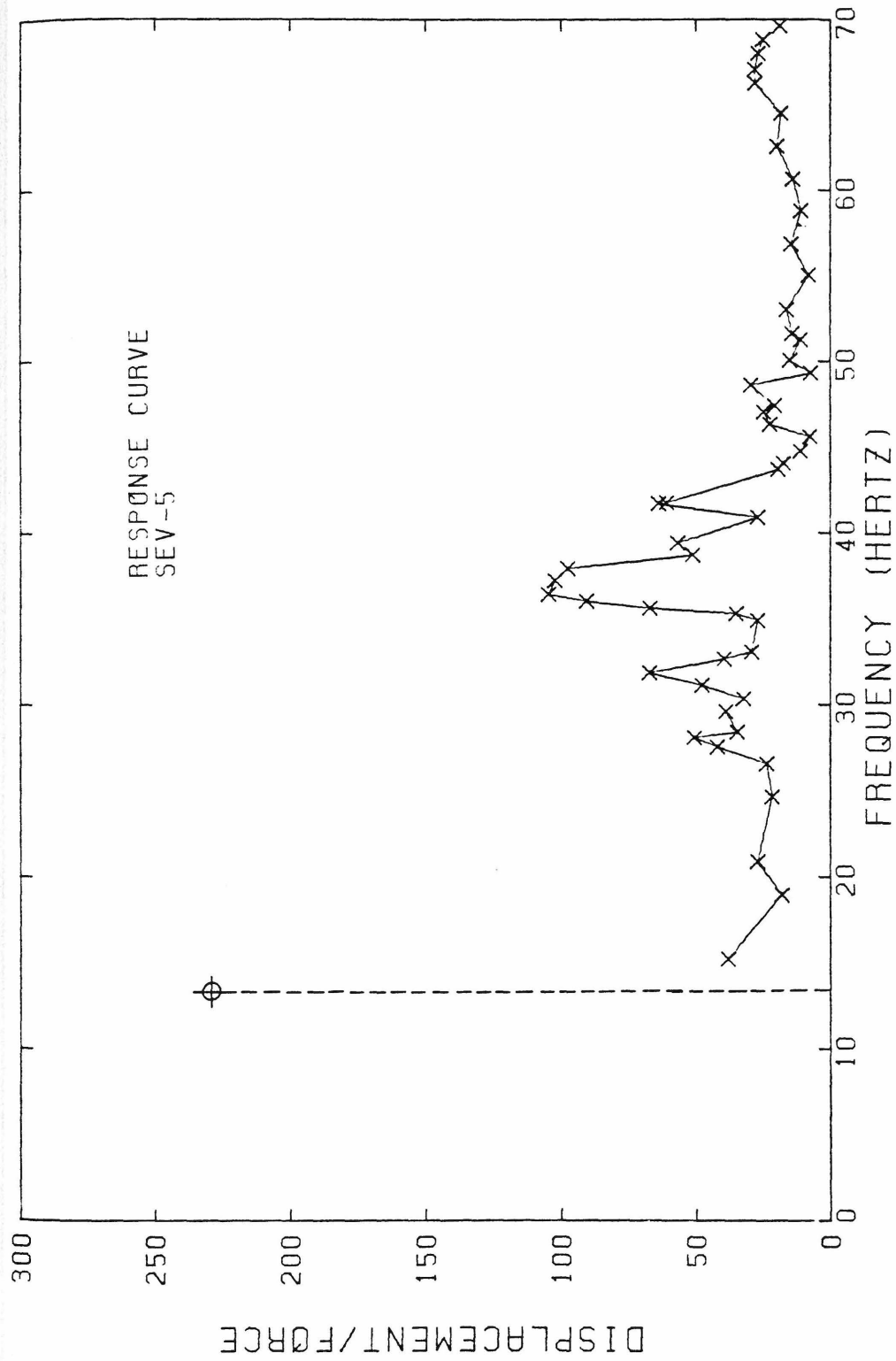


Figure 4.51. Response curve for superstructure edge vertical (SEV-5).

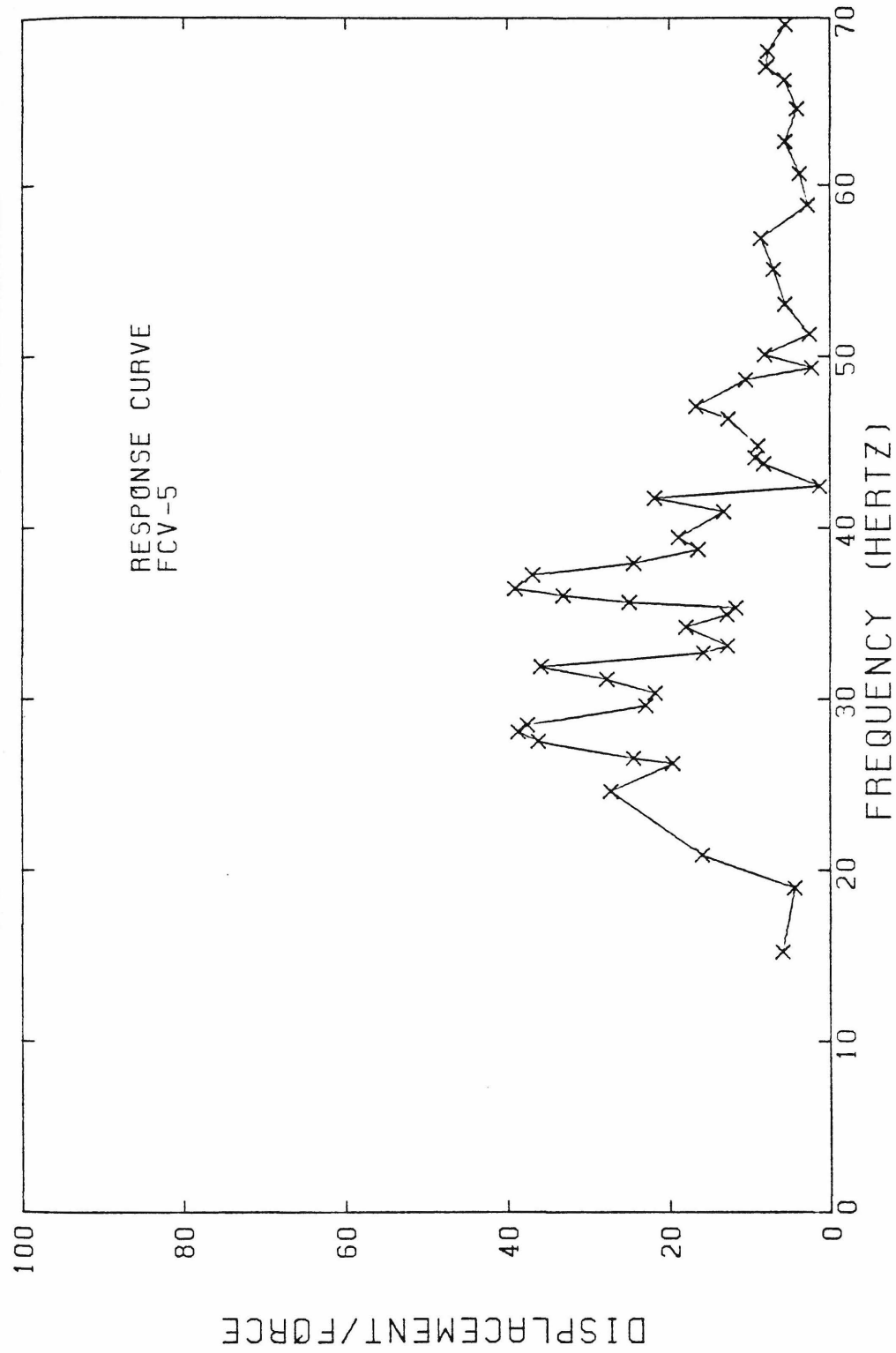


Figure 4.52. Response curve for foundation center vertical (FCV-5).

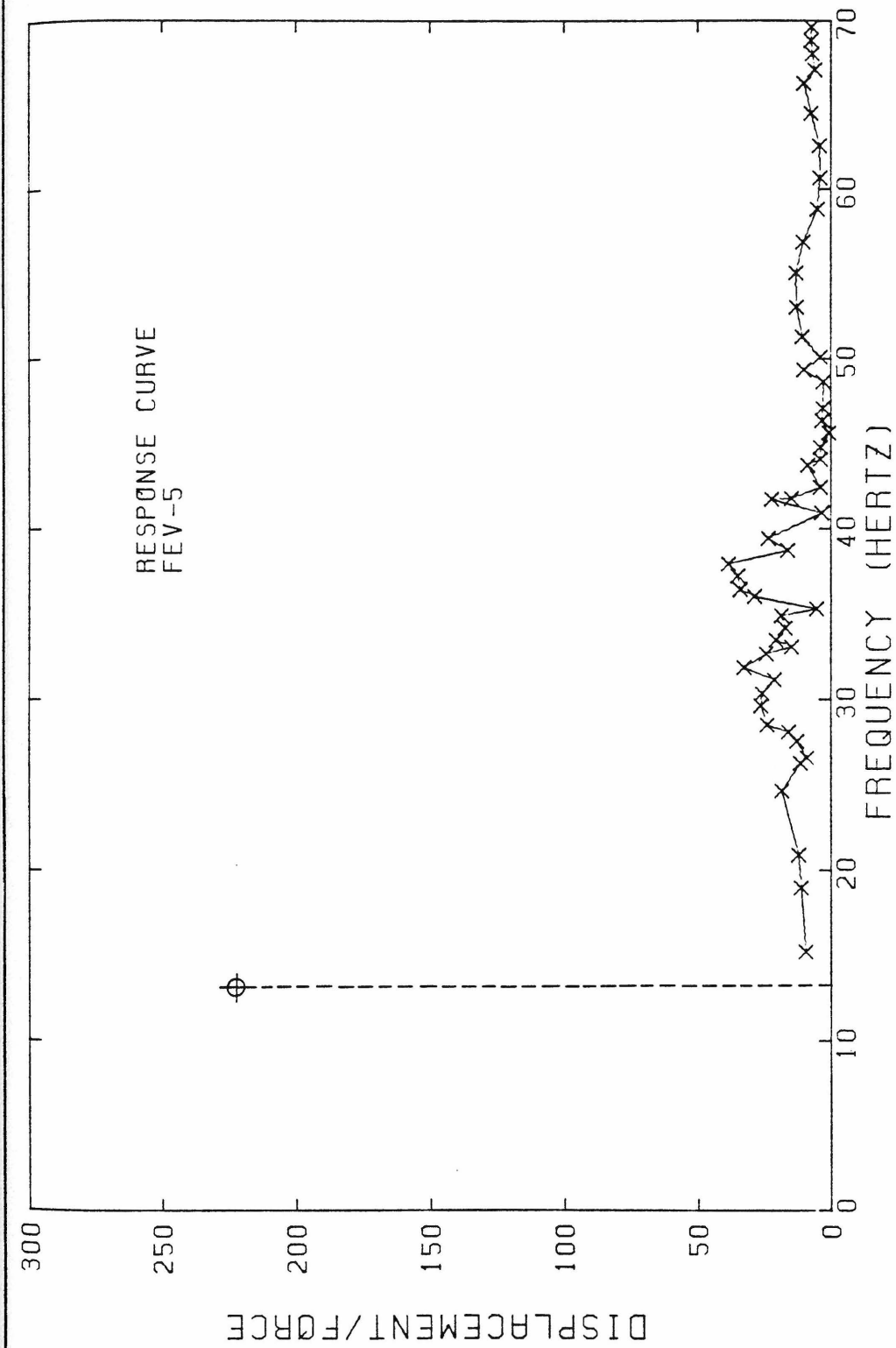


Figure 4.53. Response curve for foundation edge vertical (FEV-5).

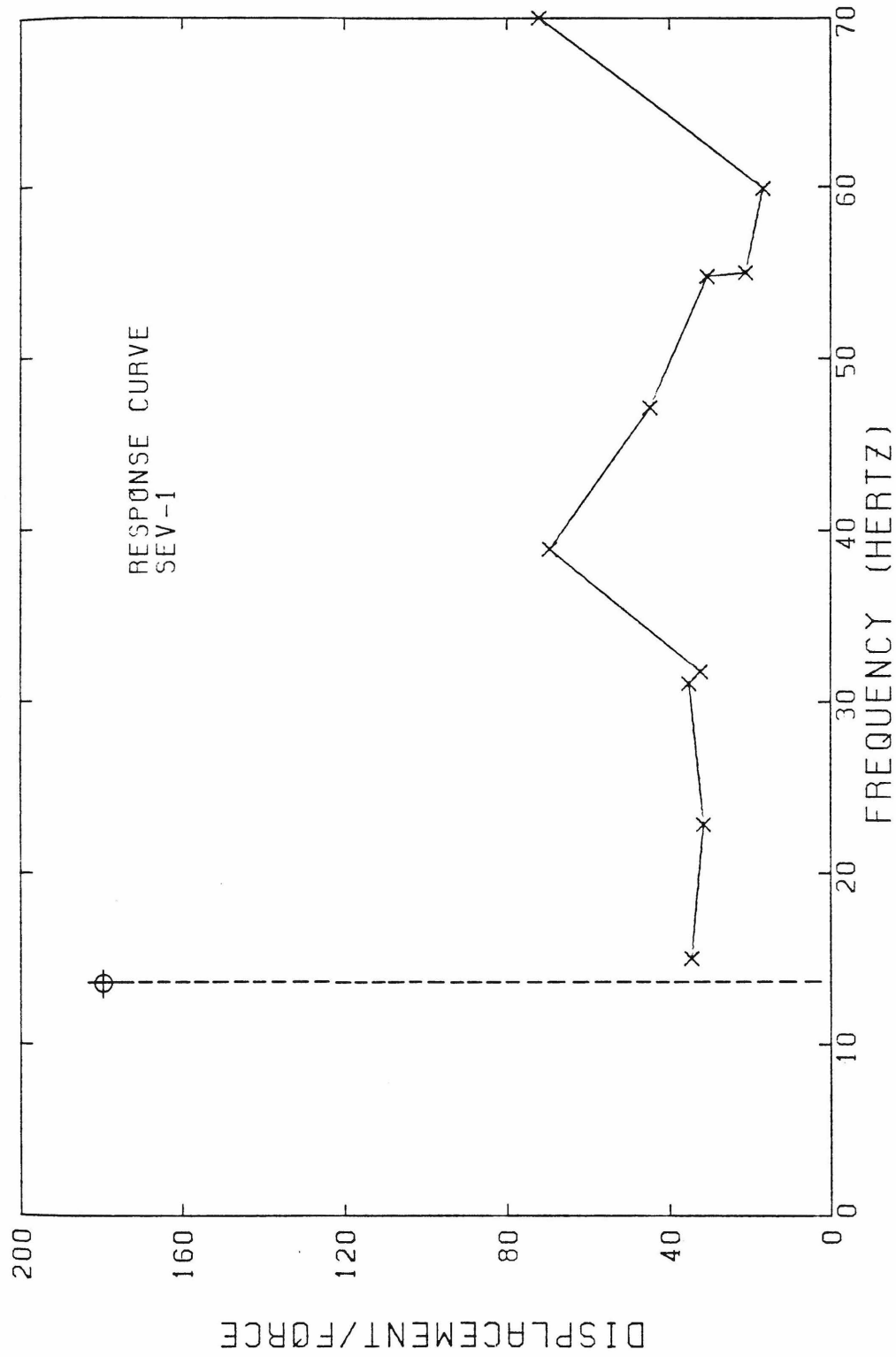


Figure 4.54. Response curve for superstructure edge vertical (SEV-1).

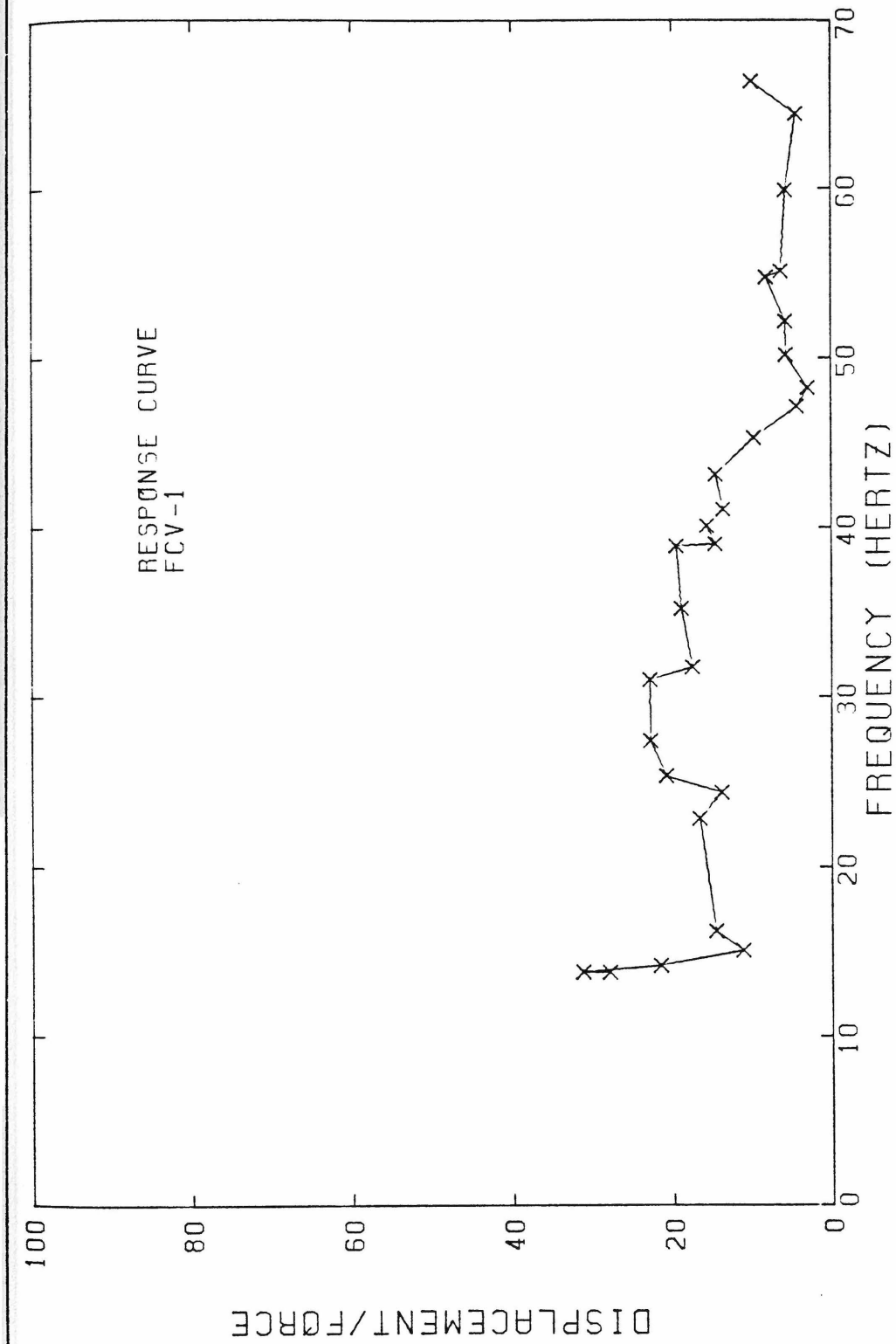


Figure 4.55. Response curve for foundation center vertical (FCV-1).

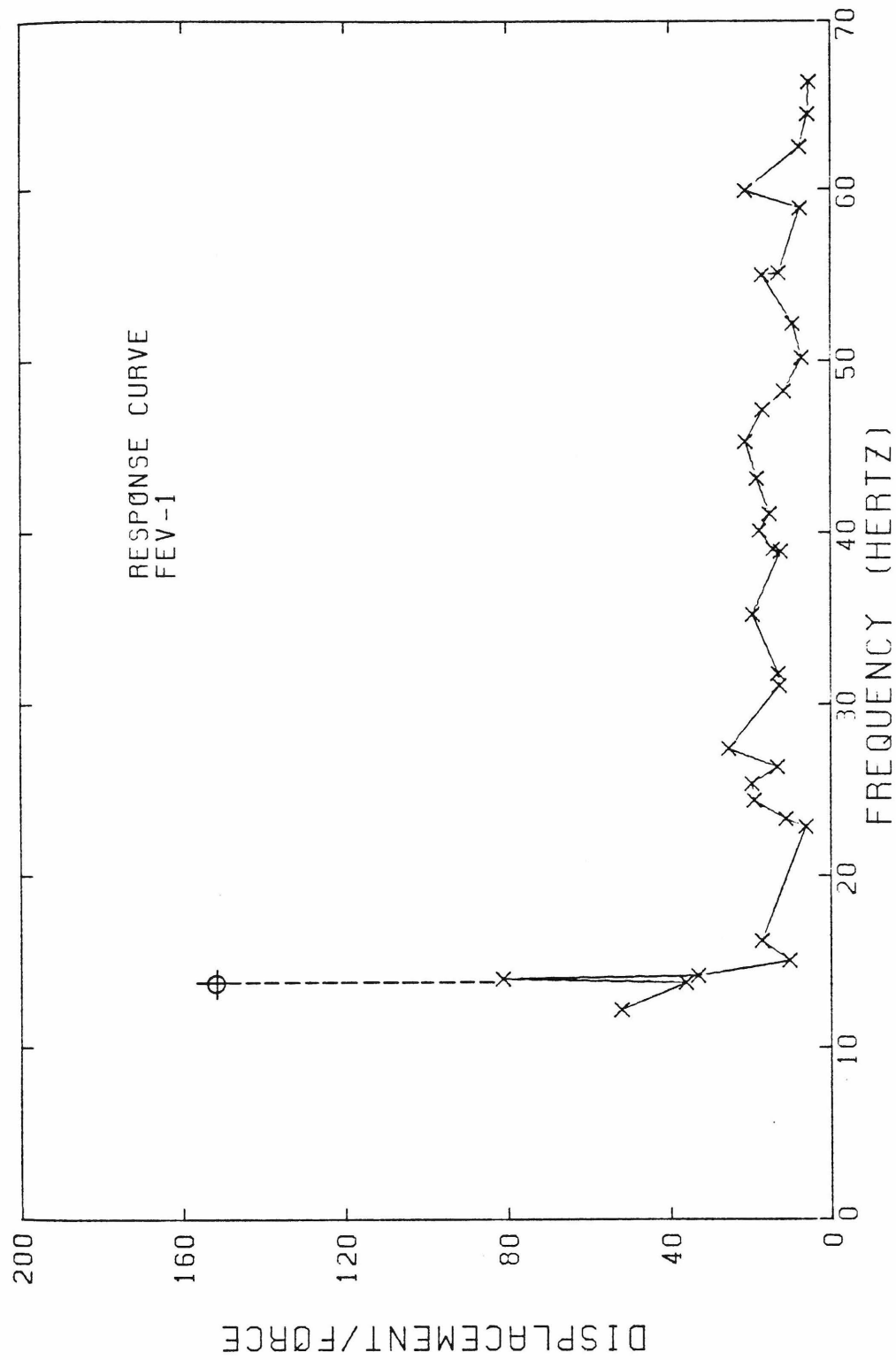


Figure 4.56. Response curve for foundation edge vertical (FEV-1).

Figures 4.28 to 4.56 can be used to support various conclusions about the response of the structure. In this paragraph, only qualitative aspects will be discussed. A more accurate determination of the modal frequencies and dampings will be presented in subsection 4.3.1.

1. The SCT records show a large peak near 12 Hertz, with no other apparent resonant behavior. This implies that the center of the structure responds significantly in only one mode.
2. In addition to the peak near 12 Hertz, SET contains additional peaks at 20 and 25 Hertz. The peak at 12 Hertz is clearly the fundamental mode, and reasoning similar to that used for the interpretation of the ambient vibration records suggests that the peaks at 20 and 25 Hertz correspond to torsional vibration. The maximum displacement of the superstructure occurs at the fundamental translatory frequency. The maximum amplitude of this response is nearly independent of embedment.
3. The amplitude of the fundamental mode peak is not the same in corresponding SCT and SET, and FCT and FET records. This is not an actual phenomenon, but a result of the test procedure. Since the purpose of the forced vibration test was to identify resonant frequencies and modal dampings, a detailed response curve was obtained only for the SCT record for the fundamental mode. The SET, FCT, and FET records were monitored to insure purely translational response. The actual amplitudes of SET,

FCT and FET relative to the superstructure center translation will be accurately determined in the more thorough mode shape measurements of the next paragraph. Detailed records for SET and FET were made only when significant torsional response became apparent. To facilitate comparison of response amplitudes, the symbol (\oplus) corresponding to the amplitude measured in the fundamental mode shape determination, has been plotted in the response curves for translatory motion. These points were not used in any of the data analysis calculations that will be discussed later.

4. Some of the translational response curves show evidence of another peak at sub-resonant frequencies. This is an artifice of the data analysis calculation which resulted from the difficulties encountered with the free-field motion measurement at 7.5 Hertz. Recall that the quadratic fit of Equation (4.1) weighed the lowest frequency point by one-half. Hence, the calculated ground motion may be significantly lower than what actually exists. Under this condition, the division by the smaller number increases both the resulting quotient and the plotted value.
5. The translational mode at 12 Hertz can also be seen in the FCT and FET records. The effect of torsion is also seen in FET, at 20 and 25 Hertz.

6. The computed quantity STR contains peaks at 20 and 25 Hertz. This indicates that the edge motion is much larger than the center motion at these two frequencies. This supports the conclusion that these two frequencies correspond to torsion.
7. The foundation translation records, FCT and FET, show a highly damped peak near 30 Hertz. This peak may indicate a second translatory mode, with strong soil-structure interaction.
8. The non-linear behavior of the structure was investigated by changing the amplitude of the excitation. No measurable effect was noticed. This may be due to the low force levels generated by the shaker at low frequencies, even with the maximum eccentricity. At the fundamental resonant frequency of approximately 12 Hertz, the force output of the shaker, at the excitation structure, was 900 lbs (4.0 kN). The attenuation of ground motion between the excitation and specimen structures reduced the effective force input to the specimen structure to approximately 100 lbs (450 N) at the maximum shaker eccentricity. The peak response amplitude of the superstructure was about 0.001 in (0.025 mm).
9. The maximum translational motion at the edge of the superstructure, due to torsion, is approximately one-quarter that of the motion due to the fundamental translational mode. This indicates that the torsional motion was significant in the specimen structure, for this type of excitation. These results are in

approximate agreement with those obtained analytically by Luco (1976).

10. The translation of the foundation edge, due to torsion, is comparable to that at the same point due to the fundamental translational mode, for the zero and full-embedment cases. The edge motion of the higher torsional frequency is significantly larger than the motion at the lower frequency. The absence of the torsional peaks at the half-embedment case is thought to be due to experimental error, since the peaks are quite narrow and could have been missed.
11. The amplitude of the foundation response in the fundamental translational mode decreases with embedment. This is shown in the records FET and FCT, in which the amplitude of the response peak decreases, and also in the ratio CTR, in which the ratio of the superstructure to foundation motion increases with embedment.
12. The vertical motions are very small. The largest vertical motion occurs at the edges of the superstructure and foundation at the fundamental mode. This indicates that foundation rocking is the most significant vertical motion. The decrease of the amplitude with embedment indicates increasing stiffening of the foundation-soil system. The vertical motions which indicate such rocking were, in general, not measured during the frequency sweep, instead, these points were measured during the more detailed mode shape measurements of the following

paragraph, and plotted on these response curves by the symbol (\oplus) to facilitate comparison. To prevent the erroneous conclusion that some of the resonant peaks have very low damping, or even no subresonant response, these extra points have not been connected to the other points by lines.

13. The amplitudes of the vertical motion of the foundation and superstructure are about the same in each embedment case. This indicates very little interfloor vertical motion.

4.2.3.2. Mode shape at resonance.

The vertical, east-west, and north-south translatory motions of the specimen structure at the fundamental resonant frequency were measured at the locations shown in Figure 3.11. At the resonant frequency, the east-west forced vibrations caused no significant north-south motions. Hence, the modal displacements consist of east-west and vertical motions, which are shown in Figures 4.57 to 4.59 for the three embedment cases. These displacements have been normalized to the displacement of the superstructure center.

As seen from these figures, the lateral translation of the superstructure and foundation masses are nearly uniform over the north-south centerline. This verifies the expected lack of torsional response. Depending on the embedment, the resonant frequency varies from 11.3 to 13.8 Hertz. At these frequencies, the SH wavelength is about 70 ft (21 m). Torsion of the foundation is caused by the variation of the

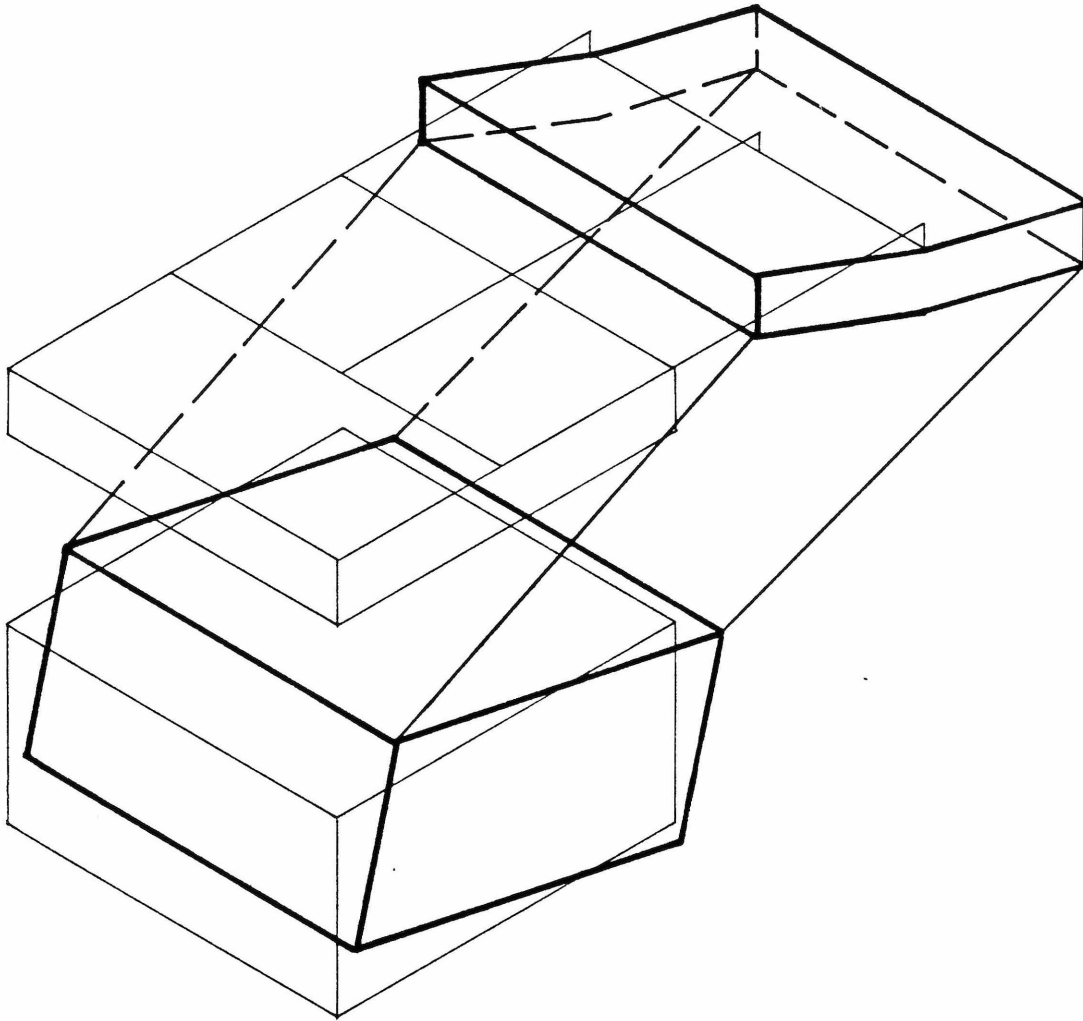


Figure 4.57. Displacements at resonance, zero-embedment. Light solid line indicates equilibrium position. Heavy line indicates maximum displacement.

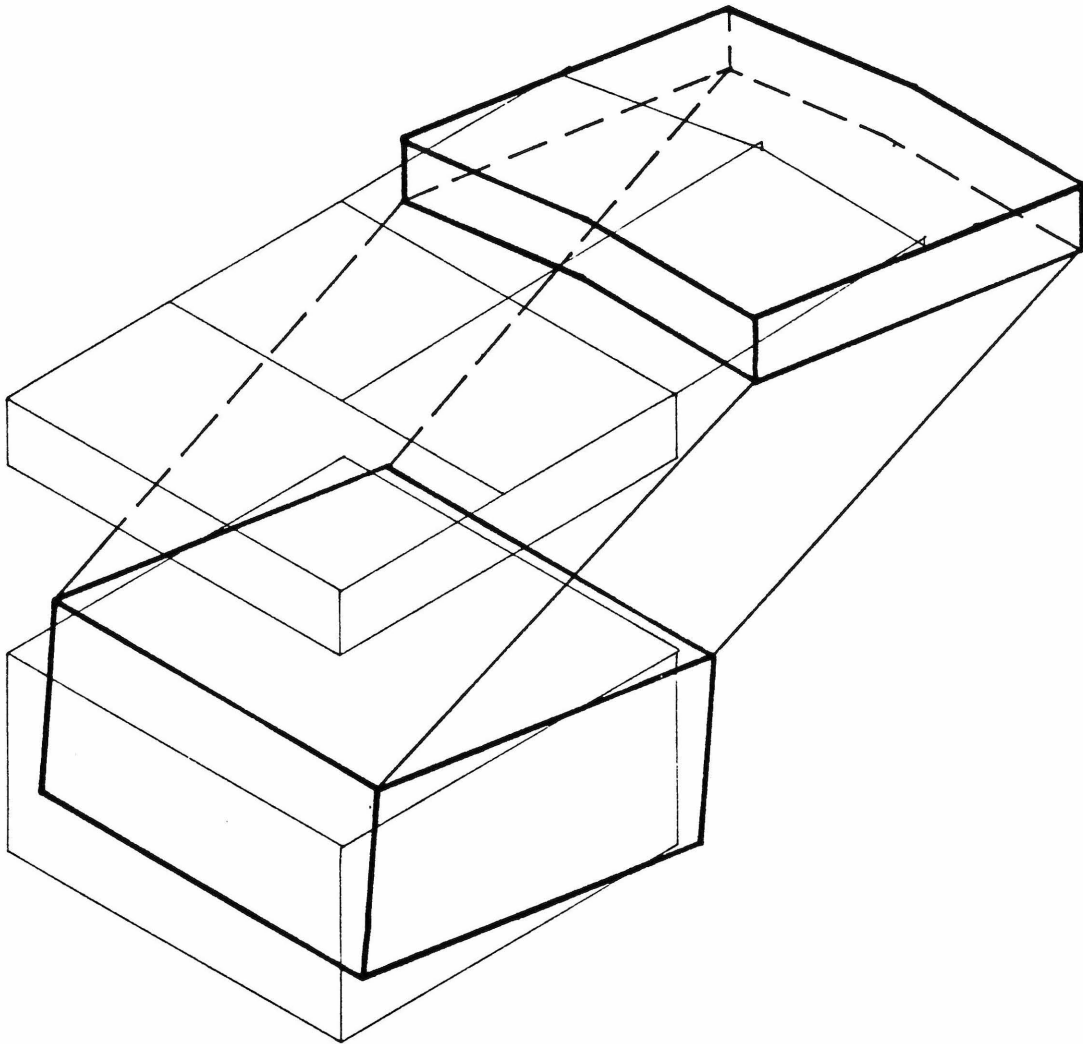


Figure 4.58. Displacements at resonance, half-embedment. Light solid line indicates equilibrium position. Heavy line indicates maximum displacement.

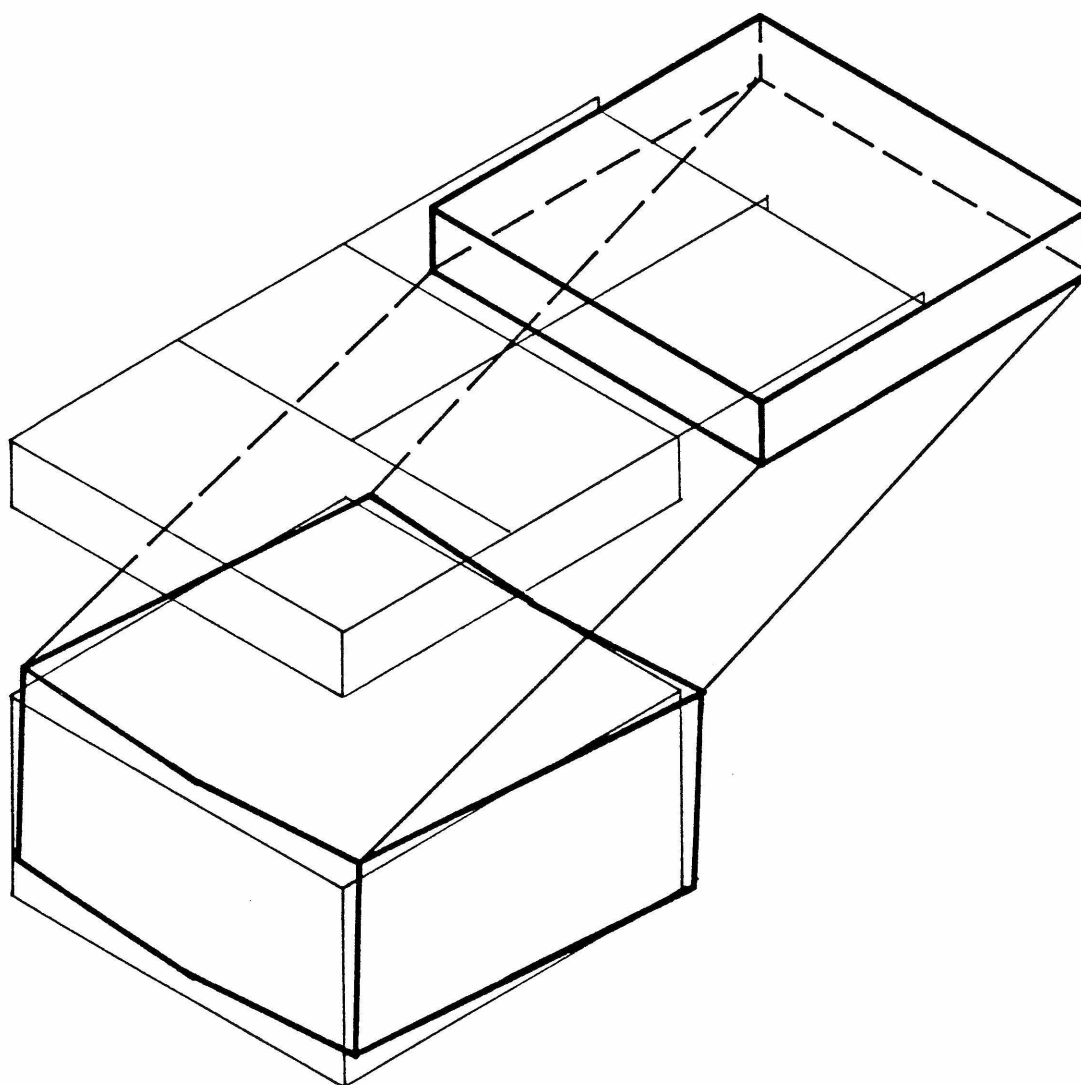


Figure 4.59. Displacements at resonance, full-embedment. Light solid line indicates equilibrium position. Heavy line indicates maximum displacement.

ground displacement over the length of the foundation. Since the foundation is small compared to the wavelength, the ground motion is essentially uniform under the foundation.

The fundamental mode response is comprised of the foundation translation, tangential displacement due to rocking, and interfloor displacement. The rocking and foundation translation, compared to the total superstructure translation, is an indication of the degree of soil-structure interaction; if the foundation-soil system were perfectly rigid, the entire superstructure translation would be due solely to interfloor displacement. It is therefore necessary to determine the contribution of each deformation to the total displacement. The rocking and translation can be found, for the assumed rigid foundation, from the lateral motion measured at the floor and at the top of the foundation walls. The rocking amplitude can also be found from the vertical displacements of the foundation floor. If the two values are in agreement, then the assumption of the rigid foundation is valid. The lateral and vertical motions of the foundation are shown normalized to the total superstructure displacement in Figure 4.60.

The two rocking amplitudes, as well as the contributions of the foundation and interfloor displacements to the total superstructure displacement, are listed in Table 4.5 shown on the following page. These displacement ratios contain some features that should be emphasized:

1. The assumption of a rigid foundation is valid since the amplitude of rocking found by the two methods is close. Because a

TABLE 4.5. Mode shape at fundamental east-west transitory resonant frequency.

Embedment in feet	Rocking angle ϕ		Contributions to total superstructure displacement			Total super- structure displacement normalized to free field
	By base vertical motion	By base horizontal motion	Foundation translation X_f/X_t	Rigid Body rocking $h\phi/X_t$	Interfloor displacement X_s/X_t	
0	0.0184	0.0183	0.061	0.210	0.729	39
2.5	N/A	0.0124	0.021	0.142	0.837	47
5.0	0.0247	0.0048	0.013	0.054	0.933	44

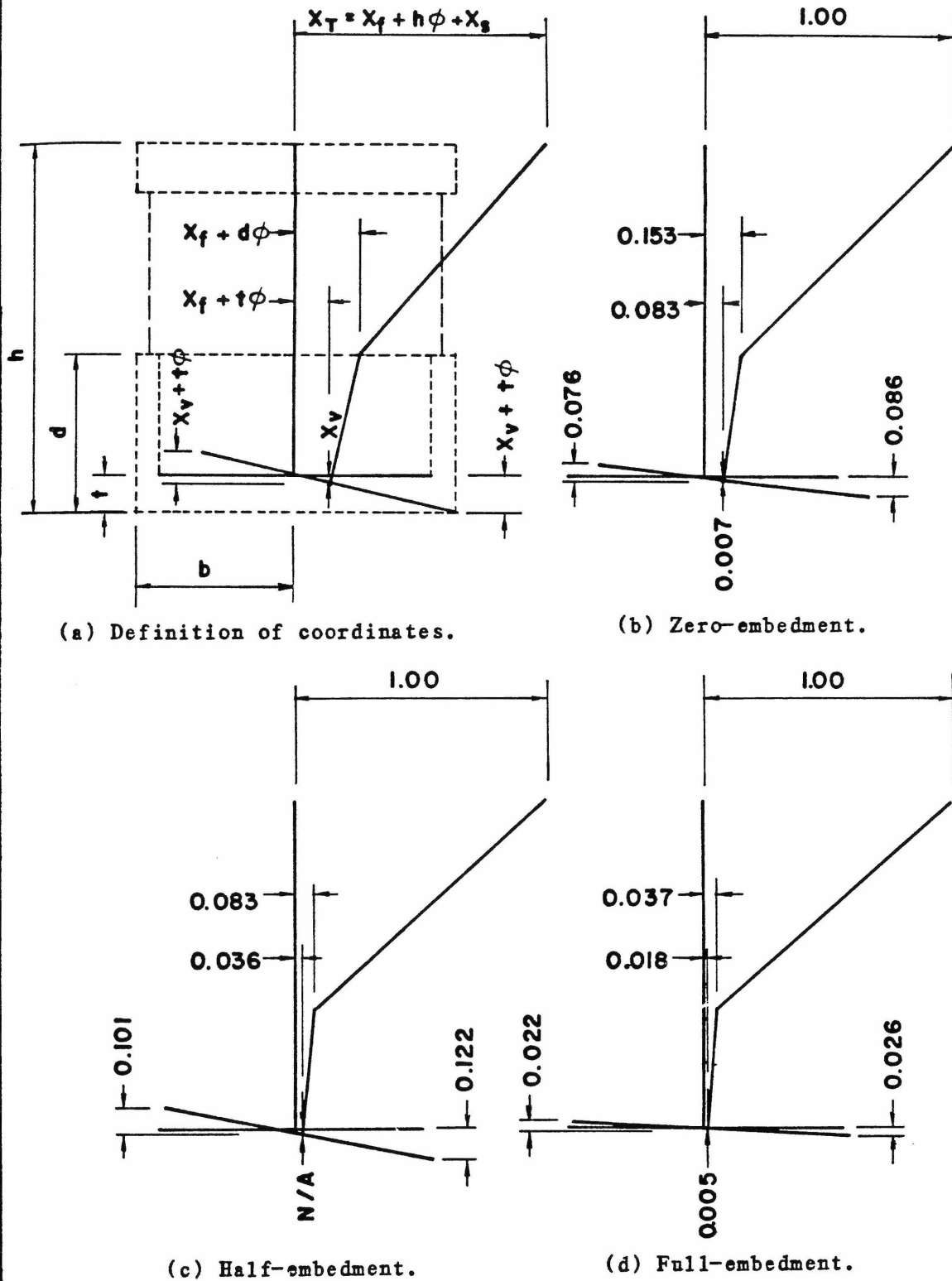


Figure 4.60. Normalized displacements of fundamental mode.

poor record was obtained at the center of the foundation in vertical motion, only one method could be used for the half-embedment case.

2. As embedment depth increases, the contribution of base translation and rocking to overall superstructure displacement decreases. Therefore, the foundation-soil system becomes stiffer with embedment.
3. There is a greater decrease in the foundation contribution to the overall displacement between the zero- and half-embedment cases than between the half- and full-embedment cases. This implies that the effect of foundation restraint becomes less sensitive to embedment depth as the depth increases.
4. The results are within the ranges reported for similar tests conducted on prototype structures. For example, Foutch (1976) found that 4% and 20% of the roof motion of Millikan Library were due to base translation and rigid body rocking, respectively, in the north-south direction.
5. The ratio of the total superstructure translation to the free-field ground motion, X_t/X_g , does not show any clear trend with embedment. The determination of this quantity, however, is subject to a small error because the results of the free-field motion studies had to be compared with the results of the forced vibration tests. As stated in subsection 4.1.2, ambient

site noise made a significant contribution to the free-field motion at the lower frequencies.

4.2.3.3. Resonance induced ground motion.

The vibration of a large structure in its fundamental mode can transmit large amounts of energy back into the soil and result in substantial changes in the near-field ground motions. This effect can be important in locating "free-field" sites for strong-motion instruments, and for cases in which multiple structure interaction can occur. Therefore, the ground motion at the specimen structure's fundamental resonant frequency was measured at the locations shown in Figure 4.61. The results of these tests are plotted in Figures 4.62 to 4.64. For comparison, the transverse free-field motion along the north-south centerline for a frequency of 15 Hertz is also plotted. Some of the key aspects of the results are:

1. Both vertical and lateral (east-west) ground motions are generated by the resonance of the structure. Lateral ground motions are induced along both axes of the structure (east-west and north-south) while vertical motions are produced only along the east-west centerline. This suggests that the vertical motions are caused by the rocking of the structure about the base, such that the north-south axis is a node line in the surface displacement field.

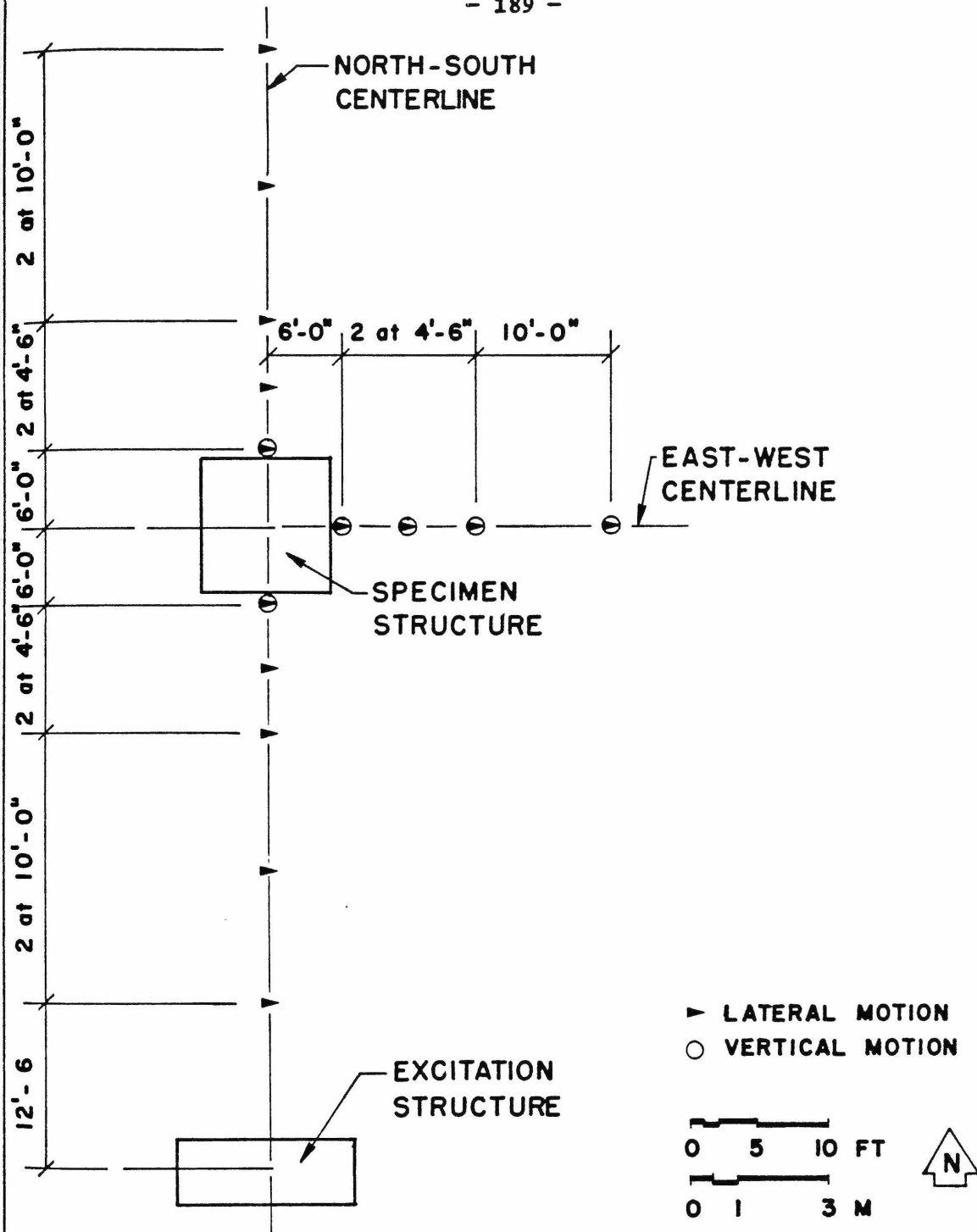
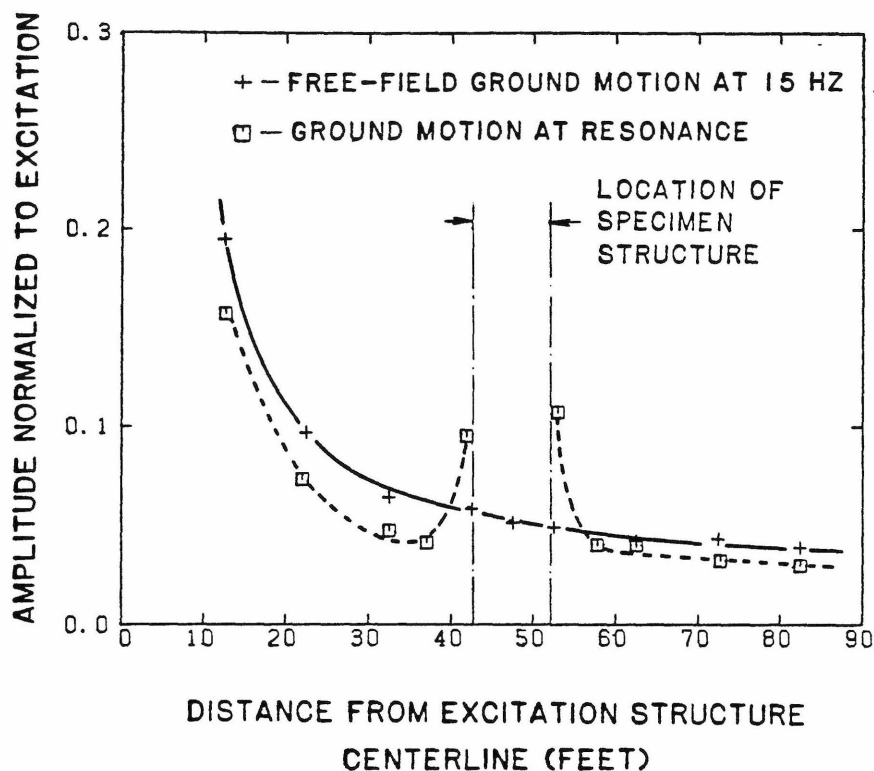
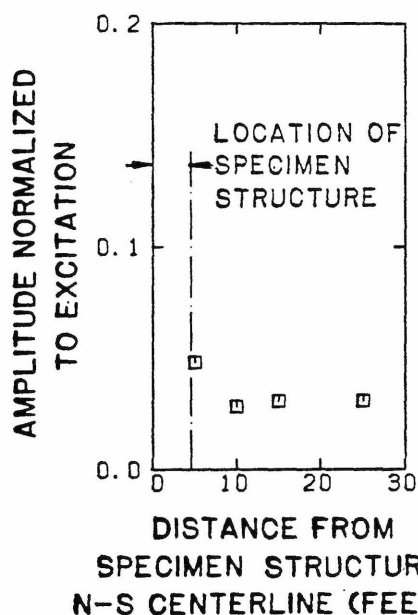


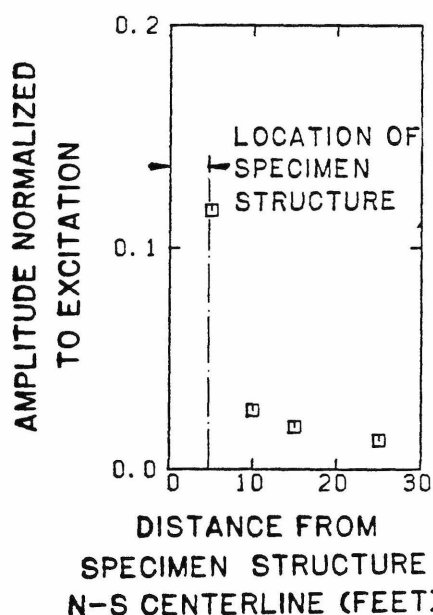
Figure 4.61. Stations for measurement of resonance-induced ground motions.



(a) Transverse motion along north-south centerline.

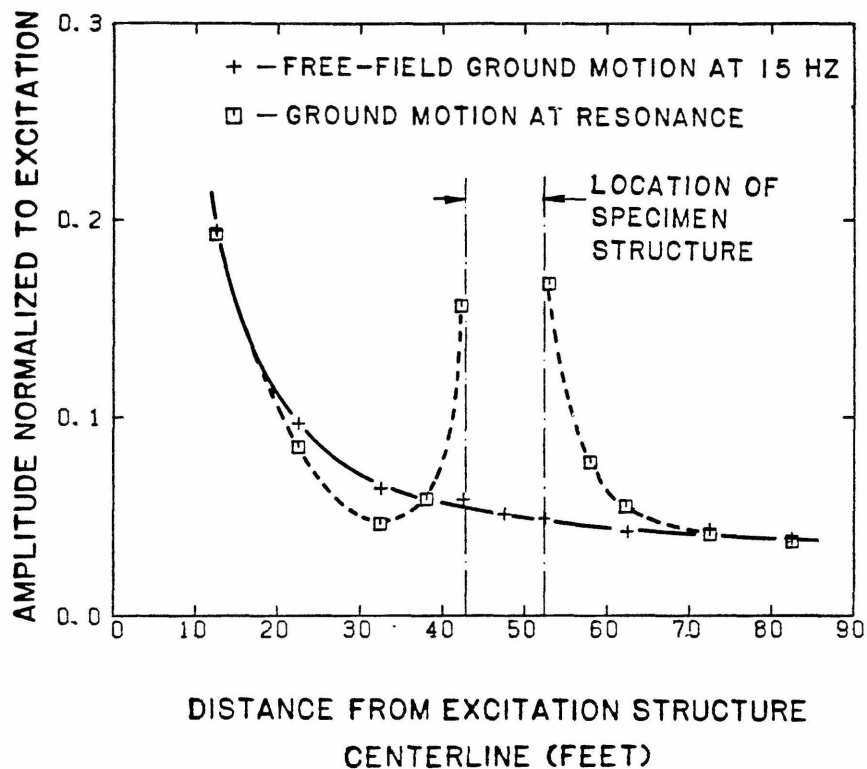


(b) Transverse motion along east-west centerline.

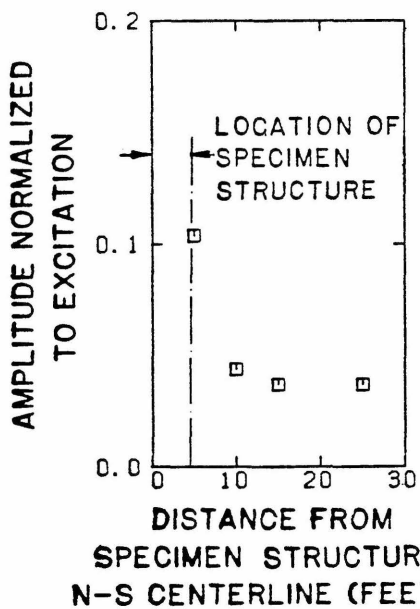


(c) Vertical motion along east-west centerline.

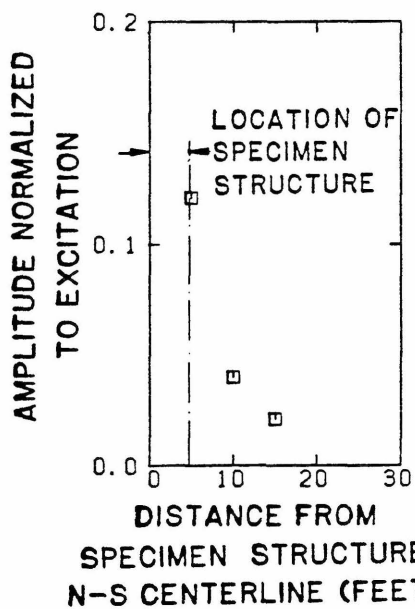
Figure 4.62. Ground-motion at resonance, zero-embedment.



(a) Transverse motion along north-south centerline.

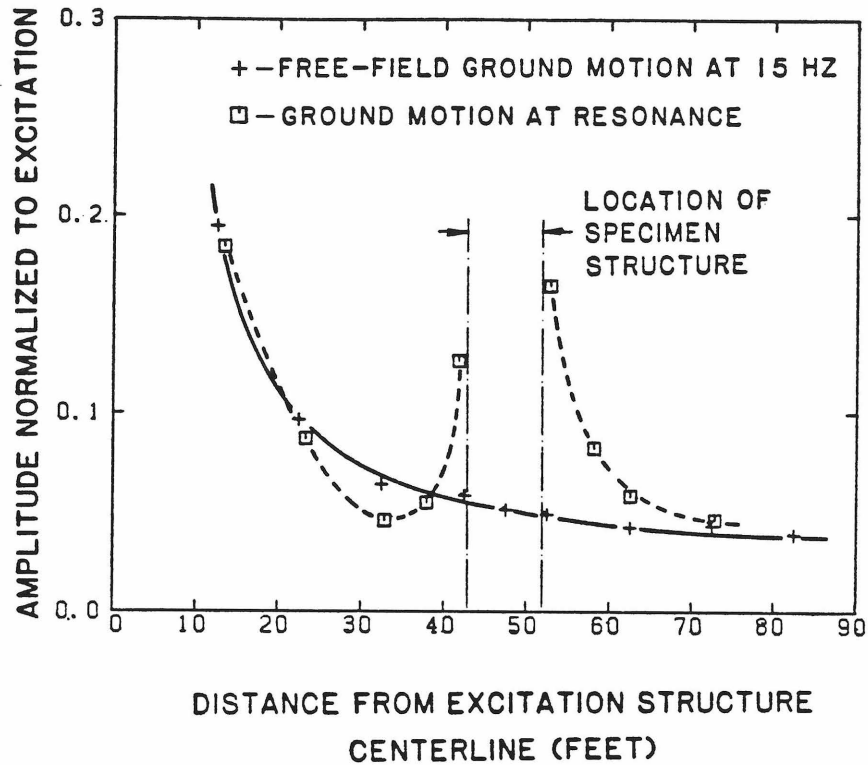


(b) Transverse motion along east-west centerline.

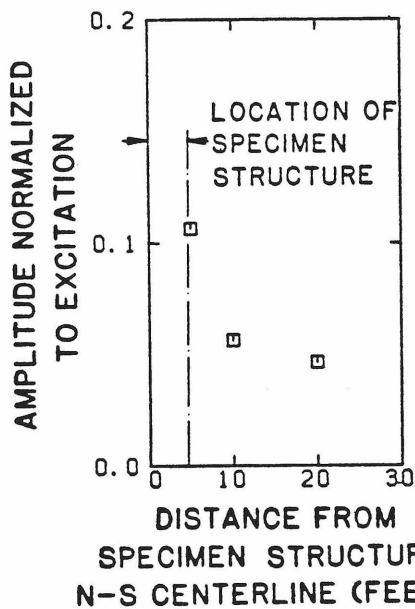


(c) Vertical motion along east-west centerline.

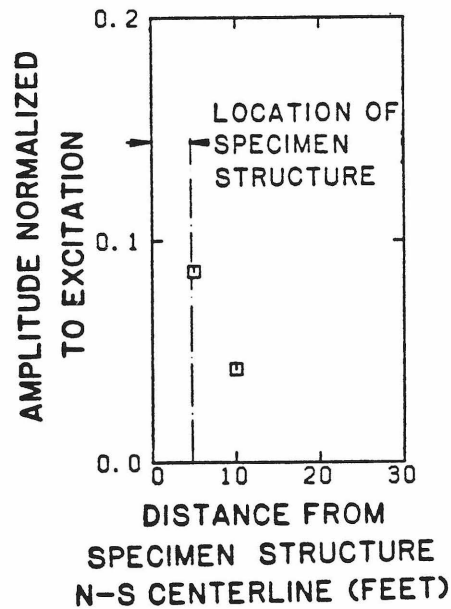
Figure 4.63. Ground-motion at resonance, half-embedment.



(a) Transverse motion along north-south centerline.



(b) Transverse motion along east-west centerline.



(c) Vertical motion along east-west centerline.

Figure 4.64. Ground-motion at resonance, full-embedment.

2. The amplitude of the induced vertical motion is approximately independent of the foundation embedment.
3. The amplitude of the horizontal induced ground motion is approximately the same for the half- and full-embedment cases, but significantly less for the zero-embedment case. This suggests that the lateral motion is primarily caused by the translation of the structure with respect to the soil.
4. The induced ground motions attenuate rapidly. There is little effect on the free-field motion beyond two or three building radii.
5. The total horizontal ground motion, at some points between the excitation and specimen structures, may actually be reduced by the resonance of the structure. This apparent reduction may be due partially to errors caused by using, in the plots, the free-field motion measured at a frequency other than the resonant frequency.

4.3. ANALYSIS OF EXPERIMENTAL RESULTS.

One of the more powerful ways to obtain the dynamic properties of a structure is to apply systems identification techniques to the results of the forced vibration tests. More specifically, these analyses can provide;

- More accurate determination of resonant frequencies and modal dampings than possible by direct interpretation of resonance curves, and
- Values for the structure and foundation stiffnesses and dampings.

The calculations used to obtain these results are described in the following subsections.

4.3.1. Determination of Equivalent Oscillators.

Scatter in the response amplitudes measured during forced vibration of the specimen structure make the accurate determination of resonant frequency and modal damping from the direct examination of the response curves difficult. Therefore, each response curve was used to develop an equivalent single degree-of-freedom (SDF) oscillator, from which the resonant frequency and damping can be found.

The SDF oscillator, defined in Figure 4.65, has a response to sinusoidal base motion described by

$$y = \frac{A(f/f_n)^2 \sin 2\pi f}{\{[1 - (f/f_n)^2]^2 + [2\zeta f/f_n]^2\}^{1/2}} \quad (4.2)$$

where

$$f_n = \frac{1}{2\pi} \sqrt{\frac{k}{m}}$$

and

$$\zeta = \frac{c}{2\sqrt{km}} \quad .$$

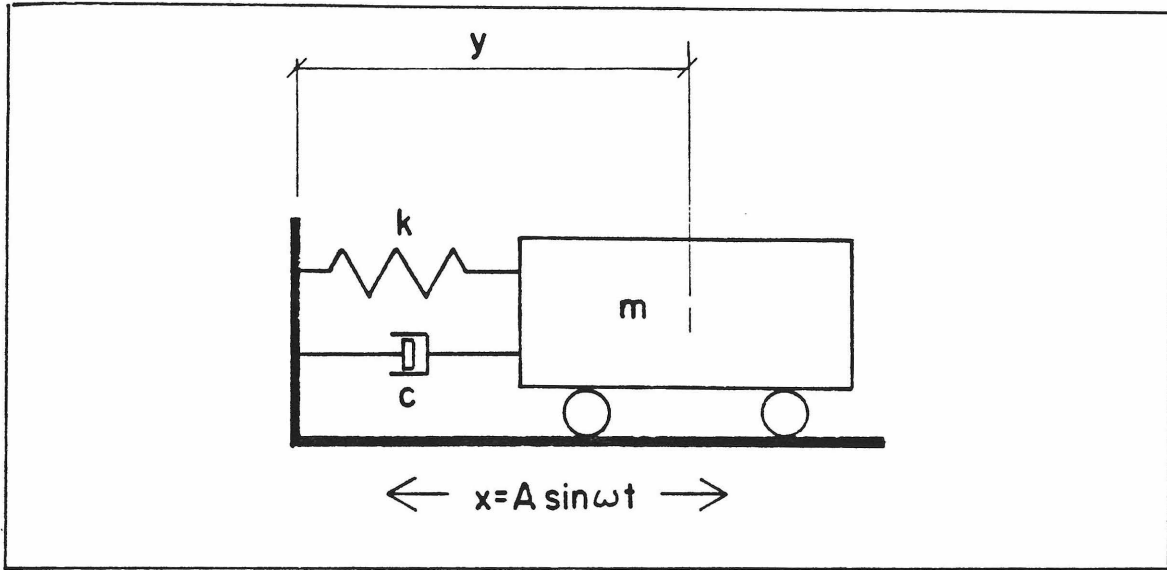


Figure 4.65. Single degree-of-freedom oscillator.

If the response of the oscillator can be made to coincide with the response of the experimental structure, then the two systems will have the same vibrational properties. The scatter in the experimental results, however, makes an exact fit impossible.

If the quantity J is defined such that

$$J = \sum_{i=1}^N [y_i - y(f_n, \zeta_n, f_i)] \quad (4.3)$$

$$= \sum_{i=1}^N \left[y_i - \frac{A f_i^2}{\{(f_n^2 - f_i^2) + (2\zeta_n f_n f_i)^2\}^{1/2}} \right] \quad (4.4)$$

where y_i is the response measured at frequency f_i ; $y(f_n, \zeta_n, f_i)$ is the response of an SDF system with natural frequency f_n , damping ratio ζ_n , at frequency f_i ; and N is the number of data points being fit; then it

is possible to minimize J by varying the values of f_n and ζ . The values of f_n and ζ which minimize J define an equivalent oscillator whose response most closely fits the measured response of a mode of the experimental structure. The values of f_n and ζ are, in this sense, the best estimates for the resonant frequency and modal damping ratio of the response mode that is being fit. Each mode of the structure will require a new fit to determine the particular equivalent oscillator. The minimization of J requires a two-dimensional minimization with respect to f_n and ζ . Following the work of Beck (1978), a computer program was written to complete the minimization. The program is listed in the Appendix.

Figure 4.66 shows a typical experimental response curve and the response of the equivalent oscillator. It should be noted that only a small bandwidth of the experimental curve is used in the fitting process. This practice emphasizes the response near resonance and reduces the possibility of errors from the contribution of other response modes.

The results of the fit, however, were found to be moderately independent of the number of points used. The minimization was more sensitive to the natural frequency than to the damping. The results of the analysis are summarized in Table 4.6. The resonant frequency and damping of the fundamental mode have been calculated from both the superstructure and foundation records. Most of the values are averages of the results obtained for different numbers of fitted points, ranging

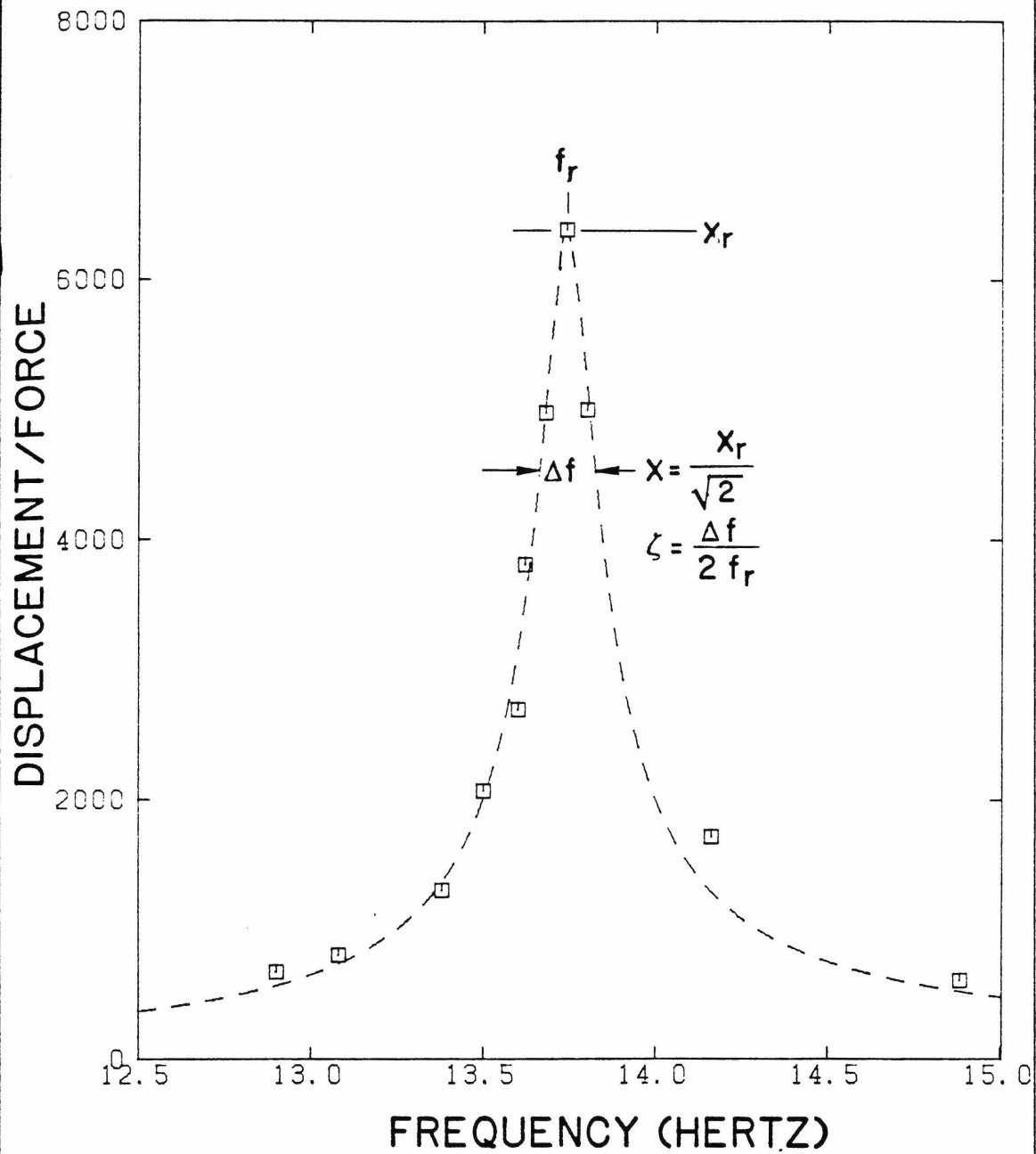


Figure 4.66. Comparison of response of fitted oscillator and experimental observations.

for example, in the case of zero-embedment, from 9 to 18 points, for the first torsional response mode.

TABLE 4.6. Modal frequencies and damping ratios from forced vibration tests by best fit to SDF system.

Mode	Zero-embedment		Half-embedment		Full-embedment	
	f_n in Hertz	ζ in percent of critical	f_n in Hertz	ζ in percent of critical	f_n in Hertz	ζ in percent of critical
Fundamental translation, from SCT	11.33	0.80	13.28	0.83	13.75	0.81
Fundamental translation, from FCT	11.30	0.76	—	—	13.70	4.4
Torsion (1) from SET	19.02	0.41	19.85	0.86	19.81	0.42
Torsion (2) from SET	24.3	0.40	24.7	0.47	25.9	—
Second translation from FCT	28.9	17.4	25.8	18.8	25.2	38.6

The following conclusions can be drawn from the results of Table 4.6.

1. Embedment of the foundation increases the fundamental frequency of the structure. Also, there is a greater change in resonant

frequency between the zero- and half-embedment cases than there is between the half- and full-embedment cases.

2. The damping ratio of the fundamental translation mode, as determined from the response of the superstructure, is independent of the embedment. This indicates that the damping is not as sensitive to embedment as the stiffness.
3. The resonant frequency and damping of the fundamental mode were calculated from the records of the foundation as well as from the superstructure. Since modal quantities are involved, the results of both calculations should be, and are, the same. The damping values, however, are substantially different for full-embedment. This can be attributed to the fewer points and poorly defined resonance peak of the foundation record, as shown in the response curves of paragraph 4.2.3.1.
4. Embedment causes a small, but consistent increase in the frequencies of the two torsional modes. The determination of the resonant frequencies of the torsional mode for the full-embedment case is imprecise because only a relatively small number of points were available for the fit.
5. No clear trend emerges for the relation of damping to embedment in the torsional modes. This may be due, in part, to the small number of data points obtained for the half- and full-embedment cases.

6. In general, increasing foundation embedment results in higher resonant frequencies. The main exception appears to be the second translatory mode, which corresponds primarily to the translation of the foundation. The resonant frequency of this mode appears to decrease with embedment. The exact values of the frequency, however, are not accurate because the motion is small and poorly defined, as shown previously in Figures 4.32, 4.38, and 4.44.
7. The damping of the second translatory mode increases substantially with embedment. While there may be some doubt in the quantitative results, inspection of the foundation response curves shows this is qualitatively correct.

4.3.2. Calculation of Translatory and Rocking Impedances.

As will be shown in Chapter 5, the response of the specimen structure to horizontally incident SH-waves can be separated into two independent groups. The first group includes the foundation and superstructure translation and the rigid body rocking degrees of freedom. The second group includes the foundation and superstructure torsional responses. The mode shape obtained at the fundamental resonance can be used to obtain estimates of the translation impedance of the foundation and superstructure, as well as the rocking impedance of the foundation. The following two paragraphs discuss the determination of these impedances. The torsional case will be discussed in subsection 4.3.3.

4.3.2.1. Determination of system stiffnesses.

Inertial forces, in a lightly damped system at resonance under harmonic excitation, can be assumed to be resisted by spring forces. Applied forces, however, are counteracted by the damping (Thomson, 1965). In this case, the response of the structure can then be separated into two systems, as shown in Figures 4.67 (a) and (b).

The spring system can be used to determine the stiffness of the foundation and superstructure, while the damping can be found from consideration of the dashpot system. The determination of damping will be the subject of paragraph 4.3.2.2.

The equations of motion of the spring system can be written as,

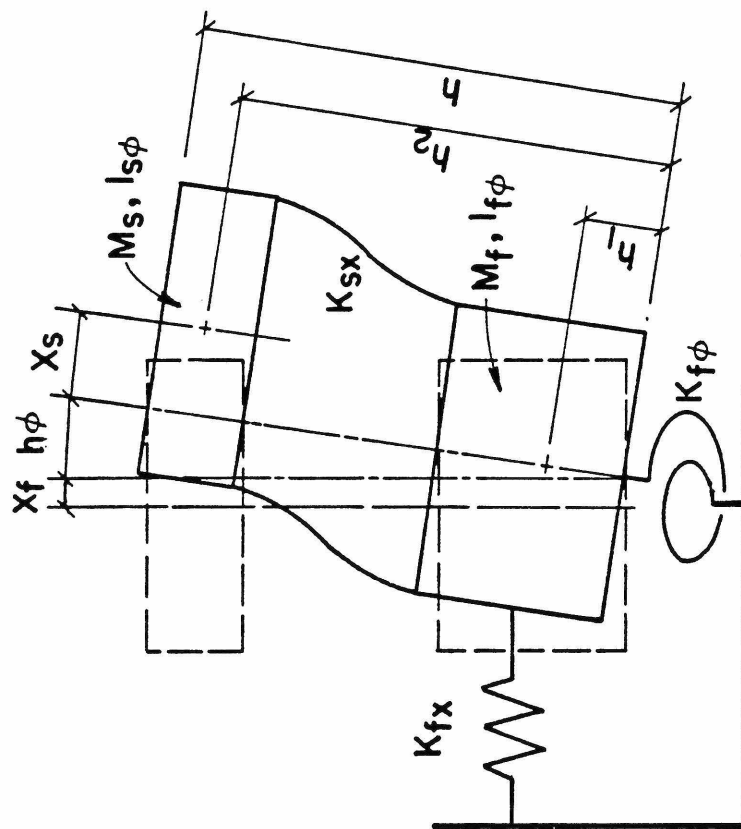
$$(M_s + M_f)\ddot{X}_f + \left[M_f \frac{h_1}{h} + M_s \frac{h_2}{h} \right] h\ddot{\phi} + M_s \ddot{X}_s = -K_{fx} X_f \quad (4.5)$$

$$(M_f h_1 + M_s h_2) \ddot{X}_f + \left[M_f \frac{h_1^2}{h} + M_s \frac{h_2^2}{h} + \frac{I_f \phi}{n} + \frac{I_s \phi}{h} \right] h\ddot{\phi} + M_s h_2 \ddot{X}_s = -K_{f\phi} \frac{h\phi}{h} \quad (4.6)$$

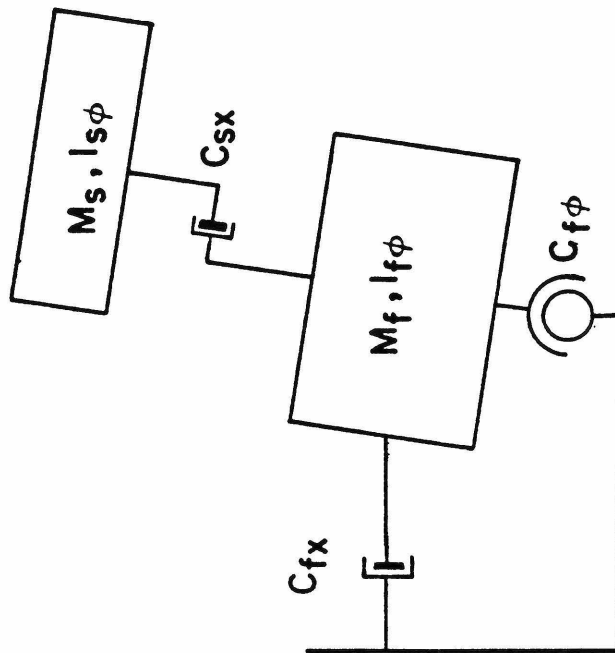
$$M_s \ddot{X}_f + M_s \frac{h_2}{h} h\ddot{\phi} + M_s \ddot{X}_s = -K_{sx} X_s \quad (4.7)$$

For sinusoidal motion,

$$\ddot{X} = -\omega^2 X \quad (4.8)$$



(a) Spring system.



(b) Dashpot system.

Figure 4.67. Mathematical models for translatory and rocking resonant motions.

Substitution of Equation (4.8) into Equations (4.5), (4.6) and (4.7) and solving for K_{sx} , K_{fx} , and $K_{f\phi}$, respectively, gives,

$$K_{sx} = M_s \omega^2 \frac{X_f}{X_s} + M_s h_2 \omega^2 \frac{h\phi}{hX_s} + M_s \omega^2 \quad (4.9)$$

$$K_{fx} = (M_f + M_s) \omega^2 + (M_f h_1 + M_s h_2) \omega^2 \frac{h\phi}{hX_f} + M_s \omega^2 \frac{X_s}{X_f} \quad (4.10)$$

$$K_{f\phi} = (M_f h_1 + M_s h_2) \omega^2 \frac{hX_f}{h} \phi + (M_f h_1^2 + M_s h_2 + I_{s\phi} + I_{f\phi}) \omega^2 + M_s h_2 \omega^2 \frac{hX_s}{h\phi} \quad (4.11)$$

The ratios X_f/X_s , $h\phi/X_s$, and $h\phi/X_f$, can be obtained from the displacement ratios listed previously in Table 4.5. Substitution of these quantities into the right hand side of Equations (4.9), (4.10), and (4.11) results in the stiffnesses of the superstructure and soil-foundation systems at the resonant frequency. These quantities are listed in Table 4.7.

The effect of embedment on the stiffness of the system leads to the following conclusions. First, the calculated stiffness of the superstructure varies with embedment. This erroneous result is a weakness of this simple approach, since the properties of the superstructure should be independent of the foundation embedment. Examination of Equation (4.9) however, shows that the calculated stiffness is dependent upon the resonant frequency and mode shape. Any errors in the determination of these quantities will have an effect on the results of the calculation. One quantity particularly susceptible to error is the base

TABLE 4.7. Superstructure and foundation-soil stiffnesses at fundamental resonant frequency by spring-system analysis.

Embedment		Superstructure Translation, K_{sx}	Foundation-soil Rocking, $K_{f\phi}$	Foundation-soil Translation, K_{fx}
Depth in feet	Ratio (d/r_o)	in lb/ft (N/m)	in lb-ft (N-m)	in lb/ft (N/m)
0	0	3.77×10^6 (5.50×10^7)	1.73×10^9 (2.34×10^9)	5.3×10^7 (7.81×10^8)
2.5	0.443	4.53×10^6 (6.61×10^7)	3.42×10^9 (4.63×10^9)	1.96×10^8 (2.84×10^9)
5.0	0.886	4.39×10^6 (6.41×10^7)	9.42×10^9 (1.28×10^{10})	3.28×10^8 (4.79×10^9)

translation, which was usually a very small quantity. Second, the soil stiffnesses K_{fx} and $K_{f\phi}$ increase substantially with embedment. The increase in stiffness indicates increasing restraint of the foundation by the soil, and is in accordance with theoretical expectations, and the observed frequencies.

Third, the ratio of the stiffnesses for the embedded to unembedded cases are plotted in Figure 4.68. A quadratic fit of the stiffness ratios, as a function of the embedment ratio, gives the following relations,

$$K_{fxe} = K_{fx}(1 + 6.2448 - 0.5088^2) \quad (4.12)$$

$$K_{f\phi e} = K_{f\phi}(1 - 0.5918 + 6.328^2) \quad (4.13)$$

The quadratic fit for the rocking stiffness ratio drops slightly below unity for small embedments. This reduction is only an artifice of the

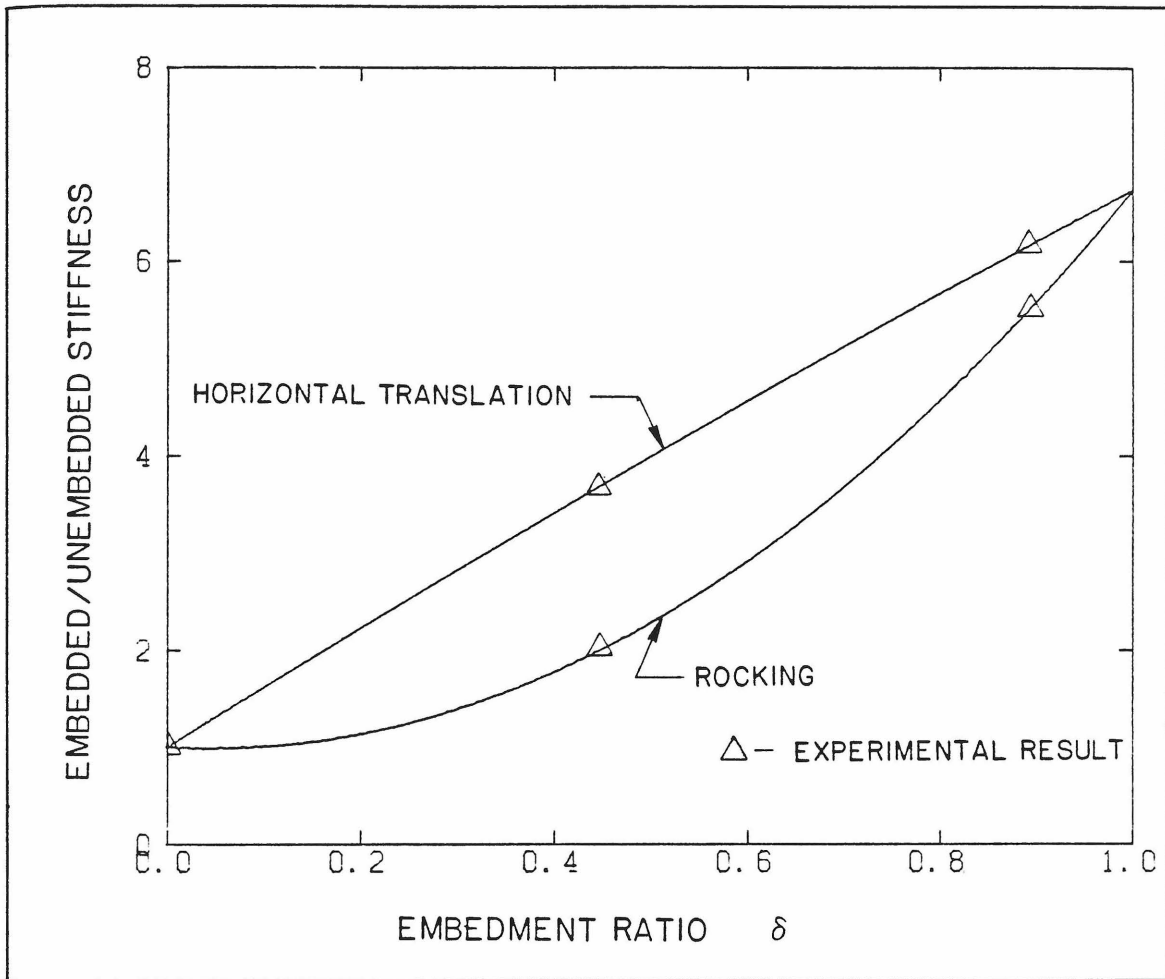


Figure 4.68. Stiffness ratios for foundation translation and rocking.

quadratic fit through the three data points. This feature is also present in the fit of the rocking damping coefficient ratio, as well.

4.3.2.2. Determination of system damping coefficients.

The system shown above in Figure 4.67 (b) can be used to estimate damping. The equations of motion of the system, considering only the

damping and d'Alembert forces of the excitation, are,

$$M_f \ddot{X}_g + M_s \ddot{X}_g = -C_{fx} \dot{X}_f \quad (4.14)$$

$$M_f h_1 \ddot{X}_g + M_s h_2 \ddot{X}_g = C_{f\phi} \frac{h\phi}{h} \quad (4.15)$$

$$M_s \ddot{X}_g = -C_{sx} \dot{X}_s \quad (4.16)$$

For sinusoidal motion,

$$\ddot{X} = \mp X \omega^2 \quad (4.17)$$

$$\dot{X} = \pm \omega X \quad (4.18)$$

Then, the following equations can be written for C_{sx} , C_{fx} , and $C_{f\phi}$, as defined previously in Figure 4.67 (b),

$$C_{fx} = \frac{1}{X_f} \omega X_g (M_f + M_s) \quad (4.19)$$

$$C_{sx} = \frac{1}{X_s} \omega X_g M_s \quad (4.20)$$

$$C_{f\phi} = \frac{h}{h\phi} \omega X_g (M_f h_1 + M_s h_2) \quad (4.21)$$

These damping coefficients are dependent upon the ratio of the superstructure displacement to the input free-field displacement listed previously in Table 4.5. Substitution of these displacement ratios into the right-hand side of Equations (4.19), (4.20), and (4.21) for each embedment case, gives the values of damping coefficient and dimensionless damping for each component of the system listed in Table 4.8.

The quantitative aspects of the effect of embedment on the damping coefficient are similar to those for stiffness. Hence, the same discussion is applicable. Figure 4.69 plots the effect of embedment on the

TABLE 4.8. Superstructure and foundation-soil damping coefficients and dimensionless damping at fundamental resonant frequency by dashpot system analysis.

Embedment		Superstructure Translation		Foundation-soil Rocking		Foundation-soil Translation	
Depth in feet	Ratio (d/r ₀)	C _{sx} in lb-sec/ft (N-sec/m)	$\frac{C_{sx}}{\sqrt{K_{sx} \cdot M_s}}$	C _{fφ} in lb-sec-ft (N-sec-m)	$\frac{C_{f\phi}}{\sqrt{K_{f\phi} \cdot I_{f\phi}}}$	C _{fx} in lb-sec/ft (N-sec/m)	$\frac{C_{fx}}{\sqrt{K_{fx} \cdot M_f}}$
0	0	1.20×10 ³ (1.75×10 ⁴)	0.013	6.67×10 ³ (9.04×10 ⁵)	0.016	4.27×10 ⁴ (6.23×10 ⁵)	0.072
2.5	0.443	1.15×10 ³ (1.68×10 ⁴)	0.015	1.09×10 ⁶ (1.48×10 ⁶)	0.071	1.37×10 ⁵ (2.00×10 ⁶)	0.121
5.0	0.886	1.29×10 ³ (1.88×10 ⁴)	0.013	3.58×10 ⁶ (4.85×10 ⁶)	0.141	2.77×10 ⁵ (4.04×10 ⁶)	0.189

damping coefficient. A quadratic fit of the plot gives the following relations,

$$C_{fxe} = C_{fx}(1 + 3.782\delta + 2.719\delta^2) \quad (4.22)$$

$$C_{f\phi e} = C_{f\phi}(1 - 2.066\delta + 7.906\delta^2) \quad (4.23)$$

4.3.3. Calculation of Torsional Properties.

The experimental results obtained for the two torsional modes contained features that made the complete characterization of the torsional response difficult. After the torsional resonant frequencies had been identified, the relative phase and amplitude of torsional response of the foundation and superstructure were measured.

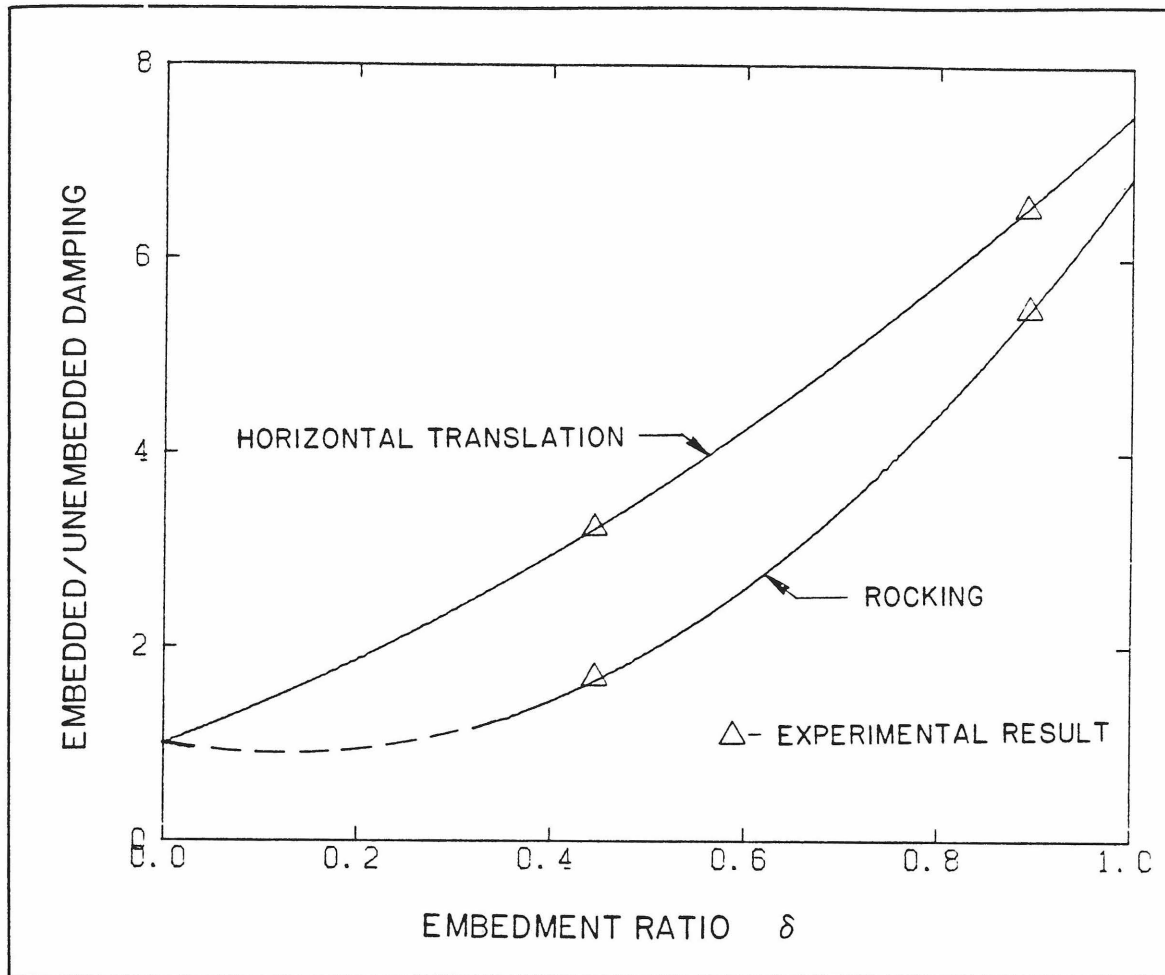


Figure 4.69. Damping ratios for foundation translation and rocking.

The torsional response was measured by placing seismometers at the locations shown in Figure 4.70. The north-south orientation of the seismometers minimized the contribution from the translational response of the structure caused by the incident SH-wave. Under ideal conditions, the SH-waves would cause no displacement at FCTN and SCTN, while the tangential displacement due to the torsional motion will be recorded at FETN and SETN. The experimental conditions, of course, were not

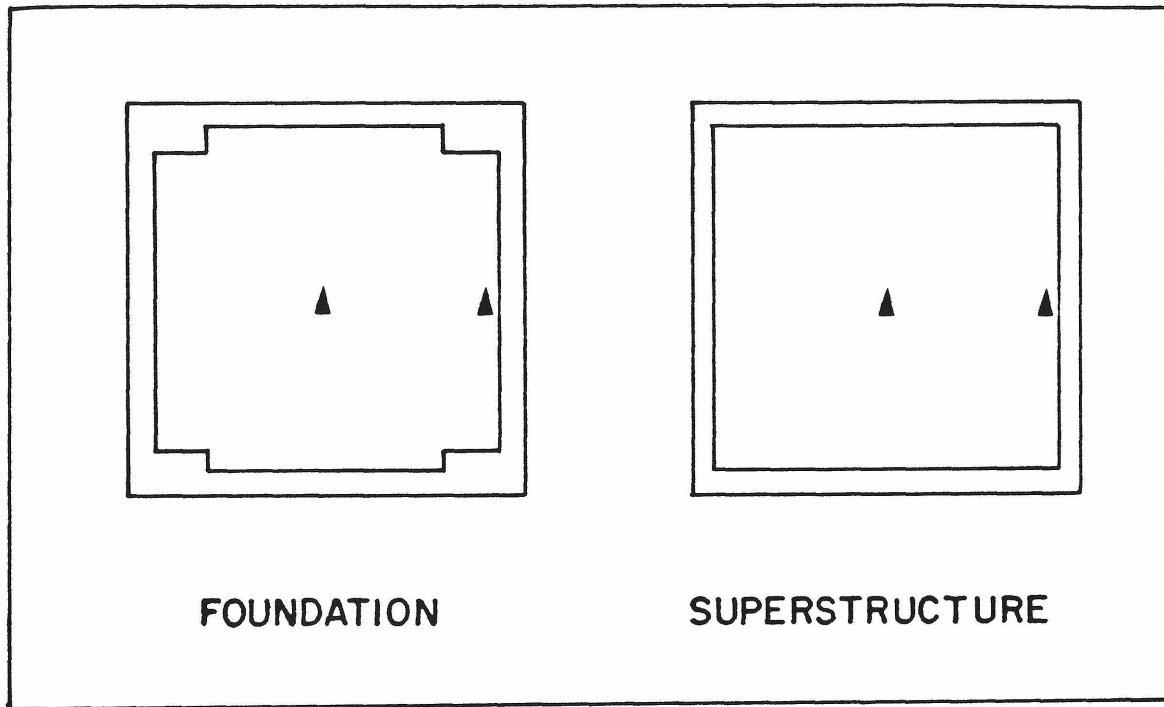


Figure 4.70. Location of seismometers for torsional mode shape measurement. Arrowheads indicate location and orientation of seismometers.

ideal, and there were small displacements at FCTN and SCTN caused by the north-south translation that had to be subtracted from the motions recorded at FETN and SETN, respectively. The corrected amplitudes of FETN and SETN are then proportional to the torsional response.

The mode shape can be further characterized by determination of the relative phase between the superstructure and foundation response. The first torsional mode should consist of the superstructure and foundation moving nearly in-phase, while the second mode response is expected to consist of motions in which the two masses move nearly 180 degrees out-of-phase. (These conditions would exist for a system with normal

modes). Table 4.9 lists the relative response amplitudes and phase of the superstructure with respect to the foundation for the three embedment cases.

TABLE 4.9. Displacement ratios and phase angles between foundation and superstructure in torsional response.

Embedment in feet	Resonant Frequency in Hertz	Displacement*		Ratio $\frac{(2)}{(1)}$	Phase Angle Between Super- structure and Foundation, in degrees
		of Founda- tion Edge (1)	of Super- struct. Edge (2)		
0	19.02	118	1816	15.4	0
	24.30	276	1347	4.9	0
2.5	19.85	9	922	102	60
	24.74	48	2820	59	120
5.0	19.81	17	2770	160	240
	25.87	100	4260	43	290

*in units of displacement/force of subsection 4.3.2.

Several features of the results shown in Table 4.9 are enumerated here. For each embedment case, the ratio between the displacements of the superstructure and foundation is larger at the lower resonant frequency than at the higher one. This is consistent with the response expected from a two-degree-of-freedom system. Furthermore, the displacement ratio of the lower torsional frequency increases with embedment. This indicates increasing foundation stiffness relative to the superstructure stiffness. There was no clear trend for the higher frequency. Finally, with the exception of the first mode of zero-

embedment, the measured phase angles are not consistent with expectations based on a lightly damped two-degree-of-freedom model.

The torsional behavior of the structure can be modelled by the two-degree-of-freedom system shown in Figure 4.71.

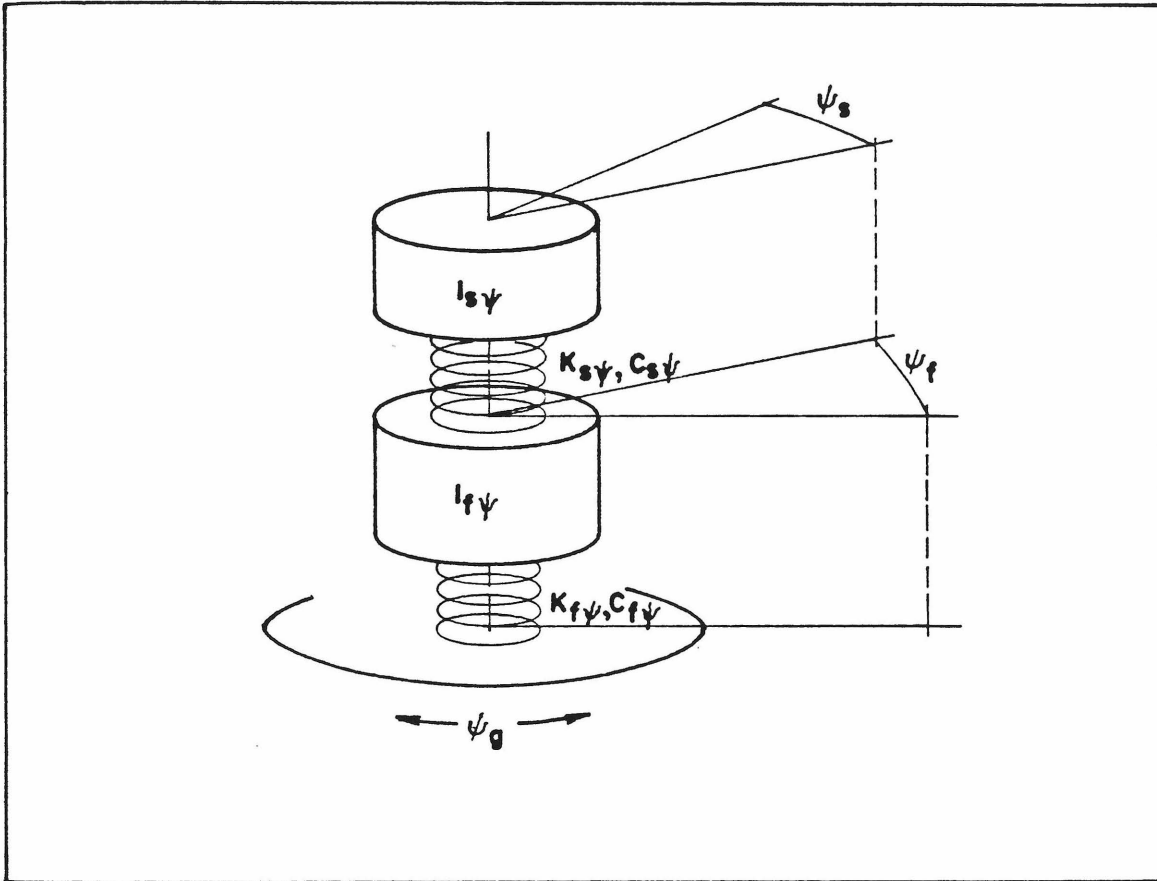


Figure 4.71. Mathematical model for two degree-of-freedom system in torsion.

It should be emphasized that the measurements used for the determination of the displacements, especially of the foundation, were difficult to obtain in the experiment. The amount of error contained in

the results may be considerable, and therefore, these results will not be used in subsequent calculations. The qualitative aspects, however, are thought to be valid.

The measurements of resonant frequency are accurate and can be used to obtain estimates of the superstructure and foundation-soil stiffnesses. As discussed in subsection 4.3.2, the resonant frequencies and mode shape can be used to determine the stiffness, while the response amplitude is required to determine damping. In this case, however, information about the mode shape is not required, since there are two conditions (the resonant frequencies) and two unknowns (the stiffnesses).

If the damping is neglected, the equations of motion are,

$$I_s \ddot{\varphi}_s + K_s \varphi (\varphi_s - \varphi_f) = 0 \quad (4.24)$$

$$I_f \ddot{\varphi}_f + K_f \varphi_f + K_s \varphi (\varphi_f - \varphi_s) = 0 \quad (4.25)$$

For steady-state response, the acceleration can be expressed in terms of the displacement by,

$$\ddot{\varphi} = -\omega^2 \varphi_x \quad (4.26)$$

The equations of motion can now be expressed solely in terms of the displacements.

$$\begin{bmatrix} K_s \varphi - I_s \omega^2 & -K_s \varphi \\ -K_s \varphi & K_s \varphi + K_f \varphi_f - I_f \omega^2 \end{bmatrix} \begin{Bmatrix} \varphi_s \\ \varphi_f \end{Bmatrix} = 0 \quad (4.27)$$

The two homogeneous algebraic equations represented in matrix form in Equation (4.27) will have trivial solutions unless the determinant of the impedance matrix identically vanishes. Ordinarily, the determinant is made to vanish by selection of the eigenvalues λ_1 and λ_2 , where $\lambda = \omega^2$. In this case, however, the resonant frequencies have been measured; it is the stiffnesses that are not known. Therefore, the eigenvalue problem becomes one of finding the values of $K_{s\phi}$ and $K_{f\phi}$ that cause the determinant to have a zero value.

Two algebraic equations result from the successive substitution of the resonant frequencies ω_1 and ω_2 into the expanded form of the matrix equation. These two equations are solved simultaneously for the stiffnesses $K_{s\phi}$ and $K_{f\phi}$,

$$K_{s\phi}K_{f\phi} - K_{f\phi}(I_{s\phi}\omega_i^2) - K_{s\phi}(I_{s\phi}\omega_i^2 + I_{f\phi}\omega_i^2) + I_{s\phi}I_{f\phi}\omega_i^4 = 0$$

$$i = 1, 2 \quad . \quad (4.28)$$

The roots of these equations, however, are complex. This result is inconsistent with the assumption of zero damping (since damping is given by the magnitude of the imaginary component) at the outset. Stated in another way, the complex roots indicate that there are no values of foundation and superstructure stiffnesses, for the two-degree-of-freedom model, that when combined with the moments of inertia of the superstructure and foundation, define a system that has the measured resonant frequencies.

In view of this situation, the interpretation of the torsional response of the system requires a more complicated model. One such

model will be presented in subsection 5.4.2, in which a hybrid calculation is given that combines both analytical and experimental results to obtain an estimate of the system properties.

4.4. COMPARISON OF RESULTS.

The response of the specimen structure to ambient vibration, ring-down, and forced vibration was measured to obtain independent estimates of the resonant frequencies and modal dampings. Since all the tests were conducted on the same structure, the results of the tests are expected to be the same, within the limits of experimental inaccuracies. Comparison of the results of these tests, as shown in Table 4.2 for the ambient vibration, Table 4.3 for the ring-down, and Table 4.6 for the forced vibration, leads to the following conclusions.

1. The resonant frequencies of the fundamental east-west translatory mode, found by the different methods, are in relative agreement with the largest discrepancy being 6%. It should be recalled that the available precision is greatest for the forced vibration tests, and least for the ring-down. This precision is expressed by the number of significant figures used to report the results.
2. In the north-south direction, the results of the ring-down and ambient vibration tests are also close. No forced vibration tests were conducted in this direction. Note that the resonant

frequency of this mode did not appear to change between the half- and full-embedment cases in the ring-down tests.

3. Torsional frequencies found from the ambient and forced vibration tests are also in agreement, although at zero-embedment the forced vibration results are about 2% lower than the ambient test results.
4. The originally supposed second resonant frequency of 21.9 Hertz found in the ambient vibration tests did not appear in the forced vibration results. The second translation frequency, found from the forced vibration tests, was heavily damped and embedment dependent, and had an approximate value of 25 to 30 Hertz.
5. In the east-west direction, the estimates of damping obtained from the ring-down and forced vibration tests were in general agreement.
6. The agreement between the results of the three tests was, in general, good. Although a more detailed description of the structure was made possible by the forced vibration tests, the characterization of the fundamental mode behavior by the ring-down and ambient vibration tests was of sufficient accuracy for many purposes. While the higher modes were not identified by the simpler tests, it should be realized that these modes generally are also of lesser importance.

7. The effect of embedment was observed in all tests. If the determination of numerical values of the system impedances had not been a goal of this study, the far simpler ambient and ring-down tests could possibly have sufficed.

4.5. CHAPTER SUMMARY.

This chapter has presented the results of several test series that were designed to determine the effects of foundation embedment on structural response.

The first series consisted of measurements of the ground motion caused by the vibration of the excitation structure. The results of this test series included the establishment of a base-line free-field ground motion, the determination of a frequency dependent function that described the amplitude of ground motion at the specimen structure site, and finally, the in situ determination of the shear wave velocity, which was found to be 1000 ft/sec (305 m/sec). This value of shear wave velocity is significantly less than the results of the preliminary tests discussed in Chapter 2. The earlier results, because they depend on "first arrival times", naturally yield the maximum velocities, while in this case, the minimum measured values were selected for their expected representation of the near-surface soil properties.

After completion of the free-field motion studies, the specimen structure was constructed with full foundation embedment. Ambient vibration, ring-down, and forced vibration tests were then conducted.

These tests were subsequently repeated for the cases of half- and non-embedment of the foundation.

The ambient vibration tests provided information that led to the identification of four modes of vibration; the fundamental translational mode in the east-west and north-south directions, and two torsional modes. The resonant frequencies were found to increase with embedment. The effect of the frequency content of the ambient vibration on the resulting Fourier amplitude spectra was also noted. Modal damping cannot be determined accurately from the Fourier amplitude spectra.

Ring-down tests were used to provide simple determinations of the fundamental modal frequencies and damping ratios.

The measurement of the response of the structure to incident SH-waves produced the most information. These tests provided data from which the resonant frequencies and modal dampings could be determined accurately by the use of an equivalent single degree-of-freedom oscillator. Four modes of response were identified; the fundamental and secondary translation in the east-west direction, and two torsional modes. Translational response in the north-south direction was not excited, since the excitation consisted of a shear wave that generated lateral motions in the east-west direction. At the fundamental resonant frequency, measurements of the mode shape and the near-field ground motion were also taken.

The results of the three types of tests were found to be in good agreement. Some of the information about the fundamental mode could be determined solely by ambient and ring-down tests. The forced vibration

tests, however, provided a more detailed characterization of the mode shape and higher modes of response.

Analysis of the results of the experiment led to the determination of the structural and foundation-soil impedances in the form of stiffness and damping values. Relations were also derived which described the effect of embedment on the stiffness and damping of the foundation-soil system in translation and rocking.

A similar attempt to calculate the torsional properties of the corresponding two-degree-of-freedom system based on the observed behavior of the specimen structure was unsuccessful. It was not possible to find values of the superstructure and foundation stiffness, that when combined with the moments of inertia of the foundation and superstructure, defined a system with the observed resonant frequencies. Hence, the torsional behavior of the specimen structure could not be modelled by a simple two-degree-of-freedom system.

CHAPTER REFERENCES.

- Beck, J.L., Determining Modes for Structures from Earthquake Records, EERL 80-01, Caltech, Pasadena, California, June, 1978.
- Ballard, R.F., Jr., "Determination of soil shear moduli at depth by in-situ vibratory techniques," Waterways Experiment Station Miscellaneous Paper, No. 4-691, Dec. 1964.
- Foutch, D.A., A Study of the Vibrational Characteristics of Two Multi-Story Buildings, EERL 76-03, Caltech, Pasadena, California, Sept. 1976.
- Fry, Z.B., "Development and evaluation of soil-bearing capacity, foundations of structures," Waterways Experiment Station Technical Report No. 3-632, Report No. 1., Vicksburg, Miss., July, 1963.
- Fung, Y.C., Foundations of Solid Mechanics, Prentice-Hall, Inc., Englewood Cliffs, N.J., 1965.
- Heukelom, W., and Foster, C.R., "Dynamic testing of pavements," Journal of the Soil Mechanics and Foundations Division, ASCE, Vol. 86, No. SM1, part 1, Feb. 1960, pp. 1-28.
- Jennings, P.C., and Kuriowa, J.H., "Vibration and soil-structure interaction tests of a nine-story reinforced concrete building," Bulletin of the Seismological Society of America, Vol. 58, No. 3, June 1968, pp. 891-916.
- Luco, J.E., "Torsional response of structures to obliquely incident seismic SH-waves," Earthquake Engineering and Structural Dynamics, Vol. 4, No. 4, Jan.-March, 1976, pp. 207-219.
- Richart, F.E., Jr., Hall, J.R., Jr., and Woods, R.D., Vibrations of Soils and Foundations, Prentice-Hall, Inc., Englewood Cliffs, N.J., 1970.
- Thomson, W.T., Vibration Theory and Applications, Prentice-Hall, Inc., Englewood Cliffs, N.J., 1965.

CHAPTER 5

RESULTS OF ANALYSIS

Many studies have examined the soil-structure interaction problem with the results ranging from the derivation of complicated integral equations and development of finite element models to the derivation of simpler equations or curves that can be used for design. In most cases, the equations presented for use in analysis or design have resulted from the numerical evaluation of more involved closed-form solutions.

In this chapter, a lumped parameter analysis will be used to determine the theoretical response of the specimen structure to SH-wave excitation. Because of the emphasis of this study, attention is focused on the effects of soil-structure interaction and, more specifically, on the effect of foundation embedment. The results of the analysis will then be compared to the experimental results.

This chapter is divided into five sections. The first section describes the analytical models that will be used for the analysis. The dynamic properties of the superstructure and the equivalent radius of the foundation are determined in the second section. In the third section, various foundation-soil impedance and embedment formulations for the fundamental mode behavior of the structure are described and compared. These formulations are then used to calculate the response of the structure in the fundamental mode. A similar analysis is conducted for the torsional response in Section 5.4. The last section summarizes the chapter.

5.1. METHODS OF ANALYSIS.

The lumped parameter method of analysis consists of the reduction of a complicated structure to a system of masses and simple spring and dashpot elements. The equations of motion of the model are then written and solved, usually by numerical means. For linear problems in soil-structure interaction, the solution is usually presented in the frequency domain. This method of analysis, compared to the finite element method, for example, is more economical and sufficiently accurate for design (Lam and Scavuzzo, 1979). Lumped parameter analysis is, however, generally limited to structures with relatively simple geometries.

In general, a one-story structure subjected to horizontally incident SH-waves along an axis of symmetry has five pertinent degrees of freedom,

- Superstructure displacement relative to the base,
- Foundation displacement relative to the soil,
- Rocking of the entire structure about the bottom of the base,
- Torsion of the superstructure about a vertical axis, relative to the base, and
- Torsion of the foundation about a vertical axis, relative to the soil.

For steady-state response to harmonic motion, the system requires the solution of ten simultaneous algebraic equations to obtain both the magnitude and phase of response for each degree of freedom. This

implies a substantial effort for such a simple problem. Fortunately, such complexity is not necessary in this case. Because of the excitation and the symmetry of the specimen structure, the structure can be separated into two uncoupled systems.

The first system has three degrees of freedom, namely those of the translations of the superstructure and foundation, as well as the rocking of the entire structure about the base. The most significant seismic behavior of prototype structures can be described by similar systems, except that additional degrees of freedom are required to represent the translatory response of additional stories. The second system represents the torsional response of the structure. In this case, two degrees of freedom, to represent the torsional behavior of the foundation and superstructure, are required. In general, the torsional response is of secondary importance in the seismic behavior of prototype structures.

Since each degree of freedom requires the solution of two equations; one for the response magnitude, the other for the relative phase; six simultaneous algebraic equations must be solved for the first system, and four equations must be solved for the second system. Because the original system resulted in a matrix of 100 (10×10) elements, while the two uncoupled systems result in two matrices with a total of 52 ($6 \times 6 + 4 \times 4$) elements, the separation of the original problem into the two simpler problems is seen to significantly reduce the amount of work required.

If the ground motion is written in the form

$$X_g = X(\omega) \sin \omega(t - y/C_s) \quad , \quad (5.1)$$

the lumped parameter models shown in Figures 5.1 and 5.2 can be developed. These two models are similar to those developed for the systems identification calculations of Section 4.3.

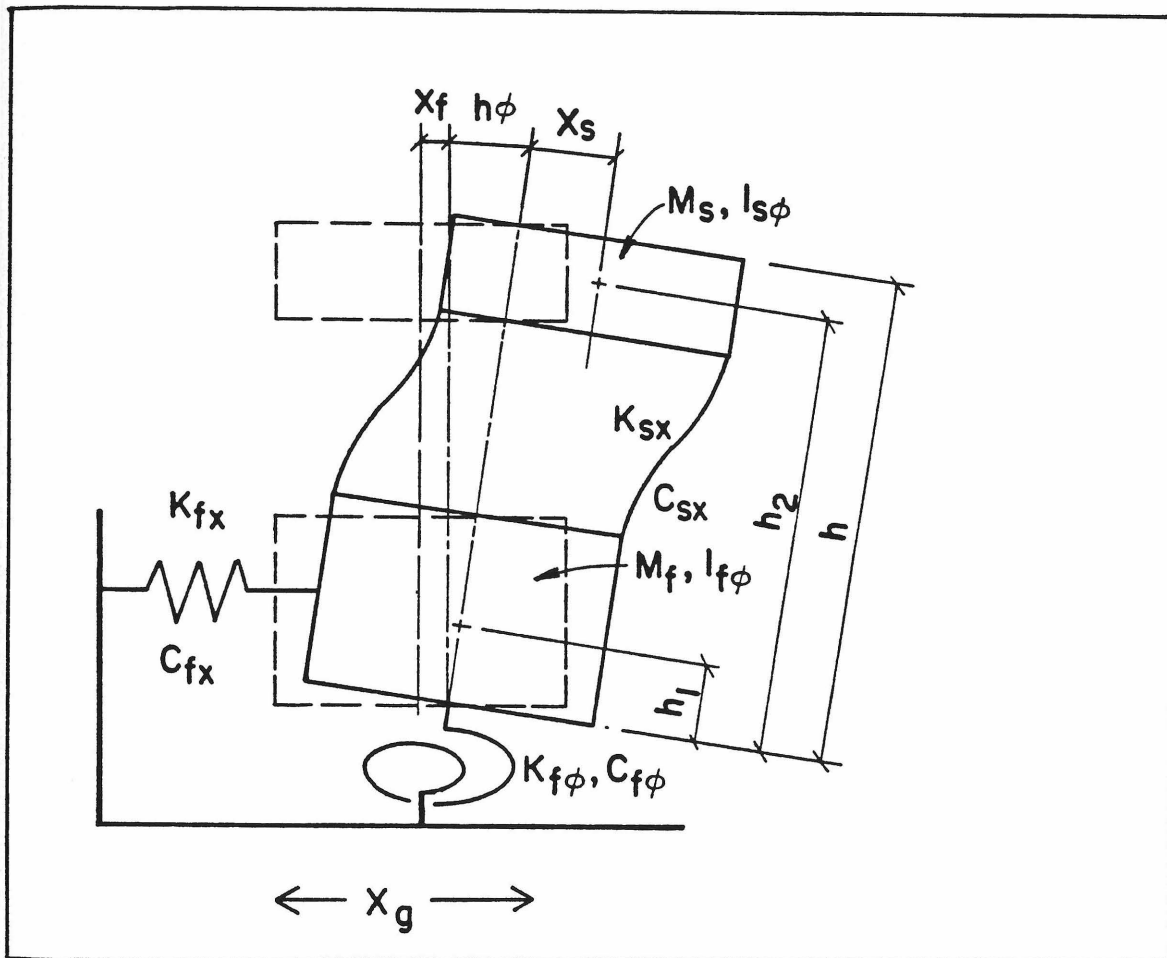


Figure 5.1. Three-degree-of-freedom model for lumped parameter analysis of foundation translation and rocking, and interfloor displacement.

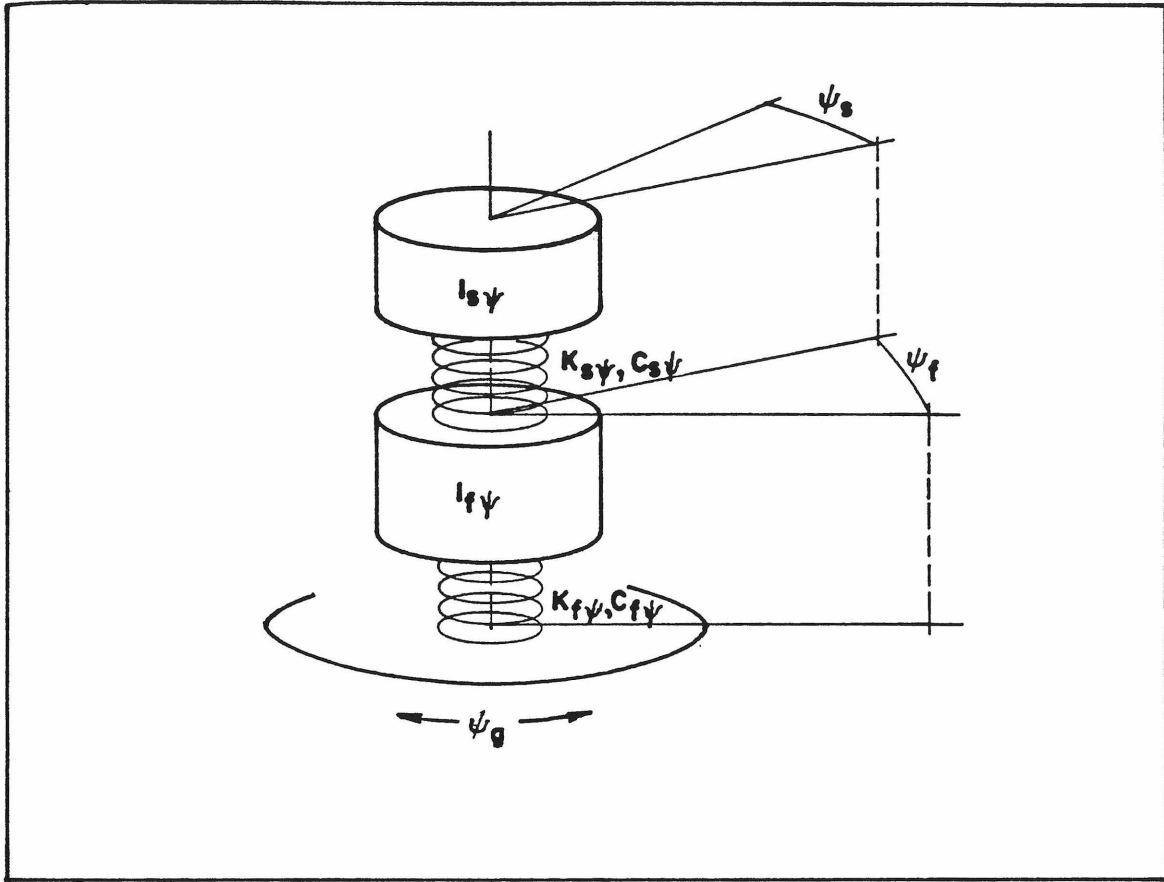


Figure 5.2. Two-degree-of-freedom model for lumped parameter analysis of foundation and superstructure torsion.

The equations of motion for the system shown in Figure 5.1 are,

$$\begin{aligned}
 M_f(\ddot{X}_f + h_1\ddot{\phi} + \ddot{X}_g) + M_s(\ddot{X}_f + h_2\ddot{\phi} + \ddot{X}_s + \ddot{X}_g) \\
 + C_{fx}\dot{X}_f + K_{fx}X_f = 0
 \end{aligned}
 \tag{5.2}$$

$$\begin{aligned}
 M_f(h_1\ddot{X}_f + h_1^2\ddot{\phi} + h_1\ddot{X}_g) + (I_s\ddot{\phi} + I_f\ddot{\phi}) + M_s(h_2\ddot{X}_f \\
 + h_2^2\ddot{\phi} + h_2\ddot{X}_s + h_2\ddot{X}_g) + C_{f\phi}\dot{\phi} + K_{f\phi}\phi = 0
 \end{aligned}
 \tag{5.3}$$

$$M_s(\ddot{X}_f + h_2\ddot{\phi} + \ddot{X}_s + \ddot{X}_g) + C_{sx}\dot{X}_s + K_{sx}X_s = 0 \quad (5.4)$$

For the steady state solutions given by,

$$X_f = A \sin \omega t + B \cos \omega t \quad (5.5a)$$

$$\phi = C \sin \omega t + D \cos \omega t \quad (5.5b)$$

$$X_s = E \sin \omega t + F \cos \omega t \quad (5.5c)$$

the following matrix equation can be written

$$[K_1] \begin{Bmatrix} A \\ B \\ C \\ D \\ E \\ F \end{Bmatrix} = \{F_1\} \quad (5.6)$$

where $[K_1]$ is given by Equation (5.7) shown on the following page and

$\{F_1\}$ is given by,

$$\begin{Bmatrix} M_f + M_s \\ 0 \\ M_f h_1 + M_s h_2 \\ 0 \\ M_s \\ 0 \end{Bmatrix} X(\omega) \omega^2 \sin \omega t \quad (5.8)$$

Solution of Equation 5.6 for the quantities A, B, C, D, E, and F leads to the following response magnitudes and phases,

$$|x_f| = A^2 + B^2 \quad (5.9a)$$

$$\theta_{xf} = \tan^{-1} \frac{B}{A} \quad (5.9b)$$

$$|\phi| = C^2 + D^2 \quad (5.9c)$$

$$\begin{bmatrix}
 K_{fx} - \omega^2(M_f + M_s) & -C_{fx}\omega & -\omega^2(M_f h_1 + M_s h_2) & 0 & -\omega^2 M_s & 0 \\
 C_{fx}\omega & k_{fx} - \omega^2(M_f + M_s) & 0 & -\omega^2(M_f h_1 + M_s h_1) & 0 & -\omega^2 M_s \\
 -\omega^2(M_f h_1 + M_s h) & 0 & K_f \phi - \omega^2(M_f h_1^2 + M_s h_2^2 + I_s \phi + I_f \phi) & -\omega C_f \phi & -\omega^2 M_s h_2 & 0 \\
 0 & -\omega^2(M_f h_1 + M_s h_2) & \omega C_f \phi & K_f \phi - \omega^2(M_f h_1^2 + M_s h_2^2 + I_s \phi + I_f \phi) & 0 & -\omega^2 M_s h_2 \\
 -\omega^2 M_s & 0 & -\omega^2 M_s h_1 & 0 & K_{sx} - \omega^2 M_s & -\omega C_{sx} \\
 0 & -\omega^2 M_s & 0 & -\omega^2 M_s h_1 & \omega C_{sx} & K_{sx} - \omega^2 M_s
 \end{bmatrix}$$

Equation (5.7)

$$\theta_d = \tan^{-1} \frac{D}{C} \quad (5.9d)$$

$$|x_s| = E^2 + F^2 \quad (5.9e)$$

$$\theta_{sx} = \tan^{-1} \frac{F}{E} \quad (5.9f)$$

In a similar way, the equations of motion for the system shown in Figure 5.2 are,

$$I_{s\phi}(\ddot{\phi}_s + \ddot{\phi}_f + \ddot{\phi}_g) + I_{f\phi}(\ddot{\phi}_f + \ddot{\phi}_g) + C_{f\phi}\dot{\phi}_f + K_{f\phi}\phi_f = 0 \quad (5.10)$$

$$I_{s\phi}(\ddot{\phi}_s + \ddot{\phi}_f + \ddot{\phi}_g) + C_{s\phi}\dot{\phi}_s + K_{s\phi}\phi_s = 0 \quad (5.11)$$

If the steady-state solutions to Equations (5.10) and (5.11) are written in the form,

$$\phi_f = \alpha \sin \omega t + \beta \cos \omega t \quad (5.12a)$$

$$\phi_s = \gamma \sin \omega t + \delta \cos \omega t \quad (5.12b)$$

the following matrix equation can be written

$$[K_2] \begin{Bmatrix} \alpha \\ \beta \\ \gamma \\ \delta \end{Bmatrix} = \{F_2\} \quad (5.13)$$

where $[K_2]$ is given by

$$\begin{bmatrix} K_{f\phi} - \omega^2(I_{s\phi} + I_{f\phi}) & -\omega C_{f\phi} & -\omega^2 I_{s\phi} & 0 \\ \omega C_{f\phi} & K_{f\phi} - \omega^2(I_{s\phi} + I_{f\phi}) & 0 & -\omega^2 I_{s\phi} \\ -\omega^2 I_{s\phi} & 0 & K_{s\phi} - \omega^2 I_{s\phi} & -\omega C_{s\phi} \\ 0 & -\omega^2 I_{\phi} & \omega C_{s\phi} & K_{s\phi} - \omega^2 I_{s\phi} \end{bmatrix} \quad (5.14)$$

and $\{F_2\}$ is given by

$$\begin{Bmatrix} 0 \\ I_s \ddot{\phi} + I_f \ddot{\phi} \\ 0 \\ I_s \ddot{\phi} \end{Bmatrix} = \ddot{\phi}_g \quad (5.15)$$

where,

$$\ddot{\phi}_g = \frac{d}{dy} \ddot{x}_g = X(\omega) \frac{\omega^3}{C_s} \cos \omega t \quad .$$

The resulting torsional response magnitudes and phase are given by,

$$|\phi_f| = \alpha^2 + \beta^2 \quad (5.16a)$$

$$\theta_{\phi_f} = \tan^{-1} \frac{\beta}{\alpha} \quad (5.16b)$$

$$|\phi_s| = \gamma^2 + \delta^2 \quad (5.16c)$$

$$\theta_{\phi_s} = \tan^{-1} \frac{\gamma}{\delta} \quad . \quad (5.16d)$$

5.2. DYNAMIC PROPERTIES

This section summarizes the calculations that were used to determine the dynamic properties of the specimen structure.

5.2.1. Superstructure Stiffness and Damping in Translation.

The columns consisted of W12 \times 22 (305 \times 102 \times 35 kg/m UB) beams welded to a bearing plate at the bottom, and to the angle frame at the top. The total length of the column was 60 in (1.52 m). The section

dimensions and properties are shown in Figure 5.3. (American Institute of Steel Construction, 1980.)

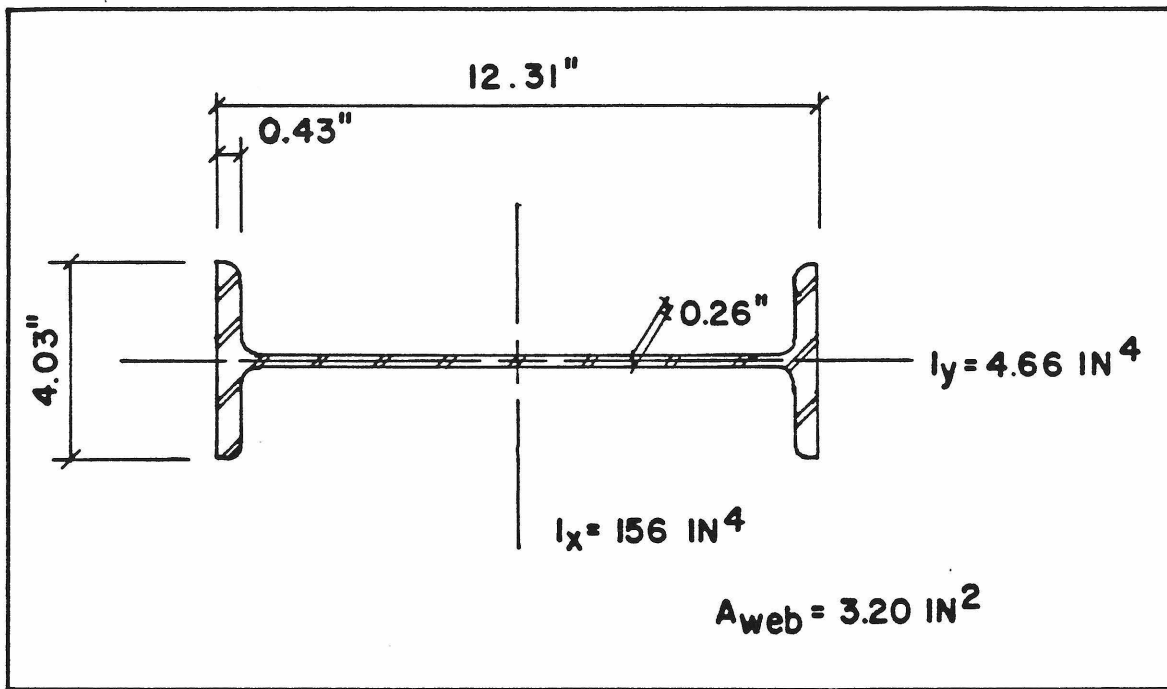


Figure 5.3. Section properties of W12 \times 22 column.

The column connections were designed to be moment resistant. In prototype structures, this condition usually means that the stiffness of the end connections is significantly greater than the stiffness of the column. Therefore, a fixed end condition can be assumed. In the specimen structure, however, several factors reduce the fixity of the end connections. The column's stiffness is, in fact, large compared to the rigidity of the end connections. Furthermore, because the width of the column is not small compared to the length, bending is not the only significant mechanism of deformation; there can also be shear. Under these

conditions, more accurate results will be obtained if the member is analyzed as part of a rigid frame subject to both bending and shear. The frame representing the specimen structure is shown in Figure 5.4. In this case, the moment distribution method can be used to obtain the column stiffness.

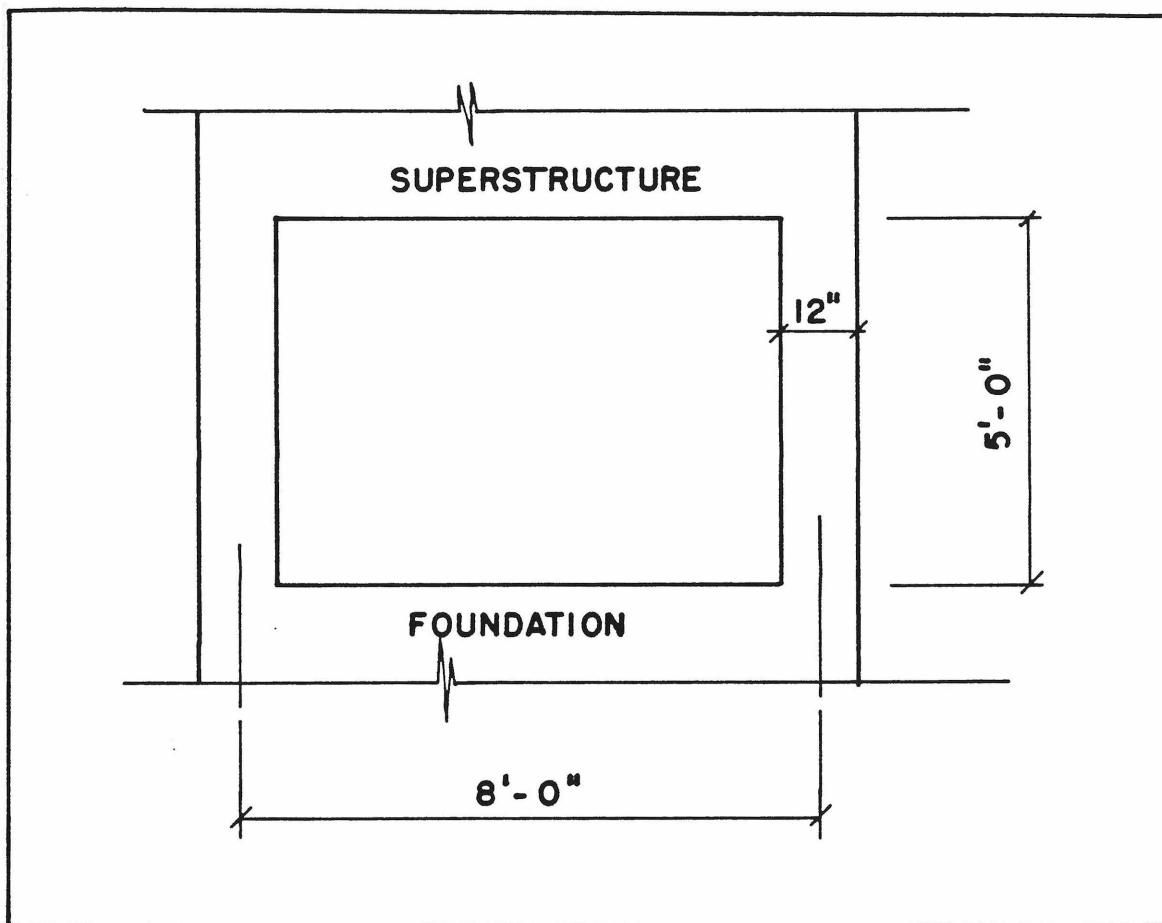


Figure 5.4. Rigid frame for column stiffness analysis.

Maugh (1946) defined a dimensionless parameter

$$j = \frac{3EI}{L^2 GA_{\text{shear}}} \quad (5.17)$$

for use in the evaluation of the stiffness and moment distribution carryover factors,

$$s = \frac{4(1+j)}{1+4j} \quad (5.18)$$

and

$$rs = \frac{2(1-2j)}{1+4j} \quad (5.19)$$

The new stiffness factor k' is defined by

$$k' = \frac{s+rs}{6} \quad (5.20)$$

The stiffness of the column is found from

$$K = k' \frac{12EI}{L^3} \quad (5.21)$$

Joint flexibility was considered by Muto (1965), who suggested increasing the clear length of the column by one-quarter of the column width at each end,

$$L = L_c + 2 \times 1/4 d \quad (5.22)$$

The column stiffness can be calculated from Equations (5.18), (5.19), (5.20), and (5.21) subject to the definition of Equation (5.22), and the relation for steel that $E = 2.6G$,

$$j = \frac{3(2.6G \text{ lb/in}^2)(156 \text{ in}^4)}{(66 \text{ in})^2(G \text{ lb/in}^2)(3.20 \text{ in}^2)} = 0.0873 \quad (5.23)$$

$$s = \frac{4(1 + 0.0873)}{1 + 4(.0873)} = 3.224 \quad (5.24)$$

$$rs = \frac{2[1 - 2(.0873)]}{1 + 4(.0873)} = 1.224 \quad (5.25)$$

$$k' = \frac{3.224 + 1.224}{6} = 0.7413 \quad (5.26)$$

Then,

$$\begin{aligned} K_{sx} &= 0.7413 \frac{12(29 \times 10^6 \text{ lb/in}^2)(156 \text{ in}^4)(12 \text{ in/ft})}{(66 \text{ in})^3} \\ &= 1.68 \times 10^6 \text{ lb/ft/col} \\ &= 6.72 \times 10^6 \text{ lb/ft} - \text{total } (9.81 \times 10^4 \text{ kN/m}). \end{aligned} \quad (5.27)$$

The structural damping is a more difficult quantity to estimate. It cannot be calculated reliably for a structure such as the specimen. Fortunately, structural damping is usually very small and does not have a significant effect on the resonant frequency. Based on experience, a damping factor ζ of 1% can be used as a reliable estimate and leads to a viscous damping coefficient of

$$\begin{aligned} C_{sx} &= 2\zeta_{sx} \sqrt{K_{sx} M_s} \\ &= 2(.01) \sqrt{6.72 \times 10^6 \text{ lb/ft} \times 550 \frac{\text{lb-sec}^2}{\text{ft}}} \\ &= 1.22 \times 10^3 \text{ lb-sec/ft } (17.4 \text{ kN-sec/m}) \end{aligned} \quad (5.28)$$

5.2.2. Superstructure Stiffness and Damping in Torsion.

The rotation of the superstructure with respect to the foundation results in the tangential deformation of the column top with respect to the center of the structure, as shown in Figure 5.5. In this case, the

rotation of the column can be neglected, and the column deformation can be resolved into successive bending deformations about the principal axes. The biaxial deformation for one column is shown in Figure 5.6.

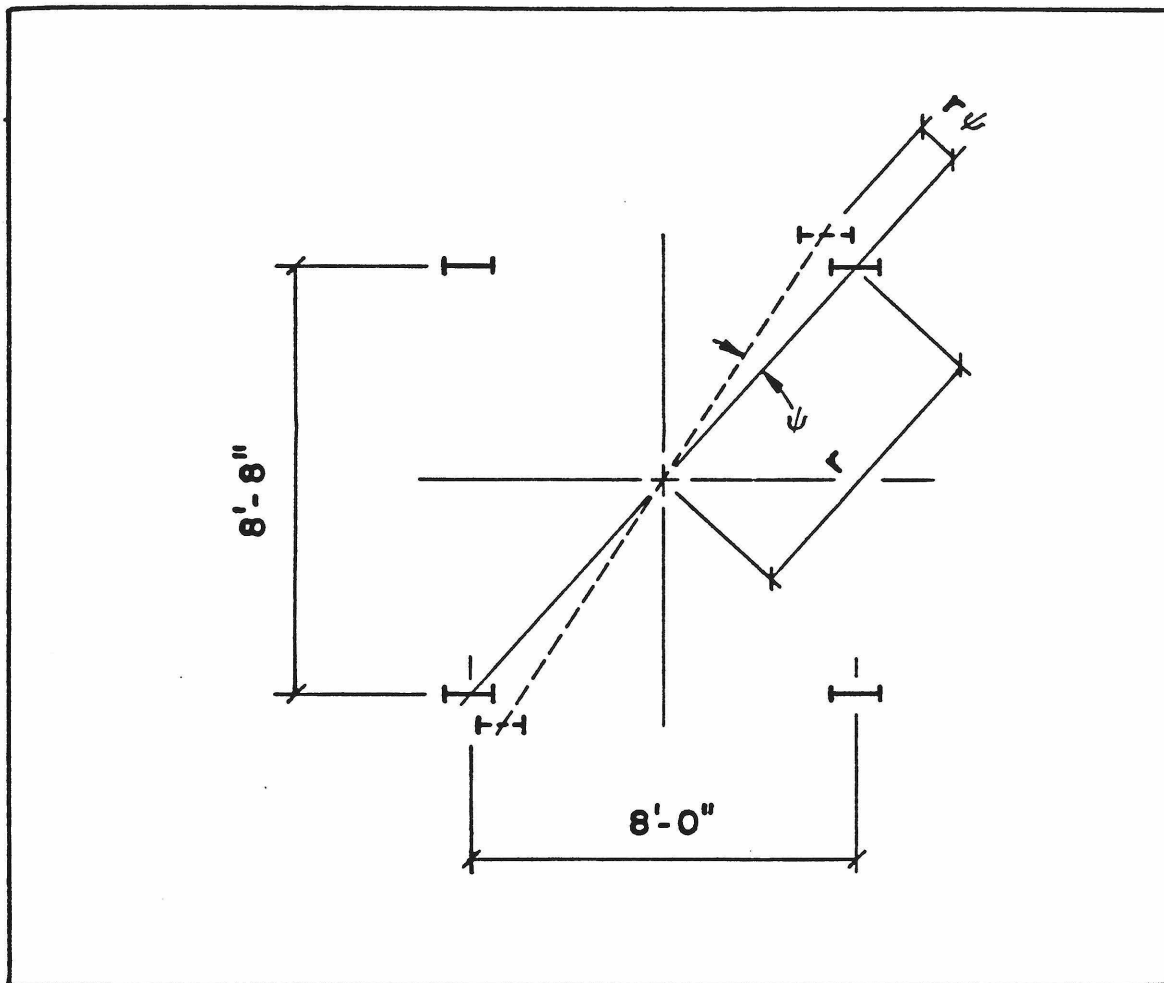


Figure 5.5. Tangential deformation of column due to superstructure rotation.

The strain energy stored in the deflected position C is independent of the path followed to reach that position from the initial position A. Therefore, the strain energy gained by following path A-C must equal the

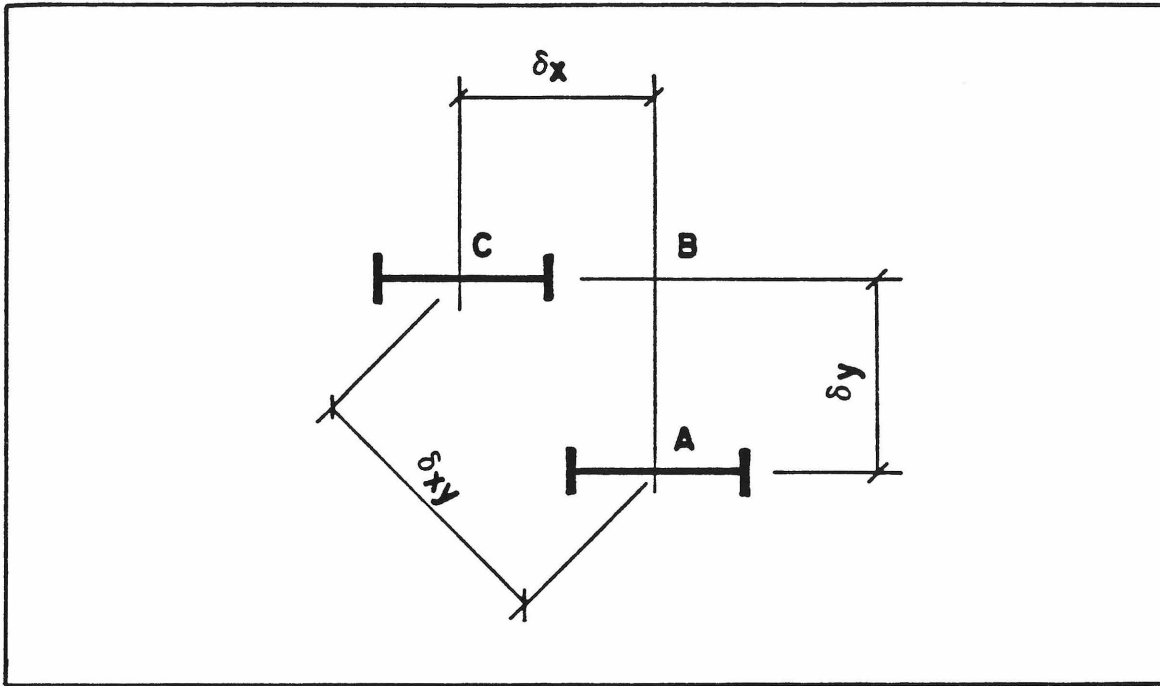


Figure 5.6. Resolution of column deformation into successive uni-axial deformations.

strain energy gained along path A-B-C. The following relations can be written

$$P_{A-C} = P_{A-B-C} \quad (5.29)$$

$$1/2 K_{xy} \delta_{xy}^2 = 1/2 K_x \delta_x^2 + 1/2 K_y \delta_y^2 \quad (5.30)$$

For a square column arrangement

$$\delta_{xy} = \sqrt{2} \delta_x = \sqrt{2} \delta_y \quad (5.31)$$

then

$$K_{xy} = 1/2 (K_x + K_y) \quad (5.32)$$

The quantities K_{xy} , K_y , and K_x are translational stiffnesses. For torsional oscillations, however, it is necessary to find the rotational stiffness. This can be accomplished by use of force and moment equilibrium. The force required to deflect the column by δ_{xy} is

$$F = K_{xy}\delta_{xy} \quad . \quad (5.33)$$

The moment required to displace the column end an angle ϕ with respect to the center of the frame, is

$$M = K_{s\phi}\phi \quad . \quad (5.34)$$

The following relations, written about the center of rotation,

$$M = Fr \quad (5.35)$$

$$\delta_{xy} = \phi r \quad (5.36)$$

where r is the distance from the axis of rotation to the column, lead to the result

$$K_{s\phi} = K_{xy}r^2 \quad . \quad (5.37)$$

Therefore, the rotational stiffness $K_{s\phi}$ can be expressed in terms of the translational stiffnesses K_x and K_y as

$$K_{s\phi} = 1/2(K_x + K_y)r^2 \quad . \quad (5.38)$$

Because the analysis in subsection 4.3.3 showed that the calculated torsional response of a simple model of the structure would probably not be close to the experimental results, two calculations for the torsional stiffness were completed. The first calculation used the properties of the structure as it was designed, the second calculation was based on the measured translational response of the structure.

In the preceding subsection, the translational stiffness K_x was found to have a value of 6.72×10^6 lb/ft (9.81×10^4 kN/m). In the y-direction, both the diagonal bracing and the columns contribute to the translational stiffness, i.e.

$$K_y = K_{col} + K_{brace} \quad . \quad (5.39)$$

The evaluation of the column stiffness K_{col} is similar to that for K_x , and the resulting value for K_{col} is 9.0×10^4 lb/ft/column (1.31×10^3 kN/m/column).

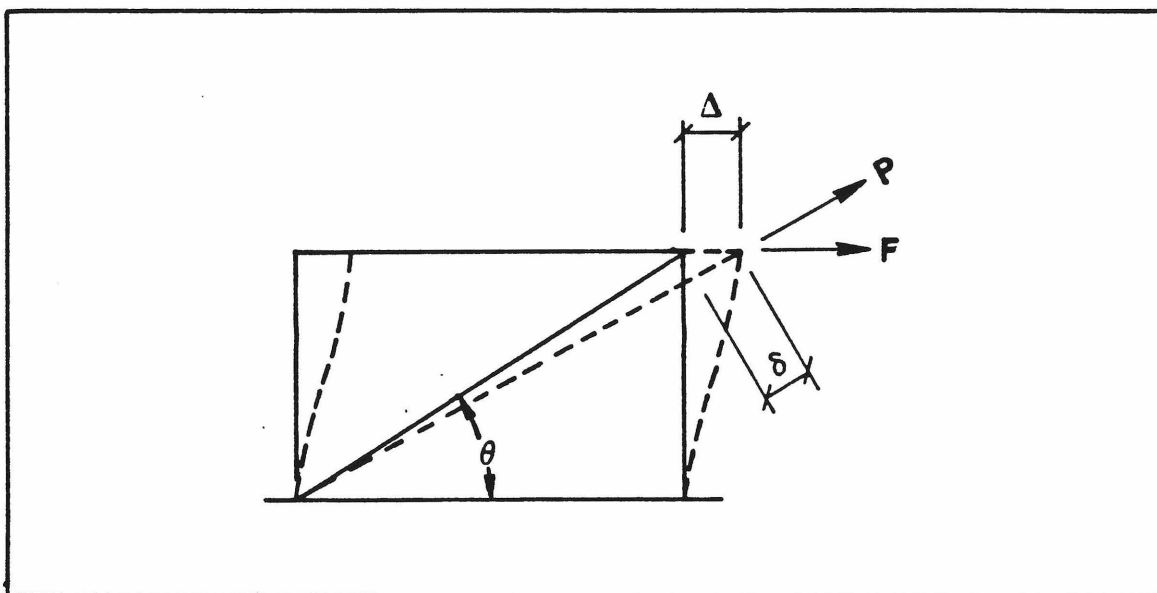


Figure 5.7. Force-displacement relations for diagonal bracing.

The x-bracing has the force-displacement relations of Figure 5.7. The stiffness of the brace, under axial load P , and displacement δ , is

$$K_{axial} = \frac{P}{\delta} = \frac{AE}{L} \quad . \quad (5.40)$$

The lateral stiffness of the brace, is given by

$$K_{\text{brace}} = \frac{F}{\Delta} \quad . \quad (5.41)$$

The axial force and displacement of the brace, P and δ , can be expressed in terms of the lateral force and displacement, F and Δ , as

$$P = F / \cos \theta \quad (5.42)$$

$$\delta = \Delta \cos \theta \quad . \quad (5.43)$$

Substitution of (5.42) and (5.43) into (5.40) leads to the following expression for the lateral stiffness of the diagonal bracing

$$\begin{aligned} K_{\text{brace}} &= \frac{AE}{L} \cos^2 \theta \\ &= \frac{(1.46 \text{ in}^2)(29 \times 10^6 \text{ lb/in}^2)(0.866)^2(12 \text{ in/ft})}{(120 \text{ in})} \\ &= 3.17 \times 10^6 \text{ lb/ft/brace} \quad (4.63 \times 10^4 \text{ kN/m/brace}) \quad . \quad (5.44) \end{aligned}$$

The total stiffness K_y is $1.31 \times 10^7 \text{ lb/ft}$ ($1.91 \times 10^5 \text{ kN/m}$), and the torsional stiffness, for $r = 6.25 \text{ ft}$ (1.9 m), is $3.85 \times 10^8 \text{ lb-ft}$ ($5.22 \times 10^5 \text{ kN-m}$). Note that the radial distance is a physical dimension of the steel frame, as opposed to the equivalent radius of the foundation. An assumed modal damping factor of 1% produces a viscous damping coefficient of $3.32 \times 10^4 \text{ lb-ft/sec}$ (45 kN-m/sec). For the superstructure system defined above, the corresponding torsional resonant frequency is 36.9 Hertz, a value much higher than either of the measured frequencies. Later, it will be shown that the effects of soil-

structure interaction cannot modify the resonant frequency to agree with the measured frequencies.

In subsection 4.3.2, the superstructure translational stiffness, as a result of the experiment, was found to have a value of 4.10×10^6 lb/ft (6.70×10^4 kN/m). Because the foundation is square, it will behave the same in both the x- and y-directions, and the difference between the two fundamental resonant frequencies can be attributed to differences in the superstructure. Neglecting interaction effects, the following relations can be used to obtain an approximate value for the translational stiffness K_y from the ratio of fundamental resonant frequencies ω_{nx} and ω_{ny} , and the stiffness K_x ,

$$\omega_{ny} \cong \sqrt{\frac{K_y}{M}} \quad (5.45)$$

$$\omega_{nx} \cong \sqrt{\frac{K_x}{M}} \quad (5.46)$$

then

$$K_y \cong \left(\frac{\omega_{ny}}{\omega_{nx}} \right)^2 K_x \quad (5.47)$$

The results of the ambient vibration tests yield an average value for $(\omega_{ny}/\omega_{nx})^2$ of 0.61. The translational stiffness K_y then has an estimated value of 2.5×10^6 lb/ft (3.65×10^4 kN/m). Use of Equation (5.38) results in a torsional stiffness $K_{s\phi}$ of 1.31×10^8 lb-ft (1.78×10^5 kN-m). The reduced value of K_y implies that the axial stiffness of the braces is much less than that originally calculated. Since the braces are short (slenderness ratio $kl/r = 61$), lateral

bending or buckling of the members is unlikely. The discrepancy in the stiffness values is most likely due to the flexibility of the end connections of the braces. The effect will be similar to those previously discussed for the columns in translation.

The viscous damping coefficient C_{sq} is assigned a value of 1.94×10^4 lb-ft-sec (26.4 kN-m-sec), which corresponds to a damping factor of 1%.

5.2.3. Equivalent Radii.

Most foundation analyses have been concerned with circular foundations. The majority of prototype structures, however, are rectangular in plan. Therefore, it is necessary to determine the radius of the circular foundation equivalent to the specimen structure foundation.

Richart, Hall, and Woods (1970) provides formulae that can be used to find the equivalent radius of a rectangular foundation in horizontal translation, rocking, and torsion. For the rectangular foundation shown in Figure 5.8, the equivalent radii are defined as,

- Horizontal translation

$$r_o = \sqrt{\frac{BL}{\pi}} \quad (5.48)$$

- Rocking

$$r_o = \sqrt[4]{\frac{BL^3}{3\pi}} \quad (5.49)$$

- Torsion

$$r_o = \sqrt[4]{\frac{BL(B^2 + L^2)}{6\pi}} \quad (5.50)$$

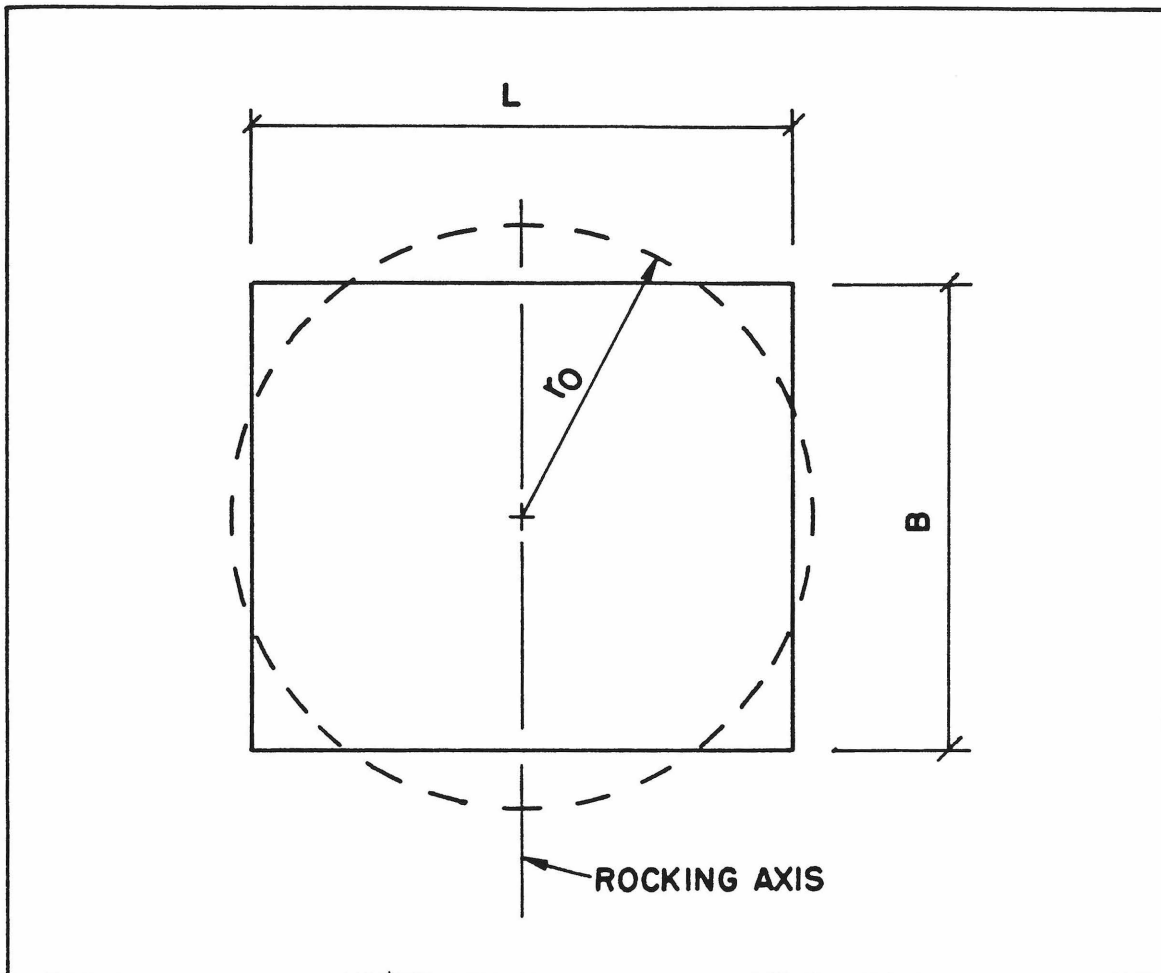


Figure 5.8. Equivalent radius for a rectangular foundation.

For the specimen structure, the equivalent radii are 5.64 ft (1.72 m) in horizontal translation and 5.71 ft (1.74 m) in torsion and rocking. Since these radii are almost equal, a value of 5.64 ft (1.72 m) will be used in subsequent analyses.

5.2.4. Soil Properties.

The soil plays an important role in the interaction phenomenon. The following values, obtained from soil tests, soil mechanics literature, and in situ measurements, will be used in the analysis of this chapter,

1. Poisson's ratio, $\nu = 0.333$; a typical value for granular materials;
2. Soil unit weight $\gamma = 95 \text{ lb/ft}^3$ (14.9 KN/m^3);
3. Soil density $\rho = 2.95 \text{ lb-sec}^2/\text{ft}^4$ (1520 kg/m^3);
4. Shear wave velocity, $C_s = 1000 \text{ ft/sec}$ (305 m/sec);
5. Shear modulus, $G = C_s^2 \rho = 2.95 \times 10^6 \text{ lb/ft}^2$ (141 MP).

5.3. FUNDAMENTAL MODE RESPONSE.

The seismic behavior of most prototype structures is governed by the fundamental mode response. In this section, lumped parameter analysis will be applied to the three-degree-of-freedom system consisting of the foundation lateral translation, interfloor displacement, and rigid body rocking. The fundamental resonant frequency and mode shape will be calculated for the three embedment cases examined experimentally.

5.3.1. Foundation-Soil Impedances.

The effect of soil-structure interaction is normally introduced into seismic analysis through the calculation of foundation-soil impedances. These impedances, in effect, model the soil as a system of

elastic springs and viscous dashpots which provide restorative and dissipative forces. In general, the values of these stiffnesses and damping coefficients are dependent upon the soil properties, size of the foundation, and excitation frequency.

The determination of these impedance values is usually based upon analytic solutions for the response of a massless plate attached to the surface of an elastic half-space. In these solutions, the input consists of harmonically varying forces or moments. The problem is quite complex because of the boundary conditions that must be observed at the contact between the plate and half-space.

These rather complicated boundary conditions have been handled by several approaches. One method, used for example by Reisner (1936), Bycroft (1956), and Hall (1967), reduces the mixed boundary value problem, in which stresses and displacements are specified over different parts of the surface, to a simpler problem in which only the boundary stresses are prescribed over the entire contact area. The resulting solution is approximate, however, as it gives rise to surface displacements which are incompatible with the rigid disk.

Gladwell (1968), Karasudhi, Keer, and Lee (1968), Veletsos and Wei (1971), and Luco and Westmann (1971), among others, simplified some of the contact conditions between the disk and half-space to obtain a solution to what is termed the relaxed mixed boundary value problem. While the two approaches differ conceptually, the impedance functions

resulting from the two methods are fairly close to each other; certainly to within the degree required for analysis or design.

The mixed boundary value problem has also been solved by use of integral equations. Bielak (1971), for instance, presents one such solution.

The usual result of these studies is the determination of frequency dependent functions for the in-phase and out-of-phase responses of the disk to unit harmonic inputs. In terms of these so-called compliance functions, the harmonic response q to an input force $F e^{i\omega t}$ can be written as

$$q e^{i\omega t} = \frac{F e^{i\omega t}}{Gr_o} (f + ig) \quad (5.51)$$

where f is associated with the in-phase response, and g with the real part of the out-of-phase response. If only the magnitudes of the force and response are considered, the above equation can be written as

$$q = \frac{F}{Gr_o} (f + ig) \quad (5.52)$$

The harmonic response q of a massless disk supported by spring and dashpot elements, with values of stiffness K and damping coefficient C respectively, is related to the harmonic force $F e^{i\omega t}$ by,

$$F e^{i\omega t} = (K + i\omega C) q e^{i\omega t} \quad (5.53)$$

If the stiffness and damping coefficient are normalized to the soil stiffness and foundation radius, then the dimensionless impedance

functions k and c result,

$$k = \frac{K}{Gr_o} \quad (5.54)$$

$$c = \frac{C\omega}{Gr_o a_o} \quad (5.55)$$

Recalling that the dimensionless frequency is defined by

$$a_o = \frac{2\pi f r_o}{C_s} = \frac{\omega r_o}{C_s} \quad (5.56)$$

Equation (5.53) can be rewritten as

$$F = Gr_o(k + ia_o c)q \quad (5.57)$$

If Equation (5.51) is rewritten in a similar form

$$F = Gr_o \left(\frac{f}{f^2 + g^2} - i \frac{g}{f^2 + g^2} \right) q \quad (5.58)$$

it can then be seen that the following equalities hold,

$$k = \left(\frac{f}{f^2 + g^2} \right) \quad (5.59)$$

$$c = - \frac{1}{a_o} \left(\frac{g}{f^2 + g^2} \right) \quad (5.60)$$

The stiffness and damping coefficient can then be expressed in terms of the compliance functions,

$$K_{fx} = Gr_o k \quad (5.61)$$

$$C_{fx} = \sqrt{G\rho} r_o^2 c \quad (5.62)$$

A similar development results in the following functions for the rocking impedances,

$$K_{f\phi} = G r_o^3 k \quad (5.63)$$

$$C_{f\phi} = \sqrt{G\rho} r_o^4 c. \quad (5.64)$$

Since the impedance functions k and c are frequency dependent, the frequency domain is normally used for dynamic analyses. The following subsections, however, will show that the frequency dependence of some of these functions is not strong, and frequency independent impedance values can often be used.

The results to be presented in the following paragraphs will be expressed in the form of the stiffness and damping coefficient functions K and C . As shown previously in Figure 5.1, the subscripts fx and $f\phi$ indicate the foundation-soil impedances for translation and rocking, respectively. The results of Bycroft, Luco and Westmann, and Veletsos and Wei were expressed in terms of the compliance functions (i.e., Equation 5.52). Therefore, it was necessary to evaluate these functions at discrete intervals in the frequency domain, calculate the corresponding value of the impedance function [Equations (5.59) and (5.60)] and finally, to perform a least squares fit to obtain the final stiffness and damping coefficient functions. Other workers, such as Hall, and Beredugo and Novak (1972), present their results in the form of stiffness and damping coefficient functions, and are therefore cited

directly without modification, except for adaptation, as necessary, to a consistent format.

Except as noted, all formulations are valid for a value of Poisson's ratio of 0. This value was chosen because all of the formulations found in the literature were valid for at least this case, and possibly, but not necessarily, for other values of ν . Based on the comparison of the impedance functions valid for the case of $\nu = 0$, a single formulation, obtained for the case of $\nu = 0.333$ (the site condition) will be selected.

5.3.1.1. Horizontal translation.

The excitation of a flat plate by a horizontal force will produce, in addition to translation, a small amount of rocking about the horizontal axis perpendicular to the force. The rotation caused by this coupling, however, is small, and is usually neglected in the analysis.

Bycroft determined frequency dependent compliance functions to describe the response of a circular plate to horizontal forces. These compliance functions lead to the following stiffness and damping coefficient functions which were obtained by the methods discussed above,

$$\begin{aligned} K_{fx} = Gr_o(4.617 - 0.4953a_o + 1.402a_o^2 - 2.253a_o^3 \\ + 1.362a_o^4 - 0.2965a_o^5) \end{aligned} \quad (5.65)$$

$$\begin{aligned} C_{fx} = \sqrt{G\rho} r_o^2(2.600 + 0.1335a_o - 0.3527a_o^2 + 0.6812a_o^3 \\ - 0.4585a_o^4 + 0.1157a_o^5) \end{aligned} \quad (5.66)$$

The static stiffness is given by

$$K_{fx}^{st} = \frac{32(1-\nu)}{7-8\nu} Gr_o \quad . \quad (5.67)$$

Veletsos and Wei, and Luco and Westmann, solved the relaxed mixed boundary value problem and obtained compliance functions valid for $0 < a_o < 10$. Because the frequency range in this experiment corresponds to the range $0 < a_o < 2.5$, the least squares fit was restricted to this smaller range to minimize errors in the fit. The resulting stiffness and damping coefficient functions are,

$$K_{fx} = 4Gr_o(1.00 - 0.0181a_o - 0.005314a_o^2 - 0.07284a_o^3 + 0.04886a_o^4 - 0.00846a_o^5) \quad (5.68)$$

$$C_{fx} = 4\sqrt{Gp} r_o^2(0.6476 + 0.07784a_o - 0.1057a_o^2 + 0.1103a_o^3 - 0.04508a_o^4 + 0.006258a_o^5) \quad . \quad (5.69)$$

The static stiffness, as a function of Poisson's ratio, is given by

$$K_{fx}^{st} = \frac{8}{2-\nu} Gr_o \quad . \quad (5.70)$$

Based on the compliance functions of Bycroft, Hall presented a quadratic fit of the stiffness and damping coefficient functions, for the interval $0 < a_o < 2$,

$$K_{fx} = Gr_o(4.573 - 0.02004a_o - 0.2122a_o^2) \quad (5.71)$$

$$C_{fx} = \sqrt{Gp} r_o^2(2.610 - 0.01257a_o + 0.1025a_o^2) \quad . \quad (5.72)$$

Beredugo and Novak examined the coupled translation and rocking of embedded foundations, and found, for the unembedded case, the impedance functions listed below,

$$K_{fx} = Gr_o \left(4.571 - 4.653 a_o + \frac{89.09 a_o}{a_o + 19.14} \right) \quad (5.73)$$

$$C_{fx} = \sqrt{G_p} r_o^2 \left(2.536 - \frac{0.1345}{a_o - 1.923} \right) . \quad (5.74)$$

The coupling terms have not been included.

Dynamic analysis is made more difficult by the frequency dependent nature of the soil impedances. Several workers have attempted to simplify these analyses by determining frequency independent impedances. In a manner similar to that used by Lysmer and Richart (1966) for the vertical vibration of a foundation, Hall determined that the following constant valued impedances,

$$K_{fx} = \frac{32(1 - \nu)}{7-8\nu} Gr_o \quad (5.75)$$

$$C_{fx} = 0.575 \left[\frac{32(1 - \nu)}{7-8\nu} \right] \sqrt{G_p} r_o^2 . \quad (5.76)$$

resulted in good agreement with the frequency dependent impedance values.

In a similar way, Parmalee, Perelman, and Lee (1969) determined these frequency independent values,

$$K_{fx} = \frac{6.77}{1.79 - \nu} Gr_o \quad (5.77)$$

$$C_{fx} = \frac{6.21}{2.54 - \nu} \sqrt{G_p} r_o^2 . \quad (5.78)$$

For a Poisson's ratio of 0, Beredugo and Novak offer these constant valued impedances,

$$K_{fx} = 4.30Gr_0 \quad (5.79)$$

$$C_{fx} = 2.70\sqrt{G_p} r_0^2 \quad (5.80)$$

The impedance functions listed above are plotted in Figures 5.9 and 5.10.

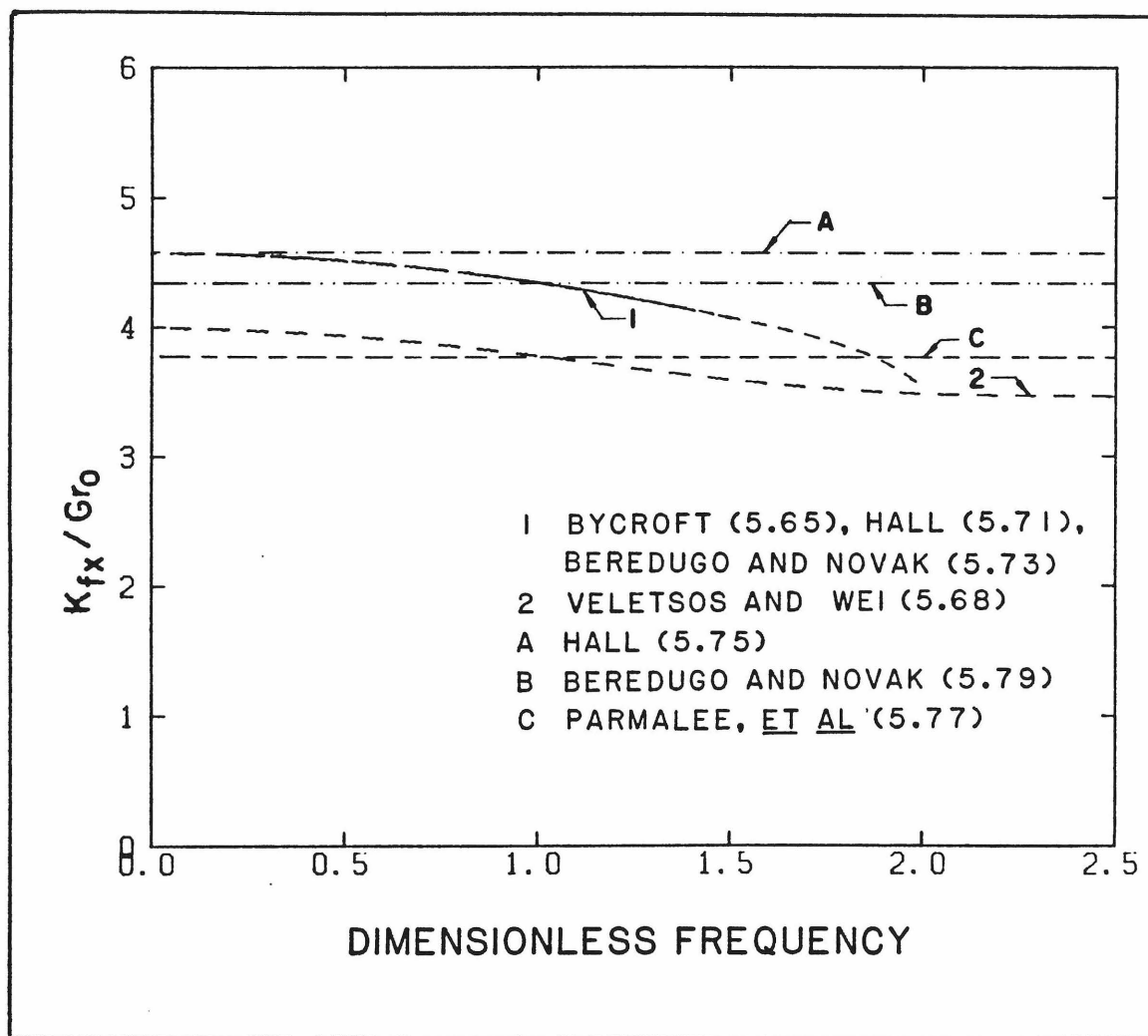


Figure 5.9. Foundation-soil stiffness for horizontal translation, $\nu = 0$.

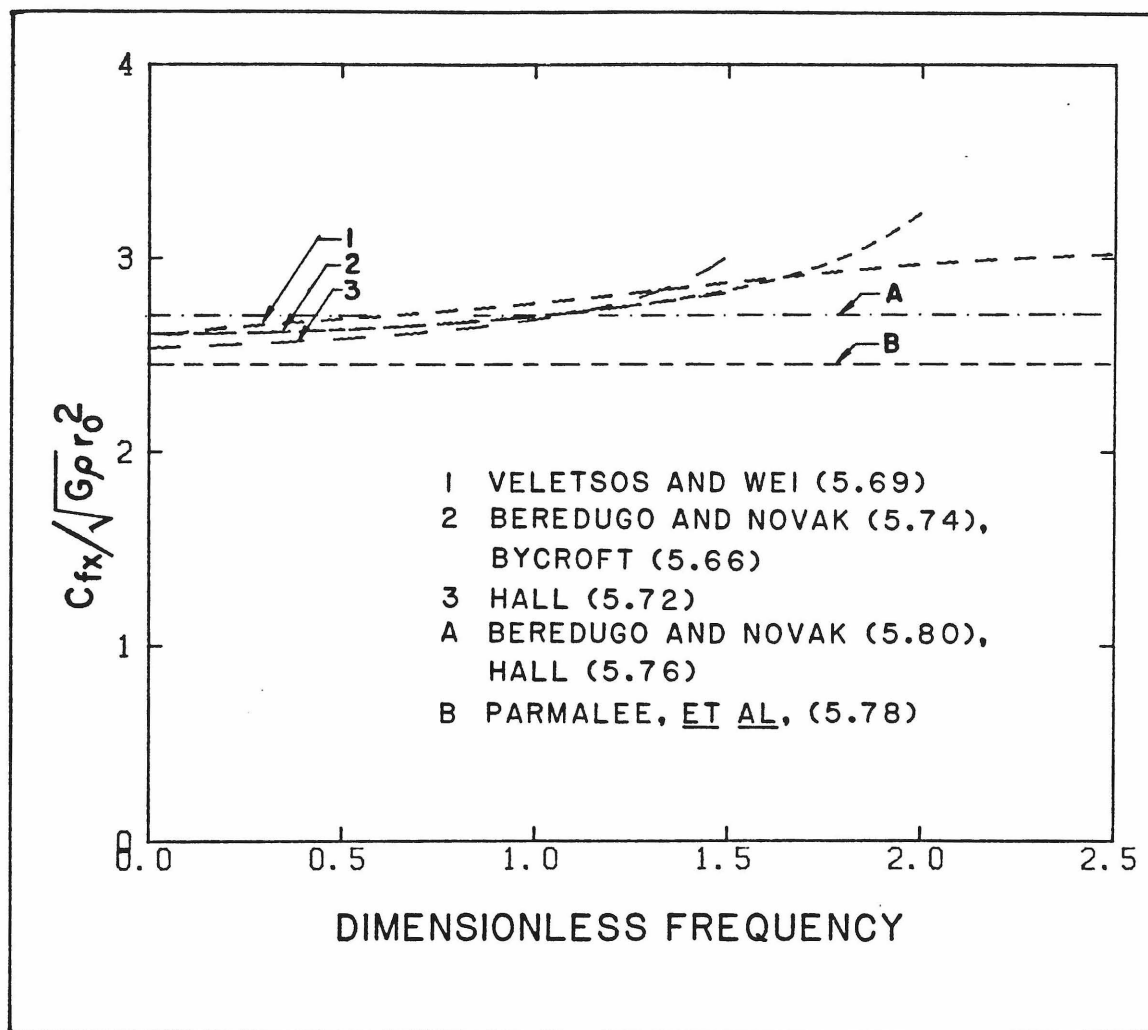


Figure 5.10. Foundation-soil damping for horizontal translation, $\nu = 0$.

Comparison of the results obtained by the different formulations shows excellent agreement among the frequency dependent functions of Bycroft, Hall, and Beredugo and Novak, and a slight variation with the results of Veletsos and Wei. The key difference between the two groups of results, in the stiffness plot, is the value of the static stiffness, i.e. for $a_0 = 0$. The frequency dependence of the various results is similar in all cases. For the plotted case of $\nu = 0$, Bycroft's

formulation leads to a static stiffness of $4.62Gr_o$, while Veletsos and Wei's formulation gives a static stiffness of $4.0Gr_o$.

The frequency independent values of Hall, Beredugo and Novak, and Parmalee, Perelman, and Lee fall within the range of the frequency dependent values. This suggests that, in the case of horizontal translation, use of frequency independent foundation impedances may not result in significant error in the analysis, while reducing the amount of effort required. Similar conclusions can be drawn from the damping coefficient functions plotted in Figure 5.10.

In order to exploit fully the existing analytical results, frequency dependent impedance functions will be used in the analyses of this chapter. While the results of Veletsos and Wei are, for the case of $\nu = 0$, slightly different from the others, this variation is reduced for the case of $\nu = 0.333$. At this value of Poisson's ratio, the static stiffnesses of Bycroft and Veletsos and Wei are $4.934Gr_o$, and $4.80Gr_o$, respectively. This is a much smaller difference than shown in Figures 5.9 and 5.10. The frequency dependence of the stiffness and damping coefficient are similar for all of the formulations. Therefore, the selection of the following functions, based on the results of Veletsos and Wei, will result in negligible differences in comparison to the other formulations,

$$\begin{aligned} K_{fx} = & 4.80Gr_o(1 - 0.001802a_o - 0.03271a_o^2 - 0.1749a_o^3 \\ & + 0.02135a_o^4 - 0.004195a_o^5) \end{aligned} \quad (5.81)$$

$$\begin{aligned}
 C_{fx} = & 4.80\sqrt{Gp} \ r_o^2 (0.580 + 0.001954a_o - 0.0130a_o^2 \\
 & + 0.01118a_o^3 - 0.00841a_o^4 + 0.001262a_o^5)
 \end{aligned} \tag{5.82}$$

These functions are valid over the range of $0 < a_o < 2.5$.

5.3.1.2. Rocking

As in the case of horizontal translation, coupling between translation and rocking will not be included in the discussion of this subsection. Bycroft found frequency dependent compliance functions, from which the following impedance functions were determined,

$$\begin{aligned}
 K_{f\phi} = & Gr_o^3 (2.6554 - 0.02323a_o - 0.6335a_o^2 - 0.6468a_o^3 \\
 & + 1.179a_o^4 - 0.4138a_o^5)
 \end{aligned} \tag{5.83}$$

$$\begin{aligned}
 C_{f\phi} = & \sqrt{Gp} \ r_o^4 (-0.0021 - 0.0351a_o + 1.632a_o^2 - 2.254a_o^3 \\
 & + 1.466a_o^4 - 0.3697a_o^5)
 \end{aligned} \tag{5.84}$$

Veletsos and Wei obtained compliance functions valid in the range $0 < a_o < 10$. The following impedance functions, valid for the range $0 < a_o < 2.5$, result,

$$\begin{aligned}
 K_{f\phi} = & 2.666 \ Gr_o^3 (1 + 0.008944a_o - 0.4630a_o^2 + 0.3705a_o^3 \\
 & - 0.1296a_o^4 + 0.01711a_o^5)
 \end{aligned} \tag{5.85}$$

$$\begin{aligned}
 C_{f\phi} = & 2.666\sqrt{Gp} \ r_o^4 (-0.0002 - 0.01130a_o + 0.4354a_o^2 \\
 & - 0.3754a_o^3 + 0.1327a_o^4 - 0.0172a_o^5)
 \end{aligned} \tag{5.86}$$

The static stiffness, found by Bycroft and by Veletsos and Wei, is dependent on Poisson's ratio

$$K_{f\phi}^{st} = \frac{8}{3(1-\nu)} Gr_o^3 \quad . \quad (5.87)$$

Hall and Beredugo and Novak, by the approach described in the previous subsection, obtained results similar to those of Bycroft.

Parmalee, Perelman, and Lee proposed the following frequency independent impedances,

$$K_{f\phi} = \frac{2.52}{1-\nu} Gr_o^3 \quad (5.88)$$

$$C_{f\phi} = \frac{0.136}{1.13-\nu} \sqrt{G\rho} r_o^4 \quad . \quad (5.89)$$

Beredugo and Novak obtained,

$$K_{f\phi} = Gr_o^3 (2.50) \quad (5.90)$$

$$C_{f\phi} = \sqrt{G\rho} r_o^4 (0.43) \quad . \quad (5.91)$$

Hall concluded that the variation of the damping with frequency was too great to allow the selection of a single frequency independent value that did not depend on the structural properties. Therefore, he defined a mass ratio,

$$B_\phi = \frac{3(1-\nu)}{8} \frac{I}{\rho r_o^5} \quad (5.92)$$

from which the dimensionless resonant frequency a_{on} could be estimated

$$a_{on} = -\frac{0.1125}{B_\phi} + \frac{1.0}{B_\phi} \sqrt{0.01265 + 1.025B_\phi} \quad . \quad (5.93)$$

The constant valued damping is dependent upon the estimated a_{on} . The

impedance values are given by,

$$K_{f\phi} = \frac{8}{3(1-\nu)} Gr_o^3 \quad (5.94)$$

$$C_{f\phi} = \frac{8}{3(1-\nu)} \sqrt{G\rho} r_o^4 (-0.001324 + 0.0483 a_{on} + 0.2089 a_{on}^2 - 0.0915 a_{on}^3) \quad (5.95)$$

The impedance functions presented above are plotted in Figures 5.11 and 5.12 for $\nu = 0$. These figures show that the variable impedances agree well with one another. Because the rocking impedances, particularly for damping, have greater dependence on frequency than those of horizontal translation, it is difficult to establish criteria for "agreement" of the constant approximations. Certainly, the constant values intersect the frequency dependent functions within the range $0 < a_o < 2$. The frequency independent stiffness values correspond generally to the static stiffness values of the frequency-dependent formulations.

In the case of Hall, it is necessary to find the mass ratio B_ϕ which leads to a value of the dimensionless resonant frequency from which the frequency independent damping can be found. For the specific case of the specimen structure, a_{on} has a value of 0.85. Substitution of this value into Equation (5.95) leads to a damping coefficient of $0.55\sqrt{G\rho} r_o^4$. It should be noted that Equation (5.95) is only another representation of the frequency dependent damping coefficient function. The same damping coefficient can be found by evaluating any of the other

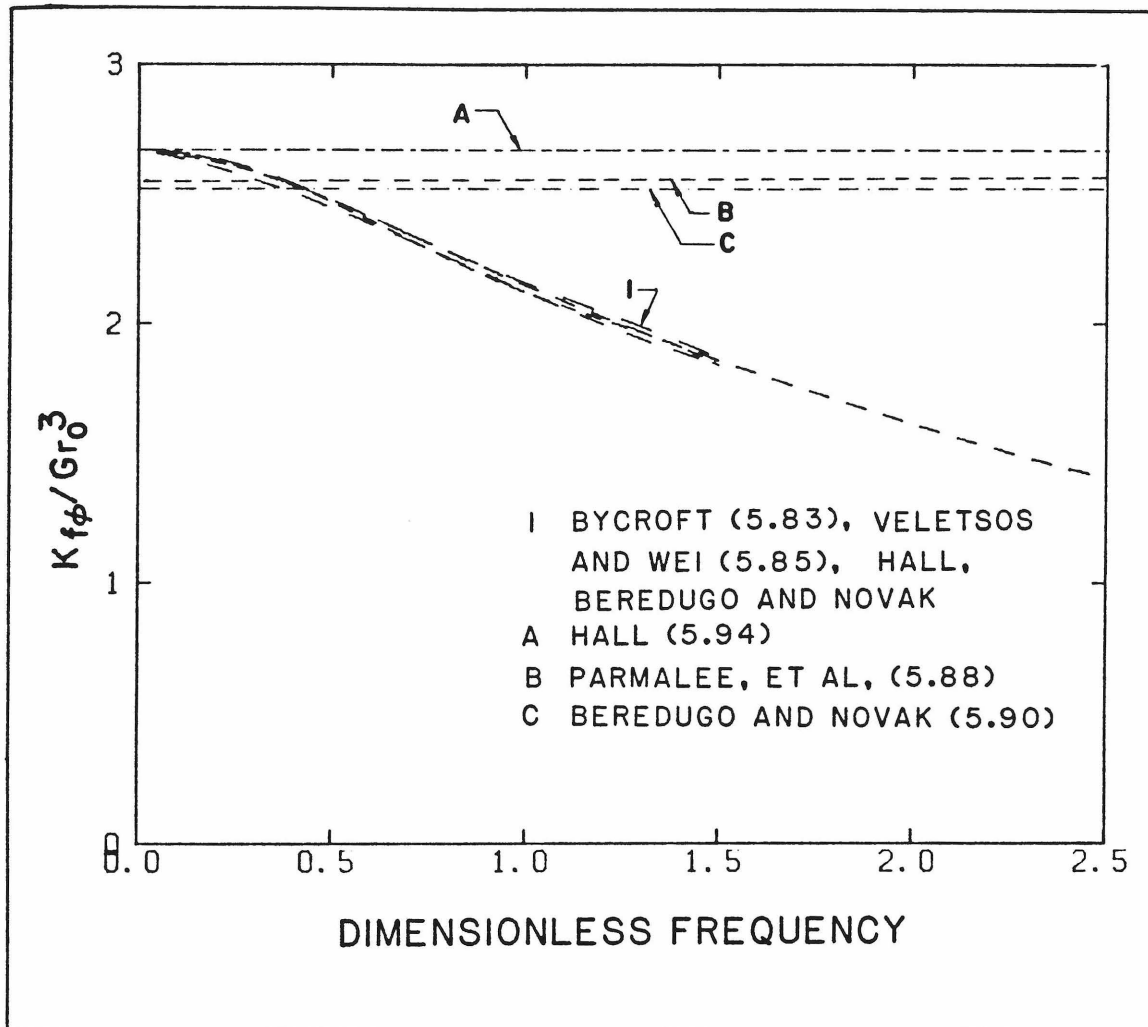


Figure 5.11. Foundation-soil stiffness for rocking $\psi = 0$.

functions [i.e. Equations (5.84) or (5.86)] at the specific value of a_{on} .

The frequency independent damping coefficient of Beredugo and Novak is valid over the range $0 < a_0 < 2.0$. The constant value corresponds to the frequency dependent function evaluated at a value of a_0 of 1. Therefore, the constant valued damping coefficient represents an average of the frequency dependent function over the range of $0 < a_0 < 2.0$. The

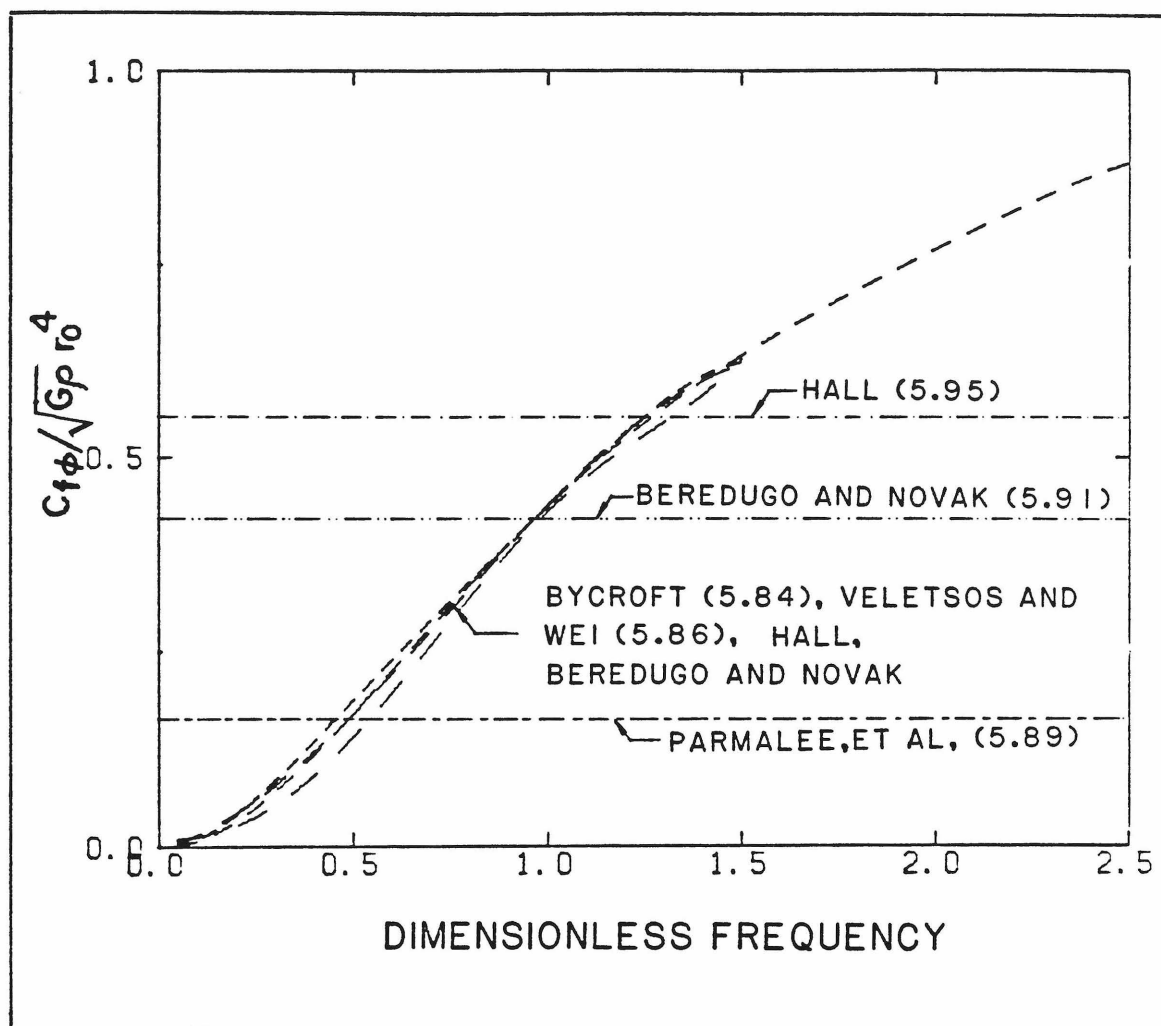


Figure 5.12. Foundation-soil damping for rocking $\nu = 0$.

frequency invariant damping coefficient of Parmalee, Perelman, and Lee corresponds to a low resonant frequency.

Selection of the impedance functions of Veletsos and Wei, evaluated for $\nu = 0.333$, results in the following functions. As in the previous paragraph, the use of these equations does not lead to major differences with the other formulations discussed above.

$$K_{f\phi} = 4.00Gr_o^3(1 + 0.1058a_o - 0.400a_o^2 + 0.3026a_o^3 - 0.1010a_o + 0.02181a_o^5) \quad (5.96)$$

$$C_{f\phi} = 4.00\sqrt{G\rho} r_o^4 (-0.0002 - 0.006734a_o + 0.3240a_o^2 - 0.2542aa_o^3 + 0.08173a_o^4 - 0.00969a_o^5) \quad (5.97)$$

5.3.2. Analysis with Unembedded Foundation.

The properties of the superstructure and foundation-soil system are used as input to the matrix equations of motion derived in Section 5.1 to obtain the dynamic response of the specimen structure. Since the foundation-soil impedances are frequency dependent, the frequency domain must be used for the analysis. The procedure for the analysis is:

1. Evaluate frequency dependent foundation-soil impedances;
2. Substitute values of system parameters into equations of motion;
3. Solve, by matrix inversion, the equations of motion for the response amplitudes and phase angles;
4. Increment to the next frequency and repeat steps 1 through 3.

The dynamic response was calculated over the range of 0 to 70 Hertz ($0 < a_o < 2.5$). The fundamental mode response of the structure is shown in Figure 5.13. Several conclusions can be drawn from the results presented in this figure.

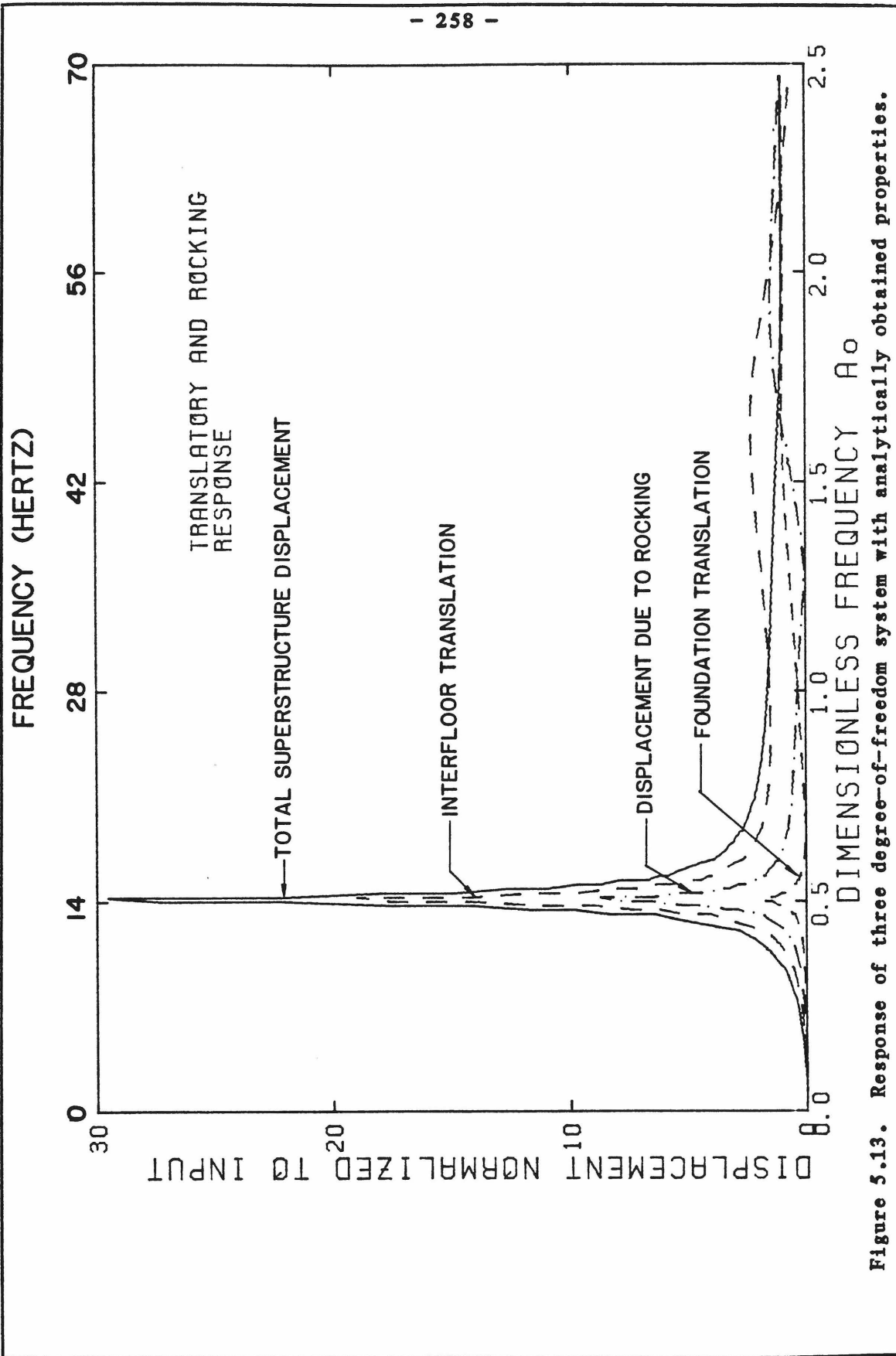


Figure 5.13. Response of three degree-of-freedom system with analytically obtained properties.

1. The fundamental resonant frequency is 14.25 Hertz, which corresponds to a value of a_o of 0.506 [$r_o = 5.64$ ft (1.7 m), $C_s=1000$ ft/sec (305 m/sec)]. This frequency is slightly higher than the experimental result of 11.33 Hertz.
2. The damping fraction, determined by the half-power method, is 1.93% of critical.
3. The foundation translation accounts for 6.34% of the total superstructure displacement, and rocking accounts for 29.5%. These fundamental mode shape values compare to the experimentally measured values of 6.1% and 21.0% respectively.
4. The total superstructure displacement is 30 times larger than the input free-field ground motion. The corresponding value measured experimentally was 39. It should be noted, as stated in paragraph 4.2.3.2, that the experimentally obtained value is not exact. The total displacement of the superstructure is also dependent upon the assumed superstructure damping ratio of 1%.
5. The frequency dependent foundation-soil impedances have the values shown in Table 5.1 at the resonant frequency. The experimentally obtained values are also shown.
6. Examination of the analytical and experimental results shows that the values of stiffness are in agreement to within 32% for translation, and 13% for rocking. In both cases, the

TABLE 5.1. Foundation-soil impedances for horizontal translation and rocking,
by evaluation of analytical formulations, and from experiment.

Motion	Static Stiffness	Dynamic Stiffness		Damping Coefficient	
		Analysis	Experiment	Analysis	Experiment
Translation	7.99×10^7 lb/ft (1.17×10^6 kN/m)	7.90×10^7 lb/ft (1.15×10^6 kN/m)	5.35×10^7 lb/ft (7.81×10^5)	2.64×10^5 lb-sec/ft (3.95×10^3 kN-sec/m)	4.27×10^4 lb/ft (6.23×10^2)
Rocking	2.12×10^7 lb-ft (2.87×10^4 kN-m)	1.99×10^9 lb-ft (2.70×10^6 kN-m)	1.73×10^9 (2.34×10^6)	5.99×10^5 lb-sec-ft (8.12×10^2 kN-sec-m)	6.67×10^5 (9.04×10^2)

analytical values are higher; this accounts for the higher calculated resonant frequency.

7. The difference between the measured and calculated damping coefficients is only 10% in rocking, but over a factor of six in translation. The higher damping coefficients and the assumed damping in the superstructure lead to a damping ratio that is twice as large as that measured experimentally.

As discussed in subsection 4.3.2.2, the experimentally determined damping coefficients are dependent upon the response amplitudes; any errors in the determination of these amplitudes will be reflected in the results. It is doubtful, however, that uncertainty in the experimental results could lead to such a large difference in the translational damping coefficient. Therefore, there may be a substantive cause for the difference.

8. Since the model contains three degrees of freedom, there are, for the undamped case, two additional response modes, one corresponding to the second translational resonance, and the other consisting primarily of rocking. These two modes do not appear in the calculated response of the structure. When the analysis was repeated without damping forces, however, these two modes did appear in the response, at frequencies of 43.5 and 57 Hertz, respectively. Recall that the experiment did indicate a second translatory frequency near 26 Hertz. The higher damping possessed by the model appears to have suppressed these other resonant frequencies.

5.3.3. Modification of Foundation-Soil System for Embedment.

A structure with an embedded foundation, in general, has a higher resonant frequency than a similar structure with an unembedded foundation. This behavior can be reflected in the analysis by increasing the foundation-soil impedance with embedment.

Foundation embedment has been modelled in two ways. The first method, introduced by Baranov (1967) and Tajimi (1969), considers the foundation to be supported on an elastic half-space and embedded in an elastic stratum. The elastic properties of the stratum may be different from those of the half-space. Beredugo and Novak offer impedance functions for translation and rocking that account for embedment in this way. Denoting the embedded impedances by a subscript "e", these functions are,

$$K_{fxe} = Gr_o(k_x + \frac{G_s}{G} \delta k_x^s) \quad (5.98)$$

$$K_{f\phi e} = Gr_o^3(k_\phi + \frac{G_s}{G} \delta k_\phi^s) \quad (5.99)$$

$$C_{fxe} = \sqrt{G\rho} r_o^2(c_x + \frac{G_s}{G} \delta c_x^s) \quad (5.100)$$

$$C_{f\phi e} = \sqrt{G\rho} r_o^4(c_\phi + \frac{G_s}{G} \delta c_\phi^s) \quad (5.101)$$

where G_s and G are the shear moduli of the stratum and half-space respectively, and δ is the embedment ratio ($\delta = d/r_o$).

The functions k_x , k_ϕ , c_x , and c_ϕ correspond to the impedances for the unembedded foundation, and were presented in the preceding sections.

These functions are dependent on frequency and Poisson's ratio. Frequency independent values can also be used to simplify the analysis.

The functions k_x^s , k_ϕ^s , c_x^s , and c_ϕ^s are the impedance functions for the sidelayer. The sidelayer functions for horizontal translation depend on the Poisson's ratio, while those for rocking do not. For a value of $\nu = .333$, the sidelayer functions are,

• Horizontal translation

$$k_x^s = -1.632\sqrt{a_o} + 6.100 \sqrt[4]{a_o} \quad 0 \leq a_o \leq 0.2 \quad (5.102)$$

$$= 2.649 + 4.448a_o - 4.930a_o^2 + 2.251a_o^3 - 0.378a_o^4$$

$$0.2 \leq a_o \leq 2.0 \quad (5.103)$$

$$c_x^s = 0.895 + \frac{49.07a_o + 207.59}{a_o^2 + 17.16a_o + 18.252}, \quad (5.104)$$

• Rocking

$$k_\phi^s = 3.142 - 0.4215a_o - 4.209a_o^2 + 7.165a_o^3$$

$$- 4.667a_o^4 + 1.093a_o^5 \quad (5.105)$$

$$c_\phi^s = 0.0144 + 5.263a_o - 4.177a_o^2 + 1.643a_o^3 - 0.2542a_o^4 \quad (5.106)$$

Frequency independent values of the sidelayer impedances can also be used to simplify the analysis

$$k_x^s = 4.05 \quad (5.107a)$$

$$c_x^s = 9.85 \quad (5.107b)$$

$$k_d^s = 2.50 \quad (5.108a)$$

$$c_d^s = 1.80 \quad (5.108b)$$

If an embedment factor Δ is defined

$$\Delta = \frac{\text{Impedance of embedded foundation}}{\text{Impedance of unembedded foundation}} \quad (5.109)$$

then the embedment factors of Beredugo and Novak can be written as,

$$\Delta_{K_{fx}} = \frac{k_x + \frac{G_s}{G} \delta k_x^s}{k_x} \quad (5.110)$$

$$\Delta_{C_{fx}} = \frac{c_x + \frac{G_s}{G} \delta c_x^s}{c_x} \quad (5.111)$$

$$\Delta_{K_{fd}} = \frac{k_d + \frac{G_s}{G} \delta k_d^2}{k_d} \quad (5.112)$$

$$\Delta_{C_{fd}} = \frac{c_d + \frac{G_s}{G} \delta c_d^s}{c_d} \quad (5.113)$$

These embedment factors contain several features that improve the potential for accuracy in comparison to the somewhat simpler solutions to be discussed later. These features include,

1. The backfill can have different elastic properties than the base material. This is important because the backfill of prototype foundation excavations does not, in general, have the same properties as the original material. Since structures are usually founded on undisturbed soils, there can be a significant difference in the properties of the two materials. The cushioning, for example, of a structure founded on very stiff soil by a softer backfill can be accounted for by this method. Slipping between the foundation and backfill can also be considered by reducing the effective stiffness of the soil.
2. The effect of embedment is frequency dependent through the sidelayer functions. The solutions to be presented subsequently do not possess this feature. It can be expected that since the foundation impedances are frequency dependent, the effect of sidelayer restraint should be also, but not necessarily in the same way as the base material.
3. Different functions have been developed for the effect of embedment on both the stiffness and damping of the translation, rocking, and torsion of the foundation.

Sidelayer effects are not explicitly used in the second method of analysis. In this method, the embedding material is assumed to have the same properties as the base material, and to have a perfect bond with the foundation. There is no direct mechanism by which the effect of different backfill materials can be accounted for. Furthermore, the additional stiffness or damping caused by embedment is assumed to be independent of the frequency. The advantage of the following formulations, however, is the significant reduction in the effort required for the analysis, the static impedance values are increased by a factor dependent solely on the embedment ratio.

Parmalee and Kudder (1974) defined a single embedment factor applicable to both the stiffness and damping of the translation and rocking motions by

$$\Delta = e^{1.10\delta} \quad . \quad (5.114)$$

Elsabee and Morray (1977) determined the following embedment factors for the translation and rocking motions,

$$\Delta_{K_{fx}} = \Delta_{C_{fx}} = 1 + \frac{2}{3} \delta \quad (5.115)$$

$$\Delta_{K_{f\phi}} = \Delta_{C_{f\phi}} = 1 + 2\delta \quad . \quad (5.116)$$

Luco, Wong and Trifunac (1975) evaluated the results of Beredugo and Novak for the the case of the backfill and base material having the same properties. An average value over the appropriate dimensionless frequency range of $0 < a_0 < 2.0$ was used to determine the following frequency independent values:

• Horizontal translation

$$\Delta_{K_{fx}} = 1 + 0.80 \delta \quad (5.117)$$

$$\Delta_{C_{f\phi}} = 1 + 3.36 \delta \quad (5.118)$$

• Rocking

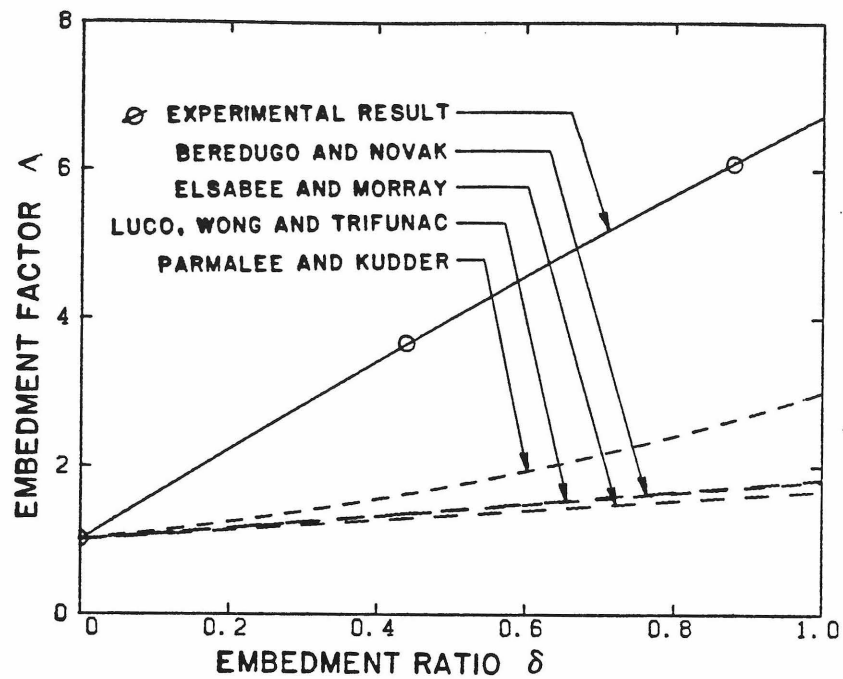
$$\Delta_{K_{f\phi}} = 1 + 2.38 \delta \quad (5.119)$$

$$\Delta_{C_{f\phi}} = 1 + 7.7 \delta \quad (5.120)$$

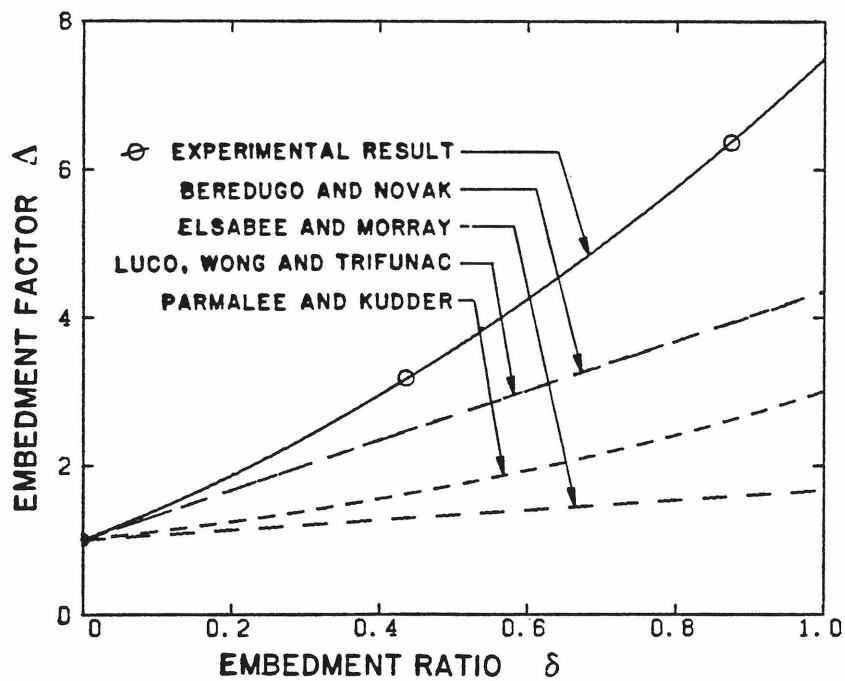
The embedment factors obtained by use of the above methods are plotted in Figures 5.14 and 5.15. For comparison, the experimentally determined embedment factors are also plotted. Because the formulations of Beredugo and Novak are frequency dependent, a frequency averaged value is plotted. This value is obtained by averaging the results obtained over the dimensionless frequency range of 0.45 to 0.60. This range was selected because the unembedded dimensionless resonant frequency was 0.506, and the embedded resonant frequencies should be slightly higher, because of the increased stiffness. The selection of the frequency range is not critical however, since the embedment factor can be shown not to vary greatly with frequency.

Some of the features exhibited in Figures 5.14 and 5.15 are highlighted here,

1. Since the results of Luco, Wong, and Trifunac are based on the frequency dependent sidelay functions of Beredugo and Novak,

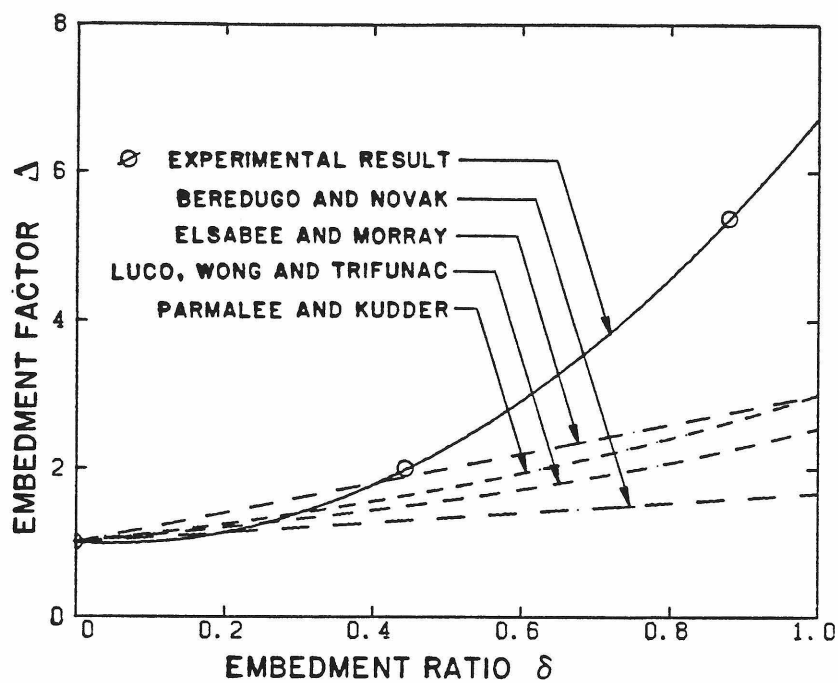


(a) Stiffness

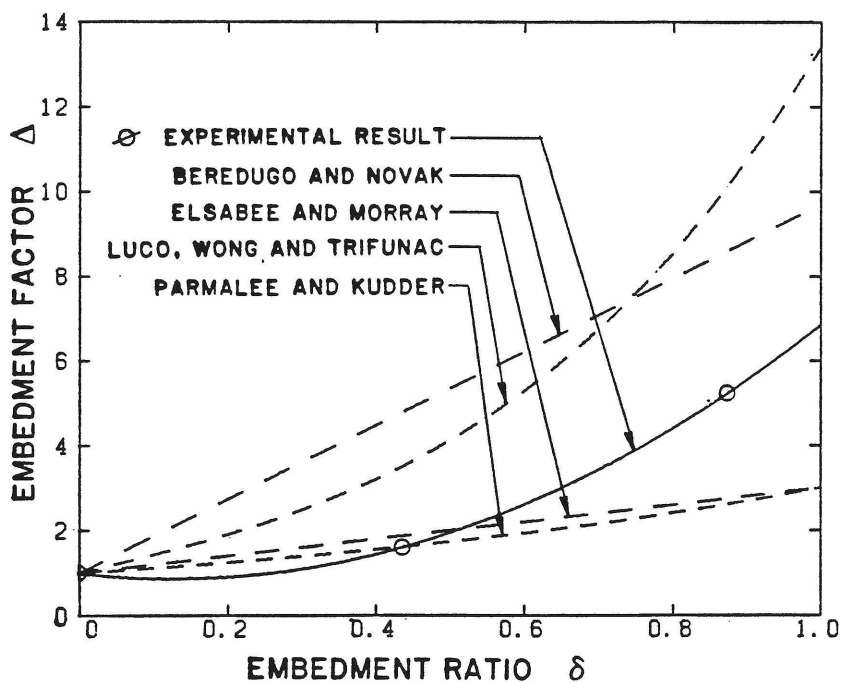


(b) Damping coefficient

Figure 5.14. Embedment factors for horizontal translation.



(a) Stiffness



(b) Damping coefficient

Figure 5.15. Embedment factors for rocking.

the relatively close agreement between these results for most cases is not surprising.

2. There are larger variations in the damping embedment factors than the stiffness damping factors. This is partially due to the fact that the formulations of Parmalee and Kudder, and Elsabee and Morray present the same embedment factor for the stiffness and damping coefficient, while different functions are presented by Luco, Wong, and Trifunac, and Beredugo and Novak.
3. Except for the case of damping of the rocking motion, the experimentally obtained embedment factors are consistently greater than the analytical factors. The experimentally obtained second-order dependence of the embedment factor on embedment ratio appears to be qualitatively supported by the theoretical results. In some cases, the experimentally obtained embedment factors appear to have values of less than unity at small embedments. As noted earlier, this is not a real phenomenon; it is a result of the imposition of a quadratic polynomial fit on the three data points.

5.3.4. Response of the Structure with Embedded Foundation.

The calculated responses of the specimen structure with foundation embedment are shown in Tables 5.2 and 5.3. In Table 5.2, the structural and foundation-soil impedances are based on the analyses of subsections 5.2.1 and 5.3.1. The embedment has been included by use of the methods

discussed in the previous subsection. The response of the structure with an unembedded foundation is also listed for comparison. Several remarks should be made about the results shown in Table 5.2.

TABLE 5.2. Effect of embedment on response of three-degree-of-freedom system. Properties of system found from analytical calculations. Effect of embedment calculated by various formulations.

Embed- ment Ratio	Resonant Frequency in Hertz	Fundamental Modal Damping in Percent of Critical	Fundamental Mode Displacement Ratios*				Calculation method
			in percent			$\frac{X_t}{X_g}$	
			$\frac{X_f}{X_t}$	$\frac{h\phi}{X_t}$	$\frac{X_s}{X_t}$		
0	14.25	1.93	6.34	29.5	64.1	29	Analysis of subsection 5.3.2
0.44 0.89	15.35 16.15	1.79 1.82	4.28 2.77	20.7 13.8	75.0 83.4	32 36	Parmalee & Kudder
0.44 0.89	15.50 16.05	1.93 1.87	5.53 4.70	18.1 13.1	76.3 82.2	29 30	Elsabec & Morray
0.44 0.89	15.20 15.95	2.96 3.33	4.60 3.55	22.2 15.6	73.2 80.8	20 17	Luco, Wong & Trifunac
0.44 0.89	15.00 15.45	3.33 3.72	4.43 3.38	24.7 21.1	70.8 75.5	17 15	Beredugo & Novak

* X_f - displacement of foundation

$h\phi$ - tangential displacement due to rocking

X_s - interfloor displacement

X_t - total superstructure displacement

X_g - ground motion amplitude

1. Embedment increases the resonant frequency of the structure.
This is consistent with the increased stiffness shown in Figures 5.14 and 5.15.
2. In most cases, the modal damping factor increases with embedment. In the cases where it does not, the embedment factor is the same for both the stiffness and damping. Where the modal damping factor increases, the embedment factor for damping is greater than the embedment factor for stiffness.
3. The contribution of foundation rocking and translation to the overall superstructure displacement decreases with embedment. This condition is consistent with the increased foundation-soil impedances.

In Table 5.3, the various embedment factor formulations described in subsection 5.3.3 have been applied to a structure having the experimentally determined impedances of the unembedded specimen structure. Recall that these impedances resulted from a simple systems identification calculation (subsection 4.3.3) that was based on the fundamental mode shape and resonant frequency. The foundation-soil impedances found this way are taken to be constant-valued over the frequency range. Since only the fundamental mode response is of immediate importance, however, the errors introduced by use of these constant-valued impedances will be small. The purpose of Table 5.3, therefore, is to show the effect of embedment on the specimen structure independent of the differences associated with the calculation of the foundation-soil

impedance values. The experimentally measured frequency, damping, and displacement ratios are also listed.

TABLE 5.3. Effect of embedment on response of three-degree-of-freedom system. Properties of system found from analytical calculations. Effect of embedment calculated by various formulations.

Embed- ment Ratio	Resonant Frequency in Hertz	Fundamental Modal Damping in Percent of Critical	Fundamental Mode Displacement Ratios				Calculation method
			in percent			$\frac{X_t}{X_g}$	
			$\frac{X_f}{X_t}$	$\frac{h\delta}{X_t}$	$\frac{X_s}{X_t}$		
0	11.33	1.32	6.00	21.0	73.0	44	Input properties from para. 4.3.2
0.44	12.00	1.38	3.95	14.2	81.9	42	Parmalee & Kudder
0.89	12.40	1.41	2.54	9.10	88.3	41	
0.44	12.05	1.45	5.08	12.2	82.7	42	Elsabee & Morray
0.89	12.35	1.31	4.26	8.66	87.1	41	
0.44	11.85	1.79	4.73	15.1	80.1	32	Luco, Wong & Trifunac
0.89	12.25	2.09	3.88	10.4	85.7	27	
0.44	11.85	2.53	3.84	16.4	79.7	23	Beredugo & Novak
0.89	12.15	2.55	2.71	13.4	83.9	21	
0	11.33	0.80	6.10	21.0	72.9	39	Measured values
0.44	13.28	0.83	2.10	14.2	83.7	47	
0.89	13.75	0.81	1.30	5.4	93.3	44	

Comparison of the experimental observations with the calculated result shows that the analyses generally underestimate the effect of embedment. This was also indicated in Figures 5.14 and 5.15 in which

the embedment factors determined by the experiment were larger than the corresponding analytical embedment factors.

The analytical and experimental results show qualitative agreement. In all cases, resonant frequencies increase with embedment, and the contribution of foundation translation and rigid body rocking to the total superstructure displacement decreases. These trends are indicative of the increased stiffness caused by foundation embedment. The modal damping factors generally increase with foundation embedment but never exceed 3%. The damping factors resulting from the analysis are, however, significantly higher than those measured experimentally, which were less than 1%. These variations are large in a relative sense, but are not of major importance in the context of structural performance.

5.3.5. Summary of Fundamental Mode Analysis.

In general, the results of the analysis are qualitatively consistent with the major features seen in the experiment, including the effects of embedment. The experimentally determined foundation-soil impedances for the unembedded case were not exactly the same as the corresponding quantities obtained from the use of analytical formulations. The effect of embedment was determined on the response of both systems.

Significant differences (by as much as a factor of two) exist between the experimental and analytical impedances for the embedded foundation. The differences in the total response caused by these individual variations were much smaller. It should be noted, however,

that the foundation geometry of the specimen structure is very simple. Very few prototype foundations have smooth straight walls and flat bases. The effect of irregularities in the foundation, such as wall footings, pile caps, and so on, may affect the response.

With the possible exception of nuclear reactor containment buildings, there are few prototype structures which are embedded to depths that approach the foundation radius. For the typical prototype structure, maximum embedment ratios between 0.2 and 0.5 can be expected. In this range, the differences among the embedment factors, and also among the theoretical and experimental results for this test, are much less. Hence, there can be some expectation that the theoretical approaches will produce reliable results.

5.4. TORSIONAL RESPONSE.

The torsional response of symmetric structures is usually considered to be unimportant in comparison to the fundamental mode response. In this study, however, since the torsional response of the structure was measured, and since some theoretical analyses do treat the problem, a lumped parameter analysis of the two-degree-of-freedom torsional model (shown in Figure 5.2) will be conducted. The format of this section will be similar to that of the previous section. The discussion of the foundation-soil impedances and embedment factors will be abbreviated, since most of the significant features have already been discussed.

5.4.1. Foundation-Soil Impedances.

Because of simpler boundary conditions, the response of an unembedded circular foundation to torsional excitation can be solved exactly. Bycroft, after Reisner and Sagoci (1944), found compliance functions that lead to the following impedance functions,

$$\begin{aligned} K_{f\phi} = & Gr_o^3(5.340 + 0.1186a_o - 1.637a_o^2 + 1.099a_o^3 \\ & - 0.3347a_o^4 - 0.0375a_o^5) \end{aligned} \quad (5.121)$$

$$\begin{aligned} C_{f\phi} = & \sqrt{Gp} r_o^4(.00936 - 0.1352a_o + 1.315a_o^2 - 0.9877a_o^3 \\ & + 0.3293a_o^4 - 0.04422a_o^5) \end{aligned} \quad (5.122)$$

The static torsional stiffness is given by

$$K_{f\phi}^{st} = \frac{16}{3} Gr_o^3 \quad (5.123)$$

Luco and Westmann expanded Bycroft's solution to include the range $0 < a_o < 10$. In the range of $0 < a_o < 2.5$, the corresponding impedance functions are,

$$\begin{aligned} K_{f\phi} = & \frac{16}{3} Gr_o^3(1.0 - 0.0298a_o - 0.06325a_o^2 - 0.2299a_o^3 \\ & + 0.2160a_o^4 - 0.04955a_o^5) \end{aligned} \quad (5.124)$$

$$\begin{aligned} C_{f\phi} = & \frac{16}{3} \sqrt{Gp} r_o^4(0.0015 + 0.1192a_o - 0.1198a_o^2 \\ & + 0.1666a_o^3 + 0.0862a_o^4 - 0.01398a_o^5) \end{aligned} \quad (5.125)$$

The torsional impedance of the soil is independent of the Poisson's ratio. Therefore, to be consistent with the impedance functions selected for the horizontal translation and rocking cases, the functions of Luco and Westmann will be used for subsequent analyses. The impedance functions for torsion are shown in Figures 5.16 and 5.17. No constant valued formulations were found in the literature.

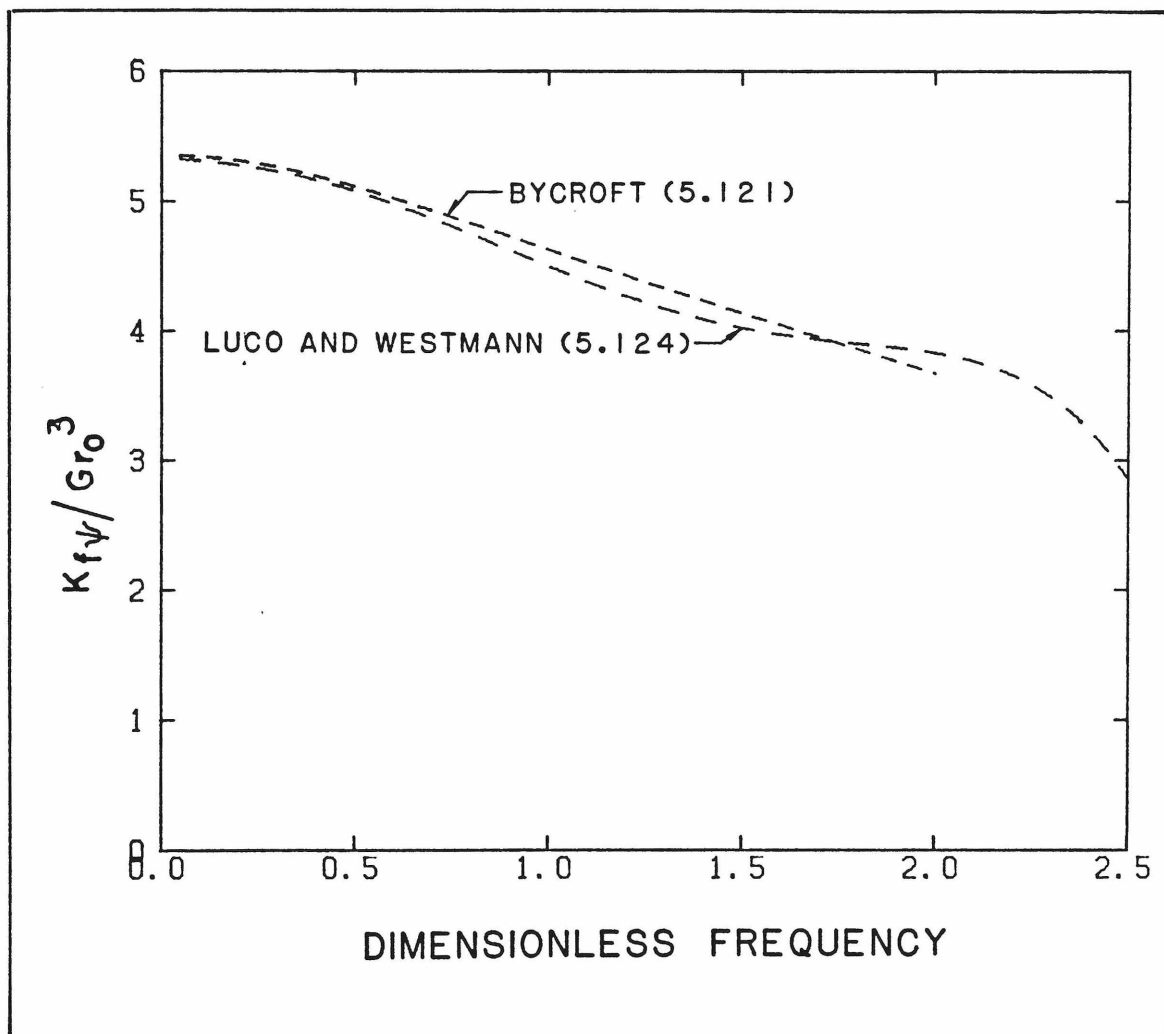


Figure 5.16. Foundation-soil stiffness for torsion, $\nu = 0$.

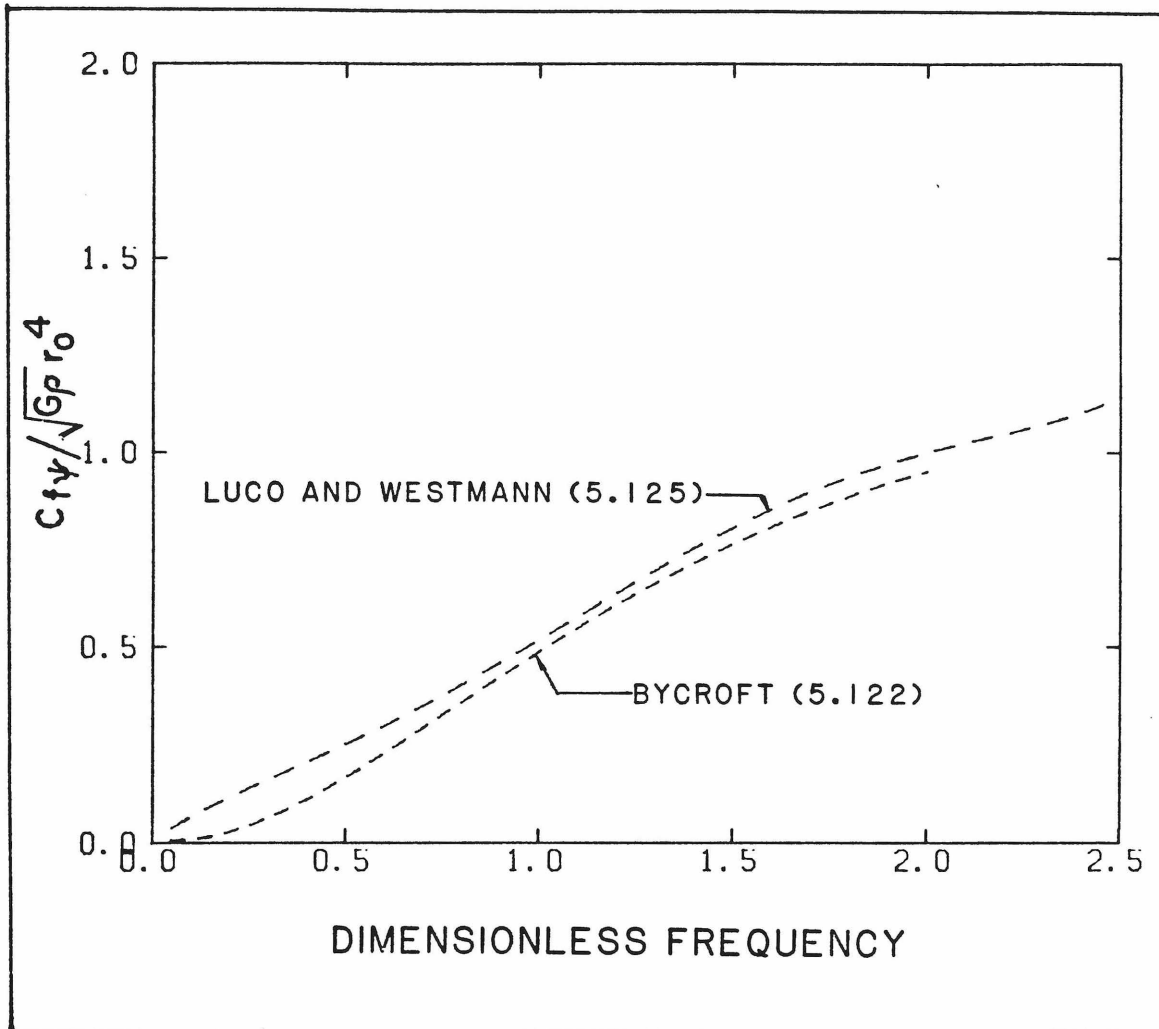


Figure 5.17. Foundation-soil damping for torsion, $\nu = 0$.

5.4.2. Analysis of Torsional Behavior with Unembedded Foundation.

Subsection 4.3.3 presented an attempt to determine the superstructure and foundation-soil stiffnesses which would define a structure that had the same resonant frequencies as the specimen. In that calculation, the moments of inertia were taken from the dimensions and masses of the specimen superstructure and foundation. The attempt was unsuccessful.

No structure, regardless of the superstructure and foundation stiffnesses having moments of inertia corresponding to the specimen structure, could have the measured resonant frequencies. This subsection will discuss further attempts at the characterization and analysis of the torsional behavior of the specimen structure, particularly for the unembedded foundation condition.

5.4.2.1. Analysis with analytically obtained properties.

Figure 5.18 shows the response of the two degree-of-freedom system defined by the following parametric values,

$$\begin{aligned} \blacksquare I_{s\phi} &= 7150 \text{ lb-sec}^2\text{-ft} \text{ (9700 N-sec}^2\text{-m)} \quad , \\ \blacksquare K_{s\phi} &= 3.85 \times 10^8 \text{ lb-ft} \text{ (5.22 } \times 10^5 \text{ kN-m)} \quad , \\ \blacksquare C_{s\phi} &= 3.32 \times 10^4 \text{ lb-sec-ft} \text{ (45 kN-sec-m)} \quad , \\ \blacksquare I_{f\phi} &= 23,620 \text{ lb-sec}^2\text{-ft} \text{ (32000 N-sec}^2\text{-m)} \quad , \\ \blacksquare K_{f\phi} &= \frac{16}{3} Gr_o^3[(a_o)] \text{ [Equation (5.124)]} \quad , \\ \blacksquare C_{f\phi} &= \frac{16}{3} \sqrt{G\rho} r_o^4[(a_o)] \text{ [Equation (5.125)]} \quad . \end{aligned}$$

The moments of inertia and the structural stiffness were calculated from the dimensions of the specimen structure. The damping coefficient of the superstructure corresponds to a fixed-base damping factor of 1%. The foundation-soil impedances resulted from the use of the analytical formulations of subsection 5.4.1. The results of the analysis indicate that the torsional resonant frequencies of the model structure are 32.5

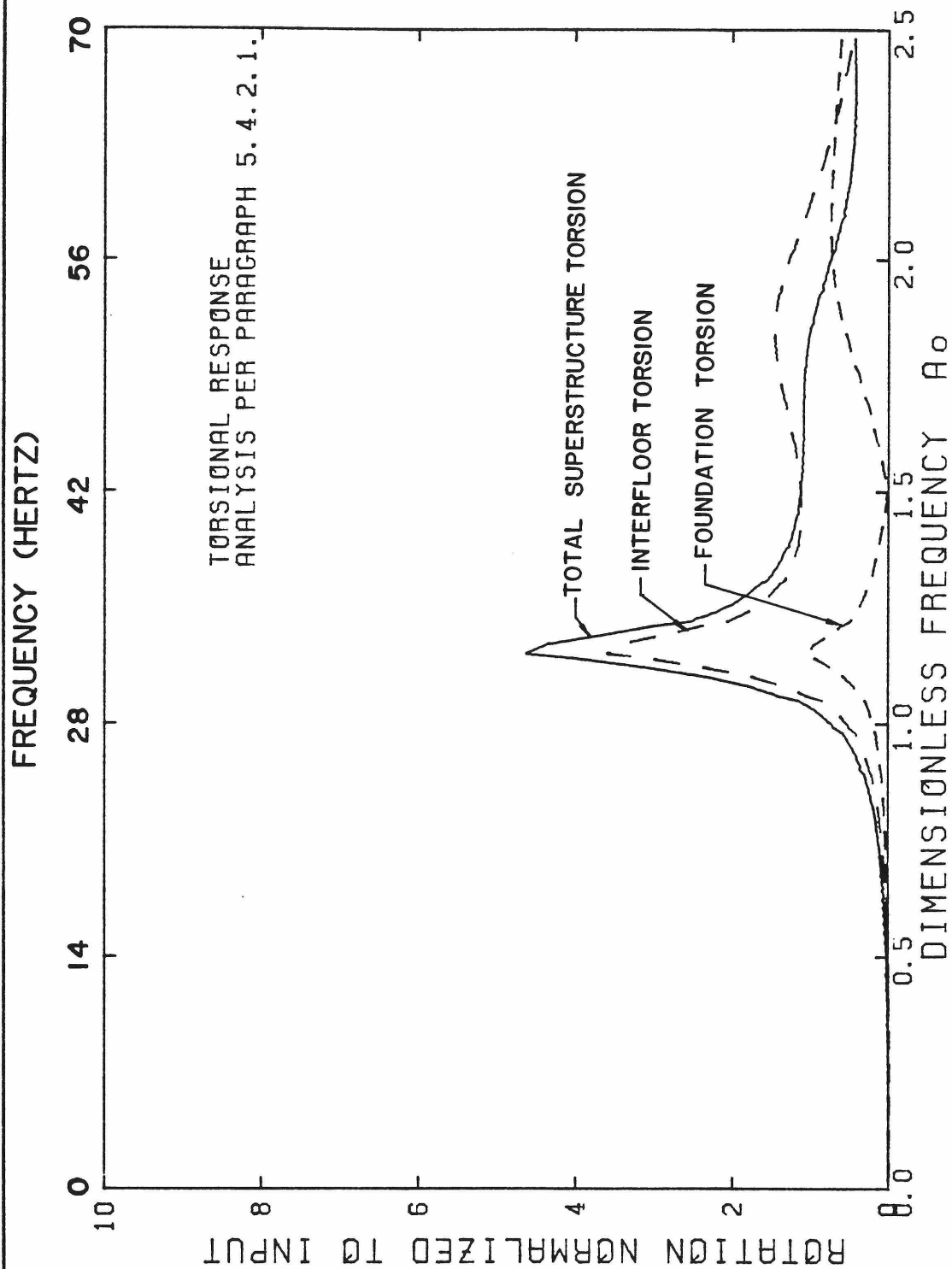


Figure 5.18. Response of two degree-of-freedom system with analytically obtained properties.

and 52.0 Hertz; the corresponding dimensionless frequencies are 1.15 and 1.85. The damping ratio of the first torsional mode is 3.1% of critical.

These calculated results do not agree with the experimental results. The lowest resonant frequency is over 50% greater than the corresponding experimental value, and the second resonant frequency is twice as large as the corresponding measured quantity. The agreement between the calculated and measured responses will be improved by the revisions introduced in the next paragraph.

5.4.2.2. Analysis with measured superstructure stiffness.

The first modification to the analysis uses the torsional stiffness of the superstructure found from the fundamental translational response of the structure in both the east-west and north-south directions (Equation 5.47). The damping coefficient again corresponds to a damping ratio of 1%. The values of the input parameters are,

$$\begin{aligned} \blacksquare I_{s\phi} &= 7150 \text{ lb-sec}^2\text{-ft} \text{ (9700 N-sec}^2\text{-m)} \quad , \\ \blacksquare K_{s\phi} &= 1.38 \times 10^8 \text{ lb-ft} \text{ (1.87} \times 10^5 \text{ kN-m)} \quad , \\ \blacksquare C_{s\phi} &= 1.94 \times 10^4 \text{ lb-sec-ft} \text{ (26.3 kN-sec-m)} \quad , \\ \blacksquare I_{f\phi} &= 23,620 \text{ lb-sec}^2\text{-ft} \text{ (32000 N-sec}^2\text{-m)} \quad , \\ \blacksquare K_{f\phi} &= \frac{16}{3} G r_o^3 [k(a_o)] \quad , \\ \blacksquare C_{f\phi} &= \frac{16}{3} \sqrt{G_p} r_o^4 [c(a_o)] \quad . \end{aligned}$$

The response is shown in Figure 5.19. The first torsional resonant frequency has decreased to 20.9 Hertz, and the second resonant frequency is 47.0 Hertz. These frequencies correspond to dimensionless frequencies of 0.74 and 1.67, respectively. The damping ratio of the first torsional mode is 1.08%. The foundation impedances, evaluated at the two resonant frequencies, have the values shown in Table 5.4.

TABLE 5.4. Foundation-soil impedances for torsion at resonant frequencies.

Resonant Frequency in Hertz	Dimensionless Frequency a_o	$k(a_o)$	$c(a_o)$	$K_{f\phi}$ in lb-ft (kN-m)	$C_{f\phi}$ in lb-ft-sec (kN-m-sec)
20.9	0.74	0.90	0.063	2.54×10^9 (3.44×10^6)	1.0×10^6 (1.33×10^3)
47.0	1.67	0.74	0.164	2.09×10^9 (2.83×10^6)	2.61×10^6 (3.4×10^6)

The first resonant frequency found by this analysis is in better agreement with the experimental response in the first mode, which is due chiefly to the torsional motion of the superstructure. The second torsional frequency, however, is still twice as large as the measured value. These comparisons show that the input properties of the superstructure used in this analysis are fairly close to those of the specimen structure.

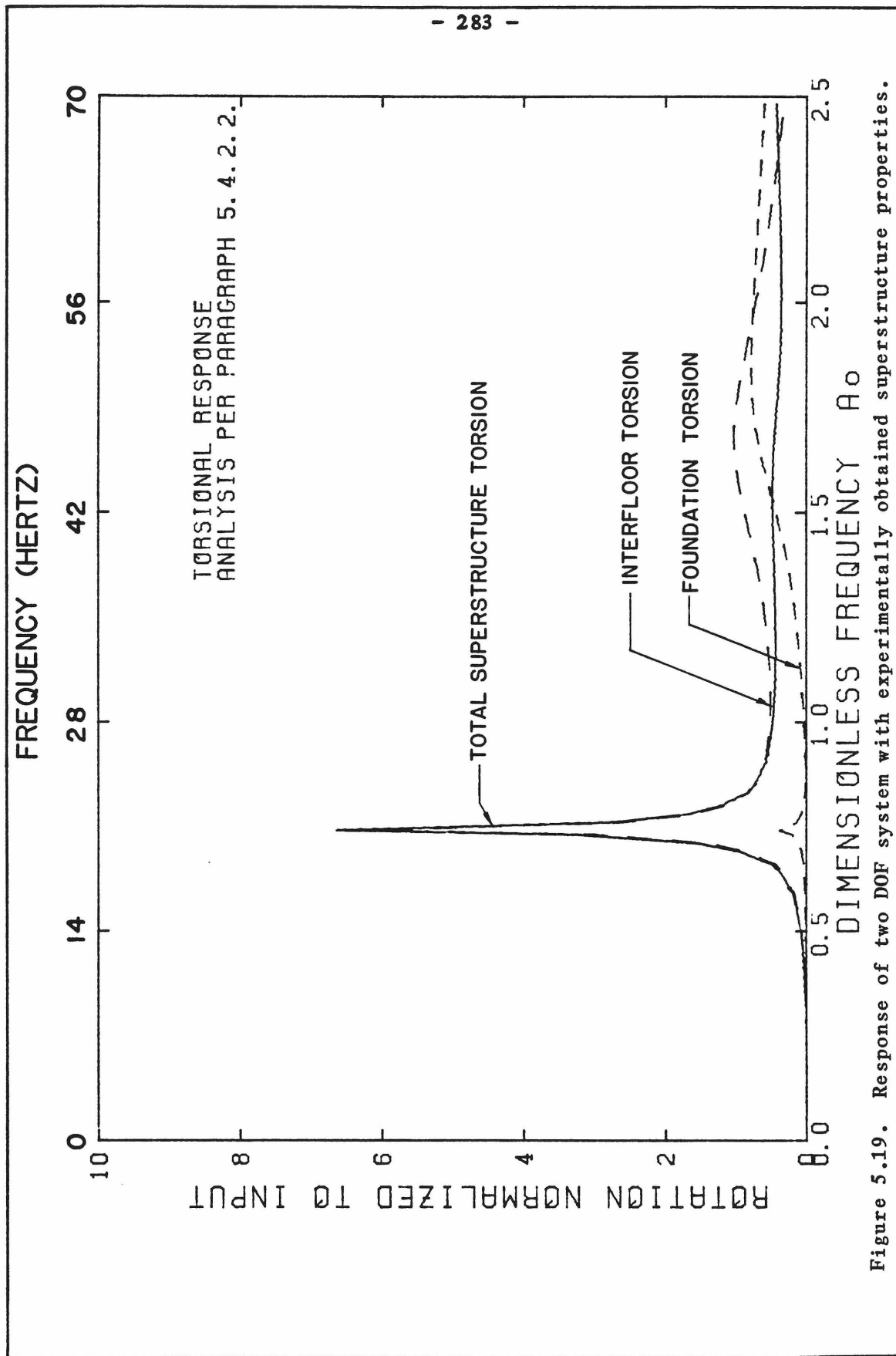


Figure 5.19. Response of two DOF system with experimentally obtained superstructure properties.

5.4.2.3. Analysis using hybrid input values.

Having now determined a value of the superstructure stiffness that leads to relative agreement in the first torsional resonant frequency, the analysis of this paragraph will attempt to determine the foundation properties to improve the agreement for the second resonant frequency.

From the close proximity of the two resonant frequencies, it appears that the two-degree-of-freedom system may be acting like a vibration absorber. Such an absorber consists of the in-series connection of two SDF oscillators, having the same natural frequency, that results in a two-degree-of-freedom system that has two distinct resonant frequencies which are separated from the individual frequencies by an amount dependent upon the relative masses of the two oscillators.

In this case, the fixed base torsional resonant frequency f_b of the superstructure is 21.5 Hertz. The two system resonant frequencies are then in the following ratios to the SDF frequency,

$$\frac{f_1}{f_b} = \frac{19.0}{21.5} = 0.88$$

$$\frac{f_2}{f_b} = \frac{24.3}{21.5} = 1.13 \quad .$$

An analysis of a vibration absorber was presented by Thomson (1965). A result of this analysis was a graph from which could be found the mass ratio necessary to define a system with the given frequency ratios. For the frequency ratios of this system, namely 0.88 and 1.13, the required mass ratio is approximately 0.06. Hence, the moment of inertia of the superstructure should be approximately 6% of the foundation moment of

inertia. Furthermore, the fixed-base resonant frequency of the foundation should be 21.5 Hertz. These two conditions lead to a foundation moment of inertia $I_{f\phi}$ of 119,060 lb-sec²-ft, and a foundation torsional stiffness $K_{f\phi}$ of 2.2×10^9 lb-ft (3.0×10^6 kN-m).

The required foundation moment of inertia is five times greater than the actual moment of inertia, while the required foundation stiffness is very close to the value obtained by the evaluation of the analytical impedance function at 21.5 Hertz (as shown in Table 5.4).

The efficacy of the vibration absorber analogy in explaining the observed behavior is demonstrated by the response shown in Figure 5.20, which was based on the following input properties,

- $I_{s\phi} = 7150 \text{ lb-sec}^2\text{-ft} \text{ (9700 N-sec}^2\text{-m)}$,
- $K_{s\phi} = 1.38 \times 10^8 \text{ (1.87} \times 10^5 \text{ kN-m)}$,
- $C_{s\phi} = 1.94 \times 10^4 \text{ lb-sec-ft} \text{ (26.3 kN-sec-m)}$,
- $I_{f\phi} = 119,060 \text{ lb-sec}^2\text{-ft} \text{ (161,400 N-sec}^2\text{-m)}$,
- $K_{f\phi} = \frac{16}{3} \text{ Gr}_o^3 [\text{k(a}_o)]$,
- $C_{f\phi} = \frac{16}{3} \sqrt{G_p} r_o^4 [(a_o)]$.

Note that these values are identical to those of the previous analysis, except that the foundation moment of inertia has been increased.

The response has resonant frequencies at 19.9 and 24.9 Hertz, a relatively good agreement with the observed values of 19.02 and 24.30 Hertz, for the unembedded case. This result shows that the use of

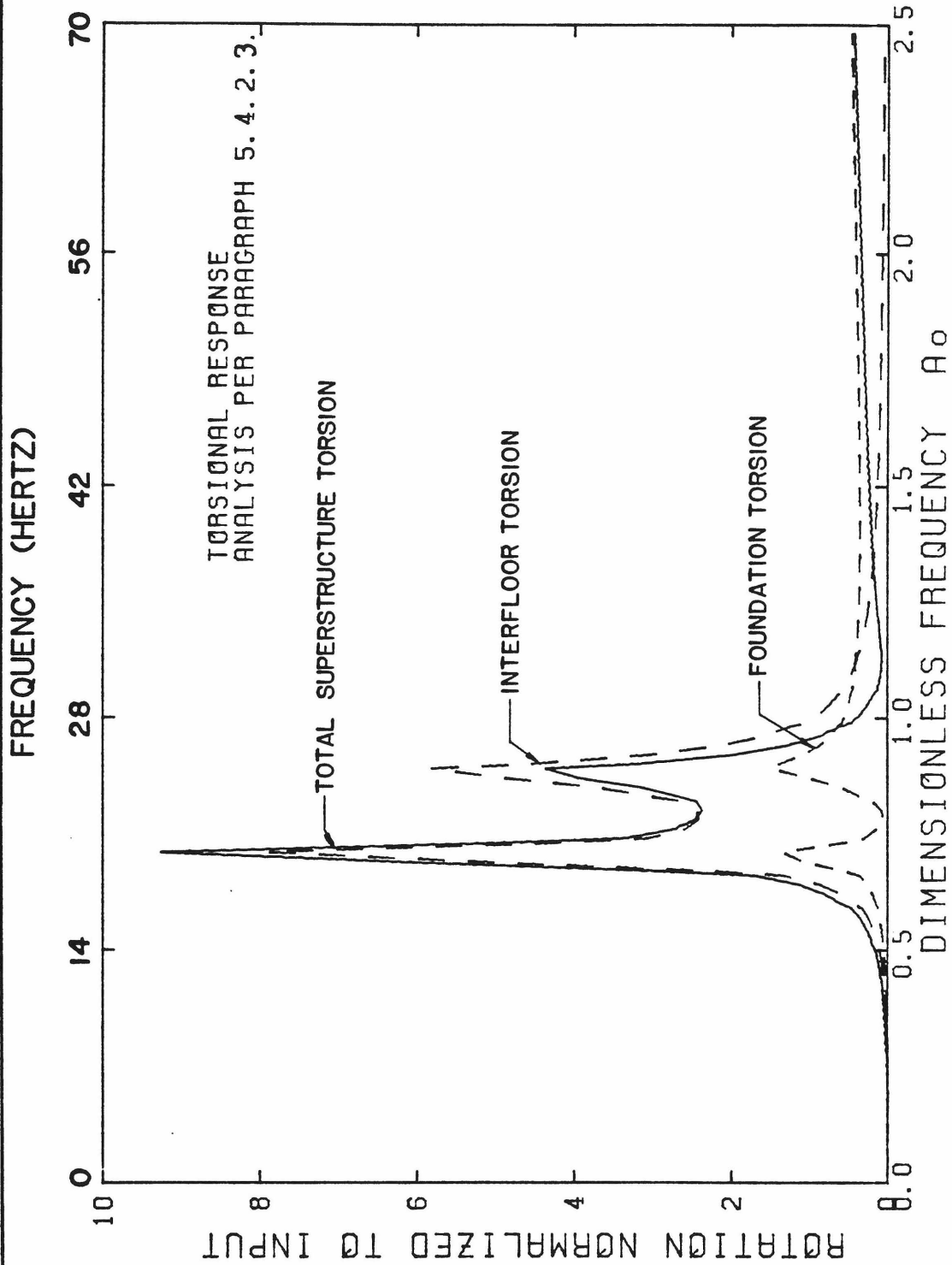


Figure 5.20. Response of two degree-of-freedom system with hybrid properties.

"modified" moment of inertia will resolve the significant differences between the response of the analytical and experimental models; if a foundation moment of inertia of 119,060 lb-ft-sec² (161 kN-m-sec²) had been used in the analysis of subsection 4.3.3, the foundation stiffness required to define a system with the experimentally measured resonant frequencies would have been very close to the value found by analysis.

Recall that the foundation-soil stiffness is dependent upon the radius of the foundation. Since the values of the analytical and experimental stiffnesses are close, the modified foundation must have approximately the same radius, and hence, plan dimensions, as the specimen foundation. Therefore only the height of the foundation can be varied to increase the moment of inertia. The modified foundation must therefore have a height of over 25 ft (7.6 m), compared to the actual height of 5.0 ft (1.5 m). This modification leads to a system that has the same resonant frequencies as experimentally observed.

Although this analysis has resulted in agreement of the torsional resonant frequencies, two problems remain unresolved. The first is the lack of agreement between the observed and calculated values for the relative phase between the foundation and superstructure motions. The second problem is to find a physical justification for the increased foundation size.

The next two subsections have no direct application to the experimental results. These analyses are presented only for completeness; to

demonstrate the effect of embedment on the response of the two-degree-of-freedom system developed in this paragraph.

5.4.3. Modification of Foundation-Soil System for Embedment.

The work of Beredugo and Novak for the translation and rocking of embedded foundations was extended by Novak and Sachs (1973) to include torsion. The resulting embedment factors are,

$$\Delta_{K_{f\phi}} = \frac{k_{\phi} + \frac{G_s}{G} \delta k_{\phi}^s}{k_{\phi}} \quad (5.127)$$

$$\Delta_{C_{f\phi}} = \frac{c_{\phi} + \frac{G_s}{G} \delta c_{\phi}^s}{c_{\phi}} \quad (5.128)$$

The functions k_{ϕ}^s and c_{ϕ}^s are frequency dependent sidelayer functions,

$$\begin{aligned} k_{\phi}^s &= 12.58 - 1.01a_o - 5.912a_o^2 & 0 \leq a_o \leq 0.2 \\ &= 12.59 - 1.885a_o - 3.3499a_o^2 + 5.335a_o^3 - 2.76a_o^4 + 0.495a_o^5 \\ & & 0.2 \leq a_o \leq 2.0 \end{aligned} \quad (5.129)$$

$$\begin{aligned} c_{\phi}^s &= 9.04a_o & 0 \leq a_o \leq 2.0 \\ &= 7.5 - \frac{3.726}{0.455 + a_o} & 0.2 \leq a_o \leq 2.0 \end{aligned} \quad (5.130)$$

Kausel and Ushijima (1979) proposed the following embedment factor for both stiffness and damping

$$\Delta_{K_{f\phi}} = \Delta_{C_{f\phi}} = 1 + 2.67 \delta \quad (5.131)$$

Luco, Wong, and Trifunac evaluated the frequency dependent results of Novak and Sachs, and obtained the following embedment factors,

$$\Delta_{K_{f\phi}} = 1 + \delta + 0.55\delta^3 \quad (5.132)$$

$$\Delta_{C_{f\phi}} = 1 + 4.2\delta + 8.2\delta^3 \quad . \quad (5.133)$$

Figure 5.22 plots the embedment factors for torsion. There were, of course, no experimentally obtained values for comparison.

5.4.4. Torsional Response of the Structure with Embedded Foundation.

The agreement between the experimental and analytical results for torsional behavior was shown, in subsection 5.4.2, to be poor for the unembedded case. To provide some assessment of the effect of embedment on torsional response, the lumped parameter model developed in paragraph 5.4.2.3 will be used here.

The resonant frequencies of the system are sensitive to the properties of the superstructure and the foundation-soil system. For the two resonant frequencies to be close to one another (as measured), it is necessary for the fixed-base resonant frequency of the superstructure to be nearly equal to the fixed-base resonant frequency of the foundation-soil system. Embedment of the foundation, however, affects the foundation-soil stiffness, but leaves the foundation moment of inertia unaffected. Therefore, the resonant frequency of the foundation will no longer be as close to the resonant frequency of the

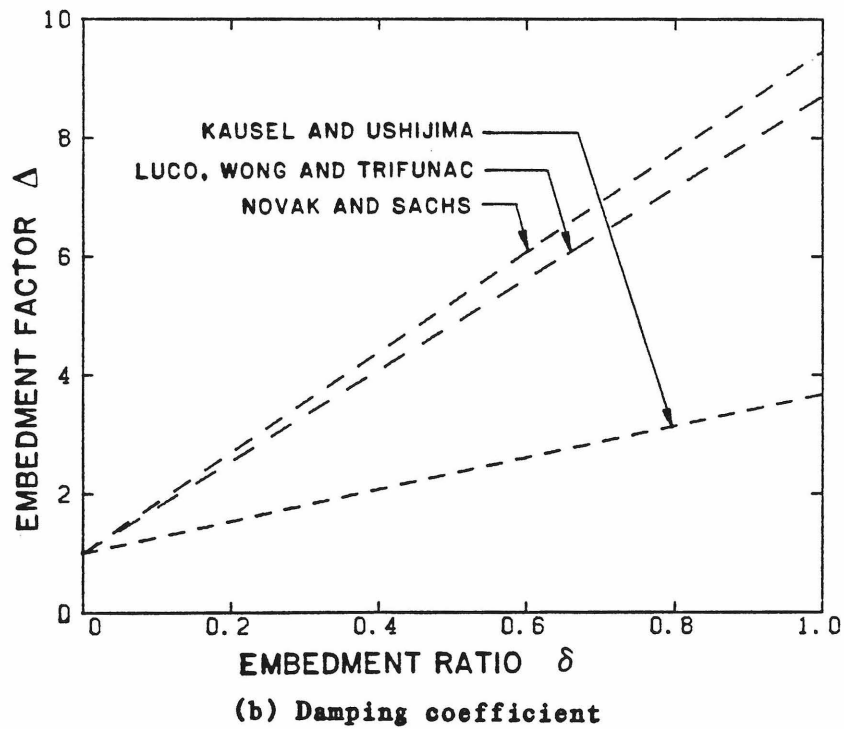
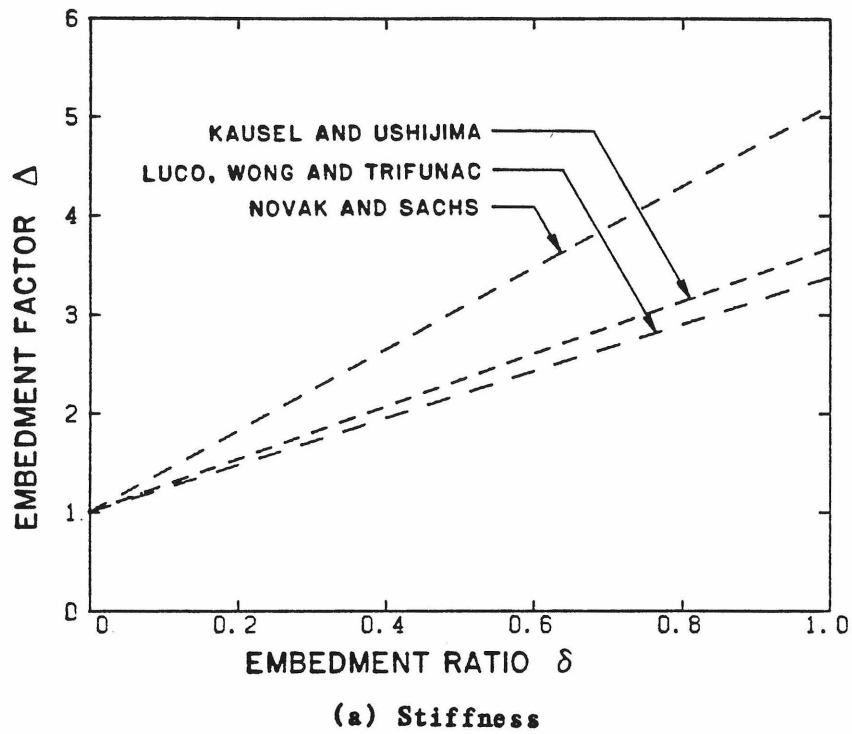


Figure 5.21. Embedment factors for torsion.

superstructure as it was in the unembedded case, and the resonant frequencies of the system will change.

Under these conditions, the two resonant frequencies of the system will not be in the close proximity that was observed experimentally. The first torsional frequency will be slightly affected by the increased foundation stiffness, but the second torsional frequency, which is primarily a foundation response, will change drastically. This feature is shown in Table 5.5, which lists the resonant frequencies, mode shapes, and modal dampings for the torsional response of the two-degree-of-freedom model with foundation embedment.

These results, compared with the experimental results listed in Table 4.8, indicate an enormous difference between the two-degree-of-freedom model and the specimen structure. Even if the model is tailored to match the behavior of the specimen structure with the unembedded foundation, the agreement cannot be maintained after the foundation is embedded. The mode shapes, represented by the ratio ϕ_f/ϕ_s , indicate that both masses move in-phase in the first mode, and are out-of-phase in the second mode. While this is consistent with a two-degree-of-freedom model with normal modes, this behavior is not seen in the measured response.

5.4.5. Summary of Torsion Analysis.

The torsional behavior of the specimen structure, regardless of the embedment condition, does not agree with the behavior predicted by the lumped parameter analysis. In such an analysis, the foundation mass is

TABLE 5.5. Effect of embedment on response of two-degree-of-freedom system for torsion. Effect of embedment calculated by various formulations.

Embedment ratio	Resonant frequency in Hertz	Modal damping in percent of critical	Mode shape ϕ_f/ϕ_s	Calculation method
0	19.9 25.0	1.63 3.2	0.149 -0.339	Analysis of para. 5.4.2.3
0.44	21.2 32.8	1.1 *	0.035 -1.13	Kausel & Ushijima (1979)
0.89	21.3 38.9	1.1 *	0.021 -1.51	
0.44	21.1 30.5	1.3 *	0.041 -.66	Luco, Wong & Trifunac (1975)
0.89	21.3 33.8	1.2 *	0.022 -.59	
0.44	21.1 30.4	1.5 *	0.042 -.66	Novak & Sachs (1973)
0.89	21.3 35.2	3.6 *	0.023 -.69	

*Response peak too highly damped to determine damping ratio.

used without modification, since the foundation-soil impedances are found from the response of a massless foundation. It has been shown that the foundation moment of inertia had to be increased five-fold in order to define a model with the resonant frequencies of the specimen. This condition is contrary to the general embedment analysis, in which only the foundation-soil impedances, and not the inertias, are dependent upon the embedment depth.

The lack of qualitative agreement between the theoretical and experimental results for the torsional response seems to indicate that a more complex phenomenon is at work in the experiment. The major cause of this difficulty is the close proximity of the two resonant frequencies, for all embedment cases.

Another interpretation of the experimental and analytical results is made possible by the radical assumption of only one torsional response mode, i.e., the second torsional response is assumed to be caused by some unrelated effect and is neglected. Under this assumption, the requirements on the two-degree-of-freedom model are reduced. As shown in paragraph 5.4.2.2, a model having a superstructure stiffness based on the observed translatory response, and values of the moments of inertia and foundation-soil impedances that are based on actual dimensions, and analytical expressions, respectively, has a torsional resonant frequency of 20.9 Hertz, which is not far from the measured frequency of 19 Hertz, for the unembedded case. If embedment factors are applied to the torsional foundation-soil impedances, this resonant frequency will increase, much like the first value in each embedment case shown in Table 5.5. The resonant frequencies will, for the cases of half- and full-embedment, then be approximately 21.2 and 21.3 Hertz, respectively. These values are consistent with the trends measured experimentally. The problem with the phase angles, however, still is not resolved.

The results of the experiment have shown that horizontally incident SH-waves can cause significant torsional motions of the foundation and superstructure. The tangential motions of both due to the torsional response were found to be the same magnitude as the translation in the fundamental mode. These results are consistent with the recent studies by Luco (1976), Wong and Luco (1978), and Luco and Wong (1982) who examined the response of structures to non-vertically incident SH-waves. These studies have shown that torsional response can make significant contributions to the overall displacement of the structure for this type of excitation.

5.5. CHAPTER SUMMARY

This chapter has presented the analysis of a five-degree-of-freedom model of the specimen structure. The analysis was simplified by separation of the model into two simpler systems: one system consisted of the superstructure and foundation translation and rigid body rocking degrees of freedom, another system consisted of the superstructure and foundation torsional motions.

Prior to the frequency domain analysis, the dynamic properties of the superstructure, and the equivalent foundation radii were calculated. The analysis included the comparison of various foundation-soil impedance formulations. Both frequency dependent and constant valued impedance formulations were shown. A consistent format was used to express these results. The difference between the various results was

small enough to permit the selection of one set of impedance functions for each type of foundation motion.

The response of the structure in the fundamental mode was then determined for the unembedded foundation case. The resonant frequencies, mode shapes, and dampings indicated that the analytical foundation-soil impedances were greater than those existing in the specimen structure. The differences, however, were not extreme.

The effect of embedment was introduced into the model by calculation of embedment factors that are applied to the foundation-soil impedances of the unembedded structure. Various methods of calculating these factors, for both stiffness and damping, were presented and plotted. In general, the effect of embedment, as observed in the experiment, was significantly greater than that predicted by the analytical formulations.

Subsequent dynamic analyses indicated that the effect of embedment on the fundamental response of the analytical model was similar to that experienced by the specimen structure. As expected, embedment increased the resonant frequency and decreased the contribution of foundation motion to the total superstructure displacement. The model also experienced increased damping with embedment, a feature not found in the experiment.

Unfortunately, the good agreement between the experimental and analytical results for the fundamental mode did not hold for torsion. Several analyses were conducted, each of which used a different combination of analytically and experimentally obtained properties. In order

to match the measured torsional frequencies, the model structure had to have a foundation moment of inertia (for the unembedded case) five times greater than that of the specimen. The foundation-soil impedances, however, were in surprising agreement.

The use of the torsional properties obtained for the unembedded case by a combination of analysis and measurement resulted in significant variations between the results of the analysis and experiment when embedment was included. While it was possible to determine the properties of the model that would give rise to behavior similar to that of the specimen structure, it was not possible to develop a consistent method of accounting for the effect of embedment.

The discrepancies between the analytical and experimental results were reduced by neglecting the second torsional frequency. In this case, the effects of embedment on the fundamental torsional frequency were more consistent with the behavior measured in the experiment.

CHAPTER REFERENCES

- American Institute of Steel Construction, Manual of Steel Construction, Eighth Edition, AISC, New York, 1980.
- Baranov, V.A., "On the calculation of excited vibrations of an embedded foundation," (in Russian) Voprosy Dynamiki i Prochnosti Polytechnical Institute of Riga, No. 14, 1967, pp. 195-206.
- Beredugo, Y.O., and Novak, M., "Coupled horizontal and rocking vibration of embedded footings," Canadian Geotechnical Journal, Vol. 9, Nov. 1972, pp 477-497.
- Bielak, J., Earthquake Response of Building-Foundation Systems, EERL 71-04, California Institute of Technology, Pasadena, California, June, 1971.
- Bycroft, G.N., "Forced vibrations of a rigid circular plate on a semi-infinite elastic space and on an elastic stratum," Philosophical Transactions of the Royal Society, Vol. A248, No. 948, 1956, pp. 327-368.
- Elsabee, F., and Morray, J.P., Dynamic Behavior of Embedded Foundations, Civil Engineering Department Report R77-33, Massachusetts Institute of Technology (MIT), Cambridge, Massachusetts, Sept. 1977.
- Gladwell, G.M.L., "Forced tangential and rocking vibration of a rigid circular disc on a semi-infinite solid," International Journal of Engineering Science, Vol. 6, 1968, pp. 591-607.
- Hall, J.R., Jr., "Coupled rocking and sliding oscillations of rigid circular footings," Proceedings of the International Symposium on Wave Propagation and Dynamic Properties of Earth Materials, University of New Mexico, 1967, pp. 139-148.
- Karasudhi, P., Keer, L.M., and Lee, S-L, "Vibratory motion of a body on an elastic half-space," ASME Journal of Applied Mechanics, Vol. 35, Series E, No. 4, Dec. 1968, pp. 697-705.
- Kausel, E., and Ushijima, R., Vertical and Torsional Stiffness of Cylindrical Footings, Civil Engineering Department Report R79-6, MIT, Cambridge, Massachusetts, Feb. 1979.
- Lam, P.C., and Scavuzzo, R.J., "Torsional structure response from free-field ground motion," Transactions of the Fifth International Conference on SMiRT, 1979, Paper K5/5.

- Luco, J.E., "Torsional response of structures for obliquely incident seismic waves," Earthquake Engineering and Structural Dynamics, Vol. 4, No. 4, Jan.-Mar., 1976, pp. 204-219.
- Luco, J.E., and Westmann, R.A., "Dynamic response of circular footings," Journal of the Engineering Mechanics Division, ASCE, Vol. 97, No. EM5, Proc. Paper 8410, Oct. 1971, pp. 1381-1395.
- Luco, J.E., and Wong, H.L., "The seismic response of structures," Bulletin of the Seismological Society of America, Vol. 72, No. 1, Feb. 1982, pp. 275-302.
- Luco, J.E., Wong H.L. and Trifunac, M.D., "A note on the dynamic response of rigid embedded foundations," International Journal of Earthquake Engineering and Structural Dynamics, Vol. 4, No. 2, Oct.-Dec. 1975, pp. 119-125.
- Lysmer, J., and Richart, F.E., Jr., "Dynamic response of circular footings," Journal of the Soil Mechanics and Foundations Division, ASCE, Vol. 97, No. SM1, Jan. 1966, pp. 66-91.
- Maugh, L.C., Statically Indeterminate Structures, John Wiley and Sons, New York, 1946.
- Muto, K., Seismic Analysis of Reinforced Concrete Buildings, Shokoku-Shu, Tokyo, 1965.
- Novak, M., and Sachs, K., "Torsional and coupled vibrations of embedded footings," International Journal of Earthquake Engineering and Structural Dynamics, Vol. 2, No. 1, July-Sept. 1973, pp 11-34.
- Parmalee, R. A., and Kudder, R. J., "Seismic soil-structure interaction of embedded buildings," Proceedings of the Fifth WCEE, Rome, 1974, pp. 1941-1950.
- Parmalee, R.A., Perelman, D.S., and Lee, S-L, "Seismic response of multiple-story structures on flexible foundations," Bulletin of the Seismological Society of America, Vol. 59, No. 3, June, 1969, pp. 1061-1070.
- Reisner, E., "Stationäre, axialsymmetrische, durch eine schüttelnde Masse erregte Schwingungen eines homogenen elastischen Halbraumes," Ingenieur Archiv, Vol. 7, 1936, pp. 381-396
- Reisner, E. and Sagoci, H.F., "Forced torsional oscillations of an elastic half-space," Journal of Applied Physics, Vol. 15, 1944, pp. 652-662.

- Richart, F.E., Jr., Hall, J.R., Jr., and Woods, R.D., Vibrations of Soils and Foundations, Prentice-Hall, Englewood Cliffs, N.J., 1970.
- Tajimi, H., "Dynamic analysis of a structure embedded in an elastic stratum," Proceedings of the Fourth WCEE, Santiago, Chile, 1969, pp. 53-69.
- Thomson, W.T., Vibration Theory and Applications, Prentice-Hall, Inc., Englewood Cliffs, N.J., 1965.
- Veletsos, A.S., and Wei, Y.T., "Lateral and rocking vibrations of footings," Structural Research at Rice, 8, Department of Civil Engineering, Rice University, Houston, Jan. 1971.
- Wong, H.L., and Luco, J.E., "Dynamic response of rectangular foundations to obliquely incident seismic waves," Earthquake Engineering and Structural Dynamics, Vol. 6, No. 1, Jan.-Mar. 1978, pp. 3-16.

CHAPTER SIX

SUMMATION

This chapter concludes the report. The first section presents a general summary of the experimental and analytical results. Principal conclusions of this study are presented and discussed in Section 6.2.

6.1. SUMMARY

This study has been concerned with the effect of foundation embedment on the response of a one-story model specimen structure subjected to ambient vibration, ring-down, and forced vibration. There were two key aspects of the experimental study. The first was the determination of the effect of embedment on the response of a foundation supporting a superstructure. Until now, embedment effects have been experimentally determined only for simple, rigid foundations. The second was the use of horizontally incident anti-plane SH-waves to provide the forced vibration. This type of excitation is more representative of prototype earthquake excitations than current forced vibration methods.

The specimen structure consisted of a rigid concrete mass superstructure supported by a welded steel frame and open-topped concrete box foundation. The structure had plan dimensions of 10 X 10 ft (3.05 m X 3.05 m), and an overall height of 11.4 ft (3.5 m). The superstructure comprised one-third of the total weight of 50,000 lbs (224 kN). The superstructure's fixed-base resonant frequency was estimated to be 17.5 Hertz for translation in the principal (east-west) direction.

The forced vibration tests required the use of a vibration generator that was installed in the excitation structure. This second structure had plan dimensions of 13×5 ft (4×1.5 m), and was located 47.5 ft (14.5 m) center-to-center, from the specimen. In this experiment, the maximum force output and operating speed of the vibration generator were 3000 lbs (13.4 kN), and 70 Hertz, respectively.

The soil at the test site was dry, cohesionless, geologically young alluvium, consisting of sands, gravels, cobbles, and boulders to a depth of 1000 ft (300 m). Soil tests and in situ measurements yielded a unit weight of 95 lb/ft^3 (14.7 kN/m^3), and a shear wave velocity, for the uppermost material, of 1000 ft/sec (305 m/sec). The calculated value of the shear modulus was $2.95 \times 10^6 \text{ lb/ft}^2$ (141 MP).

The dimensions and properties of the experimental structures and equipment led to the determination and selection of five independent dimensionless parameters,

$$\blacksquare \text{ Mass ratio; } \mu_1 = \frac{M_{\text{superstructure}}}{M_{\text{foundation}}} = 0.5$$

$$\blacksquare \text{ Mass ratio; } \mu_2 = \frac{M_{\text{total structure}}}{M_{\text{displaced soil}}} = 1.0$$

$$\blacksquare \text{ Frequency ratio; } 0.4 < f/f_n < 4.0$$

$$\blacksquare \text{ Embedment ratio; } 0 < \delta = d/r < 0.9$$

$$\blacksquare \text{ Dimensionless frequency; } 0.25 < a_o = \frac{2\pi f r_o}{c_s} < 2.5 \quad .$$

The first phase of the test program consisted of the measurement of the free-field motion generated by the vibration of the specimen structure. This phase of testing was completed prior to construction of the specimen structure. Three results were obtained from this test, i) establishment of base-line ground motion for subsequent comparison, ii) determination of the ground motion amplitude at the site of the specimen structure, and iii) determination of the shear wave velocity. The first two results were dependent upon the excitation frequency, while a single value of 1000 ft/sec (305 m/sec) was obtained as the third result.

The response of the specimen structure to ambient vibration, ring-down, and forced vibration was measured in the second phase of the experiment, for the cases of full-, half-, and non-embedment of the foundation.

The resonant frequencies of the fundamental translational modes in the east-west and north-south directions and two torsional modes were determined from Fourier amplitude spectra which were calculated from the results of the ambient vibration tests. In general, these resonant frequencies increased with embedment; a result consistent with the expected increase in stiffness. The nature of the ambient vibration was found to be important in the evaluation of the amplitude spectra, non-random ambient excitations produced spectral peaks which could be erroneously interpreted as structural responses. Because of the non-stationarity of the structure's response, no information about the modal damping was obtained from these tests.

Ring-down, or free vibration, tests were conducted to obtain an independent estimate of the fundamental resonant frequency and modal damping ratio. While the resonant frequencies showed the expected dependence on embedment, no clear trends emerged for the modal damping ratio.

The main effort of this study was directed toward the forced vibration test. Although this test required far more effort than either the ambient vibration or ring-down tests, a more detailed and accurate description of the vibrational characteristics of the structure resulted. Since the excitation consisted of lateral ground motions in the east-west direction, no information about the north-south translatory response was obtained.

The principal objective of the test was the determination of the major resonant frequencies and modes. At the fundamental frequency, more detailed measurements of the structural displacements and near-field ground motions were completed.

Four modes of response were identified, the fundamental and secondary translatory modes, and two torsional modes. The resonant frequency and damping ratio of each mode were accurately determined by use of an equivalent single degree-of-freedom oscillator. The resonant frequency and damping ratio of the oscillator were varied until the difference between the response of the oscillator and the observed response of the specimen was minimized. The parametric values that resulted in the minimization were then assumed to correspond to the particular mode of the specimen structure.

The mode shape at the fundamental resonance contained negligible torsional or north-south translatory motions. This is consistent with the long wavelength of the incident motion. At the unembedded case, translation and rocking of the foundation contributed 6% and 21%, respectively, of the total superstructure displacement. At full-embedment, increased stiffness of the foundation reduced these contributions to 1.3% and 5.4%, respectively.

The fundamental resonance of the structure introduced large near-field ground motions. Both lateral ground motion, due to the structure's translation, and vertical ground motion, due to rocking of the structure, were measured. These motions were significant within three building radii of the foundation.

The results of the three tests were in relative agreement. Ambient vibration and ring-down tests provided sufficient information for the identification of the significant structural response modes. The forced vibration tests, however, were necessary to provide additional details that would be used as a basis for the subsequent lumped parameter analyses.

Lumped parameter analysis consists of the reduction of a complicated structure to a system of lumped masses and simple spring and dashpot elements to represent the inertial, elastic, and dissipative forces. For the analysis of this study, two systems were developed. The first system consisted of the translation of the foundation and superstructure, and the rocking of the entire structure about the bottom of the base. This system was used to study the fundamental mode

response, which, from a seismic viewpoint, is the most significant for symmetric structures. The second system, of lesser importance, was comprised of the torsion, about a vertical axis, of the superstructure and the foundation. The separation of the response of the structure into the two systems resulted in a significant reduction in computational effort, while causing no decrease in accuracy.

The first application of the lumped parameter analysis was the determination of the structural and foundation-soil impedances, in terms of the stiffness and the damping coefficient, from the fundamental resonant frequency and modal displacement ratios. Since the response of the structure was measured at three foundation embedments, it was possible to obtain the following embedment factors that reflected the effect of embedment on the horizontal translation and rocking impedances of the foundation-soil system,

$$\Delta_{K_{fx}} = 1 + 6.2448 - 0.5088^2$$

$$\Delta_{C_{fx}} = 1 + 3.7828 + 2.7198^2$$

$$\Delta_{K_{f\phi}} = 1 - 0.5918 + 6.328^2$$

$$\Delta_{C_{f\phi}} = 1 - 2.0668 + 7.9068^2 \quad .$$

Values of the foundation-soil impedances were also determined by evaluation of existing analytical formulations for the specific case of the specimen structure. Both frequency-dependent and constant-valued formulations were compared. The various methods used for the original

derivations were found to yield fairly similar results, hence, only one set of impedance functions was selected for use in the analysis. In general, the impedance values resulting from the experiment were lower than those that resulted from use of analytical expressions.

Significant variations existed between the various analytical expressions that reflect the effect of embedment on the foundation-soil impedances. There was a wide range in the complexity of the formulations. The experimental values were generally greater than those contained in the literature.

Several lumped parameter analyses of the three-degree-of-freedom system were conducted to determine the accuracy of the overall analysis. For a model defined solely by parametric values resulting from the substitution of the specimen structure's physical dimensions into analytical formulations, the fundamental resonant frequencies for the cases of zero-, half- and full-embedment were 14.25, 15.25, and 15.90 Hertz. The experimental results were 11.33, 13.28, and 13.75 Hertz. The lower observed frequencies are consistent with the lower experimentally determined impedances.

The effect of embedment was also calculated for a model defined by the experimentally determined unembedded impedances. The resonant frequencies, for the three embedment cases, were 11.33, 11.94, and 12.29 Hertz. The agreement of the resonant frequencies for the unembedded cases was, of course, a part of the modelling procedure. The calculated effect of embedment was less than the observed effect of embedment, a result consistent with the comparison of the observed and analytical

embedment factors. A similar agreement existed for the calculated and measured modal displacement ratios.

The modal damping ratios resulting from the analysis ranged from 1.3% to 2.5%, in comparison to the experimental value of 0.8%, a value found at all three embedment cases. This comparison reflects, in part, the assumed fixed-base damping factor of 1%.

A similar lumped parameter analysis was conducted for a two-degree-of-freedom system representing the torsional responses. Unlike the first set of analyses, it was impossible to find impedance values of the superstructure or foundation-soil system that would define a model with the observed resonant frequencies. One system, having a foundation moment of inertia five times greater than the specimen structure, but with all other significant properties in agreement with those resulting from the evaluation of analytical expressions, did have a similar torsional response. However, the calculated relative phase of the superstructure and foundation were not in agreement with the observed values. The model also failed to reproduce the fact that the measured response did not show strong dependence on embedment for the second torsional mode.

A reinterpretation of the torsional data considering only the lower resonant frequency led to more reasonable results. In this case, a system defined by parameters resulting from the analytical formulations had behavior similar to the specimen. The embedment dependence of this system was also consistent with expectations.

6.2. CONCLUSIONS.

Some general conclusions can be drawn from the experimental and analytical results of this study. These conclusions are in addition to the specific conclusions presented at the end of the major chapters.

1. Embedment of the foundation has a significant effect on the fundamental mode response. The increased impedances of the foundation-soil system increase the resonant frequency and decrease the contribution of the foundation motion to the overall structural displacement.
2. Existing analytical methods of calculating foundation-soil impedances appear to yield results consistent with those found experimentally. The accuracy of the resulting stiffness and damping coefficient are strongly dependent on the accuracy of the estimate of the soil's shear modulus.
3. The use of incident wave forced vibration simulates the incident SH-wave excitation of prototype structures during earthquakes. An additional advantage of this type of excitation is that a large excitation mass does not have to be added to the structure.
4. The use of lumped parameter analysis to determine the dynamic response of the specimen structure led to results consistent with the experimental response. The simple geometry and form of the foundation and superstructure, in comparison to prototype structures, are much closer to the idealized conditions of

the theoretical analyses. For this reason, better agreement is expected with the analysis of the specimen structure than would be obtained for prototype structures.

5. In terms of the fundamental mode response, current analytical formulations led to fairly accurate predictions of the effect of soil-structure interaction on the resonant frequencies and mode shapes. The simplicity and small size of the superstructure, relative to the foundation, however, overemphasizes the effect of interaction in comparison to prototype structures. Since it was not possible to directly measure the individual damping ratios of the superstructure and the foundation-soil systems, a quantitative description of the accuracy of the analysis with respect to the damping cannot be made. The assumption of superstructure damping ratios of 1%, however, led to reasonable agreement. In the context of behavior of structures during earthquakes, the difference between a calculated modal damping ratio of 3%, and a measured modal damping ratio of 1% at small strains, is not important because prototype structures show much higher effective dampings during potentially damaging motions.
6. The accurate determination of the superstructure's stiffness plays an important role in the overall accuracy of the lumped parameter analysis. In the case of the one-story specimen structure's fundamental mode response, two of the three degrees of freedom involved foundation motions. In a multistory

prototype structure, many more degrees of freedom are present, yet, only two of these are due to the foundation. In this case, the superstructure plays a much larger role in the response. Reduction of a multistory structure into equivalent simple oscillators, however, allows the direct application of the analyses of this study to multistory prototypes.

7. Even though significant variations exist between the analytical and experimental values for the impedances and the embedment factors, the agreement between the results of the analyses and the experimental measurements of the overall response of the structure is much better. While the variations in the impedances and embedment factors are important from the perspective of research, they are believed to be acceptable in the analysis of most prototype structures.
8. Significant near-field ground motions were generated by the resonance of the structure in its fundamental mode. Both lateral and vertical motions, due respectively to the translation and rocking of the foundation, were created. These near-field motions must be considered in the placement of free-field strong motion instruments or in cases where multiple structure interaction, particularly of sensitive structures, may occur. The low amplitude response of the specimen structure was sufficient to generate significant motions up to three building radii from the foundation.

9. The measured presence of two torsional modes in close proximity was not consistent with the lumped parameter analysis of the two-degree-of-freedom system. These two frequencies, the second of which was expected to correspond primarily to foundation motions, showed very little dependence on the foundation embedment. This behavior may indicate the presence of interaction phenomenon more complicated than was considered in the modelling.
10. The data acquisition, reduction, and analysis procedures were carefully designed to eliminate systematic errors caused by the equipment. Independent spot checks and repetition of key measurements were made to reduce the occurrence of random errors. As a result of these safeguards, the results of the forced vibration tests are believed to be reliable and repeatable, within a few percent in amplitude and within one percent for the resonant frequencies. Larger variations are possible in the very small, non-resonant motions.
11. The experience obtained during the field measurements led to several observations about the field and laboratory equipment. In general, the seismometer/signal conditioner system was reliable and accurate. Very few problems were encountered with these instruments. Because of the wide range in the measured frequencies and amplitudes, it was necessary to calibrate each component. The development of a simple and accurate transducer whose output could be used to obtain absolute displacements,

velocities, or accelerations would represent a significant improvement in the state-of-the-art. Attempts to obtain such absolute readings with the Ranger Seismometers were unsuccessful. The use of the Statham Accelerometer, which can be calibrated absolutely, was impractical because of the accelerometer's low sensitivity.

The strip chart and magnetic tape recorders were heavy and not well suited to field use. These instruments, while portable, were not durable enough to consistently withstand the rigors of heat, dust, and adverse field conditions. The test series would have had significant delays if spare equipment had not been available.

12. The large frequency range of the forced vibration tests placed strenuous demands on the shaker and controller system. If the motion transducers were less sensitive, much of the low frequency testing would have been impossible due to the low force output of the shaker. Although the shaker system did work in this program, its operation was cumbersome because of the imprecision of the speed control. Better accuracy would be obtained if the frequency could be directly read from the controller, instead of calculated from the record. The newer solid-state controllers do offer a significant improvement in this respect, but were of insufficient electrical capacity to

generate the high frequencies required for this experiment.

The high frequencies required in this test, fortunately, are atypical of tests conducted on prototype structures.

The results of the analyses and experiments of this study suggest additional areas that require attention. First, the advantages of incident wave excitation of model and prototype structures should be used to provide further information on structural response. Second, the lack of agreement of the theoretical and experimental results regarding torsion indicates another area that requires additional research. The two degree-of-freedom lumped parameter model was inadequate to represent the behavior of the specimen structure. Finally, the effect of embedment has not been measured on prototype structures. An ambient vibration test program, conducted on a structure during backfill of the foundation excavation, would result in significant new information.

APPENDIX A

This appendix contains FORTRAN listings for the computer programs described in the text.

A.1. Data reduction program NEWDAT

```
C*****C
C
C NEWDAT IS THE MAIN DATA REDUCTION PROGRAM. IT INCLUDES THE EFFECT C
C OF SHAKER FORCE LEVEL, EXCITATION FREQUENCY, RANGER SEISMOMETER C
C CHARACTERISTICS, AND THE SIGNAL CONDITIONER GAIN TO YIELD A C
C DISPLACEMENT/FORCE AMPLITUDE. C
C C
C*****C
      DIMENSION CORAMP(4), ATTA(160), CALIB(4), NORAMP(4), RMS(4), IATTA(4)
      DIMENSION DISAMP(4)
      DIMENSION LINE(40)
      REAL NORAMP
      DO 1 K=1, 160
      ATTA(K)=0.
1      CONTINUE
C
C GAIN VALUES FOR SIGNAL CONDITIONER ATTENUATOR SETTINGS.
C
      ATTA(1)=1.
      ATTA(7)=1.964
      ATTA(13)=3.856
      ATTA(19)=7.571
      ATTA(25)=14.87
      ATTA(31)=28.50
      ATTA(37)=54.50
      ATTA(43)=108.4
      ATTA(49)=217.4
      ATTA(55)=433.6
      ATTA(101)=83.48
      ATTA(107)=163.8
      ATTA(113)=329.4
      ATTA(119)=660.9
      ATTA(125)=1334.
      ATTA(131)=2715.
      ATTA(137)=5362.
      ATTA(143)=10220.
      ATTA(149)=20440.
      ATTA(155)=39860.
C
C "LINE" IS TEXT USED TO IDENTIFY THE DATA
C
      READ(5,100) LINE
100  FORMAT(40A2)
      WRITE(6,100) LINE
      READ(5,10) N
      DO 20 I=1,N
      READ(5,30) FREQ, ECC
C
C DYNAMIC CALIBRATION FITS FOR INDIVIDUAL SEISMOMETERS.
C
      CALIB(1)=1.
      CALIB(2)=1/(-.875+.00483*FREQ-.0000279*FREQ**2)
      CALIB(3)=1/(-.996+.001798*FREQ+.00000934*FREQ**2)
      CALIB(4)=1/(-.8937+.00473*FREQ-.0000311*FREQ**2)
```

```

C  FORCE OUTPUT OF SHAKER
C
      FORCE=4.84*ECC*FREQ**2
C
C  FREE-FIELD GROUND MOTION AT SPECIMEN STRUCTURE LOCATION
C
      GROUND=-.03+.0089*FREQ-.0000878*FREQ**2
      WRITE(6,40)FREQ,ECC,FORCE
      WRITE(6,90)
      DO 50 J=1,4
      READ(5,60) IATTA(J),RMS(J)
      K=IATTA(J)+1
      CORAMP(J)=RMS(J)*CALIB(J)*ATTA(K)
      DISAMP(J)=CORAMP(J)/(FORCE*GROUND*2.*3.141593*FREQ)*10000
50  CONTINUE
      DO 70 J=1,4
      NORAMP(J)=CORAMP(J)/CORAMP(1)
      WRITE (6,80) J, IATTA(J), RMS(J), CORAMP(J), NORAMP(J), DISAMP(J)
70  CONTINUE
20  CONTINUE
10  FORMAT(I3)
30  FORMAT(F5.2,F4.2)
40  FORMAT(/,1H,'      FREQUENCY=',F5.2,' HZ '
*  ',', ECC=',F4.2,', FORCE=',F8.2,' POUNDS')
60  FORMAT(I3,F10.5)
80  FORMAT(/,1H,'      ',I1,'      ',I3,'      ',F6.4,' ',
*  'E15.7,' ',F7.4,' ',F10.2)
90  FORMAT(/,1H,'      CH  ATTN  RMS AMPL  CORR',
*  ' AMPL  NORM AMPL  DISP AMP')
      STOP
      END

```

A.1.1. Sample input to program.

```

      SEPTEMBER 17, 1981, TEST SERIES C
3
19.68 1.0
136 .933
100 .487
106 1.232
136 1.346
23.80 1.0
142 1.98
106 2.08
124 2.39
124 3.69
24.6 1.0
142 2.27
106 3.60
112 3.60
136 4.83

```

A.1.2. Sample output of program.

SEPTEMBER 17, 1981, TEST SERIES C

FREQUENCY=19.68 HZ , ECC=1.00, FORCE= 1874.54 POUNDS .

CH	ATTEN	RMS AMPL	CORR AMPL	NORM AMPL	DISP AMP
1	136	0.9330	0.5002745E 04	1.0000	1941.83
2	100	0.4870	0.4308827E 02	0.0086	16.72
3	106	1.2320	0.1995612E 03	0.0399	77.46
4	136	1.3460	0.7318267E 04	1.4629	2840.61

FREQUENCY=23.80 HZ , ECC=1.00, FORCE= 2741.57 POUNDS

CH	ATTEN	RMS AMPL	CORR AMPL	NORM AMPL	DISP AMP
1	142	1.9800	0.2023560E 05	1.0000	3736.81
2	106	2.0800	0.3570422E 03	0.0176	65.93
3	124	2.3900	0.3120556E 04	0.1542	576.26
4	124	3.6900	0.4965275E 04	0.2454	916.91

FREQUENCY=24.60 HZ , ECC=1.00, FORCE= 2928.97 POUNDS

CH	ATTEN	RMS AMPL	CORR AMPL	NORM AMPL	DISP AMP
1	142	2.2700	0.2319940E 05	1.0000	3773.33
2	106	3.6000	0.6164983E 03	0.0266	100.27
3	112	3.6000	0.1158345E 04	0.0499	188.40
4	136	4.8300	0.2609895E 05	1.1250	4244.93

A.2. Two-dimensional minimization program MINUM.

```

C*****C
C
C
C  THIS PROGRAM MINIMIZES THE VARIATION BETWEEN THE RESPONSE OF A
C  SIMPLE HARMONIC OSCILLATOR AND THE EXPERIMENTAL RESULTS. THE
C  PURPOSE IS TO OBTAIN AN ESTIMATE OF THE DAMPING AND NATURAL
C  FREQUENCY. A TWO-DIMENSIONAL MINIMIZATION IS USED.
C
C*****C

      DIMENSION F(100),Y(100),A1(3,3),B1(3),X(3),WORK(4,4),FR(3),L(3)
      DIMENSION ZE(3)
      REAL J,L

C
C  INITIALIZE AN ESTIMATE OF THE RESONANT FREQUENCY, "FREQ", AND DAMPING
C  RATIO, "ZETA".
C
      READ(5,10) FREQ
      READ(5,10) ZETA

```

```

C
C "N" IS THE NUMBER OF POINTS ON THE MEASURED RESPONSE CURVE
C
      READ(5,14) N
C
C "EPF" AND "EPZ" ARE THE INITIAL STEP-SIZES FOR THE ITERATION
C
      EPF=.05
      EPZ=.005
      DO 20 I=1,N
C
C "F" AND "Y" ARE THE ORDERED PAIRS OF THE FREQUENCY AND AMPLITUDE
C
      READ (5,15) F(I),Y(I)
20    CONTINUE
      CALL MIN (N,F,Y,FREQ,ZETA,J,A0)
      WRITE(6,21) FREQ,ZETA,J,EPF,EPZ,A0
      PEST=J
30    TEST=J
C
C THIS SECTION OF THE PROGRAM INCREMENTS THE FREQUENCY
C
35    FREQ=FREQ+EPF
      CALL MIN (N,F,Y,FREQ,ZETA,J,A0)
      WRITE(6,21) FREQ,ZETA,J,EPF,EPZ,A0
      IF (J.LT.TEST) GO TO 40
      EPF=-EPF
      FREQ=FREQ+EPF
      GO TO 45
40    TEST=J
45    FREQ=FREQ+EPF
      CALL MIN(N,F,Y,FREQ,ZETA,J,A0)
      WRITE(6,21) FREQ,ZETA,J,EPF,EPZ,A0
      IF (J.LT.TEST) GO TO 40
C
C J IS NO LONGER DECREASING. HENCE, FIND THE FREQUENCY THAT MINIMIZES
C J LOCALLY.
C
      FR(1)=FREQ-2*EPF
      FR(2)=FREQ-EPF
      FR(3)=FREQ
      WRITE(6,27)
      DO 200 K=1,3
      FREQ=FR(K)
      CALL MIN(N,F,Y,FREQ,ZETA,J,A0)
      WRITE(6,21) FREQ,ZETA,J,EPF,EPZ,A0
      L(K)=J
200    CONTINUE
C
C CALCULATE A PARABOLA TO FIT THROUGH THREE VALUES OF J
C
      A1(1,1)=FR(1)**2
      A1(1,2)=FR(1)
      A1(1,3)=1.00
      A1(2,1)=FR(2)**2
      A1(2,2)=FR(2)
      A1(2,3)=1.00
      A1(3,1)=FR(3)**2
      A1(3,2)=FR(3)
      A1(3,3)=1.00
      B1(1)=L(1)
      B1(2)=L(2)
      B1(3)=L(3)
C
C "LINEQ" IS A LIBRARY SUBROUTINE TO SOLVE THE MATRIX EQUATION.
C
      CALL LINEQ(X,B1,A1,WORK,3,4,IERR)

```

```

WRITE(6,22) X(1),X(2),X(3)
FREQ=-X(2)/(2*X(1))
C
C VALUE OF "FREQ" THAT MINIMIZES J IN ONE DIMENSION
C
CALL MIN(N,F,Y,FREQ,ZETA,J,A0)
WRITE (6,21) FREQ,ZETA,J,EPF,EPZ,A0
C
C "PEST" IS A CHECK IN CASE THE CALCULATION HAS SOME ANOMALY.
C
IF (J.GT.PEST) GO TO 80
PEST=J
46 TEST=J
C
C THIS SECTION INCREMENTS ON "ZETA".
C
ZETA=ZETA+EPZ
CALL MIN(N,F,Y,FREQ,ZETA,J,A0)
WRITE(6,21) FREQ,ZETA,J,EPF,EPZ,A0
IF (J.LT.TEST) GO TO 50
EPZ=-EPZ
ZETA=ZETA+EPZ
GO TO 55
50 TEST=J
55 ZETA=ZETA+EPZ
CALL MIN(N,F,Y,FREQ,ZETA,J,A0)
WRITE(6,21) FREQ,ZETA,J,EPF,EPZ,A0
IF (J.LT.TEST) GO TO 50
C
C J IS STARTING TO INCREASE, FIND A VALUE OF ZETA FOR A LOCAL MINIMUM.
C
ZE(1)=ZETA-2*EPZ
ZE(2)=ZETA-EPZ
ZE(3)=ZETA
WRITE(6,27)
DO 300 K=1,3
ZETA=ZE(K)
CALL MIN(N,F,Y,FREQ,ZETA,J,A0)
WRITE (6,21) FREQ,ZETA,J,EPF,EPZ,A0
L(K)=J
300 CONTINUE
A1(1,1)=ZE(1)**2
A1(1,2)=ZE(1)
A1(1,3)=1.00
A1(2,1)=ZE(2)**2
A1(2,2)=ZE(2)
A1(2,3)=1.00
A1(3,1)=ZE(3)**2
A1(3,2)=ZE(3)
A1(3,3)=1.00
B1(1)=L(1)
B1(2)=L(2)
B1(3)=L(3)
CALL LINEQ(X,B1,A1,WORK,3,4,IERR)
WRITE (6,22) X(1),X(2),X(3)
ZETA=-X(2)/(2*X(1))
C
C VALUE OF "ZETA" THAT MINIMIZES J IN ONE DIRECTION
C
CALL MIN (N,F,Y,FREQ,ZETA,J,A0)
WRITE(6,21) FREQ,ZETA,J,EPF,EPZ,A0
IF (J.GT.PEST) GO TO 80
PEST=J
56 TEST=J

```

C
C DECREASE INCREMENT SIZE FOR BETTER PRECISION.
C

```

59     EFF=ABS(EFF/2)
      EPZ=ABS(EPZ/2)
      GO TO 35
80     STOP
81     WRITE(6,23)TST
23     FORMAT('STOP AT ONE',F10.5)
27     FORMAT('          PARABOLA FIT          ')
10     FORMAT(F10.4)
14     FORMAT(I2)
15     FORMAT(F5.2,F10.4)
21     FORMAT(F12.5,F12.7,E20.7,F10.5,F10.5,E15.7)
22     FORMAT(3E15.7)
      END

```

C
C SUBROUTINE TO CALCULATE THE VALUE OF J.
C

```

      SUBROUTINE MIN (N,F,Y,FREQ,ZETA,J,A0)
      DIMENSION A(50),B(50),C(50),W(50),F(50),Y(50),D(50)
      REAL J
      SUM1=0.
      SUM2=0.
      SUM3=0.
      WNAT=FREQ*2.*3.141593
      DO 100 I=1,N
      W(I)=F(I)*2.*3.141593
      A(I)=W(I)**2/(SGRT((WNAT**2-W(I)**2)**2+(2*ZETA*WNAT*W(I))**2))
      B(I)=A(I)*Y(I)
      C(I)=A(I)**2
      SUM1=SUM1+B(I)
      SUM2=SUM2+C(I)
100    CONTINUE
      AO=SUM1/SUM2
      DO 110 I=1,N
      D(I)=(Y(I)-AO*A(I))**2
      SUM3=SUM3+D(I)
110    CONTINUE
      J=SUM3
      RETURN
      END

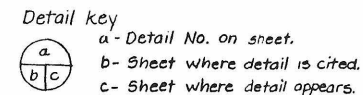
```


APPENDIX B

This appendix contains a set of contract drawings issued for the construction of the experimental structures.

for

Earthquake Engineering Laboratory
Department of Civil Engineering
Division of Engineering & Applied Science
California Institute of Technology
Pasadena, California

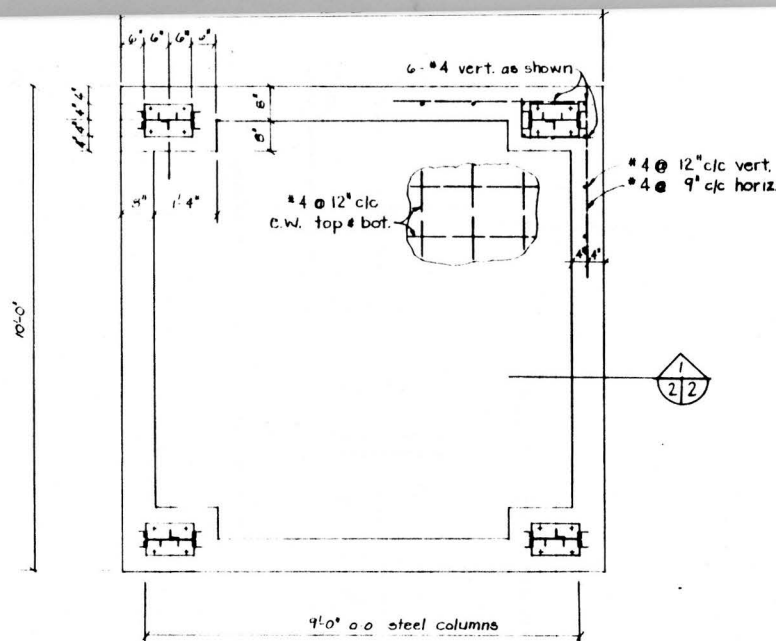


Paramount Street

Scale: $1'' = 80.00'$

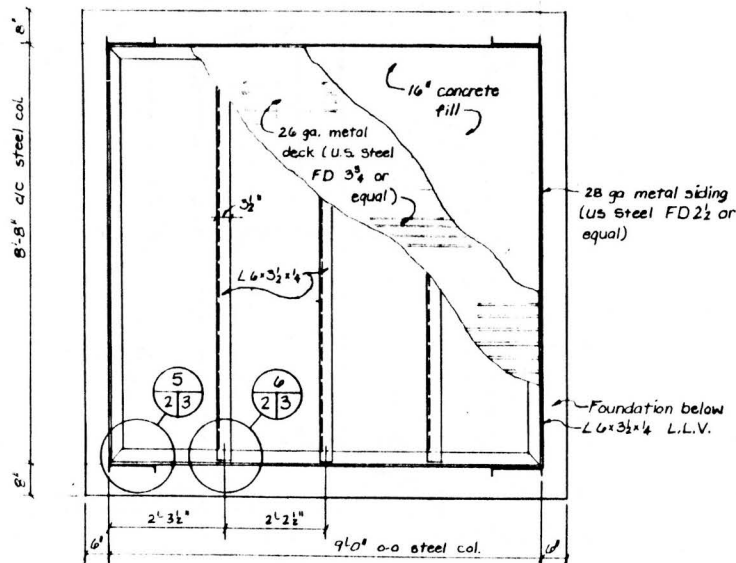


SCALE: As noted	APPROVED BY: <i>P. L. Jensen</i>	DRAWN BY <i>A. Lin</i>
DATE: March 6, 1981		REVISED
EARTHQUAKE ENGINEERING RESEARCH LABORATORY CALIFORNIA INSTITUTE OF TECHNOLOGY		
FIELD TEST STRUCTURES		DRAWING NUMBER 1 OF 5



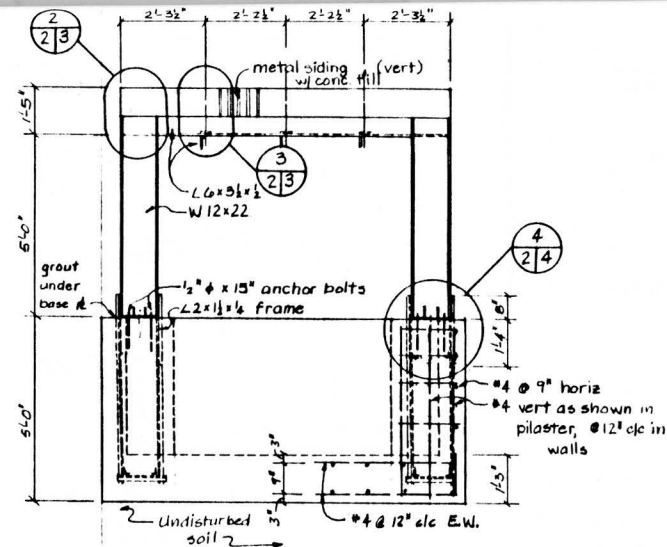
FOUNDATION PLAN

Scale: 1/2" = 1'-0"



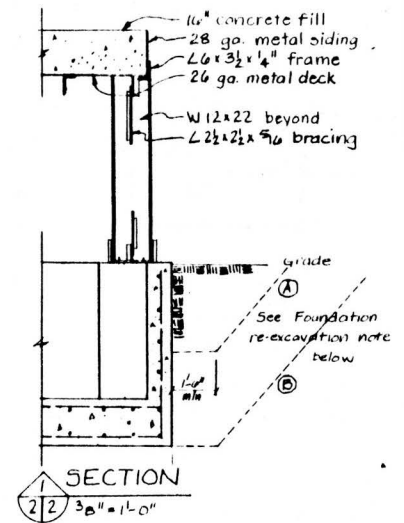
SUPERSTRUCTURE PLAN

Scale: 1/2" = 1'-0"



SOUTH ELEVATION

Scale: 3/8" = 1'-0"

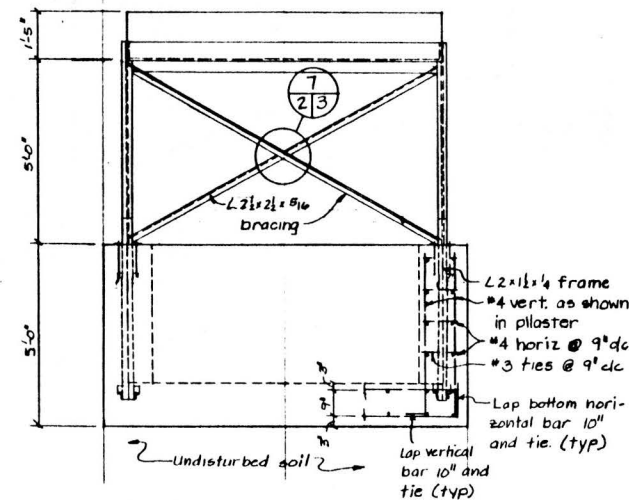


FOUNDATION RE-EXCAVATION

After completion of Phase II of testing, Contractor shall return to site and excavate to contour ① as shown above. Contractor shall return attend of Phase III and excavate around foundation to contour ②. Removed soil shall be stockpiled 25' west of specimen structure.

NOTES:

1. Structural steel shall be A-36.
2. Reinforcing steel shall be A-615 grade 60 deformed bars.
3. Superstructure concrete shall be fc = 3000 psi, with unit weight = 150 pcf.
4. Foundation concrete shall have fc = 3000 psi, and unit weight = 150 pcf.
5. Backfill shall be well graded granular material placed and compacted in 6" lifts to 110 pcf ± 5%. No cobbles larger than 3" φ may be used.
6. Total weight of superstructure concrete shall be 14,150#.
7. Total weight of foundation concrete shall be 30,000#.
8. Two (2) 6" φ x 12" cylinder samples of the foundation and superstructure concrete shall be made for weight determination.
9. Structural steel fabrication and welding shall conform to standards of AISC and AWS.
10. Concrete and reinforcing steel work shall conform to standards of ACI and CRSI.
11. Base of foundation shall be cast against undisturbed soil. Excavation shall be to ±1" of elevation shown. Excavation shall be inspected by designer prior to placement of reinforcing steel.

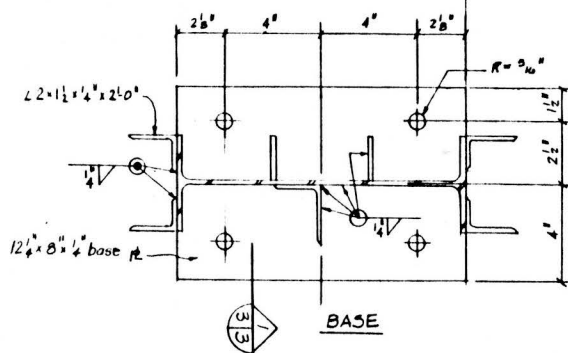
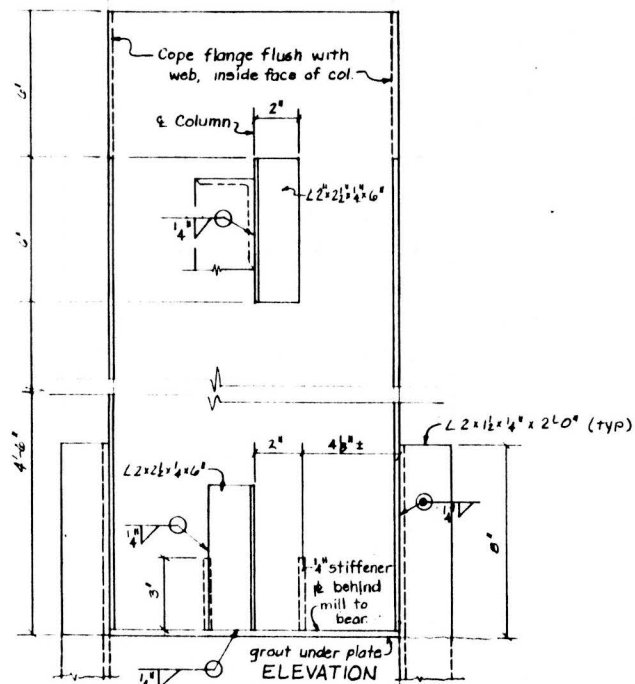
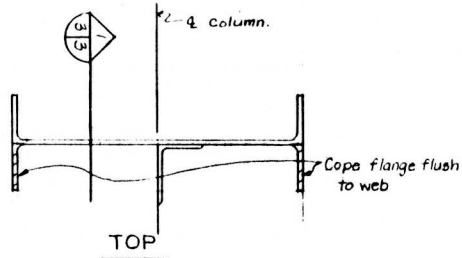


WEST ELEVATION

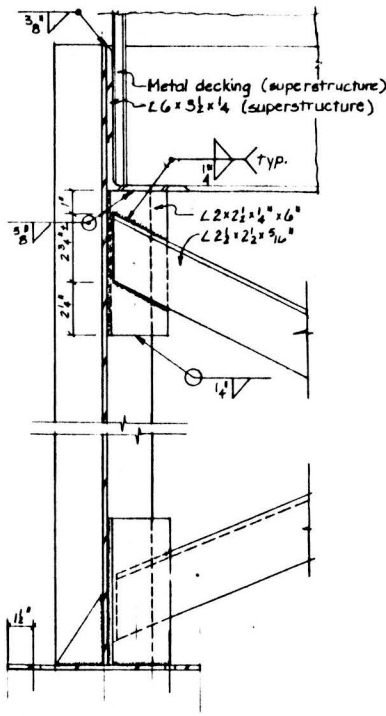
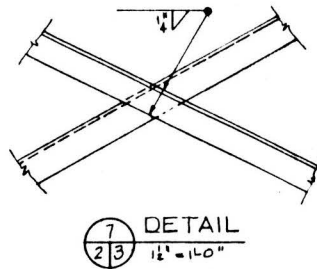
Scale: 3/8" = 1'-0"

SPECIMEN STRUCTURE
PLANS AND ELEVATIONS

SCALE: As Noted	APPROVED BY: PC Jennings	DRAWN BY: A. Lin
DATE: March 6, 1981		REVISED
EARTHQUAKE ENGINEERING RESEARCH LABORATORY CALIFORNIA INSTITUTE OF TECHNOLOGY		
FIELD TEST STRUCTURES		DRAWING NUMBER 2 OF 5

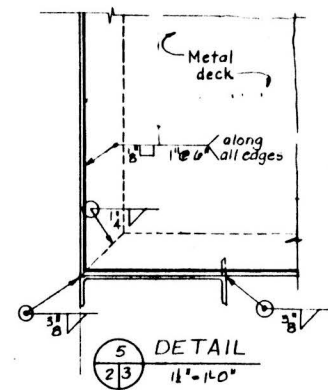


COLUMN DETAILS
Scale 3/4"=1'-0"

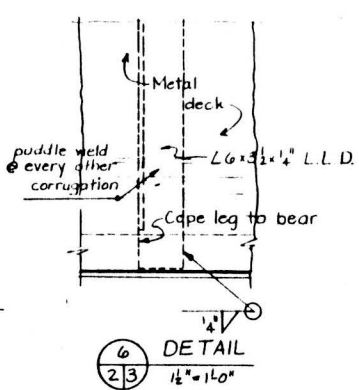


SECTION 1
3/4"=1'-0"

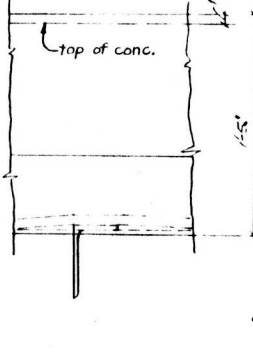
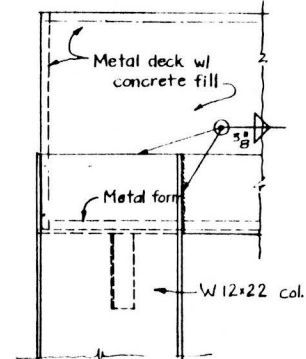
Note: Shop Drawings shall be submitted for approval prior to fabrication.



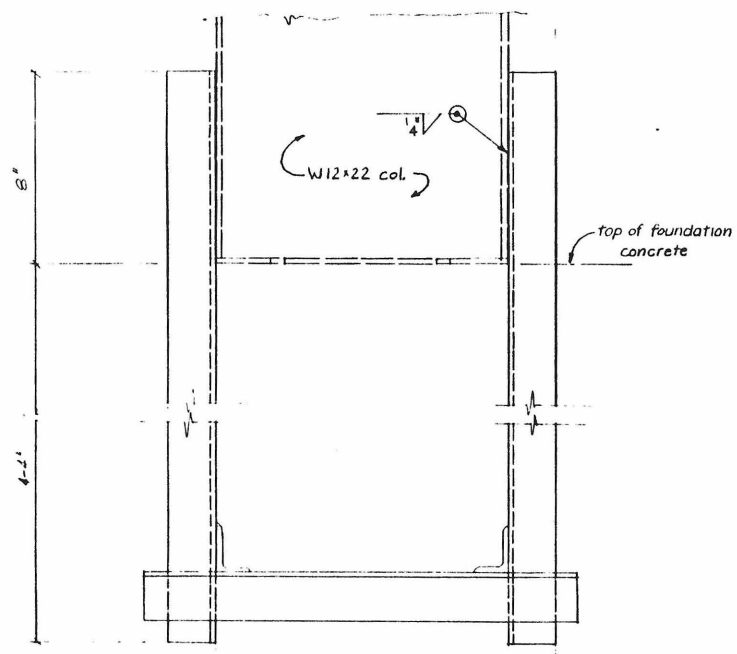
DETAIL 5
1/2"=1'-0"



DETAIL 6
1/2"=1'-0"



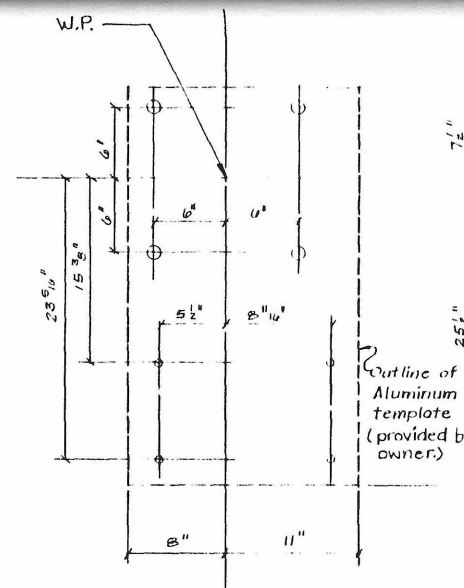
SPECIMEN STRUCTURE STRUCTURAL STEEL DETAILS		
SCALE: As Noted	APPROVED BY: <i>Ref. Test</i>	DRAWN BY A. Lin
DATE: March 6, 1981		REVISED
EARTHQUAKE ENGINEERING RESEARCH LABORATORY CALIFORNIA INSTITUTE OF TECHNOLOGY		
FIELD TEST STRUCTURES		DRAWING NUMBER 3 OF 5



SPECIMEN STRUCTURE
STRUCTURAL STEEL DETAILS

DRAWN BY A Lin
REVISED

DRAWING NUMBER
4 OF 5

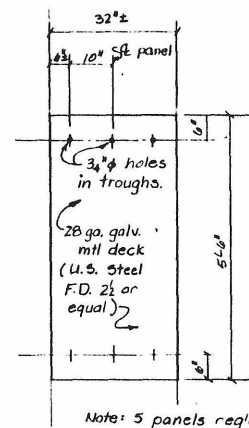


2
5 5

DETAIL

Scale $1\frac{1}{2}" = 1'-0"$

1



COVER PANEL

Scale $\frac{1}{2}'' = 1'-0''$

NOTES

1. Concrete shall be normal weight, $14 \pm 3.330 \text{ psi}$.
2. Reinforcing steel shall be A615, gr 60.
3. Structure base shall be poured against undisturbed soil within 1" of profile shown.
4. Backfill shall be placed and compacted in 6" lifts to 110 pcf $\pm 5\%$. No cobbles larger than 3" nominal shall be used.
5. Concrete and reinforcing steel work shall conform to standards of ACI and CRSI.

EXCITATION STRUCTURE

SCALE: As noted	APPROVED BY: <i>R.C. Tennant</i>	DRAWN BY: A Lin
DATE: March 6, 1961		REVISED: 4/1/61
EARTHQUAKE ENGINEERING RESEARCH LABORATORY CALIFORNIA INSTITUTE OF TECHNOLOGY		
FIELD TEST STRUCTURES		DRAWING NUMBER 5 OF 5